



TECHNISCHE UNIVERSITÄT MÜNCHEN

Ingenieur fakultät Bau Geo Umwelt

LEHRSTUHL FÜR STATIK



# Functional Adaptation with Hyperkinematics using Natural Element Method: Application for Articular Cartilage

ÖNAY CAN

Vollständiger Abdruck der von der Ingenieur fakultät Bau Geo Umwelt der Technischen Universität München zur Erlangung des akademischen Grades eines

Doktor-Ingenieurs

genehmigten Dissertation.

**Vorsitzender:** Univ.-Prof. Dr.-Ing.habil. Fabian DUDDECK

**Prüfer der Dissertation:**

1. Univ.-Prof. Dr.-Ing. Kai-Uwe BLETZINGER
2. Prof. Ellen KUHL, Ph.D.  
Stanford University/USA
3. Univ.-Prof.Dr.techn. Roman LACKNER  
Universität Innsbruck/Österreich

Die Dissertation wurde am 23.09.2014 bei der Technischen Universität München eingereicht und durch die Ingenieur fakultät Bau Geo Umwelt am 05.12.2016 angenommen.



Schriftenreihe des Lehrstuhls für Statik  
TU München

Band 35

**Önay Can**

FUNCTIONAL ADAPTATION WITH HYPERKINEMATICS USING  
NATURAL ELEMENT METHOD:  
APPLICATION FOR ARTICULAR CARTILAGE

München 2016

Veröffentlicht durch

Kai-Uwe Bletzinger  
Lehrstuhl für Statik  
Technische Universität München  
Arcisstr. 21  
80333 München

Telefon: +49(0)89 289 22422  
Telefax: +49(0)89 289 22421  
E-Mail: [kub@tum.de](mailto:kub@tum.de)  
Internet: [www.st.bgu.tum.de](http://www.st.bgu.tum.de)

ISBN: 978-3-943683-42-4

© Lehrstuhl für Statik, TU München



*to Maya and Toprak*

---

*Eline, Beline, Diline hakim ol.  
Beherrsche deine Hande, Lende, Zunge.*

---

*Buyruk  
Buyruq*

---

# Acknowledgments

Beginning of all, I would like to express my warm Gratitudes to all involving in the preparation of this long engineering essay.

It is in this stage an honour for me to return best indebtedness to my supervisor Prof. Kai-Uwe Bletzinger, for his admirable patience, understanding and judgment, power of recognition, and for his ability of empathy and self-projection. In fact, only carrying some natural aptitudes is not a reason to praise somebody, however using this skill, was a matter of decision and not a must, and this determinant initiative of Prof. Bletzinger was the most appreciable for me, and will never be forgotten.

Immediately after, I would like to address my respectful Gratitudes towards Prof. Roman Lackner. He has proven in many occasions, that he is trustful and supportive to the people who are dependent on his actions and decisions. His principle of *"multiplying the speculated time with twenty to get more rational estimation for finishing"* is still seems to be valid for my case.

I am also very grateful and feel fortunate to get the opportunity for knowing Prof. Ellen Kuhl personally. I gained lots of confidence about my work, by receiving constructive critics from this motivation emitting individual personality. I am sure that, I am neither last, nor the first one who benefits from the life energy of this inspiration-providing master of Biomechanics. I will try to keep in mind that, *"normal people sleep nights, and work daytime"*, as much as I can.

I address furthermore special thanks to Prof. Fabian Duddeck, who was always a perfect listener and advisor to me. I thank to Dr. Roland Wüchner by heart, as he was delivering help whenever it was necessary. Frau Ekkel was always very kind, polite and was assisting her help always on time.

Among many colleagues, Martin Johannes Herrenbrück is a very special one, honest, frank, a protecting loyal friend. I send hereby warm greetings to some other former Colleagues, among many, to Electra Stavropoulou, Armin Widhammer, Pablo Suarez Espinoza, Serdar Serdas and Josef Kiendl.

I prost here two dear friends, Hakan Cankaya and Ersoy Yildirim for keeping me partially in touch with real world.

Never be paid empathy was spend by my lovely sister Sultan Nilay Can, my self-sacrificing Mother Salime Can, and my upstanding Father Yusuf Can.

Lastly, apart all the other listed above, I thank to self-sacrificing mothers Silke Renner-Ehlert and beloved Günes Carmichael-Can for giving lives to my daughter Maya Frida Can and son Toprak Martin Can. As they sleep during typing these last words of my thanksgiving, i wish they dream about the future events of their lives, where they attain the "source of peace in soul and flesh" and nurse the "soil of earth", as their names state.

---

**Functional Adaptation with Hyperkinematics using Natural Element  
Method: Application for Articular Cartilage**

---

# Preclusion of this Treatise

Before starting, I would like to emphasize that this preface stands not only for the brief explanation of the scientific content of the treatise, but also proposed to be a summary of the motivation of working on it, and exploding the philosophy of best practice of constructing the survey and its content. This foreword is partially written to impose the conception of the line of action up on the reader. The abstract of the scientific elements of the work, which mainly represents the backbone of the work, will be presented thereafter.

The subject of this dissertation is a subfield of the *Biomechanics*, namely the *Continuum Biomechanics*, more specifically with focus on living fibrous soft-tissue. The initial definition of the subject will be more precisely revised after introducing initial arguments. Before starting to network the ideas behind the principle of line of action, one has to start with the formal definitions of the subject.

Biomechanics is defined as to be "*the study of the structure and function of biological systems such as humans, animals, plants, organs, and cells by means of the methods of mechanics*" Ref.[<sup>Hatze 1974</sup>]. This definition is generally accepted to be very comprehensible, and thus a redefinition is avoided and had not seen to be necessary. There are certainly similar definitions, however, older or novel, all these do neither contribute additional message, nor narrow the points of significance. However, since then, there is though some differences developed. These are mainly as a result of discrete jumps in the state of the art of disciplines contributing the field of biomechanics, namely in engineering and medical science. Many Pioneers considered the field of Mechanics as a tool which is used to understand the function of biological structure. For instance Ref.[<sup>Fung 1993</sup>] states that "*the interest in continuum biomechanics is spurred by the need for realism in the development of medical simulation*". Which more explicitly than implicitly indicates that, in the absence of this interdisciplinary interest, the field of biomechanics would never been born at all, or would not be the same which is now. This observation is well accepted and appreciated by the writer of this treatise.

Moving on, more up-to date publications about mechanobiology, state the expected *realism* above clearly enough. For instance, Ref.[<sup>Humphrey 2003</sup>] forewords his opinion on this subject by writing that, "*biomechanics has yet to reach its full potential as a consistent contributor to the improvement of health-care delivery*." This pragmatic manifest was certainly not a secret, but the achievements are spoken out now confidently as before. As background message, it is also emphasized not to forget consistent contribution. According to the subjective opinion of the writer, behind this emphasis, there is presumably the apprehension of losing the attention on continuum mechanics, by failing to hit the point of objective, or landing far beyond of the diameter of interest. If this apprehension tends to move towards anxiety or should soldier on to keep the stress level high enough for improvement, to find the answer more experience is required. However, this discussion leads to the clarification of the *best practice* and line of action of this treatise.

There is an implicative question to be answered. *The fact* is, during the development

of interdisciplinary fields, one field served and supplied logistics to another (where the practical interest focuses). *The question* is, does it take place without evolving its own structure, or vendor branch has gained also power and self-interest by involving in the proposed interdisciplinary field?

The arguments can be put on the table simultaneously, or sequentially. The latter is preferred by the writer here. Considering one single property of matter of concern here, that is anisotropy. Please recall that several fibrous soft tissue types are mechanically anisotropic, such as skin, cardio-vascular system, cartilage, tendons, ligaments and more. However, the term is in fact visited several times by the leading engineers of the field, even before the discussion of existence of a field named biomechanics. For instance S. Timoshenko and J.N. Goodier in their master piece of Ref. [S. Timoshenko 1951] mention about anisotropy, "...a certain orientation of the crystals in metals prevails, the elastic properties of the metal become different in different directions and the condition of anisotropy must be considered.". They obviously mention about the anisotropy caused by engineering process, precisely metal forming. Frankly writing, it would be quite an arrogant action to claim that, the founders of the *Theory of Elasticity* were unaware of the existence of naturally anisotropic material, because they were ridiculously unable to observe the fibrous structure of redwood. It is thus an obvious fact that, terms like anisotropy was certainly postulated earlier in the borderlines of continuum mechanics, and found another field of application; *Biomechanics*.

Keeping this example in mind, the first postulations of the hyperelastic anisotropic energy functions date not as back as foundational elements of elasticity. Fung, being accepted as one of the fathers of continuum biomechanics, mentioned about the residual stresses in arterial walls in Ref. [C.J. Chuong 1986], however first postulated the famous exponential formula for the anisotropic materials, quite later, in Ref. [Fung 1993]. Similarly, nearly before Fung, another hyperelastic anisotropic formula postulated in Ref. [J.M. Guccione 1991]. In the second work, Guccione JM et al. reached one of the first quantitative statements; "...the stiffness of passive myocardium (defined for a 20 percent equibiaxial extension) would be 2.4 to 6.6 times greater in the fiber direction than in the transverse plane...". Later works of Ogden and Holzapfel, such as in Ref. [Ogden 2003] and Ref. [Holzapfel 2008] include more specific and reliable material models based on empirical techniques and validation methods based on recent publications of themselves. Among all the contributions done until now, one is common that, the researchers and pioneers of the field of biomechanics applied the fundamental postulates of classical continuum mechanics, such as the definitions done by Green, Ref. [Green 1970].

# Contents

<b>Acknowledgement</b>	<b>iii</b>
<b>Preclusion</b>	<b>v</b>
<b>List of Abbreviations</b>	<b>ix</b>
<b>1 Soft Tissue as Biphase Mixture</b>	<b>1</b>
1.1 Introduction	2
1.2 Partial and Total Properties of the Mixture	3
1.3 Kinematics of the Mixture	5
1.4 Governing Relations	7
1.4.1 Conservation of Mass	7
1.4.2 Conservation of Translational Momentum	9
1.4.3 Conservation of Internal and Kinetic energy: An extended first law of Thermodynamics	11
1.4.4 The Entropy Inequality-Dissipation of Mixed Field	15
1.5 Assumptions, Narrowed Relations and Constitutive Restrictions	20
1.5.1 Assumptions	20
1.5.2 Narrowed Governing Relations	21
1.5.3 Constitutive Restrictions	22
1.5.4 Darcy Velocity, Saturation Rate and Pore Pressure	23
1.6 Weak Forms	27
1.6.1 Weak Form of Balance of Translational Momentum in Solid Material Coordinates	27
1.6.2 Weak Form of Conservation of Mass	30
1.7 Discretized balance equations	31
1.7.1 Matrix-Vector Form on Total Lagrangian Configuration	31
1.7.2 Newmark-Method-Consistent Material Time Derivatives	33
1.7.3 Discrete Form of the Translational Momentum Part	34
1.7.4 Discrete Form of the Conservation of Mass	39
1.8 Numerical Examples	46
1.8.1 Finite Element Implementation: Software Specifications	46
1.8.2 A Numerical Scenario: Growth of Uterine Fibroids	48
1.8.3 A Numerical Scenario: Impact on the Surrounding Tissue	52
1.8.4 A Numerical Scenario: Cartilage under Compression	57
<b>2 Hyperkinematics</b>	<b>61</b>
2.1 Introduction	61
2.2 Theory: Kinematics	63
2.2.1 Reference to Spatial: From Reference Lines to Spatial Curves	63

2.2.2	Spatial to Reference: From Spatial Curves to Reference Lines . . . . .	67
2.2.3	Material to Spatial: From Reference Curves to Spatial Curves . . . . .	70
2.3	Verification: Numerical Examples . . . . .	72
2.3.1	Push Forward: From straight Reference to the curved Spiral . . . . .	72
2.3.2	Pull Back: From curved Spiral to the straight Reference . . . . .	73
2.4	Conclusion . . . . .	75
<b>3</b>	<b>Nonlinear Strain-gradient Balance</b>	<b>77</b>
3.1	Introduction . . . . .	77
3.2	Hyper-Cauchy Equation-OM: The Governing Local Form . . . . .	80
3.3	Curved Anisotropy . . . . .	84
3.3.1	Curvature Invariant with Euler Bernoulli Ansatz . . . . .	84
3.3.2	Anisotropic Strain and Strain-gradient Energy Function - EB Ansatz . . . . .	87
3.4	FEM Implementation with Strain-gradient Effects . . . . .	90
3.4.1	Discrete Form for Finite Element Formulation . . . . .	91
3.4.2	Strain-gradient Displacement Matrix . . . . .	92
3.4.3	Numerical Examples . . . . .	96
<b>4</b>	<b>Reorientation with Strain and Gradient Effects</b>	<b>99</b>
4.1	Introduction . . . . .	99
4.2	Orthotropic Hyperelasticity . . . . .	100
4.2.1	Worm-like Chain Model . . . . .	100
4.2.2	Mechanics of the Chain Network . . . . .	101
4.2.3	Structural Tensors . . . . .	102
4.2.4	Energy Split, Stress at Integration Point and Tangent Modulus . . . . .	108
4.2.5	Simple Tension and Shear on the Orthotropic 8-chain Model . . . . .	110
4.3	Material Point Reorientation . . . . .	113
4.3.1	Strain based Reorientation . . . . .	113
4.3.2	Curvature Reorientation . . . . .	118
4.3.3	Reorientation based on the EB Material Model . . . . .	119
<b>5</b>	<b>Natural Element Method</b>	<b>123</b>
5.1	Introduction . . . . .	123
5.2	Clustered and Constrained Delaunay-Voronoi Dual . . . . .	125
5.2.1	Clustering the Delaunay Triangulation . . . . .	125
5.2.2	Constrained Voronoi Tesselation . . . . .	129
5.3	Non-sequential Nodal Integration . . . . .	135
5.3.1	Evaluation of Shape Value Matrix . . . . .	138
5.3.2	Nature of Shape Value Matrix . . . . .	143
5.4	Implementation and Examples . . . . .	146
5.5	Comparison of Different Reorientation Manifests . . . . .	150

---

<b>6 Summary</b>	<b>153</b>
6.1 Introduction . . . . .	153
6.2 Least Requirements . . . . .	153
6.3 Hyperelasticity . . . . .	154
6.4 Functional Adaptation, Abnormal Cell Growth . . . . .	154
6.5 Methodical Development . . . . .	155
<b>A Appendix A</b>	<b>157</b>
A.1 The derivatives of the spiral beam . . . . .	157
<b>B Appendix B</b>	<b>163</b>
B.1 Bending Strain and Strain Gradient energy density Function . . . . .	163
B.2 Stretching Strain and Strain Gradient energy density Function . . . . .	171
<b>C Appendix C</b>	<b>173</b>
C.1 Simo-Type geometrically exact anisotropy in hyperelastic form . . . . .	173
C.2 Tractions and Hypertractions on gradient Cauchy tetrahedra . . . . .	176
<b>D Appendix D</b>	<b>181</b>
D.1 Stationary configurational energy and kinematics . . . . .	181
D.2 Maximization of Configurational Energy . . . . .	185
<b>Bibliography</b>	<b>189</b>
<b>E Present Publication Series</b>	<b>199</b>





# List of Abbreviations

## Conceptual Declarations

---

<u>Symbol</u>	<u>Description</u>	<u>Definition</u>
$\bar{N}, \bar{G}, \bar{NG}$	Nodal, Gussian and the union sets (equations ( 5.19a, 5.19b, 5.19c in subsection 5.3.1)	$\bar{NG} = \bar{N} \cup \bar{G}$
$\bar{\mathbb{P}}$	A finite point set with cardinality 'm' in 'n' dimensions. (equation 5.1 in subsection 5.2.1.1)	$p_m : \forall p_i \in \mathbb{R}^n$
CDT	Clustered Delaunay triangulation (equation 5.8 in subsection 5.2.1.1)	—
CV	constrained Voronoi tessellation (equation 5.15b in subsection 5.2.2)	$CV = \bigcup_{p=1}^m CV^{P_i}$
$C_i$	A Delaunay feasible primitive. (equation 5.2b in subsection 5.2.1.1)	$: (\forall p_{ij} \in \mathbb{P}) \wedge (p_{ij} = p_{ik})$
DT	Delaunay triangulation of feasible primitives (equation 5.3a in subsection 5.2.1.1)	$DT = \bigcup_{i_{df} \geq 1}^{i_{df} < c} C_i$
$\mathcal{B}_\gamma$	Boundary of the constituent of the smeared continuum (equation 1.39 in subsection 1.4.2)	$\int_{\mathcal{B}_\gamma} (\cdot) da = \int_{\Omega_\gamma} div(\cdot) dv$
$\Omega^\Gamma$	Constituent of the reference control mass. (equation 1.1 in section 1.2)	$\Omega = \bigcup_\Gamma \Omega^\Gamma$
$\Omega_*^\gamma$	Constituent of the spatial control mass. (equation 1.2 in section 1.2)	$\Omega_* = \bigcup_\gamma \Omega_*^\gamma$
$att_{i1}$	Attributes for the Delaunay clustering (equation 5.4 in subsection 5.2.1.1)	—
$m, r, s$	Subscripts for material, reference and spatial domains (equation 2.24 in section 2.2.3)	$d\mathbf{X}_m^\#, d\mathbf{X}_r^\#, d\mathbf{x}_s^\#$

---

### Tensors of order Four

---

<u>Symbol</u>	<u>Description</u>	<u>Dimensions</u>
$\mathfrak{C}_e^S$	Elastic tangent moduli of solid constituent both legs in reference coordinates (equation 1.183 in subsection 1.7.3)	$[F/L^2]$
$\mathfrak{C}_p^S$	Pore-pressure tangent moduli of solid constituent both legs in reference coordinates (equation 1.183 in subsection 1.7.3)	$[F/L^2]$

---

### Tensors of order Three

---

<u>Symbol</u>	<u>Description</u>	<u>Dimensions</u>
$G$	Hyper deformation Gradient (equation 2.6 in subsection 2.2.1)	$[L^{-1}]$
$Q$	Hyperstress tensor. (equation 3.2 in section 3.2)	$[FL^{-1}]$
$H$	Hyper inverse deformation Gradient (in equation 2.13 in subsection 2.2.2)	$[L^{-1}]$

---

### Symbols of Matrix Algebra

---

<u>Symbol</u>	<u>Description</u>	<u>Size in 3D or 2D</u>
$[B^{PF}]$	Strain-displacement matrix of 9-node quadrilateral at a location (equation 3.35 in section 3.4.2)	$[4 \times 16]$
$[GB^{PF}]$	Shape function derivative wrt. global coordinates for the determination of nodal strain-gradient displacement matrix (equation 3.40 in section 3.4.2)	$[8 \times 32]$
$[G^{PF}]$	Strain-displacement matrix of 9-node quadrilateral at a location (equation 3.41 in section 3.4.2)	$[8 \times 16]$
$[N_{,\xi}]$	Shape function derivative matrix wrt. local coordinates (equation 3.33 in section 3.4.2)	$[4 \times 16]$
$\mathcal{C} _S$	Voigt-vector of Cauchy-Green strain tensor of solid constituent (equation 1.157 in subsection 1.7.1)	$[6 \times 1]$

$\mathbf{C}^{-1}  _S$	Voigt-vector of Inverse Cauchy-Green strain tensor of solid constituent (equation 1.157 in subsection 1.7.1)	$[6 \times 1]$
$\mathcal{D}_e^S$	Voigt form of the Elastic tangent moduli of solid constituent (equation 1.182 in subsection 1.7.3)	$[6 \times 6]$
$\mathcal{D}_p^S$	Voigt form of the Pore-pressure tangent moduli of solid constituent (equation 1.182 in subsection 1.7.3)	$[6 \times 6]$
$\mathbf{S}  _S$	Voigt-vector of second-Piola Kirchoff Stress tensor of solid constituent (equation 1.157 in subsection 1.7.1)	$[6 \times 1]$
$\Psi^{\overline{\text{NG}}}$	Nodal/Gaussian shape value matrix (equation ( 5.20b in subsection 5.3.1)	$[\#ng \times \#ng]$
$\Psi^{\overline{\text{N}}}$	Nodal shape value matrix (equation ( 5.20a in subsection 5.3.1)	$[\#n \times \#n]$
$\tilde{\mathbf{u}}  _S$	Element-Nodal (or Voronoi-Nodal) displacement vector (equation 1.179 in subsection 1.7.3)	$[\#dof \times 1]$
$\mathbf{K}_{LM}^{M_j \lambda}$	Element (or Voronoi-Nodal) stiffness part of node-coupling of L&M from mass remainder(j) of type pore-pressure dof (equation 1.194 in subsection 1.7.4)	$[4 \times 4]$
$\mathbf{K}_{LM}^{M_j u}$	Element (or Voronoi-Nodal) stiffness part of node-coupling of L&M from mass remainder(j) of type displacement dof (equation 1.194 in subsection 1.7.4)	$[4 \times 4]$
$\mathbf{K}_{LM}^{W \lambda}$	Element (or Voronoi-Nodal) stiffness part of node-coupling of L&M from internal energy of type pore-pressure dof (equation 1.179 in subsection 1.7.3)	$[4 \times 4]$
$\mathbf{K}_{LM}^{W u}$	Element (or Voronoi-Nodal) stiffness part of node-coupling of L&M from internal energy of type displacement dof (equation 1.179 in subsection 1.7.3)	$[4 \times 4]$
$\delta \dot{\mathbf{C}}  _S$	Voigt-vector of variation of rate of Cauchy-Green strain tensor of solid constituent (equation 1.157 in subsection 1.7.1)	$[6 \times 1]$

---

$\delta \mathcal{Q}  _S$	Voigt-vector of half variation of dyadic square of pore-pressure (G)radient of solid constituent (equation 1.159 in subsection 1.7.1)	$[6 \times 1]$
$\delta \tilde{R}^{M_j}  ^{i+1}$	Residuum of mass remainder(j) at iteration (i+1) (equation 1.194 in subsection 1.7.4)	$[1 \times 1]$
$\tilde{R}^W  ^{i+1}$	Residuum of internal energy at iteration (i+1) (equation 1.179 in subsection 1.7.3)	$[1 \times 1]$

---

### Tensors of order One

---

Symbol	Description	Dimensions
$\psi(\mathbf{X}), \psi^{-1}(\mathbf{x})$	r times differentiable forward and backward mappings. (equations 2.1a & 2.1b in section 2.2.1)	$[L]$
$\mathbf{f}_b^\gamma$	body forces acting on control volume (equation 1.34 in subsection 1.4.2)	$[F]$
$\mathbf{f}_t^\gamma$	traction forces acting on control surface (equation 1.34 in subsection 1.4.2)	$[F]$
$\mathbf{n}^{B_\gamma} da$	Infinite surface normal of the smeared continuum belonging to constituent (equation 1.39 in subsection 1.4.2)	$[L^2]$
$\mathbf{q}^\gamma$	Heat flux from the surroundings into a constituent (equation 1.61 in subsection 1.4.3)	$[F(TL)^{-1}]$
$\mathbf{t}^\gamma$	Area specific surface tractions acting on the partial surface of the smeared continuum belonging to constituent (equation 1.39 in subsection 1.4.2)	$[F/L^2]$
$\mathbf{w}^{fs}$	Darcy velocity at the smeared continuum spatial coordinate (equation 1.109 in subsection 1.5.4)	$[L^2/T^2], [L/T]$
$\mathbf{x}  _s, \mathbf{x}  _f$	Current coordinates of the solid and fluid constituents of the biphasic media (equation 1.13 in section 1.3)	$[L]$
$\tilde{\mathbf{f}}_b^\gamma$	Sum of apparent density specific body forces acting on constituent (equation 1.38 in subsection 1.4.2)	$[L/T^2]$
$\mathbf{m}^\sharp, \mathbf{m}^\flat$	The sharp and flat deformed fiber vectors (equation 3.16 in subsection 3.3.1)	$[L]$

---

$\dot{\mathbf{p}}^\gamma  _\gamma$	The rate of change of momentum of a spatial control volume (equation 1.34 in subsection 1.4.2)	[F]
$\hat{\mathbf{p}}^\gamma$	flux of momentum supply (equation 1.34 in subsection 1.4.2)	[F]
$d\mathbf{X}^\sharp, d\mathbf{X}^\flat, d\mathbf{X}^\natural$	sharp, flat and neutral reference directors (in section 2.2.1)	[L]
$d\mathbf{x}^\sharp, d\mathbf{x}^\flat, d\mathbf{x}^\natural$	sharp, flat and neutral current directors (in equation 2.9 in section 2.2.1)	[L]

---

### Tensors of order Two

---

<u>Symbol</u>	<u>Description</u>	<u>Dimensions</u>
$\dot{\mathbf{F}}  _{sS}, \dot{\mathbf{F}}  _{fF}$	rates of deformation gradients for chemically identical components of the mixture (equation 1.19 in section 1.3)	[T <sup>-1</sup> ]
$\boldsymbol{\sigma}^\gamma$	Cauchy Stress tensor of the constituent (equation 1.39 in subsection 1.4.2)	[F/L <sup>2</sup> ]
$\mathbf{D}, \mathbf{W}$	Symmetric and Skew Symmetric parts of the spatial velocity gradients (equations 1.56 & 1.57 in subsection 1.4.3)	[T <sup>-1</sup> ]
$\mathbf{F}  _F, \mathbf{F}  _S$	Deformation gradient of the smeared current coordinates wrt. the fluid & solid reference coordinates (equations 1.14 & 1.15 in section 1.3)	[–]
$\mathbf{F}  _{SF}$	Imaginary tangent mapping of reference fluid coordinates into reference solid coordinates (equation 1.143 in subsection 1.6.1)	[–]
$\mathbf{F}^{-1}  _F, \mathbf{F}^{-1}  _S$	Spatial deformation gradients of the reverse fluid&solid motions (equations 1.16 & 1.17 in section 1.3)	[–]
$\mathbf{L}  _f, \mathbf{L}  _s$	spatial velocity gradients of fluid and solid components (equations 1.21 & 1.20 in section 1.3)	[T <sup>-1</sup> ]
$\lambda \mathbf{I}$	Tensor of Pore pressure (equation 1.125 in subsection 1.5)	[F/L <sup>2</sup> ]

---

**Tensors of order Zero**


---

<b>Symbol</b>	<b>Description</b>	<b>Dimensions</b>
$\alpha^{\sharp}, \alpha^{\flat}$	Sharp and Flat axis angle changes with respect to the neutral direction (equation 3.13 in subsection 3.3.1)	$[-]$
$\check{s}^{\gamma}, \dot{\check{s}}^{\gamma}  _{\gamma}$	Apparent density specific entropy flux and the rate of it- for a constituent (equation 1.80 in subsection 1.4.4)	$[L^2/K/T^2][L^2/K/T^3]$
$\check{\Psi}^{\gamma}, \dot{\check{\Psi}}^{\gamma}  _{\gamma}$	Strain energy density of a constituent and rate of it (equations 1.84a & 1.84b in subsection 1.4.4)	$[L^2/T^2], [L^2/T^3]$
$\delta\Pi_{int}^{PF}$	Variation of internal energy depending on first order kinematics only. (equation 3.2 in section 3.2)	$[FL]$
$\delta\Pi_{int}^{QG}$	Variation of internal energy depending on second order kinematics only. (equation 3.2 in section 3.2)	$[FL]$
$\Delta S_{rev}, dS_{rev}$	Entropy Change and differential of a reversible process (equation 1.64 in subsection 1.4.4)	$[FL/K]$
$\Delta U, dU$	Change and differential of internal energy in time intervals of $\Delta t, dt$ respectively (equations 1.41 & 1.42 in subsection 1.4.3)	$[FL]$
$\dot{n}^f  _s, \dot{n}^f  _f$	Rates of fluid volume fractions (equation 1.112 in subsection 1.5.4)	$[T^{-1}]$
$\dot{n}^s  _s, \dot{n}^s  _f$	Rates of solid volume fractions (equation 1.112 in subsection 1.5.4)	$[T^{-1}]$
$\dot{\varrho}^{\gamma R}$	The rate of change of the current real density of the constituent (equation 1.33 in subsection 1.4.1)	$[FT/L^4]$
$\hat{\varrho}^{\gamma}, \dot{\varrho}^{\gamma}  _{\gamma}$	Current rate of apparent density supply and current rate of apparent density change of the constituents respectively (equations 1.24 & 1.25 in subsection 1.4.1)	$[FT/L^4]$
$\hat{m}^{\gamma}, \dot{m}^{\gamma}  _{\gamma}$	Current rate of mass supply and current rate of mass change of the constituents respectively (equations 1.24 & 1.25 in subsection 1.4.1)	$[FT/L]$

$\psi^\kappa$	Strain energy density function (per length) of EB curved anisotropy (equation 3.21 in subsection 3.3.2)	[ $F$ ]
$\rho^\Gamma, \varrho^\gamma$	The partial (apparent) densities in reference and spatial configurations (equation 1.10 in section 1.2)	[ $FT^2/L^4$ ]
$\rho^{\Gamma R}, \varrho^{\gamma R}$	The realistic (true) densities in reference and spatial configurations (equation 1.10 in section 1.2)	[ $FT^2/L^4$ ]
$A, dA$	Helmholtz free energy (Arbeit) and the differential of it (equations 1.75 & 1.76 in subsection 1.4.4)	[ $FL$ ]
$c$	The Euler-Bernoulli definition of the curvature (equation 3.14 in subsection 3.3.1)	[ $L^{-1}$ ]
$m, m_*$	Total mass of the mixture in reference and in-conjugated spatial domains (equation 1.11 in section 1.2)	[ $FT^2/L^4$ ]
$n^\Gamma, n^\gamma$	Volume fraction in reference and spatial coordinates (equation 1.5 in section 1.2)	[ $-$ ]
$Q, \delta Q$	Heat supplied and the variation of this supply by the surroundings in time intervals of $\Delta t, dt$ respectively (equations 1.41 & 1.42 in subsection 1.4.3)	[ $FL$ ]
$r$	Apparent density specific thermal source (equation 1.61 in subsection 1.4.3)	[ $L^2T^{-3}$ ]
$T$	Operation temperature of the smeared continuum (equation 1.73 in subsection 1.4.4)	[ $K$ ]
$U^\gamma, \check{U}^\gamma$	Internal energy and apparent density specific internal energy of the constituent (equation 1.41 in subsection 1.4.3)	[ $FL$ ], [ $L^2/T^2$ ]
$V^\Gamma$	Volume constituent of the reference control volume. (equation 1.3 in section 1.2)	[ $L^3$ ]
$v_*^\gamma$	Volume constituent of the spatial control volume. (equation 1.4 in section 1.2)	[ $L^3$ ]
$W, \delta W$	Mechanical work done onto the system and the variation of it in time intervals of $\Delta t, dt$ respectively (equations 1.41 & 1.42 in subsection 1.4.3)	[ $FL$ ]



$K^\gamma, \dot{K}^\gamma  _\gamma$	Current kinetic energy and rate of kinetic energy of the constituent (equation 1.51 in subsection 1.4.3)	$[FL], [FL/T]$
$S^\gamma, \dot{S}^\gamma  _\gamma$	Entropy and rate of change of entropy of the constituent (equation 1.80 in subsection 1.4.4)	$[FL/K], [FL(KT)^{-1}]$

# List of Figures

1.1	The shell script used for compiling and linking the external libraries using Intel <sup>®</sup> compiler	47
1.2	The shell script used for compiling and linking the external libraries using Abaqus <sup>®</sup> compiler	47
1.3	Schematic Drawing of various types of uterine fibroids and initial fibroid geometry . . . .	49
1.4	The development of the pore pressure distribution on the xy plane; time steps 1-20 . . . .	50
1.5	The development of the pore pressure distribution on the xz plane; time steps 1-20 . . . .	50
1.6	The development of the pore pressure distribution on the yz plane; time steps 1-20 . . . .	50
1.7	The development of the fluid fraction distribution in layered structure; time steps 12-15 . .	51
1.8	The development of the fluid fraction distribution in layered structure; time steps 15-19 . .	51
1.9	Steady state streamlines, color plot of fluid fraction, diameter scale of fluid velocity . . .	52
1.10	Model for the scenario of growth of secondary tissue on the primary one . . . . .	53
1.11	Fiber lay-up layers 1-4 . . . . .	54
1.12	Fiber lay-up layers 5-8 . . . . .	54
1.13	Fiber lay-up layers 9-12 . . . . .	54
1.14	The steady state streamlines on 4 layers of 12 . . . . .	55
1.15	The development of the fluid fraction distribution in layered structure time steps 1-7 . . .	56
1.16	The development of the fluid fraction distribution in layered structure time steps 9-19 . . .	56
1.17	Pore pressure distribution with deformation, states 1, 6, and 20 . . . . .	57
1.18	The development of the deformation of articular cartilage in between time steps 1-5 . . . .	58
1.19	The development of the deformation of articular cartilage in between time steps 6-10 . . . .	58
1.20	The development of the fluid fraction of a layer of articular cartilage; time steps 1-5 . . . .	59
1.21	The development of the fluid fraction of a layer of articular cartilage; time steps 6-10 . . . .	59
1.22	The development of the pore pressure of a layer of articular cartilage; time steps 1-5 . . . .	60
1.23	The development of the pore pressure of a layer of articular cartilage; time steps 6-10 . . . .	60
2.1	Material size subjectivity illustrated on real Human biological specimen (SEM Image taken from Ref.[ <a href="#">J.M.Clark 1991</a> ]). The original image does not contain the blue triangle. Bar=1mm)	62
2.2	Hypermatrix-matrix-vector form of mapping of the sharp spatial tangent with the neutral reference tangent and its metric. . . . .	66
2.3	Kinematics of reference tangents to spatial tangents . . . . .	67
2.4	Kinematics of spatial tangents to reference tangents . . . . .	69
2.5	Kinematics of material tangents to current tangents . . . . .	71
2.6	From straight reference to the curved spiral beam. $\alpha = \pi/6, n = 2$ . . . . .	73
2.7	From straight reference to the curved spiral beam. $\alpha = \pi/2, n = 5$ . . . . .	73
2.8	From straight reference to the curved spiral beam. $\alpha = 3\pi/2, n = 15$ . . . . .	73
2.9	From curved spiral beam reference to the straight rod. $\alpha = \pi/6, n = 2$ . . . . .	74
2.10	From curved spiral beam reference to the straight rod . $\alpha = \pi/2, n = 10$ . . . . .	74
2.11	From curved spiral beam reference to the straight rod. $\alpha = 3\pi/2, n = 20$ . . . . .	74
2.12	An example of Cauchy Tetrahedron, which demonstrates the difference in between first and second order kinematics . . . . .	75

3.1	Left: An abstract profile with fractional characteristics; Right(Ref.[ <sup>OpenStax 2016</sup> ]) :Illustration of the reality of partially fractional Muscle-Hierarchy . . . . .	78
3.2	Left: An abstract fractional profile chain with depth of 5 . . . . .	79
3.3	Development of the effective Area and Second Moment of Area values with respect to the selection of hierarchy levels of <i>Figure 3.2</i> . . . . .	80
3.4	Integration domains on which first and second order effects are acting . . . . .	83
3.5	Integration domains on which first and second order effects are acting . . . . .	83
3.6	Kinematics of a single fiber with convecting and moving coordinates at the flat, natural and sharp sections . . . . .	85
3.7	The deformation and the evolute of the spiral beam, $\alpha = 3\pi/2, n = 60$ . . . . .	87
3.8	Left: The exponential material formation in 10 time steps; Right: The normalized curvature and normalized EB bending energy of the exponential mapping . . . . .	88
3.9	Left: First Piola Kirchoff Stress tensor traction on the reference X plane and current x direction. Right: First Piola Kirchoff Stress tensor traction on the reference X plane and current y direction . . . . .	90
3.10	Left: First Piola Kirchoff Hypertress tensor traction on the reference X plane and xX First Piola Stress-Space. Right: First Piola Kirchoff Hypertress tensor traction on the reference X plane and xY First Piola Stress-Space . . . . .	90
3.11	Extending the sinusoidal spiral, undeformed Grey, deformed color plot, Legend: Deformation magnitude . . . . .	93
3.12	Extending the sinusoidal spiral, Left: PF formulation, Right:SE formulation . . . . .	93
3.13	Case1; Bending a simple beam, undeformed Grey, deformed color plot, Legend:Deformation Magnitude . . . . .	96
3.14	Deformation plots of beam bending, Left: Case2; Isotropic strain energy density function and Stretch energy density function, Right: Case3; Istropic strain energy density, Stretch energy density and Bending energy density functions . . . . .	96
3.15	Energy distribution plots of beam bending, Left: Stretch energy distribution, Right: Case3; Bending energy distribution . . . . .	97
4.1	Nonlinear deformation map with convective coordinates . . . . .	101
4.2	undeformed and deformed coordinates of the unit cell . . . . .	104
4.3	Form and the formula of the stretch on 8-chain model . . . . .	110
4.4	Second Piola Kirchoff Stress tensor components . . . . .	111
4.5	Comparison of second Piola Kirchoff and Cauchy stress component in stretch direction . . . . .	111
4.6	Form and the formula of the shear on 8-chain model . . . . .	112
4.7	Second Piola Kirchoff Stress tensor components . . . . .	112
4.8	Comparison of second Piola Kirchoff and Cauchy stress component in stretch direction . . . . .	113
4.9	Kinematics of updating the reference configuration with rotation tensor . . . . .	114
4.10	The definition of the evolution as an optimization set problem . . . . .	114
4.11	Numerical verification of maximizing the stretch in one step . . . . .	115
4.12	Numerical verification of maximizing the stretch stepwise . . . . .	115
4.13	Comparison of stretch maximizing and coaxiality optimization manifolds . . . . .	116
4.14	Pressing the Cartilage-alike profile with uniform force . . . . .	117
4.15	The coaxiality requirement . . . . .	117

4.16	Maximizing of equation (4.29) under the action of hypergradient of equation (4.36). The maximum location is found correctly and marked with a line. . . . .	119
4.17	Arbitrary surfaces of $(\hat{M}^{\natural \otimes 2} : \mathbb{K} : \hat{M}^{\natural \otimes 2})$ and the location of reorientation target. The maximum overlaps with scattered-gathered eigenvector result. . . . .	120
4.18	Maximizing of equation (4.37) under the action of hypergradient of equation (4.38). The maximum location is found correctly and marked with a line. . . . .	121
5.1	An example where 'DT' condition set does not represent challenging geometries . . . . .	126
5.2	Plausible cases of erroneous CDT . . . . .	128
5.3	3-means clustering of an object . . . . .	129
5.4	Clustering of complicated Skull geometry - Node Set is taken from AIM Shape-Visonair Ref.[P.Alliez 2006] . . . . .	130
5.5	Unconstrained Voronoi Tesselations . . . . .	131
5.6	Bulk, Surface, Edge and Corner detection . . . . .	132
5.7	Sharp Featuring of the Skull geometry - Node Set is taken from AIM Shape-Visonair Ref.[P.Alliez 2006] . . . . .	133
5.8	Constrained Voronoi Tesselations . . . . .	134
5.9	Non-sibsonian interpolation around a point. The right-most node is not included in the integration but the uppermost is. . . . .	136
5.10	Primary and secondary Voronoi tessellation for the sequential integration of the differentials	137
5.11	<i>Left:</i> Nodal Delaunay-Voronoi dual including only nodes. <i>Right:</i> Nodal/Gaussian Voronoi tessellation. Nodes in red, integrators (gauss points) in blue. . . . .	138
5.12	Location of gauss points (in blue) and nodal points (in orange) interpolated with two different linear mappings . . . . .	145
5.13	Support sizes of a surface node of a plate model . . . . .	145
5.14	A piece from an infinitely large imaginary volume with a heat source located at the origin of the elliptical split pathway . . . . .	147
5.15	Two solutions of linear momentum equation for large deformations, considering geometrical nonlinear effects only . . . . .	147
5.16	Bending directions as curvature vortexes of a beam. . . . .	148
5.17	Constrained 3d Voronoi diagramm of the described cartilage-like geometry . . . . .	148
5.18	Top: Displacement result of plate cartilage contact. Bottom: Distribution of Isotropic strain gradient energy $\mathbf{G} : \mathbf{G}$ . . . . .	149
5.19	Development of $\mathbf{G} : \hat{\mathbf{E}}_1^{\otimes 2}$ from the beginning, intermediate to the final stage of the imposed boundary condition. . . . .	149
5.20	Comparisons of different reorientation manifests . . . . .	152
C.1	Kinematics of a single fiber with convecting and moving coordinates at the flat, natural and sharp sections, Change the omega into small one . . . . .	174
C.2	From left to right, undeformed straight Cauchy tetrahedron, traction forces on deformed body hypertraction forces on deformed body. . . . .	178
C.3	Left, traction and hypertraction force factors depending on the deformation factors. Right The logarithmic ratio of traction to hypertraction forces. . . . .	179



# Soft Tissue as Biphasic Mixture

---

## Contents

---

<b>1.1</b>	<b>Introduction</b> . . . . .	<b>2</b>
<b>1.2</b>	<b>Partial and Total Properties of the Mixture</b> . . . . .	<b>3</b>
<b>1.3</b>	<b>Kinematics of the Mixture</b> . . . . .	<b>5</b>
<b>1.4</b>	<b>Governing Relations</b> . . . . .	<b>7</b>
1.4.1	Conservation of Mass . . . . .	7
1.4.2	Conservation of Translational Momentum . . . . .	9
1.4.3	Conservation of Internal and Kinetic energy: An extended first law of Thermodynamics . . . . .	11
1.4.4	The Entropy Inequality-Dissipation of Mixed Field . . . . .	15
<b>1.5</b>	<b>Assumptions, Narrowed Relations and Constitutive Restrictions</b>	<b>20</b>
1.5.1	Assumptions . . . . .	20
1.5.2	Narrowed Governing Relations . . . . .	21
1.5.3	Constitutive Restrictions . . . . .	22
1.5.4	Darcy Velocity, Saturation Rate and Pore Pressure . . . . .	23
<b>1.6</b>	<b>Weak Forms</b> . . . . .	<b>27</b>
1.6.1	Weak Form of Balance of Translational Momentum in Solid Material Coordinates . . . . .	27
1.6.2	Weak Form of Conservation of Mass . . . . .	30
<b>1.7</b>	<b>Discretized balance equations</b> . . . . .	<b>31</b>
1.7.1	Matrix-Vector Form on Total Lagrangian Configuration . . . . .	31
1.7.2	Newmark-Method-Consistent Material Time Derivatives . . . . .	33
1.7.3	Discrete Form of the Translational Momentum Part . . . . .	34
1.7.4	Discrete Form of the Conservation of Mass . . . . .	39
<b>1.8</b>	<b>Numerical Examples</b> . . . . .	<b>46</b>
1.8.1	Finite Element Implementation: Software Specifications . . . . .	46
1.8.2	A Numerical Scenario: Growth of Uterine Fibroids . . . . .	48
1.8.3	A Numerical Scenario: Impact on the Surrounding Tissue . . . . .	52
1.8.4	A Numerical Scenario: Cartilage under Compression . . . . .	57

---

## 1.1 Introduction

This chapter of the thesis is dedicated to introduce the first order kinematics and thermodynamics of biphase media using *theory of mixtures* as a floor requirement for investigating the soft biological tissue. This base requirement is either directly stated, or is imposed by the pioneers of the continuum Biomechanics.

Several elements of this general statement requires clarification. The initial one is the so called "*First order Kinematics*". The keyword brings out the possibility of postulations of higher order kinematics. This specification excludes the so called *strain gradient effects*, which is visited in the remaining chapters of the thesis. Additionally, it should be emphasized that the difference of *first order* and *higher order* kinematics are not analogous definitions of German study concepts of *Theorie Erster und Zweiter Ordnung* clarified in Ref.[[Bletzinger 2009](#)] clearly. The latter one deals with the statics and dynamics of structures with and without of the effects of geometrical, loading and material types of nonlinearities. The prior one, which is the subject of this thesis, imposes the nonlinear kinematics, in another novel way. Keeping this in mind, the first order and the second order Kinematics used in this work, both consider nonlinear geometrical effects, and thus applicable for large deformational studies.

The second keyword of the statement is the fundamental necessity of consideration of multiphase nature of the soft tissue. As stated above, the base requirement is imposed by the pioneers of the continuum Biomechanics. For instance, Fung in Ref.[[Fung 1993](#)] calls the soft tissue (irrespective of the type of the tissue) as being *pseudoelastic*, by pointing out the phenomenological cause of viscoelasticity. As can be seen by this chapter, the sources of the hysteresis, which is consistently the main difference in between the assumption of *pseudoelasticity* and true elasticity (which is in fact the true idealization, and does probably not exist at all), can be well linked to the second law of thermodynamics, in terms of the micromechanical interaction of different phases of the tissue. At this stage it would be appropriate to mention that the comprehensive mechanics of the causality of hysteresis is not an trivial task to determine. Implicitly, the reformulation of the phenomenon with the definition of *viscoelasticity* points out that the viscous effects are responsible for the pseudo-characteristics of the solid.

According to the writer of this chapter, to link the phenomenon and causality in terms of physical quantities, is still a more comprehensible approach than estimating coefficients for the rheological material models. No doubt that the latter has certainly some practical engineering advantages. However, in short, the writer had chosen the way of researcher, not the way of engineer.

The chapter is divided into seven sections. In the beginning, the properties of the biphase mixture is summarized. In the follower sections, the kinematics, the assumptions under consideration of soft-tissue in focus is presented. The weak form, and discretized equations is visited in the remaining sections. Accordingly, several different numerical examples is shown to prove applicability and completeness of the approach. The pioneering formulations can be found under the study of the theory of the mixtures by Truesdell and Toupin in Ref.[[C.Truesdell 1960](#)], and by Atkin and Craine in Ref.[[R.J.Atkin 1976](#)]. Following this

initial works, one of the first applications of the study can be found in Mow et al. in Ref.[[V.C.Mow 1980](#)]. The historical development and basics of the *theory of porous media* can be found in the notes of de Boer in Ref.[[de Boer 1996](#)], who is another founder of the macroscopic theories of the multiphase mixtures. The state of the art of the *Theory of porous media* and various numerical and experimental applications can be found in the recent editorial publication of Ehlers and Bluhm in Ref.[[W.Ehlers 2002](#)].

The writer of the thesis had used many of these works and it is stated specifically if a novel self-contribution is present or another reference is used for the source of information. Otherwise, this introductory chapter is a short and piecewise summary of the fundamental scientific works in the aforementioned references above.

## 1.2 Partial and Total Properties of the Mixture

The main aim of this section is to provide fundamental definitions. The kinematics of the mixture is developed according to these basic definitions in hand. Accordingly, the governing equations are formulated on the basis of theory of mixture, namely a thermodynamic balance and unbalance governing equations, as well as inequalities are presented.

The total material domain of the problem is a composition of a binary mixture.

$$\Omega = \bigcup_{\Gamma} \Omega^{\Gamma} = \Omega^S \cup \Omega^F \quad (1.1)$$

Another spatial domain, which is not (necessarily) kinematically conjugated with the material domain defined above, is also a composition. The principle of kinematical inconjugation of the theory presented here is abbreviated with the subscript '\*' beneath.

$$\Omega_* = \bigcup_{\gamma} \Omega_*^{\gamma} = \Omega_*^s \cup \Omega_*^f \quad (1.2)$$

The theory of porous media assumes that the total infinite and finite volumes in the material as well as in the spatial configurations do obey the principle of additive split. In this case, as indicated previously in section Ch.[1.1], a two-phase material is under consideration.

$$V = \sum_{\Gamma} V^{\Gamma} = \sum_{\Gamma} \int_{\Omega^{\Gamma}} dV^{\Gamma} = \int_{\Omega} \sum_{\Gamma} dV^{\Gamma} = \int_{\Omega} dV \quad (1.3)$$

The same series of fundamental definitions can be also made for the spatial infinite and finite volumes.

$$v_* = \sum_{\gamma} v_*^{\gamma} = \sum_{\gamma} \int_{\Omega_*^{\gamma}} dv_*^{\gamma} = \int_{\Omega_*} \sum_{\gamma} dv_*^{\gamma} = \int_{\Omega_*} dv_* \quad (1.4)$$

The volume fraction of a material constituent  $\Gamma$  in the material coordinates is depending on the material location of that constituent.

$$n^{\Gamma} = n^{\Gamma}(\mathbf{X}^{\Gamma}) \quad (1.5)$$



As well, the volume fraction in the spatial coordinates depending on the the spatial coordinates of that constituent.

$$n^\gamma = n^\gamma(\mathbf{X}^\Gamma, t) = n^\gamma(\mathbf{x}^\gamma) \quad (1.6)$$

The volume fraction determines the partial volume of that constituent in the saturated mixture.

$$\begin{aligned} V &= \sum_{\Gamma} V^\Gamma = \sum_{\Gamma} n^\Gamma V = \int_{\Omega} \sum_{\Gamma} dV^\Gamma = \int_{\Omega} \sum_{\Gamma} n^\Gamma dV = \int_{\Omega} dV \\ v_* &= \sum_{\gamma} v_*^\gamma = \sum_{\gamma} n_*^\gamma v_* = \int_{\Omega_*} \sum_{\gamma} dv_*^\gamma = \int_{\Omega_*} \sum_{\gamma} n_*^\gamma dv_* = \int_{\Omega_*} dv_* \end{aligned} \quad (1.7)$$

The in-conjugated quantities referred here again with an asterisk. To make it clear, considering the volume fractions are not necessarily equal,

$$n^\gamma(\mathbf{X}, t) \neq n_*^\gamma(\mathbf{X}_*, t) \quad (1.8)$$

To repeat it again, in general, the material domain  $\Omega$  is not the kinematic origin of the spatial domain  $\Omega_*$ . Besides, the last two equation set of equation (1.7), comprises the saturation condition.

$$\int_{\Omega} \sum_{\Gamma} n^\Gamma dV = \int_{\Omega} dV \quad \int_{\Omega_*} \sum_{\gamma} n^\gamma dv = \int_{\Omega_*} dv \quad (1.9a)$$

$$\sum_{\Gamma} n^\Gamma = n^S + n^F = 1 \quad \sum_{\gamma} n^\gamma = n^s + n^f = 1 \quad (1.9b)$$

The partial and realistic true densities are defined as,

$$\begin{aligned} \rho^{\Gamma R} &= \frac{dm^\Gamma}{dV} & \rho^\Gamma &= \frac{dm^\Gamma}{dV^\Gamma} \\ \varrho^{\gamma R} &= \frac{dm^\gamma}{dv} & \varrho^\gamma &= \frac{dm^\gamma}{dv^\gamma} \end{aligned} \quad (1.10)$$

The total mass in reference and current configurations are,

$$\begin{aligned} m &= \int_{\Omega} \sum_{\Gamma} dm^\Gamma = \int_{\Omega} \sum_{\Gamma} \rho^\Gamma dV^\Gamma = \int_{\Omega} \sum_{\Gamma} \rho^{\Gamma R} dV = \int_{\Omega} \sum_{\Gamma} n^\Gamma \rho^{\Gamma R} dV^\Gamma \\ m_* &= \int_{\Omega_*} \sum_{\gamma} dm_*^\gamma = \int_{\Omega_*} \sum_{\gamma} \varrho_*^\gamma dV_*^\gamma = \int_{\Omega_*} \sum_{\gamma} \varrho_*^{\gamma R} dV_* = \int_{\Omega_*} \sum_{\gamma} n_*^\gamma \varrho_*^{\gamma R} dV_*^\gamma \end{aligned} \quad (1.11)$$

This concludes the relationship between the partial and true densities in material and another kinematically in-conjugated spatial coordinates,

$$\rho^\Gamma = n^\Gamma \rho^{\Gamma R} \quad \varrho_*^\gamma = n_*^\gamma \varrho_*^{\gamma R} \quad (1.12)$$

This basic definitions can be found in any state of the art texts, such as Ateshian Ref.[G.A.Ateshian 2008] makes a very brief definition of these backbone identities of mixture continuum.

### 1.3 Kinematics of the Mixture

In the theory of mixtures, it is assumed that each individual constituent has its own Lagrangian mapping. Alternatively, the way of expression of motion is that, each individual component of the mixture originates from different reference coordinates, but ends and thus composes the final unique spatial current state of mixture. Specifically, the current coordinate is a result of a two-to-one mapping. For the case of solid and fluid (fiber and surrounding fluid) mixture,

$$\mathbf{x} = \mathbf{x}|_s = \mathbf{x}|_f = \mathbf{x}(\mathbf{X}|_S, t) = \mathbf{x}(\mathbf{X}|_F, t) \quad (1.13)$$

Since the coordinates are neither a state nor a process variable, the appropriate mathematical notation of *such that*:(|) is used instead of super or subscript. Since the evaluation of the current coordinates are apriorily are known (defined) to be the same<sup>1</sup>, one single current coordinate is used next, instead of two separate. However, the "matter" of the coordinate is indicated. Being considered as an gradient operator only (independent of any violation indications of material penetration), the same notation of *evaluated at* (such that) can be applied for the deformation gradient too.

$$\mathbf{F}|_F = \frac{\partial \mathbf{x}}{\partial \mathbf{X}}|_F = \mathbf{F}|_{sF} = \frac{\partial \mathbf{x}|_s}{\partial \mathbf{X}}|_F = \mathbf{F}|_{fF} = \frac{\partial \mathbf{x}|_f}{\partial \mathbf{X}}|_F \quad (1.14)$$

The deformation gradient of the solid constituent (the gradient of the current mixture evaluated at the solid reference coordinates) is similarly,

$$\mathbf{F}|_S = \frac{\partial \mathbf{x}}{\partial \mathbf{X}}|_S = \mathbf{F}|_{sS} = \frac{\partial \mathbf{x}|_s}{\partial \mathbf{X}}|_S = \mathbf{F}|_{fS} = \frac{\partial \mathbf{x}|_f}{\partial \mathbf{X}}|_S \quad (1.15)$$

Since there are two mappings and two deformation gradients, there will be necessarily another two spatial gradients of the reverse motions. The spatial gradients are -as tensor operators- inverse of the forward material gradients. The spatial gradients for the reverse fluid motion reads,

$$\mathbf{F}^{-1}|_F = \frac{\partial \mathbf{X}}{\partial \mathbf{x}}|_F = \mathbf{F}^{-1}|_{Fs} = \frac{\partial \mathbf{X}}{\partial \mathbf{x}}|_F = \mathbf{F}^{-1}|_{Ff} = \frac{\partial \mathbf{X}}{\partial \mathbf{x}}|_F \quad (1.16)$$

The spatial gradients for the reverse solid motion are,

$$\mathbf{F}^{-1}|_S = \frac{\partial \mathbf{X}}{\partial \mathbf{x}}|_S = \mathbf{F}^{-1}|_{Ss} = \frac{\partial \mathbf{X}}{\partial \mathbf{x}}|_S = \mathbf{F}^{-1}|_{Sf} = \frac{\partial \mathbf{X}}{\partial \mathbf{x}}|_S \quad (1.17)$$

In short notation, the material and the spatial (G)gradients of each constituent are,

$$\mathbf{F}|_\Gamma = \mathbf{F}|_{\gamma\Gamma} = \text{Grad}|_\Gamma \mathbf{x}|_\gamma = \text{Grad}|_\Gamma \mathbf{x} \quad (1.18a)$$

$$\mathbf{F}^{-1}|_\Gamma = \mathbf{F}^{-1}|_{\Gamma\gamma} = \text{grad}|_\gamma \mathbf{X}|_\Gamma = \text{grad}\mathbf{X}|_\Gamma \quad (1.18b)$$

<sup>1</sup>The "coordinates" are quantitatively the same, yet the "matter" as quality of course are not the same. This implies the well known "smeared" model postulated by many writers, see Ehlers Ref.[[W.Ehlers 2002](#)] for instance.

As the current mixture components originates from different reference locations, the statement of constituents do keep the same smeared configurations in another state, is still arbitrary. By specifying this another state as the state of *infinite next*<sup>2</sup>, one can state that the velocity vectors of the current components are arbitrary and thus different, even though the time derivative is evaluated at the common current coordinates. This indicates that even though there are two deformation gradients, there are in total four rates of deformation gradients. Next, only the rates which are *relevant for the formulation* are presented in this content. This *relevancy* is determined by the chemical composition. The rates of deformation gradients for chemically identical components of the mixture are,

$$\dot{\mathbf{F}}|_{sS} = \frac{\partial \dot{\mathbf{x}}|_s}{\partial \mathbf{X}|_S} = \text{Grad}|_S \dot{\mathbf{x}}|_s \quad (1.19a)$$

$$\dot{\mathbf{F}}|_{fF} = \frac{\partial \dot{\mathbf{x}}|_f}{\partial \mathbf{X}|_F} = \text{Grad}|_F \dot{\mathbf{x}}|_f \quad (1.19b)$$

The spatial velocity gradient of the solid component can be deduced from the previous equations as follows,

$$\mathbf{L}|_s = \mathbf{L}|_{ss} = \mathbf{L}|_{sf} = \frac{\partial \dot{\mathbf{x}}|_s}{\partial \mathbf{x}} = \frac{\partial \dot{\mathbf{x}}|_s}{\partial \mathbf{X}|_S} \cdot \frac{\partial \mathbf{X}|_S}{\partial \mathbf{x}} = \dot{\mathbf{F}}|_{sS} \cdot \mathbf{F}^{-1}|_S \quad (1.20)$$

$$\mathbf{L}|_s = \text{grad} \dot{\mathbf{x}}|_s = (\text{Grad}|_S \dot{\mathbf{x}}|_s \cdot) (\text{grad} \mathbf{X}|_S)$$

The spatial velocity gradient of the fluid component is kinematically identical,

$$\mathbf{L}|_f = \mathbf{L}|_{fs} = \mathbf{L}|_{ff} = \frac{\partial \dot{\mathbf{x}}|_f}{\partial \mathbf{x}} = \frac{\partial \dot{\mathbf{x}}|_f}{\partial \mathbf{X}|_F} \cdot \frac{\partial \mathbf{X}|_F}{\partial \mathbf{x}} = \dot{\mathbf{F}}|_{fF} \cdot \mathbf{F}^{-1}|_F \quad (1.21)$$

$$\mathbf{L}|_f = \text{grad} \dot{\mathbf{x}}|_f = (\text{Grad}|_F \dot{\mathbf{x}}|_f \cdot) (\text{grad} \mathbf{X}|_F)$$

Lastly, for the kinematics of the mixture, the spatial velocity gradients can be further additively splitted into symmetric and skew symmetric tensors.

$$\mathbf{L}|_\gamma = \mathbf{D}|_\gamma + \mathbf{W}|_\gamma$$

$$\mathbf{D}|_\gamma = \frac{1}{2} (\mathbf{L}|_\gamma + \mathbf{L}^T|_\gamma) \quad (1.22)$$

$$\mathbf{W}|_\gamma = \frac{1}{2} (\mathbf{L}|_\gamma - \mathbf{L}^T|_\gamma)$$

This split is for the balance equations absolutely necessary, since the true stress tensor is symmetric (for the sake of balance of angular momentum), and thus energetically orthogonal to the skew symmetric part of the spatial velocity gradient. In general, for the components

---

<sup>2</sup>continuum neighborhood of the smeared configuration

which are chemically identical, the following correlation can be written;

$$\begin{aligned} \text{chemically identical : } & \begin{cases} \gamma = s, & | \Gamma = S \\ \gamma = f, & | \Gamma = F \end{cases} \iff \\ \iff & \mathbf{L} |_{\gamma} = \dot{\mathbf{F}} |_{\gamma\Gamma} \cdot \mathbf{F}^{-1} |_{\Gamma} \\ & \mathbf{L} |_{\gamma} = \text{grad} \dot{\mathbf{x}} |_{\gamma} = (\text{Grad} |_{\Gamma} \dot{\mathbf{x}} |_{\gamma} \cdot) (\text{grad} \mathbf{X} |_{\Gamma}) \end{aligned} \quad (1.23)$$

The writer of the treatise, strongly suggests to follow the identities and correlations introduced in the section of *Kinematics of the Mixture* Ch.[1.3], in the very well written textbooks of Holzapfel Ref.[Holzapfel 2006], and Bonet&Wood Ref.[J.Bonet 2008]. Even though these books do not mention about the nature of biomaterials composed of multiple physical phases explicitly, they are still the best among many others to verify the validity of the proposed first order kinematics.

## 1.4 Governing Relations

In this section *the balance equalities* of the conservation of mass, the conservation of linear momentum, the conservation of internal and kinetic energy are introduced initially. After that, the introduction of the *inequality* of entropy for the biphasic material can be found.

### 1.4.1 Conservation of Mass

In this section, the conservation of mass for a control volume is introduced briefly. The control volume is taken as the current volume occupied by the current mixture components, and thus defines a thermodynamically open system. This indicates, that there might be a mass input into the system. At this stage of formulation, the system can be further assumed to be isolated, and accordingly the mass supply term can be neglected for the time being.

To start with, the current mass and the current rate of mass supply in terms of the current apparent (partial) density and current rate of apparent (partial) density supply can be written as,

$$m^{\gamma} = \int_{\Omega_{\gamma}} dm^{\gamma} = \int_{\Omega_{\gamma}} \varrho^{\gamma} dv \quad \hat{m}^{\gamma} = \int_{\Omega_{\gamma}} d\hat{m}^{\gamma} = \int_{\Omega_{\gamma}} \hat{\varrho}^{\gamma} dv \quad (1.24)$$

Obviously, the statement of conservation of mass requires the equality of rate of change of mass to the rate of mass supply into the volume.

$$\dot{m}^{\gamma} |_{\gamma} = \hat{m}^{\gamma} \quad (1.25)$$

Recalling the equations of rates of deformation gradients (1.19) makes it clear, why the evaluation location of the rate of current mass should be considered.

$$\dot{m}^{\gamma} |_{\gamma} = \left. \overline{\left( \int_{\Omega_{\gamma}} \varrho^{\gamma} dv \right)} \right|_{\gamma} \quad (1.26)$$

The local form of this equation can be obtained stepwise. Firstly, by pulling back the spatial total volume to the material partial volume with the determinant of the corresponding deformation gradient, one gets,

$$\dot{m}^\gamma|_\gamma = \left( \overline{\int_{\Omega_\gamma} \varrho^\gamma dv} \right) \Big|_\gamma = \left( \overline{\int_{\Omega_\gamma} \varrho^\gamma \det(\mathbf{F}|_\Gamma) dV^\Gamma} \right) \Big|_\gamma = \int_{\Omega_\gamma} \overline{\varrho^\gamma \dot{\det}(\mathbf{F}|_\Gamma)} \Big|_\gamma dV^\Gamma \quad (1.27)$$

This rate derivative<sup>3</sup> can be further partitioned to reach the local form,

$$\begin{aligned} \int_{\Omega_\gamma} \overline{\varrho^\gamma \dot{\det}(\mathbf{F}|_\Gamma)} \Big|_\gamma dV^\Gamma &= \int_{\Omega_\gamma} \left( \dot{\varrho}^\gamma|_\gamma \det(\mathbf{F}|_\Gamma) + \varrho^\gamma \overline{\dot{\det}(\mathbf{F}|_\Gamma)} \Big|_\gamma \right) dV^\Gamma \\ &= \int_{\Omega_\gamma} \left( \dot{\varrho}^\gamma|_\gamma \det(\mathbf{F}|_\Gamma) + \varrho^\gamma \frac{\partial(\det(\mathbf{F}|_\Gamma))}{\partial \mathbf{F}|_\Gamma} : \dot{\mathbf{F}}|_{\gamma\Gamma} \right) dV^\Gamma \\ &= \int_{\Omega_\gamma} \left( \dot{\varrho}^\gamma|_\gamma \det(\mathbf{F}|_\Gamma) + \varrho^\gamma \det(\mathbf{F}|_\Gamma) \mathbf{F}^{-T}|_\Gamma : \dot{\mathbf{F}}|_{\gamma\Gamma} \right) dV^\Gamma \end{aligned} \quad (1.28)$$

Where the derivative of the third invariant of a tensor with respect to the tensor itself is omitted here, and can be found elsewhere, the writer had followed the notation used by Bonet&Wood Ref.[<sup>J.Bonet 2008</sup>]. Besides the simplification of the constituent mapping of the infinite volume, the double contraction term can be further simplified by using the index notation,

$$dv = \det(\mathbf{F}|_\Gamma) dV^\Gamma \quad (1.29a)$$

$$\begin{aligned} \mathbf{F}^{-T}|_\Gamma : \dot{\mathbf{F}}|_{\gamma\Gamma} &= \left( \frac{\partial \mathbf{X}|_\Gamma}{\partial \mathbf{x}} \right)_{Ji} \left( \frac{\partial \dot{\mathbf{x}}|_\gamma}{\partial \mathbf{X}|_\Gamma} \right)_{iJ} \\ &= \left( \frac{\partial \dot{\mathbf{x}}|_\gamma}{\partial \mathbf{x}} \right)_{ii} = \text{tr}(\text{grad} \dot{\mathbf{x}}|_\gamma) = \text{tr}(\mathbf{L}|_\gamma) = \text{div}(\dot{\mathbf{x}}|_\gamma) \end{aligned} \quad (1.29b)$$

The final global form becomes;

$$\begin{aligned} \dot{m}^\gamma &= \int_{\Omega_\gamma} \left( \dot{\varrho}^\gamma|_\gamma \det(\mathbf{F}|_\Gamma) + \varrho^\gamma \det(\mathbf{F}|_\Gamma) \mathbf{F}^{-T}|_\Gamma : \dot{\mathbf{F}}|_{\gamma\Gamma} \right) dV^\Gamma \\ &= \int_{\Omega_\gamma} \left( \dot{\varrho}^\gamma|_\gamma + \varrho^\gamma \text{div}(\dot{\mathbf{x}}|_\gamma) \right) dV^\Gamma \end{aligned} \quad (1.30)$$

and the local inhomogeneous form is then;

$$\dot{\varrho}^\gamma|_\gamma + \varrho^\gamma \text{div}(\dot{\mathbf{x}}|_\gamma) = \hat{\varrho}^\gamma \quad (1.31)$$

---

<sup>3</sup>Please note that the integrand is time dependent, the integration variable as the reference real volume of the constituent is predetermined, and this time-invariant.

Considering that the component under consideration is *intrinsically incompressible*, by getting it together with equation (1.12) the following alternative inhomogeneous form is achieved,

$$\hat{\varrho}^\gamma = \overline{(n^\gamma \varrho^{\gamma R})} \Big|_\gamma + n^\gamma \varrho^{\gamma R} \operatorname{div}(\dot{\mathbf{x}}|_\gamma) = \dot{n}^\gamma|_\gamma \varrho^{\gamma R} + n^\gamma|_\gamma \dot{\varrho}^{\gamma R} + n^\gamma \varrho^{\gamma R} \operatorname{div}(\dot{\mathbf{x}}|_\gamma) \quad (1.32)$$

The final form of the balance of mass equation in terms of volume fractions is as follows;

$$\dot{\varrho}^{\gamma R} = 0 \quad \Rightarrow \quad \dot{n}^\gamma|_\gamma + n^\gamma \operatorname{div}(\dot{\mathbf{x}}|_\gamma) = \frac{\hat{\varrho}^\gamma}{\varrho^{\gamma R}} \quad (1.33)$$

The first identity of the final form of the equation of conservation of mass in equation (1.33), implies the concept of *intrinsic incompressibility*. Concerning the numerics of the continuum solid mechanics, the conservation of mass is usually omitted. The main reason of this is that, the focus of the classical continuum solid mechanics is usually based on single-phase materials, or on thermodynamically closed systems. The writer suggests Zienkiewicz&Taylor Ref.[<sup>O.C.Zienkiewicz 2000c</sup>], which cover also numerical applications of the subject. Since the topic covers two-phase mixture, the equation of conservation of mass (1.33) will be used in the following chapters and sections.

### 1.4.2 Conservation of Translational Momentum

Verbally, the conservation of momentum requires that the total sum of external, (body and traction) forces should be balanced by the rate of change of momentum. For a thermodynamically open system, the rate of change of momentum has a further *supply term*. In global form,

$$-\dot{\mathbf{p}}^\gamma|_\gamma + \mathbf{f}_b^\gamma + \mathbf{f}_t^\gamma + \hat{\mathbf{p}}^\gamma = \mathbf{0}$$

with,

$$\begin{aligned} \dot{\mathbf{p}}^\gamma|_\gamma &: \text{rate of change of momentum of a spatial control volume} \\ \mathbf{f}_b^\gamma &: \text{body forces acting on control volume} \\ \mathbf{f}_t^\gamma &: \text{traction forces acting on control surface} \\ \hat{\mathbf{p}}^\gamma &: \text{flux of momentum supply} \end{aligned} \quad (1.34)$$

Each of which is investigated and finally summed individually. Starting with the rate of change of momentum of the body in global form, which results in;

$$\begin{aligned} \dot{\mathbf{p}}^\gamma|_\gamma &= \frac{\partial \left( \int_{\Omega_\gamma} \varrho^\gamma \dot{\mathbf{x}}|_\gamma dv \right)}{\partial t} \Big|_\gamma \\ &= \int_{\Omega_\gamma} \dot{\varrho}^\gamma|_\gamma \dot{\mathbf{x}}|_\gamma dv + \int_{\Omega_\gamma} \varrho^\gamma \ddot{\mathbf{x}}|_\gamma dv + \int_{\Omega_\gamma} \varrho^\gamma \dot{\mathbf{x}}|_\gamma \mathbf{F}^{-T}|_\Gamma : \dot{\mathbf{F}}|_{\Gamma} dv \\ &= \int_{\Omega_\gamma} \dot{\varrho}^\gamma|_\gamma \dot{\mathbf{x}}|_\gamma dv + \int_{\Omega_\gamma} \varrho^\gamma \ddot{\mathbf{x}}|_\gamma dv + \int_{\Omega_\gamma} \varrho^\gamma \dot{\mathbf{x}}|_\gamma \operatorname{div}(\dot{\mathbf{x}}|_\gamma) dv \end{aligned} \quad (1.35)$$

The rate of change of momentum term can be further reduced by taking the conservation of mass equation into consideration. The compressible form of the conservation of mass equation (1.33) multiplied by the velocity of the current constituent at the spatial coordinates gives;

$$\varrho^\gamma \operatorname{div}(\dot{\mathbf{x}}|_\gamma) \dot{\mathbf{x}}|_\gamma = \hat{\varrho}^\gamma \dot{\mathbf{x}}|_\gamma - \dot{\varrho}^\gamma|_\gamma \dot{\mathbf{x}}|_\gamma \quad (1.36)$$

Inserting this expression back into equation (1.35) gives;

$$\dot{\mathbf{p}}^\gamma|_\gamma = \int_{\Omega_\gamma} (\hat{\varrho}^\gamma \dot{\mathbf{x}}|_\gamma + \varrho^\gamma \ddot{\mathbf{x}}^\gamma|_\gamma) dv \quad (1.37)$$

The body forces with the consideration of the apparent density-specific body forces<sup>4</sup>, in global form;

$$\mathbf{f}_b^\gamma = \int_{\Omega_\gamma} \varrho^\gamma \check{\mathbf{f}}_b^\gamma dv \quad (1.38)$$

Where the apparent density specific quantities are abbreviated with a breve symbol. The surface traction (on the system, not by the system) is, -according to the definition of Cauchy Ref.[C.Truesdell 1960]-is the surface integral of the true stress projected on the surface outward normals. These bunch of statements are in fact covering the definition of stress in continuum mechanics, and can be found anywhere else then the reference given in the paragraph itself.

$$\mathbf{f}_t^\gamma = \int_{\mathcal{B}_\gamma} \mathbf{t}^\gamma da = \int_{\mathcal{B}_\gamma} \boldsymbol{\sigma}^\gamma \cdot \mathbf{n}^{\mathcal{B}_\gamma} da = \int_{\Omega_\gamma} \operatorname{div}(\boldsymbol{\sigma}^\gamma) dv \quad (1.39)$$

The last point, namely the conversion of surface integral into the volume integral is due to the very well-known Gauss divergence Ref.[Mueller 2009] theorem. Combining all together, one gets the final local form of the balance of translational momentum equation evaluated in the spatial coordinates.

$$\operatorname{div}(\boldsymbol{\sigma}^\gamma) + \varrho^\gamma (\check{\mathbf{f}}_b^\gamma - \ddot{\mathbf{x}}|_\gamma) - \hat{\varrho}^\gamma \dot{\mathbf{x}}|_\gamma + \dot{\mathbf{p}}^\gamma = \mathbf{0} \quad (1.40)$$

It should be noted that the third term which is related to the mass source of the system is a natural conclusion of the enforcement of the conservation of mass into the rate of momentum part of the conservation of translational momentum equation as done in identity (1.36). The mass source has in this context no momentum contribution as long as stated otherwise. The reason of this assumption is that, the time integral of the apparent density flux does not coexist (yet) with the spatial velocity of the constituent. There is a balance of rate as stated in the equation of conservation of mass, but this does not indicate that, in the current time the source term is already gathered into the existing mass.

---

<sup>4</sup>The apparent density specific forces in this context refer dimensionally to forces per matter, thus has the same units of body acceleration

### 1.4.3 Conservation of Internal and Kinetic energy: An extended first law of Thermodynamics

The first law of thermodynamics verbally states that, *no matter what process occur, there exist a property of the universe, called energy, which can not change, neither can be destroyed nor can be produced.* This statement can be found in many early works, the writer had followed the definitions done in more recent publications and books, such as Sonntag et. all. Ref.[[R.E.Sonntag 1998](#)] and deHoff Ref.[[deHoff 2006](#)]. Especially the latter one is more appropriate for the study of Thermodynamics in material science.

This verbal statement in terms of different types of energy terms can be formulated. For a given interval of time,

$$U(t^*) - U(t^* - \Delta t) = \Delta U = Q + W + \dot{W}$$

$\Delta U$  : Change of internal energy in the time interval of  $\Delta t$

$Q$  : Heat supplied by the surroundings towards to the system in the time interval of  $\Delta t$

$W$  : Mechanical work done onto the system in the time interval of  $\Delta t$

$\dot{W}$  : Other types of work done onto the system in the time interval of  $\Delta t$

(1.41)

According to this statement, any change in the internal energy of the system should be (is) balanced by the thermal, mechanical or any means of energy influx (outflux) into (outside to) the system. The differential form of equation (1.41) for infinite changes is,

$$dU = \delta Q + \delta W + \delta \dot{W} \quad (1.42)$$

Quite purposely, a differential operator is usually used for the infinite change in the internal energy, whereby a variation operator is used for the energy supplies to the system. The reason beyond this notation is the fact that, the internal energy is a *state function*, but the heat supplied, the mechanical work done onto the system and other types of energy inputs are *process variables*<sup>5</sup>. The underlying meaning of a *state function* in the current context is implicitly given in the definition of first law of thermodynamics. A change of state function depends only on the initial and the final states of a system, not on the path. Since the internal energy has to be conserved, no matter how, if many different systems are supplied with the same amount of thermal and mechanical energies, the change in their internal energy has to be the same, being independent of the path. However, otherwise is not necessarily true, i.e. the pressure (as pressure of a fluid at a time instant or as the volumetric part of the true stress tensor) of a system in equilibrium (say in the absence of pressure gradients), is also a state function but not conserved. There is of course a variation of differential *equations* which govern the spatial and temporal change of pressure, and thus indicate a type of conservation of pressure, but it is not a generic law, which can be

<sup>5</sup>Refer to Dehoff Ref.[[deHoff 2006](#)] for an elaborate survey of *state functions and process variables*



compared with the first law of thermodynamics. The law can be extended for a spatially inhomogeneous system by considering the infinite changes in the kinetic energy as well.

$$dU + dK = \delta Q + \delta W \quad (1.43)$$

Where the kinetic energy of the system is also taken as a state function. In this context, the internal energy is driven by the mechanical stress-strain contractions (Helmholtz type free energy), and the relative thermal fluctuations. The kinetic energy is driven by the averaged spatial rates of the system inertia. Any other magnetic, electrical or chemical potentials which can be considered additionally as conserved quantities are omitted here. The temporal integral form of the equation of conservation of energy is,

$$\int_t^{t+\Delta t} \dot{U} dt + \int_t^{t+\Delta t} \dot{K} dt = \int_t^{t+\Delta t} \hat{Q} dt + \int_t^{t+\Delta t} \hat{W} dt \quad (1.44)$$

The notation of differential and variational forms of corresponding state functions and process variables are kept for the equation above. The state functions undergo rate type of change, where the process variables enter the equation system in terms of fluxes, as done in the previous sections. They all change temporally. The temporal local form, which include the spatial integrations and are all evaluated at the current spatial configuration. Those become then;

$$\dot{U}^\gamma |_\gamma + \dot{K}^\gamma |_\gamma = \hat{Q}^\gamma |_\gamma + \hat{W}^\gamma |_\gamma \quad (1.45)$$

Next, each term is introduced after each other. Like previously, the apparent density specific internal energy of a constituent is abbreviated with breve symbol, see  $\check{U}^\gamma$  beneath.

$$U^\gamma = \int_{\Omega_\gamma} \varrho^\gamma \check{U}^\gamma dv \quad (1.46)$$

The rate is then,

$$\begin{aligned} \dot{U}^\gamma |_\gamma &= \left. \frac{\partial \left( \int_{\Omega_\gamma} \varrho^\gamma \check{U}^\gamma dv \right)}{\partial t} \right|_\gamma \\ &= \int_{\Omega_\gamma} \dot{\varrho}^\gamma |_\gamma \check{U}^\gamma dv + \int_{\Omega_\gamma} \varrho^\gamma \dot{\check{U}}^\gamma |_\gamma dv + \int_{\Omega_\gamma} \varrho^\gamma \check{U}^\gamma \mathbf{F}^{-T} |_\Gamma : \dot{\mathbf{F}} |_{\Gamma\Gamma} dv \\ &= \int_{\Omega_\gamma} \dot{\varrho}^\gamma |_\gamma \check{U}^\gamma dv + \int_{\Omega_\gamma} \varrho^\gamma \dot{\check{U}}^\gamma |_\gamma dv + \int_{\Omega_\gamma} \varrho^\gamma \check{U}^\gamma \text{div}(\dot{\mathbf{x}} |_\gamma) dv \end{aligned} \quad (1.47)$$

The third term can be reduced by using the compressible form of the equation of conservation of mass (1.36),

$$\varrho^\gamma \text{div}(\dot{\mathbf{x}} |_\gamma) \check{U}^\gamma = \hat{\varrho}^\gamma \check{U}^\gamma - \dot{\varrho}^\gamma |_\gamma \check{U}^\gamma \quad (1.48)$$

Inserting this expression back into equation (1.47), gives the final local form of the rate of change of internal energy in terms of the apparent density specific internal energy and other partial quantities.

$$\dot{U}^\gamma |_\gamma = \int_{\Omega_\gamma} \left( \hat{\varrho}^\gamma \check{U}^\gamma + \varrho^\gamma \dot{\check{U}}^\gamma |_\gamma \right) dv \quad (1.49)$$

Moving forward, the kinetic energy caused by the average rate of change of coordinate of the constituent can be defined as;

$$K^\gamma = \frac{1}{2} \int_{\Omega_\gamma} \varrho^\gamma \dot{\mathbf{x}}|_\gamma \cdot \dot{\mathbf{x}}|_\gamma dv \quad (1.50)$$

The rate of kinetic energy can be obtained by following similar steps of getting the rate of internal energy.

$$\dot{K}^\gamma|_\gamma = \frac{1}{2} \frac{\partial \left( \int_{\Omega_\gamma} \varrho^\gamma \dot{\mathbf{x}}|_\gamma \cdot \dot{\mathbf{x}}|_\gamma dv \right)}{\partial t} \Bigg|_\gamma = \frac{1}{2} \int_{\Omega_\gamma} \hat{\varrho}^\gamma \|\dot{\mathbf{x}}|_\gamma\|^2 dv + \int_{\Omega_\gamma} \varrho^\gamma \dot{\mathbf{x}}|_\gamma \cdot \ddot{\mathbf{x}}|_\gamma dv \quad (1.51)$$

The first term of the right hand side of equation (1.51) as being the mechanical energy, is nothing but the rate of work done by the external surface tractions and body forces.

$$\hat{W}^\gamma = \mathbf{f}_b^\gamma \cdot \dot{\mathbf{x}}|_\gamma + \mathbf{f}_t^\gamma \cdot \dot{\mathbf{x}}|_\gamma \quad (1.52)$$

By neglecting the body forces at this stage, the mechanical work done by the singular action of surface tractions is;

$$\mathbf{f}_t^\gamma \cdot \dot{\mathbf{x}}|_\gamma = \int_{\mathcal{B}_\gamma} \mathbf{t}^\gamma \cdot \dot{\mathbf{x}}|_\gamma da = \int_{\mathcal{B}_\gamma} \boldsymbol{\sigma}^\gamma \cdot \mathbf{n}^{\mathcal{B}_\gamma} \cdot \dot{\mathbf{x}}|_\gamma da = \int_{\mathcal{B}_\gamma} (\boldsymbol{\sigma}^{\gamma T} \cdot \dot{\mathbf{x}}|_\gamma) \cdot \mathbf{n}^{\mathcal{B}_\gamma} da \quad (1.53)$$

and by applying the divergence theorem at this stage one gets;

$$\mathbf{f}_t^\gamma \cdot \dot{\mathbf{x}}|_\gamma = \int_{\mathcal{B}_\gamma} (\boldsymbol{\sigma}^{\gamma T} \cdot \dot{\mathbf{x}}|_\gamma) \cdot \mathbf{n}^{\mathcal{B}_\gamma} da = \int_{\Omega_\gamma} \text{div} (\boldsymbol{\sigma}^{\gamma T} \cdot \dot{\mathbf{x}}|_\gamma) dv \quad (1.54)$$

The spatial divergence can be further simplified by turning into the index notation. For the equation below, the symmetry property<sup>6</sup> of Cauchy stress tensor is taken into account,

$$\text{div} (\boldsymbol{\sigma}^{\gamma T} \cdot \dot{\mathbf{x}}|_\gamma) = \frac{\partial}{\partial x_i} (\sigma_{ij}^\gamma (\dot{x}|_\gamma)_j) = \frac{\partial \sigma_{ij}^\gamma}{\partial x_i} (\dot{x}|_\gamma)_j + \sigma_{ji}^\gamma \frac{\partial (\dot{x}|_\gamma)_j}{\partial x_i} \quad (1.55)$$

Back, in terms of tensorial notation,

$$\begin{aligned} \text{div} (\boldsymbol{\sigma}^{\gamma T} \cdot \dot{\mathbf{x}}|_\gamma) &= \text{div} (\boldsymbol{\sigma}^\gamma) \cdot \dot{\mathbf{x}}|_\gamma + \boldsymbol{\sigma}^\gamma : \text{grad} \dot{\mathbf{x}}|_\gamma \\ &= \text{div} (\boldsymbol{\sigma}^\gamma) \cdot \dot{\mathbf{x}}|_\gamma + \boldsymbol{\sigma}^\gamma : \mathbf{L}|_\gamma \\ &= \text{div} (\boldsymbol{\sigma}^\gamma) \cdot \dot{\mathbf{x}}|_\gamma + \boldsymbol{\sigma}^\gamma : \mathbf{D}|_\gamma \end{aligned} \quad (1.56)$$

Where the second equation results as a conclusion of the definition of spatial velocity gradient, and the last equation is due to the orthogonality of Cauchy stress tensor (as being symmetric) to a skew symmetric tensor. This pure algebraic fact is written to state formally that the spin tensor does not contribute into the first law of thermodynamics.

$$\boldsymbol{\sigma}^\gamma : \mathbf{W}|_\gamma = 0 \quad (1.57)$$

<sup>6</sup>The conservation of angular momentum is implied here

Recalling the equation of conservation of (translational) momentum (1.40)<sup>7</sup> is multiplied with the spatial velocity,

$$\operatorname{div}(\boldsymbol{\sigma}^\gamma) \cdot \dot{\boldsymbol{x}}|_\gamma = -\varrho^\gamma \left( \check{\boldsymbol{f}}_b^\gamma - \ddot{\boldsymbol{x}}|_\gamma \right) \cdot \dot{\boldsymbol{x}}|_\gamma + \hat{\varrho}^\gamma \dot{\boldsymbol{x}}|_\gamma \cdot \dot{\boldsymbol{x}}|_\gamma - \hat{\boldsymbol{p}}^\gamma \cdot \dot{\boldsymbol{x}}|_\gamma \quad (1.58)$$

Inserting this back into equation (1.56),

$$\boldsymbol{f}_t^\gamma \cdot \dot{\boldsymbol{x}}|_\gamma = -\varrho^\gamma \left( \check{\boldsymbol{f}}_b^\gamma - \ddot{\boldsymbol{x}}|_\gamma \right) \cdot \dot{\boldsymbol{x}}|_\gamma + \hat{\varrho}^\gamma \dot{\boldsymbol{x}}|_\gamma \cdot \dot{\boldsymbol{x}}|_\gamma - \hat{\boldsymbol{p}}^\gamma \cdot \dot{\boldsymbol{x}}|_\gamma + \boldsymbol{\sigma}^\gamma : \boldsymbol{D}|_\gamma \quad (1.59)$$

Together with the previously neglected power caused by the body forces, the total global form of the mechanical energy supplied into the system by one constituent becomes;

$$\begin{aligned} \hat{W}^\gamma &= \boldsymbol{f}_b^\gamma \cdot \dot{\boldsymbol{x}}|_\gamma + \boldsymbol{f}_t^\gamma \cdot \dot{\boldsymbol{x}}|_\gamma \\ &= \int_{\Omega_\gamma} \left( \varrho^\gamma \ddot{\boldsymbol{x}}|_\gamma \cdot \dot{\boldsymbol{x}}|_\gamma + \hat{\varrho}^\gamma \dot{\boldsymbol{x}}|_\gamma \cdot \dot{\boldsymbol{x}}|_\gamma - \hat{\boldsymbol{p}}^\gamma \cdot \dot{\boldsymbol{x}}|_\gamma + \boldsymbol{\sigma}^\gamma : \boldsymbol{D}|_\gamma \right) dv \end{aligned} \quad (1.60)$$

The final contribution of energy is due to the thermal source and heat input from the surroundings towards to the system,

$$\hat{Q}^\gamma = \int_{\Omega_\gamma} \varrho^\gamma r dv - \int_{\mathcal{B}_\gamma} \boldsymbol{q}^\gamma \cdot \boldsymbol{n}^{\mathcal{B}_\gamma} da = \int_{\Omega_\gamma} \varrho^\gamma r dv - \int_{\Omega_\gamma} \operatorname{div}(\boldsymbol{q}^\gamma) dv \quad (1.61)$$

The integral form of all contributions inserted back into the master equation of first law of thermodynamics (1.45) leads into,

$$\begin{aligned} 0 &= \int_{\Omega_\gamma} \left( \hat{\varrho}^\gamma \check{U}^\gamma + \varrho^\gamma \check{U}^\gamma|_\gamma \right) dv \\ &\quad + \frac{1}{2} \int_{\Omega_\gamma} \hat{\varrho}^\gamma \|\dot{\boldsymbol{x}}|_\gamma\|^2 dv + \int_{\Omega_\gamma} \varrho^\gamma \dot{\boldsymbol{x}}|_\gamma \cdot \ddot{\boldsymbol{x}}|_\gamma dv \\ &\quad + \int_{\Omega_\gamma} \left( -\varrho^\gamma \ddot{\boldsymbol{x}}|_\gamma \cdot \dot{\boldsymbol{x}}|_\gamma - \hat{\varrho}^\gamma \dot{\boldsymbol{x}}|_\gamma \cdot \dot{\boldsymbol{x}}|_\gamma + \hat{\boldsymbol{p}}^\gamma \cdot \dot{\boldsymbol{x}}|_\gamma - \boldsymbol{\sigma}^\gamma : \boldsymbol{D}|_\gamma \right) \\ &\quad - \int_{\Omega_\gamma} \varrho^\gamma r dv + \int_{\Omega_\gamma} \operatorname{div}(\boldsymbol{q}^\gamma) dv \end{aligned} \quad (1.62)$$

The homogeneous integrand results in the local form, which was searched.

$$\hat{\varrho}^\gamma \check{U}^\gamma + \varrho^\gamma \check{U}^\gamma|_\gamma - \frac{1}{2} \hat{\varrho}^\gamma \|\dot{\boldsymbol{x}}|_\gamma\|^2 + \hat{\boldsymbol{p}}^\gamma \cdot \dot{\boldsymbol{x}}|_\gamma - \boldsymbol{\sigma}^\gamma : \boldsymbol{D}|_\gamma - \varrho^\gamma r + \operatorname{div}(\boldsymbol{q}^\gamma) = 0 \quad (1.63)$$

For this final form, any source for internal energy is omitted for the sake of simplicity. Before moving into the next section, a last but necessary comment is let here about the notation. With the time derivatives for example in  $\check{U}^\gamma|_\gamma$  it is not the intent to mean the material time derivative. The motion, -as expressed previously- is taken to be Lagrangian, and time derivatives indicate only, that the quantities associated with one component undergo a change of rate, which is depending on a single coordinate, which is shared by two constituents. Since this single coordinate has two different time derivatives (again not the material or spatial meant here), it should be expressed which time derivative is taken.

<sup>7</sup>This back-insertion of this multiplication is necessary for further derivations

### 1.4.4 The Entropy Inequality-Dissipation of Mixed Field

Until this point, the *Balance equations* of the *Governing relations* are introduced. In this sub-section, entropy inequality is introduced shortly. Initially, continuum mechanical definition of entropy is going to be done briefly. Shortly after, the dissipation inequality, namely the *second law of thermodynamics* is going to be made both verbally and formally. Immediately after, *Helmholtz free energy* as a state function is going to be defined. This results in the so-called *strain energy density function*, which defines the main *constitutive relation*<sup>8</sup> of thermoelasticity. The other types of state functions, like *Entalpy and Gibbs free energies* are omitted in this scope.

#### 1.4.4.1 Change of Entropy as a State Function

The micromechanical definition of entropy, defined as *the system in equilibrium has the configuration of the most probable macrostate*, is omitted here, and can be find elsewhere Ref.[[D.F.Styer 2007](#)]. The continuum mechanical macroscopic definition of entropy follows rather initial postulates and supporting theoretical statements. The definition starts with the relation of entropy with the heat supply into the system. For any process, which is not necessarily a cyclic one, the integral on the left hand side and the fraction on the right hand side are state functions, and the differentials of those state functions respectively.

$$\Delta S_{rev} [A \rightarrow B] = \int_A^B \frac{\delta Q_{rev}}{T} \quad dS_{rev} = \frac{\delta Q_{rev}}{T} \quad (1.64)$$

With the subscript it is not meant that the heat transfer has reversible properties, rather it is meant that the process from state A to state B has took place reversibly, i.e. without dissipation or loss of energy. Energy is globally not lost, first law of thermodynamics holds, but it can be still dissipated to the surroundings, or converted in another form. The situation in correlation (1.64) can be partially achieved for slow enough, aka almost reversible processes.

Remembering the definition of a state function, it is not only a declaration that the temperature specific variation of heat absorbtion of equation (1.64) is a state function. It can be shown Ref.[[R.E.Sonntag 1998](#)] i.e. for Carnot cycle that the cyclic integral of the aforementioned quantity for reversible process has zero value. Again, the reversible process should fulfill the following criteria for a cycle;

$$\Delta S_{rev} [A \rightarrow B] + \Delta S_{rev} [B \rightarrow C] + \Delta S_{rev} [C \rightarrow D] + \Delta S_{rev} [D \rightarrow A] = 0 \quad (1.65)$$

Since the integral is a state function, for two different processes one being reversible, if the amount of heat exchange and operation temperature is same the other irreversible, the change of entropy should be the same.

$$\Delta S_{irr} [A \rightarrow B] = \Delta S_{rev} [A \rightarrow B] \quad (1.66)$$

The second law states that, for any irreversible process, there is a transfer and production of entropy, where the production is always greater then zero. The notion of positive production

<sup>8</sup>potential function of the elastic part of pseudo-elasticity; material law

is interpreted in statistical physics as *most probable tends to happen*, and thus indicates a direction of the real processes. For continuum mechanical definition the differential local form, the infinite change of entropy of a system Ref.[<sup>deHoff 2006</sup>],

$$dS_{irr}^{sys} = dS_{irr}^{trans} + dS_{irr}^{prod} \quad dS_{irr}^{prod} > 0 \quad (1.67)$$

The verbal definition of second law states that, " *There is a property of the universe, called its entropy, which always changes in the same direction no matter what process occur* Ref.[<sup>deHoff 2006</sup>]" . The main agreement which can be also phenomenologically proven is that, the irreversible process has an entropy transfer and production term. On the other side, the system undergoing a reversible process can only, absorb the entropy.

$$\begin{aligned} \Delta S_{irr} [A \rightarrow B] &= \Delta S_{irr}^{trans} [A \rightarrow B] + \Delta S_{irr}^{prod} [A \rightarrow B] \\ &= \Delta S_{rev} [A \rightarrow B] = \Delta S_{rev}^{trans} [A \rightarrow B] + \Delta S_{rev}^{prod} [A \rightarrow B] \quad (1.68) \\ &= \Delta S_{rev}^{trans} [A \rightarrow B] \end{aligned}$$

Equation (1.67) together with equation (1.68) leads into the following conclusion,

$$\begin{aligned} \Delta S_{irr}^{trans} [A \rightarrow B] &= \Delta S_{rev}^{trans} [A \rightarrow B] - \Delta S_{irr}^{prod} [A \rightarrow B] \\ \implies \Delta S_{irr}^{trans} [A \rightarrow B] &< \Delta S_{rev}^{trans} [A \rightarrow B] \end{aligned} \quad (1.69)$$

Which results into the following integral and differential forms,

$$\int_A^B \frac{\delta Q_{irr}}{T} < \int_A^B \frac{\delta Q_{rev}}{T} \quad \frac{\delta Q_{irr}}{T} < \frac{\delta Q_{rev}}{T} = dS \quad (1.70)$$

First and second inequalities show that, for isothermal processes, the reversible heat transfer takes the maximum. For cyclic processes, the change in state function entropy is zero. This gives the well known *Clausius Inequality* in integral form,

$$\oint_A^A \frac{\delta Q}{T} \leq 0 \quad (1.71)$$

The strictness of the inequality is removed, since there is no information about the reversibility of the heat transfer made. The time integral form of equations (1.70) and (1.71) are,

$$\int_t^{t+\Delta t} \frac{\hat{Q}}{T} dt \leq \int_t^{t+\Delta t} \dot{S} dt \quad \implies \quad \left. \frac{\hat{Q}^\gamma}{T} \right|_\gamma \leq \dot{S}^\gamma |_\gamma \quad (1.72)$$

Where the composition and corresponding time derivatives are considered in the last form of the equation. This rate form is taken to be consistent with the previous balance equations, namely, conservation of mass, translational momentum and the internal and kinetic energy sum.

### 1.4.4.2 Combined Statement and Helmholtz Free Energy

From the definition of entropy, for as reversible process, the process variation of total heat transfer and production of the system can be expressed in terms of temperature and entropy differential as follows,

$$\delta Q_{rev} = TdS \quad (1.73)$$

Inserting this back into the first law of thermodynamics, equation (1.42), one gets,

$$dU = TdS + \delta W \quad (1.74)$$

This equation, where the alternative energy sources are omitted, is known as *the combined statement of first and second laws of thermodynamics*. The state function of Helmholtz free energy and its differential are defined as<sup>9</sup>,

$$A = U - TS \quad \implies \quad dA = dU - SdT - TdS \quad (1.75)$$

Inserting the combined statement into the Helmholtz free energy;

$$dA = TdS + \delta W - SdT - TdS = \delta W - SdT \quad (1.76)$$

Which indicates that the differential of Helmholtz free energy for isothermal and reversible processes is balanced by the variations of mechanical work (*A:Arbeit*) done on to the system. This is most probably the main reason that in the theory of elasticity, the so called strain energy density function is abbreviated as the Helmholtz free energy density state function.

### 1.4.4.3 Second law of Thermodynamics for the two phase mixture

In this part, another form of *the combined statement of second and first law* is done. This statement is performed by considering the second law of Thermodynamics as the master relation, and thus results in an inequality. The strain energy density function is enforced into this inequality in order to quantify admissible ranges for positive dissipation. Recalling the temporal and spatial differential form of the second law (1.72),

$$\frac{\hat{Q}^\gamma}{T^\gamma} \leq \dot{S}^\gamma |_\gamma \quad (1.77)$$

The temperature specific total heat gain, consisting of a heat source and heat transfer becomes then,

$$\frac{\hat{Q}^\gamma}{T^\gamma} = \int_{\Omega_\gamma} \frac{1}{T^\gamma} \varrho^\gamma r^\gamma dv - \int_{\mathcal{B}_\gamma} \frac{\mathbf{q}^\gamma}{T^\gamma} \cdot \mathbf{n}^{\mathcal{B}_\gamma} da = \int_{\Omega_\gamma} \frac{1}{T^\gamma} \varrho^\gamma r^\gamma dv - \int_{\Omega_\gamma} \text{div} \left( \frac{\mathbf{q}^\gamma}{T^\gamma} \right) dv \quad (1.78)$$

The symbol of *evaluated at:* is not anymore used for process variables of heat and work, since they are anyway given in rate form. The apparent, or partial density specific entropy has the form,

$$S^\gamma = \int_{\Omega_\gamma} \varrho^\gamma \tilde{s}^\gamma dv \quad (1.79)$$

---

<sup>9</sup>By means of differentiation by parts

The rate of this quantity can be obtained by using the conservation of mass,

$$\dot{S}^\gamma|_\gamma = \int_{\Omega_\gamma} \left( \hat{\varrho}^\gamma \check{s}^\gamma + \varrho^\gamma \dot{\check{s}}^\gamma|_\gamma \right) dv \quad (1.80)$$

Previously, the constituents of the mixtures were assumed to obey the balance laws independent of each other. Each constituent had its own conservation of mass equation, translational momentum balance equation and finally, combined internal and kinetic energy conservation equation. Some of the interactions in between the constituents are donated by momentum or energy input to the system, but their origin were not addressed. In opposite, for the case of entropy inequality, the mixture is considered as a whole.

$$\sum_{\gamma:f,s} \dot{S}^\gamma|_\gamma \geq \sum_{\gamma:f,s} \int_{\Omega_\gamma} \frac{1}{T^\gamma} \varrho^\gamma r dv - \sum_{\gamma:f,s} \int_{\Omega_\gamma} \text{div} \left( \frac{\mathbf{q}^\gamma}{T^\gamma} \right) dv \quad (1.81)$$

The local form together with equation (1.80) becomes,

$$\sum_{\gamma:f,s} \left( \hat{\varrho}^\gamma \check{s}^\gamma + \varrho^\gamma \dot{\check{s}}^\gamma|_\gamma - \frac{1}{T^\gamma} \varrho^\gamma r + \text{div} \left( \frac{\mathbf{q}^\gamma}{T^\gamma} \right) \right) \geq 0 \quad (1.82)$$

The Helmholtz free energy in the integral form, together with spatial mass free energy, internal energy and entropy, rewritten again,

$$\begin{aligned} A^\gamma &= U^\gamma - T^\gamma S^\gamma \\ A^\gamma &= \int_{\Omega_\gamma} \varrho^\gamma \check{\Psi}^\gamma dv \\ U^\gamma &= \int_{\Omega_\gamma} \varrho^\gamma \check{U}^\gamma dv \\ S^\gamma &= \int_{\Omega_\gamma} \varrho^\gamma \check{s}^\gamma dv \end{aligned} \quad (1.83)$$

The strain energy density function<sup>10</sup>, and the rate of change of it are given then in local form,

$$\check{\Psi}^\gamma = \check{U}^\gamma - T^\gamma \check{s}^\gamma \quad (1.84a)$$

$$\dot{\check{\Psi}}^\gamma|_\gamma = \dot{\check{U}}^\gamma|_\gamma - \dot{T}^\gamma|_\gamma \check{s}^\gamma - \dot{\check{s}}^\gamma|_\gamma T^\gamma \quad (1.84b)$$

The second term in equation (1.82) can be deduced from equation (1.84b)

$$\begin{aligned} \varrho^\gamma \dot{\check{s}}^\gamma|_\gamma &= -\varrho^\gamma \frac{\dot{\check{\Psi}}^\gamma|_\gamma}{T^\gamma} + \varrho^\gamma \frac{\dot{\check{U}}^\gamma|_\gamma}{T^\gamma} - \varrho^\gamma \frac{\dot{T}^\gamma|_\gamma \check{s}^\gamma}{T^\gamma} \\ &= (T^\gamma)^{-1} \left( -\varrho^\gamma \dot{\check{\Psi}}^\gamma|_\gamma + \varrho^\gamma \dot{\check{U}}^\gamma|_\gamma - \varrho^\gamma \dot{T}^\gamma|_\gamma \check{s}^\gamma \right) \end{aligned} \quad (1.85)$$

<sup>10</sup>The strain energy functions is defined as the apparent density (in spatial domain) specific Helmholtz free energy of the constituent

The second term of equation (1.85) can be replaced by the rate of change of internal energy from the equation of conservation of energy;

$$(T^\gamma)^{-1} \varrho^\gamma \dot{U}^\gamma |_\gamma = (T^\gamma)^{-1} \left( -\hat{\varrho}^\gamma \check{U}^\gamma + \frac{1}{2} \hat{\varrho}^\gamma \|\dot{\mathbf{x}} |_\gamma\|^2 - \hat{\mathbf{p}}^\gamma \cdot \dot{\mathbf{x}} |_\gamma \right. \\ \left. + \boldsymbol{\sigma}^\gamma : \mathbf{D} |_\gamma + \varrho^\gamma r - \text{div}(\mathbf{q}^\gamma) \right) \quad (1.86)$$

After successful replacement, the following form for the rate of partial density specific entropy rate is obtained;

$$\varrho^\gamma \dot{s}^\gamma |_\gamma = (T^\gamma)^{-1} \left( -\varrho^\gamma \dot{\Psi}^\gamma |_\gamma - \hat{\varrho}^\gamma \check{U}^\gamma + \frac{1}{2} \hat{\varrho}^\gamma \|\dot{\mathbf{x}} |_\gamma\|^2 - \hat{\mathbf{p}}^\gamma \cdot \dot{\mathbf{x}} |_\gamma \right. \\ \left. + \boldsymbol{\sigma}^\gamma : \mathbf{D} |_\gamma + \varrho^\gamma r - \text{div}(\mathbf{q}^\gamma) - \varrho^\gamma \dot{T}^\gamma |_\gamma \check{s}^\gamma \right) \quad (1.87)$$

Inserting this expression into the final dissipation inequality (1.82) yields;

$$\sum_{\gamma:f,s} \left( \dot{s}^\gamma |_\gamma - \frac{\hat{Q}^\gamma}{T^\gamma} \right) = \sum_{\gamma:f,s} (T^\gamma)^{-1} \left[ T^\gamma \hat{\varrho}^\gamma \check{s}^\gamma - \varrho^\gamma \dot{\Psi}^\gamma |_\gamma - \hat{\varrho}^\gamma \check{U}^\gamma + \frac{1}{2} \hat{\varrho}^\gamma \|\dot{\mathbf{x}} |_\gamma\|^2 - \hat{\mathbf{p}}^\gamma \cdot \dot{\mathbf{x}} |_\gamma \right. \\ \left. + \boldsymbol{\sigma}^\gamma : \mathbf{D} |_\gamma + \varrho^\gamma r - \text{div}(\mathbf{q}^\gamma) - \varrho^\gamma \dot{T}^\gamma |_\gamma \check{s}^\gamma - \varrho^\gamma r + T^\gamma \text{div} \left( \frac{\mathbf{q}^\gamma}{T^\gamma} \right) \right] \geq 0 \quad (1.88)$$

Further insertion of equation (1.84b), gives one the internal energy-free version of the inequality;

$$\sum_{\gamma:f,s} \left( \dot{s}^\gamma |_\gamma - \frac{\hat{Q}^\gamma}{T^\gamma} \right) = \sum_{\gamma:f,s} (T^\gamma)^{-1} \left[ -\hat{\varrho}^\gamma \check{\Psi}^\gamma - \varrho^\gamma \dot{\Psi}^\gamma |_\gamma + \frac{1}{2} \hat{\varrho}^\gamma \|\dot{\mathbf{x}} |_\gamma\|^2 - \hat{\mathbf{p}}^\gamma \cdot \dot{\mathbf{x}} |_\gamma \right. \\ \left. + \boldsymbol{\sigma}^\gamma : \mathbf{D} |_\gamma - \text{div}(\mathbf{q}^\gamma) - \varrho^\gamma \dot{T}^\gamma |_\gamma \check{s}^\gamma + T^\gamma \text{div} \left( \frac{\mathbf{q}^\gamma}{T^\gamma} \right) \right] \geq 0 \quad (1.89)$$

Heat flux related quantities can be further reduced by spreading the divergence of temperature specific heat flux term as follows;

$$T^\gamma \text{div} \left( \frac{\mathbf{q}^\gamma}{T^\gamma} \right) = T^\gamma \frac{\partial \left( q_i^\gamma (T^\gamma)^{-1} \right)}{\partial x_i} = \text{div}(\mathbf{q}^\gamma) - (T^\gamma)^{-1} \text{grad}(T^\gamma) \cdot \mathbf{q}^\gamma \quad (1.90)$$

Replacing this result of this term;

$$\sum_{\gamma:f,s} \left( \dot{s}^\gamma |_\gamma - \frac{\hat{Q}^\gamma}{T^\gamma} \right) = \sum_{\gamma:f,s} (T^\gamma)^{-1} \left[ -\hat{\varrho}^\gamma \check{\Psi}^\gamma - \varrho^\gamma \dot{\Psi}^\gamma |_\gamma + \frac{1}{2} \hat{\varrho}^\gamma \|\dot{\mathbf{x}} |_\gamma\|^2 - \hat{\mathbf{p}}^\gamma \cdot \dot{\mathbf{x}} |_\gamma \right. \\ \left. + \boldsymbol{\sigma}^\gamma : \mathbf{D} |_\gamma - \varrho^\gamma \dot{T}^\gamma |_\gamma \check{s}^\gamma - \frac{\text{grad}(T^\gamma)}{T^\gamma} \cdot \mathbf{q}^\gamma \right] \geq 0 \quad (1.91)$$



In common parenthesis of partial density and partial density input;

$$\sum_{\gamma:f,s} \left( \dot{S}^\gamma |_\gamma - \frac{\hat{Q}^\gamma}{T^\gamma} \right) = \sum_{\gamma:f,s} (T^\gamma)^{-1} \left[ \varrho^\gamma \left( -\dot{\Psi}^\gamma |_\gamma - \dot{T}^\gamma |_\gamma \check{s}^\gamma \right) + \hat{\varrho}^\gamma \left( -\check{\Psi}^\gamma + \frac{1}{2} \|\dot{\mathbf{x}} |_\gamma \|^2 \right) \right. \\ \left. - \hat{\mathbf{p}}^\gamma \cdot \dot{\mathbf{x}} |_\gamma + \boldsymbol{\sigma}^\gamma : \mathbf{D} |_\gamma - \frac{\text{grad}(T^\gamma)}{T^\gamma} \cdot \mathbf{q}^\gamma \right] \geq 0 \quad (1.92)$$

The equation above is known as a special version of Clausius-Duhem inequality. Stress tensors, spatial rate of the deformation gradients and strain energy functions are involved in this version of the governing relation. The main assumptions can be applied on this combined version of second and first laws, and lead into a weak form, which can be merged into the numerical methods for solving partial differential equations.

## 1.5 Assumptions, Narrowed Relations and Constitutive Restrictions

In this section, the previously given governing relations are simplified according to the assumptions, which will be postulated in this section. Immediately after, the consistency of number of field variables with the number of equations are compared. Since the number of equations in hand are strictly depending on the assumptions done (under assumptions done, energy equation can be reduced to the balance of momentum), the impact on the determinability of the system is discussed.

### 1.5.1 Assumptions

The list of assumptions done are,

*Assumption1:* The solid phase of the mixture is taken to be fully incompressible. The realistic density of the solid phase does not undergo temporal changes.

$$\dot{\varrho}^{sR} |_s = 0 \quad (1.93)$$

*Assumption2:* Similarly, the fluid phase of the mixture is taken to be fully incompressible. The realistic density of the fluid phase does not undergo temporal changes either.

$$\dot{\varrho}^{fR} |_f = 0 \quad (1.94)$$

*Assumption3:* The temporal differential of the temperature field is neglected. The processes are assumed to find place isothermally, for both phases, the rate of change of the temperature is ignored.

$$\dot{T}^\gamma |_\gamma = 0 \quad (1.95)$$

## 1.5. Assumptions, Narrowed Relations and Constitutive Restrictions 21

*Assumption4:* The process is assumed to take place in equal temperatures for the solid and fluid phases. The temperature gradients are not only neglected in between phases, but also in the phases.

$$T^s = T^f = T \quad \text{grad}(T^\gamma) = \mathbf{0} \quad (1.96)$$

*Assumption5:* The process is quasi-static for both phases.

$$\ddot{\mathbf{x}}^\gamma = \mathbf{0} \quad (1.97)$$

*Assumption6:* No mass supply into any phase.

$$\hat{\varrho}^\gamma = 0 \quad (1.98)$$

*Assumption7:* No body forces applied on the system for any constituent.

$$\check{\mathbf{f}}_b^s = \check{\mathbf{f}}_b^f = \mathbf{0} \quad (1.99)$$

### 1.5.2 Narrowed Governing Relations

In this subsection the simplifications according to the assumptions introduced above are presented.

*Simplification 1:* Saturation condition and partial density equations

$$\sum_{\gamma} n^\gamma = n^s + n^f = 1 \quad \varrho^s = n^s \varrho^{sR} \quad \varrho^f = n^f \varrho^{fR} \quad (1.100)$$

*Simplification 2:* Generic equations for conservation of mass for incompressible materials

$$\hat{\varrho}^{sR} = 0 \quad \Rightarrow \quad \dot{n}^s|_s + n^s \text{div}(\dot{\mathbf{x}}|_s) = \frac{\hat{\varrho}^s}{\varrho^{sR}} \quad (1.101a)$$

$$\hat{\varrho}^{fR} = 0 \quad \Rightarrow \quad \dot{n}^f|_f + n^f \text{div}(\dot{\mathbf{x}}|_f) = \frac{\hat{\varrho}^f}{\varrho^{fR}} \quad (1.101b)$$

With the further assumption of no mass source;

$$\hat{\varrho}^s = 0 \quad \Rightarrow \quad \dot{n}^s|_s + n^s \text{div}(\dot{\mathbf{x}}|_s) = 0 \quad (1.102a)$$

$$\hat{\varrho}^f = 0 \quad \Rightarrow \quad \dot{n}^f|_f + n^f \text{div}(\dot{\mathbf{x}}|_f) = 0 \quad (1.102b)$$

*Simplification 3:* The generic balance of translational momentum equations,

$$\text{div}(\boldsymbol{\sigma}^s) + \varrho^s (\check{\mathbf{f}}_b^s - \ddot{\mathbf{x}}|_s) - \hat{\varrho}^s \dot{\mathbf{x}}|_s + \hat{\mathbf{p}}^s = \mathbf{0} \quad (1.103a)$$

$$\text{div}(\boldsymbol{\sigma}^f) + \varrho^f (\check{\mathbf{f}}_b^f - \ddot{\mathbf{x}}|_f) - \hat{\varrho}^f \dot{\mathbf{x}}|_f + \hat{\mathbf{p}}^f = \mathbf{0} \quad (1.103b)$$

With the assumptions of quasi-static process, lack of body forces and lack of mass source the translational balance of momentum equation set reduce to;

$$\hat{\rho}^s = 0, \quad \check{\mathbf{f}}_b^s = \mathbf{0}, \quad \check{\mathbf{x}}|_s = \mathbf{0} \quad \Rightarrow \quad \text{div}(\boldsymbol{\sigma}^s) + \hat{\mathbf{p}}^s = \mathbf{0} \quad (1.104a)$$

$$\hat{\rho}^f = 0, \quad \check{\mathbf{f}}_b^f = \mathbf{0}, \quad \check{\mathbf{x}}|_f = \mathbf{0} \quad \Rightarrow \quad \text{div}(\boldsymbol{\sigma}^f) + \hat{\mathbf{p}}^f = \mathbf{0} \quad (1.104b)$$

*Simplification 4:* The generic inequality of the Clausius-Duhem,

$$\begin{aligned} \sum_{\gamma:f,s} \left( \dot{S}^\gamma|_\gamma - \frac{\dot{Q}^\gamma}{T^\gamma} \right) = \sum_{\gamma:f,s} (T^\gamma)^{-1} \left[ \rho^\gamma \left( -\dot{\Psi}^\gamma|_\gamma - \dot{T}^\gamma|_\gamma \check{s}^\gamma \right) + \hat{\rho}^\gamma \left( -\dot{\Psi}^\gamma + \frac{1}{2} \|\dot{\mathbf{x}}|_\gamma\|^2 \right) \right. \\ \left. - \hat{\mathbf{p}}^\gamma \cdot \dot{\mathbf{x}}|_\gamma + \boldsymbol{\sigma}^\gamma : \mathbf{D}|_\gamma - \frac{\text{grad}(T^\gamma)}{T^\gamma} \cdot \mathbf{q}^\gamma \right] \geq 0 \end{aligned} \quad (1.105)$$

The lack of mass input, lack of temperature gradients, and the assumption of isothermal process reduces the dissipation inequality as,

$$\begin{aligned} \hat{\rho}^\gamma = 0, \quad \text{grad}(T^\gamma) = \mathbf{0}, \quad \dot{T}^\gamma|_\gamma = 0 \quad T = T^s = T^f \quad \Rightarrow \\ \sum_{\gamma:f,s} \dot{D}^\gamma|_\gamma = \sum_{\gamma:f,s} T^{-1} \left[ \boldsymbol{\sigma}^\gamma : \mathbf{D}|_\gamma - \rho^\gamma \dot{\Psi}^\gamma|_\gamma + -\hat{\mathbf{p}}^\gamma \cdot \dot{\mathbf{x}}|_\gamma \right] \geq 0 \end{aligned} \quad (1.106)$$

*Simplification 5:* The simple agreement of fluid solid interaction, requires the momentum inputs to be balanced by each other.

$$\hat{\mathbf{p}}^s + \hat{\mathbf{p}}^f = \mathbf{0} \quad (1.107)$$

### 1.5.3 Constitutive Restrictions

The equations in hand for solving initial/boundary value problem -which is not explicitly stated yet- are 3 equations from the saturation and partial density relations, 2 conservation of mass equations, 3 of each in total 6 conservation of translational momentum equations, and finally 3 equations from the momentum interaction balance of constituents. According to the sum, in total 14 equations in local form are present. Additionally, the real densities in material coordinates of the constituents are known, namely 2 equalities for  $\rho^s, \rho^f$  are in hand. Those 2 equalities from the assumption of full incompressibility<sup>11</sup>, are not counted on the side of *knowns*. At final stage, one has 16 equations. The balance of angular momentum requires the true stress tensors  $\boldsymbol{\sigma}^s$  and  $\boldsymbol{\sigma}^f$  to be symmetric. Instead of considering the balance of angular momentum equation, one can admit that the number of field variables of each stress tensor to be 6, instead of 9. Furthermore, it should be stated here that, the balance of energy is not considered in this context, because in the absence of electrical, thermal and chemical effects, it does not supply more information than the conservation of

<sup>11</sup>since these are enforced completely into the other balance/unbalance equations/inequalities

translational momentum equation does.

The number of field variables are, 6 from the fluid and solid mappings ( $\mathbf{x}|_f$  and  $\mathbf{x}|_s$ ), 12 from the fluid and solid stresses ( $\boldsymbol{\sigma}^s$  and  $\boldsymbol{\sigma}^f$ ), 6 from the fluid and solid momentum inputs ( $\hat{\mathbf{p}}^s$  and  $\hat{\mathbf{p}}^f$ ), 2 from the fluid and solid spatial partial densities ( $n^f$  and  $n^s$ ), 2 spatial (yet material) fluid and solid real densities ( $\rho^{fR}$  and  $\rho^{sR}$ ) and lastly 2 variables from the apparent densities of fluid and solid phases ( $\varrho^f$  and  $\varrho^s$ ). At the end, according to the total sum, one has 30 field variables.

In mechanics, the equations which are closing the aforementioned significantly underestimated system (16-30=-14), are known to be the *constitutive relations*. To enclose the system, there are stress to gradients of mappings relationship postulates to be made. The nature of the constitutive law, is usually determined by the Helmholtz free energy function for the solids, and follows empirical statements for the case of fluids. The free energies are to be found in the entropy inequality and balance of energy equation, which are not counted to be one of the field equations, and thus not considered as a field variable here. Therefore, the resulting fact is, there are in total 12 (each 6) postulates made defining those constitutive relationships.

$$\boldsymbol{\sigma}^s = \boldsymbol{\sigma}^s (\text{Grad}|_S \mathbf{x}, \dots) \quad \boldsymbol{\sigma}^f = \boldsymbol{\sigma}^f (\text{Grad}|_F \mathbf{x}, \dots) \quad (1.108)$$

However, this function might be depending on further internal parameters, or field variables as already indicated. The same postulate can be also made for one of the momentum inputs, fore instance to the fluid constituent only, ( $\hat{\mathbf{p}}^f = \hat{\mathbf{p}}^f (\dots)$ ). The sort of dependency is consistently postulated in the following sections. A similar postulate is not done here for the case of solid phase, not to cause a conflict with the interaction equation, namely *Narrowed Governing Relations number 6*.

At the end, 12 true stress relations and 3 Ansatz relationships for the momentum input to the fluid (in total 15) are present. The final sum as the number of knowns minus the number of unknowns is, (16+15-30=-1), indicates that the system is singular. To close this redundancy, an additional unknown will be introduced in the next sections, which will enforce the saturation, and close the constitutive dependency in equation (1.108) and the fluid momentum input.

#### 1.5.4 Darcy Velocity, Saturation Rate and Pore Pressure

The definitions which are done in this subsection are necessary for constitutive modeling, building the weak form, and the finite element formulation. The *natural element* formulation are taken under consideration in a separate chapter (Ch.[5]).

### 1.5.4.1 Darcy Velocity

Darcy velocity<sup>12</sup> in soil mechanics has been known as the *velocity of the fluid molecules in the pores*. In the context of theory of mixtures, Darcy velocity is defined as the relative and thus objective spatial velocity of fluid constituent observed by the solid constituent.

$$\mathbf{w}^{fs} = \dot{\mathbf{x}}|_f - \dot{\mathbf{x}}|_s \quad (1.109)$$

It (equation (1.109)) is spatially and temporally objective, independent of the rate of the global coordinate observer.

### 1.5.4.2 Rate Form of the Saturation Condition

Rate form of the following condition is necessary to move on;

$$n^s + n^f = 1 \quad (1.110)$$

It is self-evident that the solid spatial rate form is homogeneous.

$$\dot{n}^s|_s + \dot{n}^f|_s = 0 \quad (1.111)$$

The rates of solid and volume fractions with respect to the solid fluid velocities are,

$$\begin{aligned} \dot{n}^s|_s &= \frac{\partial n^s}{\partial \mathbf{x}} \cdot \dot{\mathbf{x}}|_s = \text{grad}(n^s) \cdot \dot{\mathbf{x}}|_s & \dot{n}^f|_f &= \frac{\partial n^f}{\partial \mathbf{x}} \cdot \dot{\mathbf{x}}|_f = \text{grad}(n^f) \cdot \dot{\mathbf{x}}|_f \\ \dot{n}^s|_f &= \frac{\partial n^s}{\partial \mathbf{x}} \cdot \dot{\mathbf{x}}|_f = \text{grad}(n^s) \cdot \dot{\mathbf{x}}|_f & \dot{n}^f|_s &= \frac{\partial n^f}{\partial \mathbf{x}} \cdot \dot{\mathbf{x}}|_s = \text{grad}(n^f) \cdot \dot{\mathbf{x}}|_s \end{aligned} \quad (1.112)$$

The relative rate of fluid volume fraction can be represented in terms of the Darcy velocity,

$$\dot{n}^f|_f - \dot{n}^f|_s = \frac{\partial n^f}{\partial \mathbf{x}} \cdot \dot{\mathbf{x}}|_f - \frac{\partial n^f}{\partial \mathbf{x}} \cdot \dot{\mathbf{x}}|_s = \frac{\partial n^f}{\partial \mathbf{x}} \cdot (\dot{\mathbf{x}}|_f - \dot{\mathbf{x}}|_s) = \text{grad}(n^f) \cdot \mathbf{w}^{fs} \quad (1.113)$$

Inserting the solid rate of the fluid volume fraction back into the equation (1.111),

$$\dot{n}^s|_s + \dot{n}^f|_f - \text{grad}(n^f) \cdot \mathbf{w}^{fs} = 0 \quad (1.114)$$

The solid rate of the solid volume fraction, and the fluid rate of the fluid volume fraction can be well recalled from the reduced version of conservation of mass equations.

$$\dot{n}^s|_s = -n^s \text{div}(\dot{\mathbf{x}}|_s) = -n^s \text{tr}(\text{grad}(\dot{\mathbf{x}}|_s)) = -n^s \text{tr}(\mathbf{L}|_s) = -n^s \text{tr}(\mathbf{D}|_s) \quad (1.115a)$$

$$\dot{n}^f|_f = -n^f \text{div}(\dot{\mathbf{x}}|_f) = -n^f \text{tr}(\text{grad}(\dot{\mathbf{x}}|_f)) = -n^f \text{tr}(\mathbf{L}|_f) = -n^f \text{tr}(\mathbf{D}|_f) \quad (1.115b)$$

Where, the second equality is a tensorial identity, the third is the definition of spatial velocity gradient which is defined previously, and final equality is another basic tensorial identity,

<sup>12</sup>Some writers Ref.[<sup>Smith 2013</sup>] prefer the term *seepage*, some Ref.[<sup>J.W.Delleur 2007</sup>] prefer *pore velocity*. Here the very initial Ref.[<sup>H.Darcy 1856</sup>] definition *Darcy velocity* is taken.

which states that the skew symmetric tensors are trace-free. Inserting the last form of the volume fraction rates into the equation (1.114),

$$n^s \mathbf{D}|_s : \mathbf{I} + n^f \mathbf{D}|_f : \mathbf{I} + \text{grad}(n^f) \cdot \mathbf{w}^{fs} = 0 \quad (1.116)$$

gives the final form of the rate form of the saturation equation in terms of the stretch tensors, gradient of the fluid volume fraction and the relative fluid velocity. This equation (1.116) is used to define permeability and enables to move on with the weak form of the equation system.

### 1.5.4.3 Effective Stress and Pore Pressure

Closure of the system of equations should not violate the second law of thermodynamics, which is not considered in the set of field (in)equalities. Recalling the narrowed version of the Clausius-Duhem inequality after considering the assumptions,

$$\boldsymbol{\sigma}^s : \mathbf{D}|_s - \varrho^s \dot{\Psi}^s|_s + \hat{\mathbf{p}}^s \cdot \dot{\mathbf{x}}|_s + \boldsymbol{\sigma}^f : \mathbf{D}|_f - \varrho^f \dot{\Psi}^f|_f + \hat{\mathbf{p}}^f \cdot \dot{\mathbf{x}}|_f \geq 0 \quad (1.117)$$

Rearranging the terms and imposing the first replacement below,

$$-\hat{\mathbf{p}}^s \cdot \dot{\mathbf{x}}|_s - \hat{\mathbf{p}}^f \cdot \dot{\mathbf{x}}|_f = -\hat{\mathbf{p}}^f \cdot (\dot{\mathbf{x}}|_s - \dot{\mathbf{x}}|_f) = -\hat{\mathbf{p}}^f \cdot \mathbf{w}^{fs} \quad (1.118a)$$

$$-\varrho^s \dot{\Psi}^s|_s - \varrho^f \dot{\Psi}^f|_f + \boldsymbol{\sigma}^s : \mathbf{D}|_s + \boldsymbol{\sigma}^f : \mathbf{D}|_f - \hat{\mathbf{p}}^f \cdot \mathbf{w}^{fs} \geq 0 \quad (1.118b)$$

The rate of strain energy density function  $\dot{\Psi}^s|_s$  is defined per spatial density, recall equation (1.83). The spatial volume specific Helmholtz free energy is denoted by *grave hat* notation.

$$\dot{\Psi}^s|_s = \varrho^s \dot{\Psi}^s|_s \quad (1.119)$$

This assumption is a conclusion of the fact that, the rate of the Helmholtz energy is free, not the energy, which is arbitrarily integrated in time. Defining the Helmholtz free energy flux, similar to equation (1.83) one gets;

$$\dot{\mathcal{A}}^s = \int_{\Omega_s} \varrho^s \dot{\Psi}^s dv = \int_{\Omega_s} \dot{\Psi}^s|_s dv = \int_{\Omega_s} \dot{\Psi}^s|_s dV^S \quad (1.120)$$

The above statement of (1.120) is conform with (1.84a) and (1.84b). In many context, the Helmholtz free energy is meant to be material volume specific one, as shown in the last integral of equation (1.120). Together with the last comments, equation (1.118b) can be represented by the spatial volume specific free energies as follows,

$$-\dot{\Psi}^s|_s - \dot{\Psi}^f|_f + \boldsymbol{\sigma}^s : \mathbf{D}|_s + \boldsymbol{\sigma}^f : \mathbf{D}|_f - \hat{\mathbf{p}}^f \cdot \mathbf{w}^{fs} \geq 0 \quad (1.121)$$

Recalling the rate form of the saturation equation (1.116), over-scaling it with an arbitrary parameter  $\lambda$ , and adding it to the last form of the entropy inequality leads into;

$$\begin{aligned} & -\dot{\Psi}^s|_s - \dot{\Psi}^f|_f \\ & + (\boldsymbol{\sigma}^s + \lambda n^s \mathbf{I}) : \mathbf{D}|_s + (\boldsymbol{\sigma}^f + \lambda n^f \mathbf{I}) : \mathbf{D}|_f \\ & + \left( \lambda \text{grad}(n^f) - \hat{\mathbf{p}}^f \right) \cdot \mathbf{w}^{fs} \geq 0 \end{aligned} \quad (1.122)$$

Remembering that the fluid part is fully incompressible and postulating another intermediate assumption that the flow is inviscid, there is only the rate of current volume specific Helmholtz free energy is remaining<sup>13</sup>,

$$\begin{aligned}
\dot{\Psi}^s|_s &= (\det(\mathbf{F}|_S))^{-1} \dot{\Psi}^s|_s = (\det(\mathbf{F}|_S))^{-1} \frac{\partial \Psi}{\partial \mathbf{C}|_S} : \overline{(\mathbf{F}^T|_S \cdot \dot{\mathbf{F}}|_S)} \Big|_s \\
&= (\det(\mathbf{F}|_S))^{-1} \frac{\partial \Psi}{\partial \mathbf{C}|_S} : \left( \dot{\mathbf{F}}^T|_{sS} \cdot \mathbf{F}|_S + \mathbf{F}^T|_S \cdot \dot{\mathbf{F}}|_{sS} \right) \\
&= (\det(\mathbf{F}|_S))^{-1} \frac{\partial \Psi}{\partial \mathbf{C}|_S} : \left( \mathbf{F}^T|_S \cdot \mathbf{L}^T|_S \cdot \mathbf{F}|_S + \mathbf{F}^T|_S \cdot \mathbf{L}|_S \cdot \mathbf{F}|_S \right) \\
&= (\det(\mathbf{F}|_S))^{-1} \frac{\partial \Psi}{\partial \mathbf{C}|_S} : \left( \mathbf{F}^T|_S \cdot 2\mathbf{D}|_S \cdot \mathbf{F}|_S \right) \\
&= 2(\det(\mathbf{F}|_S))^{-1} \left[ \mathbf{F}|_S \cdot \frac{\partial \Psi}{\partial \mathbf{C}|_S} \cdot \mathbf{F}^T|_S \right] : \mathbf{D}|_S \\
&= (J^{-1}|_S \mathbf{F}|_S \cdot \mathbf{S}_e^S \cdot \mathbf{F}^T|_S) : \mathbf{D}|_S = \boldsymbol{\sigma}_e^s : \mathbf{D}|_S
\end{aligned} \tag{1.123}$$

The initial replacement of the determinant of solid deformation gradient results from equation (1.120). After this conversion, the time derivative can be taken with respect to the strain tensors with material coordinate base vectors. The part of the stress tensor depending on the material-specific free energy function is the so called *effective stress tensor*. Back substitution of effective stress into the last version of dissipation inequality results in;

$$(\boldsymbol{\sigma}^s + \lambda n^s \mathbf{I} - \boldsymbol{\sigma}_e^s) : \mathbf{D}|_s + (\boldsymbol{\sigma}^f + \lambda n^f \mathbf{I}) : \mathbf{D}|_f + \left( \lambda \text{grad}(n^f) - \hat{\mathbf{p}}^f \right) \cdot \mathbf{w}^{fs} \geq 0 \tag{1.124}$$

According to the definition of effective stress and pore pressure, the first two terms in the equation above are free of dissipation. The true total stresses of solid and fluid constituents are then,

$$\boldsymbol{\sigma}^s = \boldsymbol{\sigma}_e^s - \lambda n^s \mathbf{I} \quad \boldsymbol{\sigma}^f = -\lambda n^f \mathbf{I} \tag{1.125}$$

The meaning of parameter lambda, introduced for closing the slightly overestimated system of equations gets clearness now. The parameter acts as a penalty parameter of pressure, reducing the effective stress, which is proportional to the volume fraction of each component. The initial expectation of that the volume fraction is proportional with the pore pressure and inversely proportional with the total stress of the solid phase is in fact a deception. One can not expect high pore pressures from almost (densely) filled void-free continuum solid. The opposite of this can be explained by means of the intrinsic dependence of parameter lambda to the other field parameters and roleplayers, volume fraction being among them. Returning back, the dissipation can be summarized as;

$$\left( \lambda \text{grad}(n^f) - \hat{\mathbf{p}}^f \right) \cdot \mathbf{w}^{fs} \geq 0 \tag{1.126}$$

<sup>13</sup>The intermediate steps of the equation (1.123) can be verified by any tensor algebra reference, such as Ref. [J.Bonet 2008]

#### 1.5.4.4 Momentum input constitutive law

For the postulate of constitutive law for the momentum input to the fluid constituent, one should consider the thermodynamic consistency, i.e. no violation of Darcy velocity dependent dissipation inequality. One postulate<sup>14</sup> can be done accordingly,

$$\begin{aligned} \hat{\mathbf{p}}^f &= \lambda \text{grad} \left( n^f \right) - \beta \mathbf{w}^{fs} \\ \left( \lambda \text{grad} \left( n^f \right) - \hat{\mathbf{p}}^f \right) \cdot \mathbf{w}^{fs} &= \beta \left| \mathbf{w}^{fs} \right|^2 \geq 0 \quad \Leftrightarrow \quad \beta \geq 0 \end{aligned} \quad (1.127)$$

Recalling the momentum equation for fluid with body forces,

$$\text{div} \left( \boldsymbol{\sigma}^f \right) + \varrho^f \check{\mathbf{f}}_b^f + \hat{\mathbf{p}}^f = \mathbf{0} \quad (1.128)$$

According to this equation, by replacing the fluid true stress with fluid pore pressure the momentum input becomes,

$$\hat{\mathbf{p}}^f = \text{div} \left( \lambda n^f \mathbf{I} \right) - \varrho^f \check{\mathbf{f}}_b^f \quad (1.129)$$

In indicial notation,

$$\frac{\partial \left( \lambda n^f \delta_{ij} \right)}{\partial x_i} = n^f \text{grad} \left( \lambda \right)_i \delta_{ij} + \lambda \text{grad} \left( n^f \right)_i \delta_{ij} = n^f \text{grad} \left( \lambda \right)_j + \lambda \text{grad} \left( n^f \right)_j \quad (1.130)$$

Inserting this expression back into the constitutive law for the momentum input to the fluid gives the final expression for the determination of the Darcy velocity,

$$\begin{aligned} n^f \text{grad} \left( \lambda \right) + \lambda \text{grad} \left( n^f \right) - \varrho^f \check{\mathbf{f}}_b^f &= \lambda \text{grad} \left( n^f \right) - \beta \mathbf{w}^{fs} \\ \Rightarrow \quad \mathbf{w}^{fs} &= \beta^{-1} \left( \varrho^f \check{\mathbf{f}}_b^f - n^f \text{grad} \left( \lambda \right) \right) \end{aligned} \quad (1.131)$$

## 1.6 Weak Forms

In this section, the weak forms of conservations of balance, translational momentum and mass differential equations are introduced after each other. The weak forms in spatial coordinates are pulled back into solid material coordinates, and the cumulative weak forms are presented in terms of the solid material coordinates.

### 1.6.1 Weak Form of Balance of Translational Momentum in Solid Material Coordinates

For a quasi-static process, the balance of momentum equations in the absence of mass input and in the presence of body forces become,

$$\text{div} \left( \boldsymbol{\sigma}^s \right) + \varrho^s \check{\mathbf{f}}_b^s + \hat{\mathbf{p}}^s = \mathbf{0} \quad (1.132a)$$

$$\text{div} \left( \boldsymbol{\sigma}^f \right) + \varrho^f \check{\mathbf{f}}_b^f + \hat{\mathbf{p}}^f = \mathbf{0} \quad (1.132b)$$

<sup>14</sup>The parameter  $\beta$  postulated here can be seen as the *Impermeability* and depends on the current morphology of the continuum neighborhood.



The virtual power principle gives the variational power of each balance equation under variational changes of spatial velocities.

$$\begin{aligned}\delta\dot{W}^s &= \int_{\Omega_s} \left( \operatorname{div}(\boldsymbol{\sigma}^s) + \varrho^s \check{\mathbf{f}}_b^s + \hat{\mathbf{p}}^s \right) \cdot \delta\dot{\mathbf{x}}|_s \, dv = 0 \\ \delta\dot{W}^f &= \int_{\Omega_f} \left( \operatorname{div}(\boldsymbol{\sigma}^f) + \varrho^f \check{\mathbf{f}}_b^f + \hat{\mathbf{p}}^f \right) \cdot \delta\dot{\mathbf{x}}|_f \, dv = 0\end{aligned}\quad (1.133)$$

Since the stresses are functions of deformation gradients, this weak form includes second gradients of the displacements and can be further weakened by integration by parts. The virtual power supplied by the divergence of true stress is,

$$\operatorname{div}(\boldsymbol{\sigma}^\gamma) \cdot \delta\dot{\mathbf{x}}|_\gamma = \operatorname{div}(\boldsymbol{\sigma}^{\gamma T} \cdot \delta\dot{\mathbf{x}}|_\gamma) - \boldsymbol{\sigma}^\gamma : \delta\mathbf{D}|_\gamma \quad (1.134)$$

The more weakened version of virtual power equation set becomes;

$$\begin{aligned}\int_{\Omega_s} (\boldsymbol{\sigma}^s : \delta\mathbf{D}|_s) \, dv &= \int_{\Omega_s} \operatorname{div}(\boldsymbol{\sigma}^{sT} \cdot \delta\dot{\mathbf{x}}|_s) \, dv + \int_{\Omega_s} \varrho^s \check{\mathbf{f}}_b^s \cdot \delta\dot{\mathbf{x}}|_s \, dv + \int_{\Omega_s} \hat{\mathbf{p}}^s \cdot \delta\dot{\mathbf{x}}|_s \, dv \\ \int_{\Omega_f} (\boldsymbol{\sigma}^f : \delta\mathbf{D}|_f) \, dv &= \int_{\Omega_f} \operatorname{div}(\boldsymbol{\sigma}^{fT} \cdot \delta\dot{\mathbf{x}}|_f) \, dv + \int_{\Omega_f} \varrho^f \check{\mathbf{f}}_b^f \cdot \delta\dot{\mathbf{x}}|_f \, dv + \int_{\Omega_f} \hat{\mathbf{p}}^f \cdot \delta\dot{\mathbf{x}}|_f \, dv\end{aligned}\quad (1.135)$$

By the application of Gauss divergence theorem, the first integrals on the right hand side of the equations can be represented by means of the surface tractions,

$$\begin{aligned}\int_{\Omega_s} (\boldsymbol{\sigma}^s : \delta\mathbf{D}|_s) \, dv &= \int_{\Omega_s} \mathbf{t}^s \cdot \delta\dot{\mathbf{x}}|_s \, da + \int_{\Omega_s} \varrho^s \check{\mathbf{f}}_b^s \cdot \delta\dot{\mathbf{x}}|_s \, dv + \int_{\Omega_s} \hat{\mathbf{p}}^s \cdot \delta\dot{\mathbf{x}}|_s \, dv \\ \int_{\Omega_f} (\boldsymbol{\sigma}^f : \delta\mathbf{D}|_f) \, dv &= \int_{\Omega_f} \mathbf{t}^f \cdot \delta\dot{\mathbf{x}}|_f \, da + \int_{\Omega_f} \varrho^f \check{\mathbf{f}}_b^f \cdot \delta\dot{\mathbf{x}}|_f \, dv + \int_{\Omega_f} \hat{\mathbf{p}}^f \cdot \delta\dot{\mathbf{x}}|_f \, dv\end{aligned}\quad (1.136)$$

The rate form of the saturation condition combined with the balance of conservation of mass can be formulated as follows,

$$\mathbf{I} : n^s \mathbf{D}|_s + \mathbf{I} : n^f \mathbf{D}|_f + \frac{1}{3} (\mathbf{I} : \mathbf{I}) \left( \operatorname{grad}(n^f) \cdot \mathbf{w}^{fs} \right) = 0 \quad (1.137)$$

With the dot product of fluid true stress tensor,

$$n^s \boldsymbol{\sigma}^f : \mathbf{D}|_s + n^f \boldsymbol{\sigma}^f : \mathbf{D}|_f + \frac{\operatorname{tr}(\boldsymbol{\sigma}^f)}{3} \left( \operatorname{grad}(n^f) \cdot \mathbf{w}^{fs} \right) = 0 \quad (1.138)$$

The virtual power caused by the fluid stress can be represented in terms of the virtual rate of solid spin tensor as,

$$\begin{aligned}\boldsymbol{\sigma}^f : \delta\mathbf{D}|_f &= -\frac{n^s}{n^f} \boldsymbol{\sigma}^f : \delta\mathbf{D}|_s + \lambda n^f \left( \operatorname{grad}(n^f) \cdot \delta\mathbf{w}^{fs} \right) \\ &= \boldsymbol{\sigma}^f : \delta\mathbf{D}|_s - \frac{1}{n^f} \boldsymbol{\sigma}^f : \delta\mathbf{D}|_s + \lambda n^f \left( \operatorname{grad}(n^f) \cdot \delta\mathbf{w}^{fs} \right) \\ &= \boldsymbol{\sigma}^f : \delta\mathbf{D}|_s + \lambda \mathbf{I} : \delta\mathbf{D}|_s + \lambda n^f \left( \operatorname{grad}(n^f) \cdot \delta\mathbf{w}^{fs} \right)\end{aligned}\quad (1.139)$$

Replacing the left hand side of equation (1.136) with equation (1.139) leads a complicated cumulative weak form. It is in general not suggested<sup>15</sup> to punish the strong form, namely the original balance of equation of mass and translational momentum with the variations of the realistic test functions. Instead, both strong forms (fluid and solid) are projected onto the test functions of variations of the solid velocity, to get more weaker, however in a more simplified manner. The accumulated virtual power equation becomes thereafter,

$$\begin{aligned} \delta\dot{W} &= \delta\dot{W}^s + \delta\dot{W}^f \\ &= \int_{\Omega_s} \left( \text{div}(\boldsymbol{\sigma}^s) + \varrho^s \check{\mathbf{f}}_b^s + \hat{\mathbf{p}}^s + \text{div}(\boldsymbol{\sigma}^f) + \varrho^f \check{\mathbf{f}}_b^f + \hat{\mathbf{p}}^f \right) \cdot \delta\dot{\mathbf{x}}|_s \, dv = 0 \end{aligned} \quad (1.140)$$

Imposing the fact that the momentum input should be canceled by each other, assuming that the body forces are equal, and spreading the divergence operator into the total sum of true stresses with effective stresses and pore pressures,

$$\begin{aligned} \delta\dot{W} &= \int_{\Omega_s} \left( \text{div}(\boldsymbol{\sigma}_e^s - n^s \lambda \mathbf{I} - n^f \lambda \mathbf{I}) + \check{\mathbf{f}}_b(\varrho^s + \varrho^f) \right) \cdot \delta\dot{\mathbf{x}}|_s \\ &= \int_{\Omega_s} \left( \text{div}(\boldsymbol{\sigma}_e^s - \lambda \mathbf{I}) + \check{\mathbf{f}}_b(\varrho^s + \varrho^f) \right) \cdot \delta\dot{\mathbf{x}}|_s \, dv = 0 \end{aligned} \quad (1.141)$$

Following the same procedure,

$$\int_{\Omega_s} ((\boldsymbol{\sigma}_e^s - \lambda \mathbf{I}) : \delta \mathbf{D}|_s) \, dv = \int_{\Omega_s} \dot{\mathbf{t}}^s \cdot \delta\dot{\mathbf{x}}|_s \, da + \int_{\Omega_s} (\varrho^s + \varrho^f) \check{\mathbf{f}}_b \cdot \delta\dot{\mathbf{x}}|_s \, dv \quad (1.142)$$

Where the traction vector is not corresponding to the real true stress traction. Similarly, although there is no direct physical correspondence (or not straightly expressible if there is any), it is assumed that there is a mapping exists in between the material fluid and solid coordinates<sup>16</sup>. Accordingly, there is a tangent mapping in between those two material tangents,

$$\mathbf{F}|_{SF} = \frac{\partial \mathbf{X}|_S}{\partial \mathbf{X}|_F} = \left( \frac{\partial \mathbf{x}|_s}{\partial \mathbf{X}|_S} \right)^{-1} \cdot \frac{\partial \mathbf{x}|_f}{\partial \mathbf{X}|_F} = \mathbf{F}^{-1}|_S \cdot \mathbf{F}|_F \quad (1.143)$$

Since the pull-back operation is kinematically multiplicative, first pulling back the current fluid tensors to the fluid material tensors, and then pulling back to those fluid material tensors into the solid material coordinates is identical to pulling back all the tensors from current coordinates to the solid material coordinates. By doing so, the virtual internal power becomes;

$$\begin{aligned} \delta\dot{W}^{int} &= \int_{\Omega_S} \left( (\mathbf{S}_e^s - \lambda \mathbf{C}^{-1}) : \delta \dot{\mathbf{E}}|_s \right) \, dV^S \\ &= \int_{\Omega_S} \frac{1}{2} \left( (\mathbf{S}_e^s - \lambda \mathbf{C}^{-1}) : \delta \dot{\mathbf{C}}|_s \right) \, dV^S \end{aligned} \quad (1.144)$$

<sup>15</sup>the writer did not observe references, which performs the action other way around

<sup>16</sup>The physical existence of this mapping would indicate that one reference phase turns into other reference phase, which indicates in fact a very fast chemical phase transition. This type of processes are neglected, as stated in the section of Ch.[1.5]. Nevertheless, a mathematical tangent mapping is definable and necessary, and thus defined.

### 1.6.2 Weak Form of Conservation of Mass

As done for the conservation of translational momentum, for the conservation of mass, the integral form of the cumulative sum of the mixture is considered.

$$\int_{\Omega_s} \left( \dot{n}^s|_s + \dot{n}^f|_f + n^s \operatorname{div}(\dot{\mathbf{x}}|_s) + n^f \operatorname{div}(\dot{\mathbf{x}}|_f) \right) dv = 0 \quad (1.145)$$

Replacing the first two components with equation (1.114),

$$\int_{\Omega_s} \left( \operatorname{grad}(n^f) \cdot \mathbf{w}^{fs} + n^s \operatorname{div}(\dot{\mathbf{x}}|_s) + n^f \operatorname{div}(\dot{\mathbf{x}}|_f) \right) dv = 0 \quad (1.146)$$

Applying further modification on the last two terms to eliminate solid volume fraction and fluid velocity,

$$\int_{\Omega_s} \left[ \operatorname{grad}(n^f) \cdot \mathbf{w}^{fs} + (1 - n^f) \operatorname{div}(\dot{\mathbf{x}}|_s) + n^f \left( \operatorname{div}(\dot{\mathbf{x}}|_s) + \operatorname{div}(\mathbf{w}^{fs}) \right) \right] dv = 0 \quad (1.147)$$

Recalling the following divergence to gradient tensor identity,

$$\operatorname{div}(n^f \mathbf{w}^{fs}) = \operatorname{grad}(n^f) \cdot \mathbf{w}^{fs} + n^f \operatorname{div}(\mathbf{w}^{fs}) \quad (1.148)$$

Replacing the first and the fourth terms with this identity, and adding the second and the third terms gives the final expression for the cumulative conservation of mass equation in integral form, free of fluid velocity and solid fraction.

$$\int_{\Omega_s} \left( \operatorname{div}(\dot{\mathbf{x}}|_s) + \operatorname{div}(n^f \mathbf{w}^{fs}) \right) dv \quad (1.149)$$

The weak form is then,

$$\int_{\Omega_s} \left( \operatorname{div}(\dot{\mathbf{x}}|_s) + \operatorname{div}(n^f \mathbf{w}^{fs}) \right) \delta \lambda dv \quad (1.150)$$

Applying integration by parts to the second term,

$$\begin{aligned} \int_{\Omega_s} \operatorname{div}(n^f \mathbf{w}^{fs}) \delta \lambda dv &= \int_{\Omega_s} \operatorname{div}(n^f \mathbf{w}^{fs} \delta \lambda) dv - \int_{\Omega_s} n^f \mathbf{w}^{fs} \cdot \operatorname{grad}(\delta \lambda) dv \\ &= \int_{\Omega_s} (n^f \mathbf{w}^{fs} \delta \lambda) \cdot \mathbf{n} da - \int_{\Omega_s} n^f \mathbf{w}^{fs} \cdot \operatorname{grad}(\delta \lambda) dv \end{aligned} \quad (1.151)$$

The internal weak form becomes,

$$\delta \hat{M}^{int} = \int_{\Omega_s} \operatorname{div}(\dot{\mathbf{x}}|_s) \delta \lambda dv - \int_{\Omega_s} n^f \mathbf{w}^{fs} \cdot \operatorname{grad}(\delta \lambda) dv \quad (1.152)$$

Recalling the *Ansatz* for the relative fluid velocity including the pore impermeability coefficient;

$$\delta \hat{M}^{int} = \int_{\Omega_s} \operatorname{tr}(\mathbf{D}|_s) \delta \lambda dv + \int_{\Omega_s} \beta^{-1} (n^f)^2 \operatorname{grad}(\lambda) \cdot \operatorname{grad}(\delta \lambda) dv \quad (1.153)$$

For the material frame formulation the gradients of the second term should be pulled back to the solid material gradients as follows,

$$\mathit{grad}(\lambda) \cdot \mathit{grad}(\delta\lambda) = \mathbf{F}^{-T}|_s \cdot \mathit{Grad}(\lambda) \cdot \mathbf{F}^{-T}|_s \cdot \mathit{Grad}(\delta\lambda) = \mathit{Grad}(\lambda) \cdot \mathbf{C}^{-1}|_s \cdot \mathit{Grad}(\delta\lambda) \quad (1.154)$$

Additionally, from the long expression of equation (1.123) one gets;

$$\mathbf{D}|_s = \frac{1}{2} \mathbf{F}^{-T}|_s \cdot \dot{\mathbf{C}}|_s \cdot \mathbf{F}^{-1}|_s \quad (1.155)$$

Using these identities, the final form in the solid material coordinates ends up;

$$\begin{aligned} \delta \dot{M}^{int} &= \int_{\Omega_s} \mathbf{I} : \mathbf{D}|_s \delta\lambda dv + \int_{\Omega_s} [\mathbf{C}^{-1}|_s : (\mathit{Grad}(\lambda) \otimes \mathit{Grad}(\delta\lambda))] dv \\ &= \int_{\Omega_s} \left[ J^{-1}|_s \mathbf{C}^{-1}|_s : \dot{\mathbf{C}}|_s \right] \delta\lambda dV^S \\ &\quad + \int_{\Omega_s} \left[ \beta^{-1} (n^f)^2 J^{-1}|_s \mathbf{C}^{-1}|_s : (\mathit{Grad}(\lambda) \otimes \mathit{Grad}(\delta\lambda)) \right] dV^S \end{aligned} \quad (1.156)$$

## 1.7 Discretized balance equations

The linearized field equations are to be solved for final verification. For this purpose, finite element method, as well as natural element method(see Ch.[5]) are used. Higher order tensorial quantities are represented in terms of matrix algebra, if necessary Voigt-type notations are applied. Following this, the total Lagrangian approximations are presented. The necessary material time derivations based on Newmark's method are presented briefly. Finally, the matrix-vector algebraic form are linearized for preparing the system of equations for an iterative solution.

### 1.7.1 Matrix-Vector Form on Total Lagrangian Configuration

For the matrix-vector notations of the tensors, calligraphy symbols<sup>17</sup> are used. The tensors which are converted into Voigt notation are namely, the second Piola-Kirchhoff stress tensor, the Cauchy strain tensor and the inverse of it, and the dyad of material gradient of pore pressure variable  $\lambda$  with the variation of material gradient of it.

$$\begin{aligned} \mathbf{s}|_s &= [S_{XX}^S, S_{YY}^S, S_{ZZ}^S, S_{XY}^S, S_{YZ}^S, S_{ZX}^S]^T \\ \mathbf{c}|_s &= [C_{XX}^S, C_{YY}^S, C_{ZZ}^S, 2C_{XY}^S, 2C_{YZ}^S, 2C_{ZX}^S]^T \\ \mathbf{c}^{-1}|_s &= \left[ (C^{-1})_{XX}^S, (C^{-1})_{YY}^S, (C^{-1})_{ZZ}^S, (C^{-1})_{XY}^S, (C^{-1})_{YZ}^S, (C^{-1})_{ZX}^S \right]^T \\ \delta \dot{\mathbf{c}}|_s &= \left[ \delta \dot{C}_{XX}^S, \delta \dot{C}_{YY}^S, \delta \dot{C}_{ZZ}^S, 2\delta \dot{C}_{XY}^S, 2\delta \dot{C}_{YZ}^S, 2\delta \dot{C}_{ZX}^S \right]^T \end{aligned} \quad (1.157)$$

<sup>17</sup>Throughout the treatise, other forms of symbols are also used. If the notation changes, the information will follow. Please refer to the front-page of *List of Abbreviations*.

The missing coefficients in the off-diagonal terms of the inverse Cauchy strain tensor are dropped on purpose, because this tensor acts as a pulled back stress tensor in the weak form. The total variational weak form is;

$$\begin{aligned}
\delta\dot{W}^{int} + \delta\dot{M}^{int} &= \int_{\Omega_S} \frac{1}{2} \left( (\mathbf{S}_e^s - \lambda \mathbf{C}^{-1}) : \delta\dot{\mathbf{C}}|_s \right) dV^S \\
&+ \int_{\Omega_s} \left[ J^{-1}|_s \mathbf{C}^{-1}|_s : \dot{\mathbf{C}}|_s \right] \delta\lambda dV^S \\
&+ \int_{\Omega_s} \left[ \beta^{-1} (n^f)^2 J^{-1}|_s \mathbf{C}^{-1}|_s : (\text{Grad}(\lambda) \otimes \text{Grad}(\delta\lambda)) \right] dV^S
\end{aligned} \tag{1.158}$$

Using the symmetry property of the inverse Cauchy strain tensor, the last double contraction can be reformulated,

$$\begin{aligned}
\mathbf{C}^{-1}|_s : (\text{Grad}(\lambda) \otimes \text{Grad}(\delta\lambda)) &= \mathbf{C}^{-1}|_s : \frac{1}{2} [\text{Grad}(\lambda) \otimes \text{Grad}(\delta\lambda) + \text{Grad}(\delta\lambda) \otimes \text{Grad}(\lambda)] \\
&= \mathbf{C}^{-1}|_s : \frac{\delta}{2} (\text{Grad}(\lambda) \otimes \text{Grad}(\lambda)) \\
&= (\mathbf{c}^{-1}|_s)^T \cdot \delta\mathbf{Q}|_s
\end{aligned} \tag{1.159}$$

Now the right hand side of the contraction can be also represented in 6 to 1 Voigt notation.

$$\begin{aligned}
&\frac{1}{2} \left[ \delta \frac{\partial^2 \lambda}{\partial X^2}, \quad \delta \frac{\partial^2 \lambda}{\partial Y^2}, \quad \delta \frac{\partial^2 \lambda}{\partial Z^2}, \quad \delta \frac{\partial \lambda}{\partial X} \frac{\partial \lambda}{\partial Y}, \quad \delta \frac{\partial \lambda}{\partial Y} \frac{\partial \lambda}{\partial Z}, \quad \delta \frac{\partial \lambda}{\partial Z} \frac{\partial \lambda}{\partial X} \right]^T \\
&= \frac{1}{2} \left[ 2 \frac{\partial \delta \lambda}{\partial X} \frac{\partial \lambda}{\partial X}, \quad 2 \frac{\partial \delta \lambda}{\partial Y} \frac{\partial \lambda}{\partial Y}, \quad 2 \frac{\partial \delta \lambda}{\partial Z} \frac{\partial \lambda}{\partial Z}, \right. \\
&\quad \left. \frac{\partial \delta \lambda}{\partial X} \frac{\partial \lambda}{\partial Y} + \frac{\partial \lambda}{\partial X} \frac{\partial \delta \lambda}{\partial Y}, \quad \frac{\partial \delta \lambda}{\partial Y} \frac{\partial \lambda}{\partial Z} + \frac{\partial \lambda}{\partial Y} \frac{\partial \delta \lambda}{\partial Z}, \quad \frac{\partial \delta \lambda}{\partial Z} \frac{\partial \lambda}{\partial X} + \frac{\partial \lambda}{\partial Z} \frac{\partial \delta \lambda}{\partial X} \right]^T \approx \delta\mathbf{Q}|_s
\end{aligned} \tag{1.160}$$

The matrix-vector notation is certainly nonlinear, and is visited in the next chapters in detail. The total variational weak form in matrix-vector notation is then,

$$\begin{aligned}
\delta\dot{W}^{int} + \delta\dot{M}^{int} &= \frac{1}{2} \int_{\Omega_S} \left( \delta\dot{\mathbf{c}}^T|_s \cdot (\mathbf{S}_e^s - \lambda \mathbf{c}^{-1}) \right) dV^S \\
&+ \int_{\Omega_s} \left( J^{-1}|_s \dot{\mathbf{c}}^T|_s \cdot \mathbf{c}^{-1}|_s \right) \delta\lambda dV^S \\
&+ \int_{\Omega_s} \left( \beta^{-1} (n^f)^2 J^{-1}|_s \delta\mathbf{Q}^T|_s \cdot \mathbf{c}^{-1}|_s \right) dV^S
\end{aligned} \tag{1.161}$$

### 1.7.2 Newmark-Method-Consistent Material Time Derivatives

The Newmark method and the algorithm of it are usually used for conditionally stable time integration of rate dependent discrete forms of weak differential equations. Since the inertial effects are neglected, only the time derivatives are presented here. Newmark postulated in his original work Ref. [Newmark 1959], fourth order and third order series expansions for displacement and the velocity (not necessarily spatial) respectively. With the notation which is adapted to finite deformation theory,

$$\begin{aligned} \mathbf{u}(\mathbf{X}, t) &= \mathbf{u}(\mathbf{X}, t - \Delta t) + \Delta t \dot{\mathbf{u}}(\mathbf{X}, t - \Delta t) \\ &+ \frac{(\Delta t)^2}{2} \ddot{\mathbf{u}}(\mathbf{X}, t - \Delta t) + \frac{(\Delta t)^3}{6} \dddot{\mathbf{u}}(\mathbf{X}, t - \Delta t) + \dots \end{aligned} \quad (1.162)$$

$$\dot{\mathbf{u}}(\mathbf{X}, t) = \dot{\mathbf{u}}(\mathbf{X}, t - \Delta t) + \Delta t \ddot{\mathbf{u}}(\mathbf{X}, t - \Delta t) + \frac{(\Delta t)^2}{2} \dddot{\mathbf{u}}(\mathbf{X}, t - \Delta t) + \dots$$

The effect of the remainders can be manipulated by applying a variable coefficient to the last terms of the expansions. The newmark type deformation and the rate (spatial or material material) of deformation are given as;

$$\begin{aligned} \mathbf{u}(\mathbf{X}, t) &= \mathbf{u}(\mathbf{X}, t - \Delta t) + \Delta t \dot{\mathbf{u}}(\mathbf{X}, t - \Delta t) + \frac{(\Delta t)^2}{2} \ddot{\mathbf{u}}(\mathbf{X}, t - \Delta t) + \beta_1 (\Delta t)^3 \dddot{\mathbf{u}}(\mathbf{X}, t - \Delta t) \\ \dot{\mathbf{u}}(\mathbf{X}, t) &= \dot{\mathbf{u}}(\mathbf{X}, t - \Delta t) + \Delta t \ddot{\mathbf{u}}(\mathbf{X}, t - \Delta t) + \beta_2 (\Delta t)^2 \dddot{\mathbf{u}}(\mathbf{X}, t - \Delta t) \end{aligned} \quad (1.163)$$

Assuming there is (was)-at least backward-linear acceleration field, one gets the following expression.

$$\ddot{\mathbf{u}}(\mathbf{X}, t - \Delta t) = \frac{\ddot{\mathbf{u}}(\mathbf{X}, t) - \ddot{\mathbf{u}}(\mathbf{X}, t - \Delta t)}{\Delta t} \quad (1.164)$$

Inserting the rate of acceleration term into equation (1.163), one gets deformation, velocity and acceleration dependent Newmark series,

$$\begin{aligned} \mathbf{u}(\mathbf{X}, t) &= \mathbf{u}(\mathbf{X}, t - \Delta t) + \Delta t \dot{\mathbf{u}}(\mathbf{X}, t - \Delta t) \\ &+ \left( \frac{1}{2} - \beta_1 \right) (\Delta t)^2 \ddot{\mathbf{u}}(\mathbf{X}, t - \Delta t) + \beta_1 (\Delta t)^2 \ddot{\mathbf{u}}(\mathbf{X}, t) \\ \dot{\mathbf{u}}(\mathbf{X}, t) &= \dot{\mathbf{u}}(\mathbf{X}, t - \Delta t) + (1 - \beta_2) \Delta t \ddot{\mathbf{u}}(\mathbf{X}, t - \Delta t) + \beta_2 \Delta t \ddot{\mathbf{u}}(\mathbf{X}, t) \end{aligned} \quad (1.165)$$

The current velocity and the current acceleration are considered to be unknowns. The current acceleration from the first equation above yields into;

$$\begin{aligned} \ddot{\mathbf{u}}(\mathbf{X}, t) &= \frac{1}{\beta_1 (\Delta t)^2} \mathbf{u}(\mathbf{X}, t) - \frac{1}{\beta_1 (\Delta t)^2} \mathbf{u}(\mathbf{X}, t - \Delta t) \\ &- \frac{1}{\beta_1 \Delta t} \dot{\mathbf{u}}(\mathbf{X}, t - \Delta t) - \left( \frac{1}{2\beta_1} - 1 \right) \ddot{\mathbf{u}}(\mathbf{X}, t - \Delta t) \end{aligned} \quad (1.166)$$

Inserting this expression into the second equation gives;

$$\begin{aligned} \dot{\mathbf{u}}(\mathbf{X}, t) &= \dot{\mathbf{u}}(\mathbf{X}, t - \Delta t) + (1 - \beta_2) \Delta t \ddot{\mathbf{u}}(\mathbf{X}, t - \Delta t) \\ &+ \frac{\beta_2}{\beta_1 \Delta t} \mathbf{u}(\mathbf{X}, t) - \frac{\beta_2}{\beta_1 \Delta t} \mathbf{u}(\mathbf{X}, t - \Delta t) \\ &- \frac{\beta_2}{\beta_1} \dot{\mathbf{u}}(\mathbf{X}, t - \Delta t) - \left( \frac{\beta_2}{2\beta_1} - \beta_2 \right) \Delta t \ddot{\mathbf{u}}(\mathbf{X}, t - \Delta t) \end{aligned} \quad (1.167)$$

Neglecting at this stage the terms causing inertial effects, namely acceleration,

$$\dot{\mathbf{u}}(\mathbf{X}, t) = \frac{\beta_2}{\beta_1 \Delta t} \mathbf{u}(\mathbf{X}, t) - \frac{\beta_2}{\beta_1 \Delta t} \mathbf{u}(\mathbf{X}, t - \Delta t) + \left( 1 - \frac{\beta_2}{\beta_1} \right) \dot{\mathbf{u}}(\mathbf{X}, t - \Delta t) \quad (1.168)$$

Taking that the series is expanded around the initial time, in the material configuration, leaves one with the following identities;

$$t - \Delta t = t_0 \quad \Rightarrow \quad \mathbf{u}(\mathbf{X}, t - \Delta t) = \mathbf{x}(\mathbf{X}, t_0) - \mathbf{X} = \mathbf{0}, \quad \dot{\mathbf{u}}(\mathbf{X}, t - \Delta t) = \mathbf{0} \quad (1.169)$$

The Newmark consistent material time derivative becomes;

$$\dot{\mathbf{u}}(\mathbf{X}, t) = \frac{\beta_2}{\beta_1 t} \mathbf{u}(\mathbf{X}, t) \quad (1.170)$$

This material time derivative can be applied for each variable with homogeneous initial conditions.

### 1.7.3 Discrete Form of the Translational Momentum Part

Apart from the pore pressure term, the discrete form of the first addend of equation (1.161), can be found elsewhere. However, for the sake of completeness and adaptedness to the following sections, the derivation proposed by Zienkiewicz Ref. [O.C. Zienkiewicz 2000b] is re-introduced here. For this purpose, the vector form of the variation of the Cauchy strain tensor is given again;

$$\delta \mathbf{C} |_S = [\delta C_{XX}^S, \delta C_{YY}^S, 2\delta C_{ZZ}^S, 2\delta C_{XY}^S, 2\delta C_{YZ}^S, 2\delta C_{ZX}^S]^T \quad (1.171)$$

The rate form is dropped on purpose. Instead of variation of rate, the rate of variation is taken and this rate is evaluated numerically, which is going to be presented in the next sections. The variation in tensor notation becomes;

$$\frac{1}{2} \delta \mathbf{C} |_S = \frac{1}{2} (\delta \mathbf{F}^T |_S \cdot \mathbf{F} |_S + \mathbf{F}^T |_S \cdot \delta \mathbf{F} |_S) \quad (1.172)$$

In indicial notation,

$$\begin{aligned}
\frac{1}{2}(\delta C|_S)_{IJ} &= \frac{1}{2}((\delta F^T|_S)_{Ii}(F|_S)_{iJ} + (F^T|_S)_{Ii}(\delta F|_S)_{iJ}) \\
&= \frac{1}{2}((\delta F|_S)_{iI}(F|_S)_{iJ} + (F|_S)_{iI}(\delta F|_S)_{iJ}) \\
&= \frac{1}{2}\left(\frac{\partial(\delta x|_S)_i}{\partial(X|_S)_I}(F|_S)_{iJ} + (F|_S)_{iI}\frac{\partial(\delta x|_S)_i}{\partial(X|_S)_J}\right) \\
&= \frac{1}{2}\left(\frac{\partial(\delta u|_S)_i}{\partial(X|_S)_I}(F|_S)_{iJ} + (F|_S)_{iI}\frac{\partial(\delta u|_S)_i}{\partial(X|_S)_J}\right)
\end{aligned} \tag{1.173}$$

Back substitution into equation (1.172) gives with the summation convention over index  $i$ ;

$$\frac{1}{2}\delta\mathbf{C}|_S = \frac{1}{2} \begin{bmatrix} \delta C_{11}^S \\ \delta C_{22}^S \\ \delta C_{33}^S \\ 2\delta C_{12}^S \\ 2\delta C_{23}^S \\ 2\delta C_{31}^S \end{bmatrix} = \begin{bmatrix} (F|_S)_{i1}(\delta u|_S)_{i,1} \\ (F|_S)_{i2}(\delta u|_S)_{i,2} \\ (F|_S)_{i3}(\delta u|_S)_{i,3} \\ (F|_S)_{i1}(\delta u|_S)_{i,2} + (F|_S)_{i2}(\delta u|_S)_{i,1} \\ (F|_S)_{i2}(\delta u|_S)_{i,3} + (F|_S)_{i3}(\delta u|_S)_{i,2} \\ (F|_S)_{i3}(\delta u|_S)_{i,1} + (F|_S)_{i1}(\delta u|_S)_{i,3} \end{bmatrix} \tag{1.174}$$

Applying the natural element shape value interpolation, on the deformations, variation of deformations and their material gradients leads into the following representations;

$$\begin{aligned}
(u|_S)_i &\approx \sum_L^{\# \text{ shape neigh.}} N^L(\tilde{u}|_S)_i^L & (\delta u|_S)_i &\approx \sum_L^{\# \text{ shape neigh.}} N^L(\delta\tilde{u}|_S)_i^L \\
(u|_S)_{i,J} &\approx \sum_L^{\# \text{ shape neigh.}} N_{,J}^L(\tilde{u}|_S)_i^L & (\delta u|_S)_{i,J} &\approx \sum_L^{\# \text{ shape neigh.}} N_{,J}^L(\delta\tilde{u}|_S)_i^L
\end{aligned} \tag{1.175}$$

The approximate vector form of the variation of the half Cauchy strain tensor is then,

$$\frac{1}{2}\delta\mathbf{C}|_S \approx \sum_L^{\# \text{ ngh}} \begin{bmatrix} (F|_S)_{i1} N_{,1}^L(\delta\tilde{u}|_S)_i^L \\ (F|_S)_{i2} N_{,2}^L(\delta\tilde{u}|_S)_i^L \\ (F|_S)_{i3} N_{,3}^L(\delta\tilde{u}|_S)_i^L \\ (F|_S)_{i1} N_{,2}^L(\delta\tilde{u}|_S)_i^L + (F|_S)_{i2} N_{,1}^L(\delta\tilde{u}|_S)_i^L \\ (F|_S)_{i2} N_{,3}^L(\delta\tilde{u}|_S)_i^L + (F|_S)_{i3} N_{,2}^L(\delta\tilde{u}|_S)_i^L \\ (F|_S)_{i3} N_{,1}^L(\delta\tilde{u}|_S)_i^L + (F|_S)_{i1} N_{,3}^L(\delta\tilde{u}|_S)_i^L \end{bmatrix} = \sum_L^{\# \text{ ngh}} \mathbf{B}^L|_S \cdot (\delta\tilde{\mathbf{u}}|_S)^L \tag{1.176}$$



The nonlinear strain displacement matrix is in full form is;

$$\mathbf{B}^L|_S = \begin{bmatrix} (F|_S)_{11} N_{,1}^L & (F|_S)_{21} N_{,1}^L & (F|_S)_{31} N_{,1}^L \\ (F|_S)_{12} N_{,2}^L & (F|_S)_{22} N_{,2}^L & (F|_S)_{32} N_{,2}^L \\ (F|_S)_{13} N_{,3}^L & (F|_S)_{23} N_{,3}^L & (F|_S)_{33} N_{,3}^L \\ (F|_S)_{11} N_{,2}^L + (F|_S)_{12} N_{,1}^L & (F|_S)_{21} N_{,2}^L + (F|_S)_{22} N_{,1}^L & (F|_S)_{31} N_{,2}^L + (F|_S)_{32} N_{,1}^L \\ (F|_S)_{12} N_{,3}^L + (F|_S)_{13} N_{,2}^L & (F|_S)_{22} N_{,3}^L + (F|_S)_{23} N_{,2}^L & (F|_S)_{32} N_{,3}^L + (F|_S)_{33} N_{,2}^L \\ (F|_S)_{13} N_{,1}^L + (F|_S)_{11} N_{,3}^L & (F|_S)_{23} N_{,1}^L + (F|_S)_{21} N_{,3}^L & (F|_S)_{33} N_{,1}^L + (F|_S)_{31} N_{,3}^L \end{bmatrix} \quad (1.177)$$

The discrete form of the internal energy as a sum of neighboring nonlinear strain displacement interpolators becomes;

$$\delta \tilde{W}^{int} = \sum_L^{\#ngh} (\delta \tilde{\mathbf{u}}|_S)^L \cdot \int_{\Omega_S} \left( (\mathbf{B}^L|_S)^T \cdot (\mathbf{S}_e^S - \lambda \mathbf{C}^{-1}) \right) dV^S \quad (1.178)$$

The first order truncation gives the residuum in between two subsequent iterations,

$$\begin{aligned} \delta \tilde{R}^W|^{i+1} (\tilde{\mathbf{u}}|_S, \tilde{\lambda}) &= \delta \tilde{W}^{int}|^{i+1} (\tilde{\mathbf{u}}|_S, \tilde{\lambda}) - \delta \tilde{W}^{int}|^i (\tilde{\mathbf{u}}|_S, \tilde{\lambda}) \\ &= \sum_L^{\#ngh} \sum_M^{\#ngh} (\delta \tilde{\mathbf{u}}|_S)^L \cdot \mathbf{K}_{LM}^{Wu} \cdot (d\tilde{\mathbf{u}}|_S)^M + \sum_L^{\#ngh} \sum_M^{\#ngh} (\delta \tilde{\mathbf{u}}|_S)^L \cdot \mathbf{K}_{LM}^{W\lambda} (d\tilde{\lambda})^M \end{aligned} \quad (1.179)$$

The component of the tangent stiffness caused by neighbor nodes L and M, and supplied by the translational momentum equation depending on only deformation can be shown as;

$$\begin{aligned} \mathbf{K}_{LM}^{Wu} &= \frac{\partial}{\partial (\tilde{\mathbf{u}}|_S)^M} \int_{\Omega_S} \left( (\mathbf{B}^L|_S)^T \cdot (\mathbf{S}_e^S - \lambda \mathbf{C}^{-1}) \right) dV^S \\ &= \int_{\Omega_S} \left( \frac{\partial (\mathbf{B}^L|_S)^T}{\partial (\tilde{\mathbf{u}}|_S)^M} \cdot (\mathbf{S}_e^S - \lambda \mathbf{C}^{-1}) \right) dV^S + \int_{\Omega_S} \left( (\mathbf{B}^L|_S)^T \cdot \frac{\partial (\mathbf{S}_e^S - \lambda \mathbf{C}^{-1})}{\partial (\tilde{\mathbf{u}}|_S)^M} \right) dV^S \end{aligned} \quad (1.180)$$

The second addend known as the material tangent stiffness can be formulated by chain rule,

$$\begin{aligned} \mathbf{K}_{LM}^{WuMat} &= \int_{\Omega_S} \left( (\mathbf{B}^L|_S)^T \cdot \frac{\partial (\mathbf{S}_e^S - \lambda \mathbf{C}^{-1})}{\partial (\tilde{\mathbf{u}}|_S)^M} \right) dV^S \\ &= \int_{\Omega_S} \left( (\mathbf{B}^L|_S)^T \cdot \frac{\partial (\mathbf{S}_e^S - \lambda \mathbf{C}^{-1})}{\partial (\mathbf{C}|_S)} \cdot \frac{\partial (\mathbf{C}|_S)}{\partial (\tilde{\mathbf{u}}|_S)^M} \right) dV^S \\ &= \int_{\Omega_S} \left( (\mathbf{B}^L|_S)^T \cdot \frac{\partial (\mathbf{S}_e^S - \lambda \mathbf{C}^{-1})}{\partial (\mathbf{C}|_S)} \cdot 2 (\mathbf{B}^M|_S) \right) dV^S \\ &= \int_{\Omega_S} \left( (\mathbf{B}^L|_S)^T \cdot \mathcal{D}^S \cdot (\mathbf{B}^M|_S) \right) dV^S \end{aligned} \quad (1.181)$$

The coefficient 2 at the third equation of (1.181) is a result of equation (1.176). The matrix form of the total tangent moduli can be decomposed into effective and pore pressure tangent moduli.

$$\mathcal{D}^S = \mathcal{D}_e^S + \mathcal{D}_p^S = 2 \frac{\partial \mathcal{S}_e^S}{\partial (\mathcal{C}|_S)} + 2 \frac{\partial (-\lambda \mathcal{C}^{-1})}{\partial (\mathcal{C}|_S)} \quad (1.182)$$

The coefficient 2 can be eliminated by considering the definition of the material modulus, which is based on Green-Lagrange strain function. Both in tensor and voigt notations, the following holds

$$\begin{aligned} \mathbf{e}_e^S &= \frac{\partial^2 \Psi}{\partial (\mathbf{E}|_S)^2} \Rightarrow \frac{1}{2} \mathbf{e}_e^S = \frac{\partial \mathcal{S}_e^S}{\partial \mathcal{C}|_S} = 2 \frac{\partial^2 \Psi}{\partial (\mathcal{C}|_S)^2} = \frac{1}{2} \frac{\partial^2 \Psi}{\partial (\mathbf{E}|_S)^2} \Rightarrow \frac{1}{2} \mathfrak{D}_e^S = \frac{\partial \mathcal{S}_e^S}{\partial \mathcal{C}|_S} \\ \frac{1}{2} \mathbf{e}_p^S &= \frac{\partial (-\lambda \mathcal{C}^{-1}|_S)}{\partial \mathcal{C}|_S} \Rightarrow \frac{1}{2} \mathfrak{D}_p^S = \frac{\partial (-\lambda \mathcal{C}^{-1})}{\partial (\mathcal{C}|_S)} \end{aligned} \quad (1.183)$$

The tangent moduli of pore pressure term can be evaluated as,

$$\mathbf{0} = -\lambda \frac{\partial \mathbf{I}}{\partial \mathcal{C}|_S} = -\lambda \frac{\partial (\mathcal{C}^{-1}|_S \cdot \mathcal{C}|_S)}{\partial \mathcal{C}|_S} = \frac{\partial (-\lambda \mathcal{C}^{-1}|_S)}{\partial \mathcal{C}|_S} \cdot \mathcal{C}|_S - \lambda \mathcal{C}^{-1}|_S \cdot \frac{\partial \mathcal{C}|_S}{\partial \mathcal{C}|_S} \quad (1.184)$$

In indicial notation then,

$$\begin{aligned} \frac{1}{2} (\mathbf{e}_p^S)_{INKL} C_{NM}^S &= \lambda (C^S)_{IO}^{-1} \frac{\partial C_{OM}^S}{\partial C_{KL}^S} \\ \frac{1}{2} (\mathbf{e}_p^S)_{INKL} C_{NM}^S (C^S)_{MJ}^{-1} &= \frac{1}{2} (\mathbf{e}_p^S)_{INKL} \delta_{NJ} = \frac{1}{2} (\mathbf{e}_p^S)_{IJKL} \\ &= \lambda (C^S)_{IO}^{-1} \frac{\partial C_{OM}^S}{\partial C_{KL}^S} (C^S)_{MJ}^{-1} \\ (\mathbf{e}_p^S)_{IJKL} &= \lambda (C^S)_{IO}^{-1} (\delta_{OK} \delta_{ML} + \delta_{OL} \delta_{MK}) (C^S)_{MJ}^{-1} \\ &= \lambda \left( (C^S)_{IK}^{-1} (C^S)_{JL}^{-1} + (C^S)_{IL}^{-1} (C^S)_{JK}^{-1} \right) \end{aligned} \quad (1.185)$$

At the last equation, the symmetry property of the inverse Cauchy strain tensor is used. The fourth order identity tensor which is used above is not a definition, but the result of the derivative of a second order tensor with itself as shown beneath;

$$\mathcal{I}_{IJKL} = \frac{\partial A_{IJ}}{\partial A_{KL}} = \frac{1}{2} \frac{\partial (A_{IJ} + A_{JI})}{\partial A_{KL}} = \frac{1}{2} (\delta_{IK} \delta_{JL} + \delta_{JK} \delta_{IL}) \quad (1.186)$$

For practical purposes, the element (or Voronoi-Nodal) stiffness matrices are splitted into *material*, *geometric* and if necessary also in *volumetric* parts. The names of the additive splitting originates from the classical Finite-element context, and named after the same analogy. As stated, the reason is to catch simplicity in the complicated derivations of the

necessary matrix-vector system of equations. The geometric stiffness matrix component can be obtained by the linearization<sup>18</sup> of the geometric residual scalar,

$$\begin{aligned} \delta \tilde{R}^{WuGeo} |^{i+1} &= (\delta \tilde{\mathbf{u}} |_S)^L \cdot \mathbf{K}_{LM}^{WuGeo} \cdot (d\tilde{\mathbf{u}} |_S)^M \\ &= (\delta \tilde{\mathbf{u}} |_S)^L \cdot \int_{\Omega_S} \left( \frac{\partial (\mathbf{B}^L |_S)^T}{\partial (\tilde{\mathbf{u}} |_S)^M} \cdot (\mathbf{S}_e^S - \lambda \mathbf{C}^{-1}) \right) \cdot (d\tilde{\mathbf{u}} |_S)^M dV^S \end{aligned} \quad (1.187)$$

The directional derivative can be considered in the total variational weak form, where the strain displacement matrix is not introduced yet,

$$\begin{aligned} (\delta \tilde{\mathbf{u}} |_S)^L \cdot \mathbf{K}_{LM}^{WuGeo} \cdot (d\tilde{\mathbf{u}} |_S)^M &= \int_{\Omega_S} \left( \frac{\partial (\delta \mathbf{C} |_S / 2)^L}{\partial (\tilde{\mathbf{u}} |_S)^M} : (\mathbf{S}_e^S - \lambda \mathbf{C}^{-1}) \right) \cdot (d\tilde{\mathbf{u}} |_S)^M dV^S \\ &= \int_{\Omega_S} \left( \frac{\partial (\delta \mathbf{C} |_S / 2)_{IJ}^L}{\partial (\tilde{u} |_S)_j^M} (\mathbf{S}_e^S - \lambda \mathbf{C}^{-1})_{IJ} \right) (d\tilde{u} |_S)_j^M dV^S \end{aligned} \quad (1.188)$$

Recalling equation (1.173),

$$\begin{aligned} \frac{1}{2} (\delta \mathbf{C} |_S)_{IJ} &= \frac{1}{2} \left( \frac{\partial (\delta u |_S)_i}{\partial (X |_S)_I} (F |_S)_{iJ} + (F |_S)_{iI} \frac{\partial (\delta u |_S)_i}{\partial (X |_S)_J} \right) \\ &= \frac{1}{2} \left( \frac{\partial (\delta u |_S)_i}{\partial (X |_S)_I} \left( \delta_{iJ} + \frac{\partial (u |_S)_i}{\partial X_J} \right) + \left( \delta_{iI} + \frac{\partial (u |_S)_i}{\partial X_I} \right) \frac{\partial (\delta u |_S)_i}{\partial (X |_S)_J} \right) \\ &\approx \frac{1}{2} \left[ \left( \sum_L N_{,I}^L (\delta \tilde{u} |_S)_i^L \right) \left( \delta_{iJ} + \sum_M N_{,J}^M (\tilde{u} |_S)_i^M \right) \right. \\ &\quad \left. + \left( \delta_{iI} + \sum_M N_{,I}^M (\tilde{u} |_S)_i^M \right) \left( \sum_L N_{,J}^L (\delta \tilde{u} |_S)_i^L \right) \right] \\ &= \frac{1}{2} \left[ \left( \sum_L N_{,I}^L (\delta \tilde{u} |_S)_i^L \right) \left( \delta_{iJ} + \sum_M N_{,J}^M \delta_{ij} (\tilde{u} |_S)_j^M \right) \right. \\ &\quad \left. + \left( \delta_{iI} + \sum_M N_{,I}^M \delta_{ij} (\tilde{u} |_S)_j^M \right) \left( \sum_L N_{,J}^L (\delta \tilde{u} |_S)_i^L \right) \right] \end{aligned} \quad (1.189)$$

<sup>18</sup>The types of notation and terminology for the linearizations applied in this context belong originally to Bonet Ref.[J.Bonnet 2008]

The focus is however a derivative of a specific variation;

$$\begin{aligned}
\frac{1}{2} \frac{\partial (\delta C |_S)_{IJ}^L}{\partial (\tilde{u} |_S)_j^M} &= \frac{1}{2} \frac{\partial}{\partial (\tilde{u} |_S)_j^M} \left[ \left( N_{,I}^L (\delta \tilde{u} |_S)_i^L \right) \left( \delta_{iJ} + \sum_M N_{,J}^M \delta_{ij} (\tilde{u} |_S)_j^M \right) \right. \\
&\quad \left. + \left( \delta_{iI} + \sum_M N_{,I}^M \delta_{ij} (\tilde{u} |_S)_j^M \right) \left( N_{,J}^L (\delta \tilde{u} |_S)_i^L \right) \right] \quad (1.190) \\
&= \frac{1}{2} \left[ \left( N_{,I}^L (\delta \tilde{u} |_S)_i^L \right) N_{,J}^M \delta_{ij} + N_{,I}^M \delta_{ij} \left( N_{,J}^L (\delta \tilde{u} |_S)_i^L \right) \right] \\
&= \delta \tilde{u} |_S_i^L N_{,I}^L N_{,J}^M \delta_{ij}
\end{aligned}$$

Inserting this expression back into the equation (1.188) gives the tensorial form of the geometric stiffness matrix.

$$\mathbf{K}_{LM}^{WuGeo} = \int_{\Omega_S} (\text{Grad}(N^L) \otimes \text{Grad}(N^M) : \mathbf{S} |_S) \mathbf{I} dV^S \quad (1.191)$$

The tangent stiffness matrix depending on the pore pressure lagrangean parameter is,

$$\begin{aligned}
\mathbf{K}_{LM}^{W\lambda} &= \frac{\partial}{\partial \lambda^M} \int_{\Omega_S} \left( (\mathbf{B}^L |_S)^T \cdot (\mathbf{s}_e^S - \lambda \mathbf{c}^{-1}) \right) dV^S \\
&= \frac{\partial}{\partial \lambda^M} \int_{\Omega_S} \left( (\mathbf{B}^L |_S)^T \cdot \left( \mathbf{s}_e^S - \sum_M N^M \lambda^M \mathbf{c}^{-1} \right) \right) dV^S \quad (1.192) \\
&= - \int_{\Omega_S} N^M (\mathbf{B}^L |_S)^T \cdot \mathbf{c}^{-1} dV^S
\end{aligned}$$

Which is in fact a vector value (a redundant matrix), coupling the pore pressure to the deformations. In this section, the geometric, material and pore pressure dependent nonlinearities considering the weak form of the translational momentum equation are presented. In the next section the discrete form based on the weak formulation of the conservation of mass are presented.

#### 1.7.4 Discrete Form of the Conservation of Mass

The tangent stiffness matrices of the following matrix-vector form is to be found.

$$\begin{aligned}
\delta \dot{M}^{int} &= \int_{\Omega_s} \left( J^{-1} |_s \dot{\mathbf{c}}^T |_s \cdot \mathbf{c}^{-1} |_s \right) \delta \lambda dV^S \\
&\quad + \int_{\Omega_s} \left( \beta^{-1} (n^f)^2 J^{-1} |_s \delta \mathbf{Q}^T |_s \cdot \mathbf{c}^{-1} |_s \right) dV^S \quad (1.193)
\end{aligned}$$

There will be several tangent components produced from the identity above. Therefore, a careful subdivision of the equation above, and the corresponding tangent operations are to

be performed.

$$\begin{aligned} \delta \tilde{R}^{M_1 | i+1} (\tilde{\mathbf{u}} |_S, \tilde{\lambda}) &= \delta \tilde{M}_1^{int | i+1} (\tilde{\mathbf{u}} |_S, \tilde{\lambda}) - \delta \tilde{M}_1^{int | i} (\tilde{\mathbf{u}} |_S, \tilde{\lambda}) \\ &= \sum_L \sum_M^{\#ngh \#ngh} (\delta \tilde{\lambda})^L \mathbf{K}_{LM}^{M_1 u} \cdot (d\tilde{\mathbf{u}} |_S)^M + \sum_L \sum_M^{\#ngh \#ngh} (\delta \tilde{\lambda})^L \mathbf{K}_{LM}^{M_1 \lambda} (d\tilde{\lambda})^M \end{aligned} \quad (1.194)$$

Despite of the fact that, the first component of the stiffness matrix is a vector, and the second one is a scalar, for the consistency of the assembly of individual addends, those all will be presented as matrices as done previously. The first derivative is,

$$\begin{aligned} \delta \tilde{\lambda}^L \mathbf{K}_{LM}^{M_1 u} &= \frac{\partial}{\partial (\tilde{\mathbf{u}} |_S)^M} \int_{\Omega_s} \left( J^{-1} |_s \dot{\mathbf{c}}^T |_s \cdot \mathbf{c}^{-1} |_s \right) N^L \delta \tilde{\lambda} dV^S \\ &= \mathbf{K}_{LM}^{M_1 u J} + \mathbf{K}_{LM}^{M_1 u Geo} + \mathbf{K}_{LM}^{M_1 u Mat} \end{aligned} \quad (1.195)$$

The individual components are, firstly the tangents originated by the determinant of the solid deformation gradient 'J',

$$\begin{aligned} \mathbf{K}_{LM}^{M_1 u J} &= \int_{\Omega_s} N^L \left( \dot{\mathbf{c}}^T |_s \cdot \mathbf{c}^{-1} |_s \right) \otimes \frac{\partial (J^{-1} |_s)}{\partial (\tilde{\mathbf{u}} |_S)^M} dV^S \\ &= \int_{\Omega_s} N^L \left( \dot{\mathbf{c}}^T |_s \cdot \mathbf{c}^{-1} |_s \right) \otimes \left( \frac{\partial (det \mathbf{C} |_s)^{-1/2}}{\partial \mathbf{C} |_s} : \frac{\partial \mathbf{C} |_s}{\partial (\tilde{\mathbf{u}} |_S)^M} \right) dV^S \\ &= \int_{\Omega_s} N^L \left( \dot{\mathbf{c}}^T |_s \cdot \mathbf{c}^{-1} |_s \right) \otimes \left( \frac{-(det \mathbf{C} |_s)^{-3/2}}{2} \frac{\partial (det \mathbf{C} |_s)}{\partial \mathbf{C} |_s} : \frac{\partial \mathbf{C} |_s}{\partial (\tilde{\mathbf{u}} |_S)^M} \right) dV^S \\ &= \int_{\Omega_s} N^L \left( \dot{\mathbf{c}}^T |_s \cdot \mathbf{c}^{-1} |_s \right) \otimes \left( -\frac{1}{2} (J^{-1} |_s)^3 \frac{\partial (det \mathbf{C} |_s)}{\partial \mathbf{C} |_s} : \frac{\partial \mathbf{C} |_s}{\partial (\tilde{\mathbf{u}} |_S)^M} \right) dV^S \\ &= \int_{\Omega_s} N^L \left( \dot{\mathbf{c}}^T |_s \cdot \mathbf{c}^{-1} |_s \right) \otimes \left( -\frac{1}{2} (J^{-1} |_s)^3 (det \mathbf{C} |_s) (\mathbf{C} |_s)^{-T} : \frac{\partial \mathbf{C} |_s}{\partial (\tilde{\mathbf{u}} |_S)^M} \right) dV^S \\ &= \int_{\Omega_s} N^L \left( \dot{\mathbf{c}}^T |_s \cdot \mathbf{c}^{-1} |_s \right) \otimes \left( -\frac{1}{2} (J^{-1} |_s)^2 (\mathbf{c}^{-1} |_s)^T \cdot \frac{\partial (\mathbf{C} |_s)^M}{\partial (\tilde{\mathbf{u}} |_S)^M} \right) dV^S \\ &= \int_{\Omega_s} N^L \left( \dot{\mathbf{c}}^T |_s \cdot \mathbf{c}^{-1} |_s \right) \otimes \left( -\frac{1}{2} (J^{-1} |_s)^2 (\mathbf{c}^{-1} |_s)^T \cdot \frac{\partial (\mathbf{B}^M |_s \cdot (\tilde{\mathbf{u}} |_S)^M)}{\partial (\tilde{\mathbf{u}} |_S)^M} \right) dV^S \\ &= \int_{\Omega_s} -\frac{1}{2} (J^{-1} |_s)^2 N^L \left( \dot{\mathbf{c}}^T |_s \cdot \mathbf{c}^{-1} |_s \right) \otimes \left[ (\mathbf{c}^{-1} |_s)^T \cdot \mathbf{B}^M |_s \right. \\ &\quad \left. + \left( (\tilde{\mathbf{u}} |_S)^M \right)^T \cdot \mathbf{I} (Grad (N^M) \otimes Grad (N^M) : \mathbf{C}^{-1} |_s) \right] dV^S \end{aligned} \quad (1.196)$$

The material parts,

$$\begin{aligned}
\mathbf{K}_{LM}^{M_1 u Mat} &= \int_{\Omega_s} N^L \left( J^{-1} |_s (\dot{\mathbf{c}} |_s)^T \cdot \frac{\partial (\mathbf{c}^{-1} |_s)^M}{\partial (\tilde{\mathbf{u}} |_s)^M} \right) dV^S \\
&= \int_{\Omega_s} N^L \left( J^{-1} |_s (\dot{\mathbf{c}} |_s)^T \cdot \frac{\partial (\mathbf{c}^{-1} |_s)}{\partial (\mathbf{c} |_s)} \cdot \frac{\partial (\mathbf{c} |_s)^M}{\partial (\tilde{\mathbf{u}} |_s)^M} \right) dV^S \quad (1.197) \\
&= \int_{\Omega_s} N^L \left( J^{-1} |_s (\dot{\mathbf{c}} |_s)^T \cdot \left( -\frac{1}{2\lambda} \mathfrak{D}_p^S \right) \cdot \mathbf{B}^M |_s \right) dV^S
\end{aligned}$$

and finally geometric part(s),

$$\begin{aligned}
\mathbf{K}_{LM}^{M_1 u Geo} &= \int_{\Omega_s} N^L \left( J^{-1} |_s (\mathbf{c}^{-1} |_s)^T \cdot \frac{\partial (\dot{\mathbf{c}} |_s)^M}{\partial (\tilde{\mathbf{u}} |_s)^M} \right) dV^S \\
&= \int_{\Omega_s} N^L \left( J^{-1} |_s \frac{\beta_2}{\beta_1 t} (\mathbf{c}^{-1} |_s)^T \cdot \frac{\partial (\mathbf{c} |_s)^M}{\partial (\tilde{\mathbf{u}} |_s)^M} \right) dV^S \\
&= \int_{\Omega_s} N^L \left( J^{-1} |_s \frac{\beta_2}{\beta_1 t} (\mathbf{c}^{-1} |_s)^T \cdot \frac{\partial (\mathbf{B}^M |_s \cdot (\tilde{\mathbf{u}} |_s)^M)}{\partial (\tilde{\mathbf{u}} |_s)^M} \right) dV^S \\
&= \int_{\Omega_s} N^L \left( J^{-1} |_s \frac{\beta_2}{\beta_1 t} (\mathbf{c}^{-1} |_s)^T \cdot (\mathbf{B}^M |_s) \right) dV^S \\
&+ \int_{\Omega_s} N^L \left( J^{-1} |_s \frac{\beta_2}{\beta_1 t} ((\tilde{\mathbf{u}} |_s)^M)^T \cdot \frac{\partial (\mathbf{B}^M |_s)^T}{\partial (\tilde{\mathbf{u}} |_s)^M} \cdot \mathbf{c}^{-1} |_s \right) dV^S \\
&= \int_{\Omega_s} N^L \left( J^{-1} |_s \frac{\beta_2}{\beta_1 t} (\mathbf{c}^{-1} |_s)^T \cdot (\mathbf{B}^M |_s) \right) dV^S \\
&+ \int_{\Omega_s} N^L \left( J^{-1} |_s \frac{\beta_2}{\beta_1 t} ((\tilde{\mathbf{u}} |_s)^M)^T \cdot \mathbf{I} (Grad(N^M) \otimes Grad(N^M) : \mathbf{C}^{-1} |_s) \right) dV^S \quad (1.198)
\end{aligned}$$

Where the last addend of the material parts is not written because of a simple reason which is visited here immediately. This could be pointed out before evaluating the material stiffness part of the weak form of translational momentum equation (1.181). The neighbor sum of the integrals with the integrand under discussion multiplied with the increment of

the direction of the directional derivative has the form<sup>19</sup>,

$$\begin{aligned} & \sum_M^{\#ngh} \int_{\Omega_s} \left( (\tilde{\mathbf{u}}|_s)^M \right)^T \cdot \mathbf{I} \left( \text{Grad}(N^M) \otimes \text{Grad}(N^M) : \mathbf{C}^{-1}|_s \right) \cdot (d\tilde{\mathbf{u}}|_s)^M dV^S \\ &= \sum_M^{\#ngh} \int_{\Omega_s} \left( (\tilde{\mathbf{F}}|_s \cdot d\tilde{\mathbf{F}}|_s) : \mathbf{C}^{-1}|_s \right) dV^S = 0 \end{aligned} \quad (1.199)$$

Additionally, the first residuum of the discretized version of the conservation of mass is linear in pore pressure Lagrangian multiplier. Secondly, the material rate of the vector form of the Cauchy can be evaluated by using the Newmark-consistent time derivative.

$$\mathbf{K}_{LM}^{M_1\lambda} = \mathbf{0} \quad (1.200a)$$

$$\tilde{\mathbf{C}}|_s = \dot{\mathbf{C}}|_s \sum_O^{\#ngh} N^O \left( \dot{\mathbf{C}}|_s \right)^O = \frac{\beta_2}{\beta_1 t} \sum_O^{\#ngh} N^O \left( \tilde{\mathbf{c}}|_s \right)^O = \frac{\beta_2}{\beta_1 t} \sum_O^{\#ngh} N^O \left( \mathbf{B}|_s \right)^O \cdot (\tilde{\mathbf{u}}|_s)^O \quad (1.200b)$$

Using this additional numerical approximation and considering the neglected term, the final stiffness addends of the first part of the mass balance weak form becomes;

$$\begin{aligned} & \mathbf{K}_{LM}^{M_1uJ} + \mathbf{K}_{LM}^{M_1uGeo} + \mathbf{K}_{LM}^{M_1uMat} = \\ & \int_{\Omega_s} -\frac{1}{2} (J^{-1}|_s)^2 N^L \left( \tilde{\mathbf{C}}^T|_s \cdot \mathbf{c}^{-1}|_s \right) \otimes \left( (\mathbf{c}^{-1}|_s)^T \cdot \mathbf{B}^M|_s \right) dV^S \\ & + \int_{\Omega_s} N^L \left( J^{-1}|_s \frac{\beta_2}{\beta_1 t} (\mathbf{c}^{-1}|_s)^T \cdot (\mathbf{B}^M|_s) \right) dV^S \\ & + \int_{\Omega_s} N^L \left( J^{-1}|_s \left( \tilde{\mathbf{C}}|_s \right)^T \cdot \left( -\frac{1}{2\lambda} \mathfrak{D}_p^S \right) \cdot \mathbf{B}^M|_s \right) dV^S \end{aligned} \quad (1.201)$$

For the linearization of the second part<sup>20</sup> of the weak mass balance equation, the following residuum parts should be introduced;

$$\begin{aligned} \delta \tilde{R}^{M_2}|^{i+1} \left( \tilde{\mathbf{u}}|_s, \tilde{\lambda} \right) &= \delta \tilde{M}_2^{int}|^{i+1} \left( \tilde{\mathbf{u}}|_s, \tilde{\lambda} \right) - \delta \tilde{M}_2^{int}|^i \left( \tilde{\mathbf{u}}|_s, \tilde{\lambda} \right) \\ &= \sum_L^{\#ngh} \sum_M^{\#ngh} \left( \delta \tilde{\lambda} \right)^L \mathbf{K}_{LM}^{M_2u} \cdot (d\tilde{\mathbf{u}}|_s)^M + \sum_L^{\#ngh} \sum_M^{\#ngh} \left( \delta \tilde{\lambda} \right)^L \mathbf{K}_{LM}^{M_2\lambda} \left( d\tilde{\lambda} \right)^M \end{aligned} \quad (1.202)$$

<sup>19</sup>The proof could not be found by the writer of the treatise, after long literature survey of most frequently cited finite element method texts

<sup>20</sup>Remember that the weak form of the conservation of mass was divided into two parts for the sake of simplicity

Before taking the directional derivative, the exact (approximated) form of the Lagrangian multiplier gradient should be introduced.

$$\begin{aligned} \left( \delta \tilde{\mathbf{Q}}|_S \right)^L &= \frac{\delta \tilde{\lambda}}{2} \left[ 2N_{,1}^L \frac{\partial \lambda}{\partial X} \quad , \quad 2N_{,2}^L \frac{\partial \lambda}{\partial Y} \quad , \quad 2N_{,3}^L \frac{\partial \lambda}{\partial Z} \quad , \right. \\ &\quad \left. N_{,1}^L \frac{\partial \lambda}{\partial Y} + \frac{\partial \lambda}{\partial X} N_{,2}^L \quad , \quad N_{,2}^L \frac{\partial \lambda}{\partial Z} + \frac{\partial \lambda}{\partial Y} N_{,3}^L \quad , \quad N_{,3}^L \frac{\partial \lambda}{\partial X} + \frac{\partial \lambda}{\partial Z} N_{,1}^L \right]^T \\ &= \delta \tilde{\lambda} (\mathbf{\Gamma}|_S)^L \end{aligned} \quad (1.203)$$

The tangent stiffness of the second part of the conservation of mass with the tangent depending on only the deformation is,

$$\begin{aligned} \delta \tilde{\lambda}^L \mathbf{K}_{LM}^{M_2u} &= \frac{\partial}{\partial (\tilde{\mathbf{u}}|_S)^M} \int_{\Omega_s} \left( \delta \tilde{\lambda}^L \beta^{-1} (n^f)^2 J^{-1}|_S (\mathbf{\Gamma}^L|_S)^T \cdot \mathbf{c}^{-1}|_S \right) dV^S \\ &= \mathbf{K}_{LM}^{M_2uJ} + \mathbf{K}_{LM}^{M_2uMat} \end{aligned} \quad (1.204)$$

Using the first narrowed assumption (see chapter Ch.[1.5.2]), namely the saturation condition, one can express the fluid volume fraction in terms of the determinant of the solid deformation gradient and true densities.

$$n^f = 1 - n^s = 1 - \frac{\varrho^s}{\varrho^{sR}} = 1 - \frac{\varrho^s}{\rho^{sR}} = 1 - \frac{dm/dv}{dm/dV^S} = 1 - \frac{dV^S}{dv} = 1 - n^S \frac{dV}{dv} = 1 - n^S J^{-1}|_S \quad (1.205)$$

The total derivative of the jacobian dependent terms with respect to jacobian itself is,

$$\frac{\partial \left( (n^f)^2 J^{-1}|_S \right)}{J^{-1}|_S} = -2n^S (1 - n^S J^{-1}|_S) J^{-1}|_S + (1 - n^S J^{-1}|_S)^2 \quad (1.206)$$

Applying the same analogy of equation (1.196),

$$\begin{aligned} \mathbf{K}_{LM}^{M_2uJ} &= \int_{\Omega_s} -\frac{1}{2} (J^{-1}|_s)^2 \left( (n^f)^2 J^{-1}|_S \right)_{,J^{-1}|_S} \\ &\quad \left( (\mathbf{\Gamma}^L|_S)^T \cdot \mathbf{c}^{-1}|_S \right) \otimes \left( (\mathbf{c}^{-1}|_S)^T \cdot \mathbf{B}^M|_S \right) dV^S \end{aligned} \quad (1.207)$$

The material part, with the same analogy to equation (1.197),

$$\mathbf{K}_{LM}^{M_2uMat} = \int_{\Omega_s} \beta^{-1} (n^f)^2 J^{-1}|_S (\mathbf{\Gamma}^L|_S)^T \cdot \left( -\frac{1}{2\lambda} \mathfrak{D}_p^S \right) \cdot \mathbf{B}^M|_S dV^S \quad (1.208)$$

And the last term, in a straightforward way,

$$\mathbf{K}_{LM}^{M_2\lambda} = \int_{\Omega_s} \left( \beta^{-1} (n^f)^2 J^{-1}|_S \frac{\partial (\mathbf{\Gamma}^L|_S)^T}{d\tilde{\lambda}^M} \cdot \mathbf{c}^{-1}|_S \right) dV^S \quad (1.209)$$



The derivative of Lagrangian multiplier gradient vector with respect to the nodal increment of Lagrangian multiplier is,

$$\begin{aligned} \frac{\partial (\boldsymbol{\Gamma}^L|_S)}{d\tilde{\lambda}^M} &= \frac{1}{2} [2N_{,1}^L N_{,1}^M, \quad 2N_{,2}^L N_{,2}^M, \quad 2N_{,3}^L N_{,3}^M, \\ &\quad N_{,1}^L N_{,2}^M + N_{,1}^M N_{,2}^L, \quad N_{,2}^L N_{,3}^M + N_{,2}^M N_{,3}^L, \quad N_{,3}^L N_{,1}^M + N_{,3}^M N_{,1}^L]^T \end{aligned} \quad (1.210)$$

Finally, the total nodal tangent stiffness matrix with individual components can be summed up together as;

$$\begin{aligned} \mathbf{K} &= \mathbf{K}_{LM}^{WuMat} + \mathbf{K}_{LM}^{WuGeo} + \mathbf{K}_{LM}^{W\lambda} + \mathbf{K}_{LM}^{M_1uJ} + \mathbf{K}_{LM}^{M_1uGeo} \\ &\quad + \mathbf{K}_{LM}^{M_1uMat} + \mathbf{K}_{LM}^{M_2uJ} + \mathbf{K}_{LM}^{M_2uMat} + \mathbf{K}_{LM}^{M_2\lambda} \\ &= \int_{\Omega_S} \left( (\mathbf{B}^L|_S)^T \cdot \mathcal{D}^S \cdot (\mathbf{B}^M|_S) \right) dV^S \\ &\quad + \int_{\Omega_S} \left( \text{Grad}(N^L) \otimes \text{Grad}(N^M) : \mathbf{S}|_S \right) \mathbf{I} dV^S \\ &\quad - \int_{\Omega_S} N^M (\mathbf{B}^L|_S)^T \cdot \mathbf{c}^{-1} dV^S \\ &\quad + \int_{\Omega_S} -\frac{1}{2} (J^{-1}|_S)^2 N^L \left( \tilde{\mathbf{C}}^T|_S \cdot \mathbf{c}^{-1}|_S \right) \otimes \left( (\mathbf{c}^{-1}|_S)^T \cdot \mathbf{B}^M|_S \right) dV^S \\ &\quad + \int_{\Omega_S} N^L \left( J^{-1}|_S \frac{\beta_2}{\beta_1 t} (\mathbf{c}^{-1}|_S)^T \cdot (\mathbf{B}^M|_S) \right) dV^S \\ &\quad + \int_{\Omega_S} N^L \left( J^{-1}|_S (\tilde{\mathbf{C}}|_S)^T \cdot \left( -\frac{1}{2\lambda} \mathfrak{D}_p^S \right) \cdot \mathbf{B}^M|_S \right) dV^S \\ &\quad + \int_{\Omega_S} -\frac{1}{2} (J^{-1}|_S)^2 \left( (n^f)^2 J^{-1}|_S \right)_{,J^{-1}|_S} \left( (\boldsymbol{\Gamma}^L|_S)^T \cdot \mathbf{c}^{-1}|_S \right) \otimes \left( (\mathbf{c}^{-1}|_S)^T \cdot \mathbf{B}^M|_S \right) dV^S \\ &\quad + \int_{\Omega_S} \beta^{-1} (n^f)^2 J^{-1}|_S (\boldsymbol{\Gamma}^L|_S)^T \cdot \left( -\frac{1}{2\lambda} \mathfrak{D}_p^S \right) \cdot \mathbf{B}^M|_S dV^S \\ &\quad + \int_{\Omega_S} \left( \beta^{-1} (n^f)^2 J^{-1}|_S \frac{\partial (\boldsymbol{\Gamma}^L|_S)^T}{d\tilde{\lambda}^M} \cdot \mathbf{c}^{-1}|_S \right) dV^S \end{aligned} \quad (1.211)$$

The individual components in terms of matrix format;

$$\begin{aligned}
& \begin{bmatrix} K_{11} & K_{12} & K_{13} & K_{14} \\ K_{21} & K_{22} & K_{23} & K_{24} \\ K_{31} & K_{32} & K_{33} & K_{34} \\ K_{41} & K_{42} & K_{43} & K_{44} \end{bmatrix} = \begin{bmatrix} K_{11}^{WuMat} & K_{12}^{WuMat} & K_{13}^{WuMat} & 0 \\ K_{21}^{WuMat} & K_{22}^{WuMat} & K_{23}^{WuMat} & 0 \\ K_{31}^{WuMat} & K_{32}^{WuMat} & K_{33}^{WuMat} & 0 \\ 0 & 0 & 0 & 0 \end{bmatrix} + \begin{bmatrix} K_{11}^{WuGeo} & 0 & 0 & 0 \\ 0 & K_{22}^{WuGeo} & 0 & 0 \\ 0 & 0 & K_{33}^{WuGeo} & 0 \\ 0 & 0 & 0 & 0 \end{bmatrix} \\
& + \begin{bmatrix} 0 & 0 & 0 & K_1^{W\lambda} \\ 0 & 0 & 0 & K_2^{W\lambda} \\ 0 & 0 & 0 & K_3^{W\lambda} \\ 0 & 0 & 0 & 0 \end{bmatrix} + \begin{bmatrix} 0 & 0 & 0 & 0 \\ 0 & 0 & 0 & 0 \\ 0 & 0 & 0 & 0 \\ K_1^{M_1uJ} & K_2^{M_1uJ} & K_3^{M_1uJ} & 0 \end{bmatrix} \\
& + \begin{bmatrix} 0 & 0 & 0 & 0 \\ 0 & 0 & 0 & 0 \\ 0 & 0 & 0 & 0 \\ K_1^{M_1uGeo} & K_2^{M_1uGeo} & K_3^{M_1uGeo} & 0 \end{bmatrix} + \begin{bmatrix} 0 & 0 & 0 & 0 \\ 0 & 0 & 0 & 0 \\ 0 & 0 & 0 & 0 \\ K_1^{M_1uMat} & K_2^{M_1uMat} & K_3^{M_1uMat} & 0 \end{bmatrix} \\
& + \begin{bmatrix} 0 & 0 & 0 & 0 \\ 0 & 0 & 0 & 0 \\ 0 & 0 & 0 & 0 \\ K_1^{M_2uJ} & K_2^{M_2uJ} & K_3^{M_2uJ} & 0 \end{bmatrix} + \begin{bmatrix} 0 & 0 & 0 & 0 \\ 0 & 0 & 0 & 0 \\ 0 & 0 & 0 & 0 \\ K_1^{M_2uMat} & K_2^{M_2uMat} & K_3^{M_2uMat} & 0 \end{bmatrix} + \begin{bmatrix} 0 & 0 & 0 & 0 \\ 0 & 0 & 0 & 0 \\ 0 & 0 & 0 & 0 \\ 0 & 0 & 0 & K^{M_2u\lambda} \end{bmatrix} \\
& \hspace{15em} (1.212)
\end{aligned}$$

## 1.8 Numerical Examples

In this section there are in total 3 different numerical examples are presented. The first one represents the growth of an initially spherical biological structure, as a result of excessive fluid feeding at some prescribed arterial locations. The effect of growing volume on some surrounding tube-like primary tissue is investigated in the second example. The third example is related to vertical contact of the articular cartilage with the meniscus tissue. All the models generated here consist of Hexahedral elements only, with tri-linear shape functions. There is a single difference of the element formulation of the typical 8-Node Hexahedral framework, which is the number of integration points. The elements contain layers, and therefore has at least 8 integration points, or more are assigned depending on the number of layers. For each layer there are 4 integration points taken, and on the plane Gauss quadrature rule is applied. In the thickness direction Simpson's rule finishes the complete integration. Before giving the examples, the details of the written code is presented next.

### 1.8.1 Finite Element Implementation: Software Specifications

The discretized form of the equations evaluated in section Ch.[1.7] were successfully implemented via Finite Element Method (FEM), as well as the Natural Element Method (NEM - see Ch.[5]). In this subsection, only the FEM code is presented with details, instructions and limitations.

The code is compatible with Linux-Environment<sup>21</sup>. Some user defined & embedded noncommercial (public and free) software libraries together with self-written makefiles provide compilation and execution of the presented software solution. Since moderate to large systems of equations aimed to be solved by the writer of the treatise, sparse matrix storage methods and solvers which are capable of dealing with sparse matrix-vector algebra are implemented and used. The sparse matrix-vector library contains basic yet efficient linear-algebra operators, such as multiplication and addition of arbitrary sparse matrices, and explicit inversions of large sparse matrices. The programming has been chosen to be C++, and compilers with the general public license Ref.[[GNU 2009](#)] agreements are used. Object oriented features such as class inheritance, polymorphism, encapsulation and function overloading (virtual functions) are fully benefited from. The writer preferred to be guided by the referend Ref.[[Yang 1996](#)], since the special focus of the treatise on engineering applications. For solving the large system of equations, mainly the Pardiso<sup>©</sup> sparse solver developed by the Pardiso<sup>©</sup> Solver Project Team Ref.[[Pardiso 2009](#)] is used. One of the very initial versions of the solver was embedded into Intel-math kernel library<sup>©</sup> project Ref.[[Library-MKL 2008](#)], the sparse solver Pardiso<sup>©</sup> is accessed indirectly from Intel-MKL<sup>©</sup> library. In addition to these, optionally another *makefile* procedure is applied to generate Abaqus<sup>©</sup> software Ref.[[Simulia 2011](#)] output database (.odb) binary types of outputs. The Application Programming Interface (API) library of software Abaqus<sup>©</sup> is intensively used for this purpose as well. The code written would be also sufficient without

---

<sup>21</sup>CentOS release 5.11 (final)

these aforementioned add-ons, nevertheless, issues such as performance and visual aids supplied by those commercial and public license software products convinced the writer to do it so. Additional to those listed above, the personal pre- and postprocessor GiD<sup>©</sup> Ref.[personal post processor GiD 2009] and Metapost<sup>©</sup> of Beta Systems Ref.[Beta 2009] are used for figures generated in the next section of examples.

```

1  #!/bin/csh -f
2  echo Deleting the old data...
3  rm TPM_CAN_RTM_BIG.cpp TPM_CAN_RTM_BIG.exe TPM_CAN_RTM_BIG.o
4  echo Combining the cpp-s...
5  cat tpm_main.cpp allocaters.cpp gauss.cpp global_functions.cpp linear_algebra.cpp readers.cpp writers.cpp odb_writers.cpp>>TPM_CAN_RTM_BIG.cpp
6
7  if ( $#argv > 0 ) then
8      set source = "$argv[1]"
9  else
10     set source = "TPM_CAN_RTM_BIG"
11 endif
12
13 #echo Setting the library path...
14
15 #LD_LIBRARY_PATH=$LD_LIBRARY_PATH:"YOURPATH/tpm_can_rtm/tpm/lib"
16
17 #setenv LD_LIBRARY_PATH ./lib
18
19 echo Compiling...
20 icpc -o -cwxlib -Kc++eh -fPIC -Krtti -Kc++ -pc64 -restrict -DABQ_LINUX -DABQ_LNX86_64 -DFOR_TRAIL -DHAS_BOOL -DASSERT_ENABLED -D_BSD_TYPES
21 -D_BSD_SOURCE -D_GNU_SOURCE -D_POSIX_SOURCE -D_XOPEN_SOURCE_EXTENDED -D_XOPEN_SOURCE -DHAVE_OPENGL -DHKS_OPEN_GL -DTYPE_NAME=typename -DGL_GLEXT_PROTOTYPES
22 -D_LARGEFILE64_SOURCE -D_FILE_OFFSET_BITS=64 -we101 -we120 -we117 -we556 -we144 -we268 -we1224 -we167 -we880 -o0 -I./include ./$source.cpp
23
24
25 echo Linking...
26 icpc -cwxlib -fPIC -Wl,-Bdynamic -i-dynamic -o ./$source.exe ./$source.o -L./lib -LABQDDB_Odb -LABQSMACdbApi -LABQSMACdbCore -LABQSMACdbCoreGeom
27 -LABQSMACdbAttrEO -LABQSMACdbBasicUtils -LABQSMACdbShared -LABQSMACdbCoreUtils -LABQCAE_StableTime -LABQSMACdbMem -LABQSMACdbGeom -LABQSMARomDiagEx
28 -LABQSMASpUmaCore -LABQSMASimInterface -LABQSMAMtxCoreModule -lpthread

```

Figure 1.1: The shell script used for compiling and linking the external libraries using Intel<sup>©</sup> compiler

```

1  #!/bin/csh -f
2  echo Deleting the old data...
3  rm TPM_CAN_RTM_BIG.cpp TPM_CAN_RTM_BIG.exe TPM_CAN_RTM_BIG.o
4  echo Combining the cpp-s...
5  cat tpm_main.cpp csr_Matrix.cpp solver.cpp allocaters.cpp contact.cpp master_surface.cpp gauss.cpp tpm_stiff.cpp
6  tpm_internal.cpp global_functions.cpp linear_algebra.cpp readers.cpp
7  writers.cpp odb_writers.cpp layup.cpp>>TPM_CAN_RTM_BIG.cpp
8
9  if ( $#argv > 0 ) then
10     set source = "$argv[1]"
11 else
12     set source = "TPM_CAN_RTM_BIG"
13 endif
14
15 #echo Setting the library path...
16
17 #LD_LIBRARY_PATH=$LD_LIBRARY_PATH:"YOURPATH/tpm_can_rtm/tpm/lib"
18
19 #setenv LD_LIBRARY_PATH ./lib
20
21 echo Compiling and Linking...
22
23 abq6111 make job=TPM_CAN_RTM_BIG.cpp

```

Figure 1.2: The shell script used for compiling and linking the external libraries using Abaqus<sup>©</sup> compiler

After this short information about the environment of the software, the contents of the individual files of the code of biphasic media can be summarized next. The files in alphabetical order;

- *Abq\_TPM\_MASTER\_MAKEFILE.csh*: Makefile compiling and generating the master file and executable using API library
- *allocaters.cpp*: includes local and global allocations

- *csr\_Matrix.h & csr\_Matrix.cpp*: compressed sparse row matrix library declarations and definitions
- *gauss.cpp*: integration point specific functions
- *global\_functions.cpp*: functions relevant to the global matrix parameters
- *headers.h*: main header file including the class declarations
- *input.inp*: any input file in Abaqus<sup>©</sup> format, this file is parsed by readers
- *Intel\_TPM\_MASTER\_MAKEFILE.csh*: Intel makefile compiling and generating the master file and executable
- *linear\_algebra.cpp*: some functions of linear algebra used for small matrix-vector operations
- *natural\_bc.inp*: the nodal natural boundary conditions
- *neumann\_bc.inp*: the nodal essential boundary conditions
- *odb\_writers.cpp*: functions generating the output database
- *readers.cpp*: readers and parsers of the input files, model and boundary conditions
- *TPM\_MASTER.cpp & TPM\_MASTER.exe*: the master file and the executable of the master file
- *tpm\_internal.cpp*: functions of internal residuals of conservation of mass and translational momentum
- *tpm\_main.cpp*: the main function
- *tpm\_stiff.cpp*: functions of element stiffnesses of conservation of mass and translational momentum
- *writers.cpp*: any type of writers for post-processing or manual debugging purposes

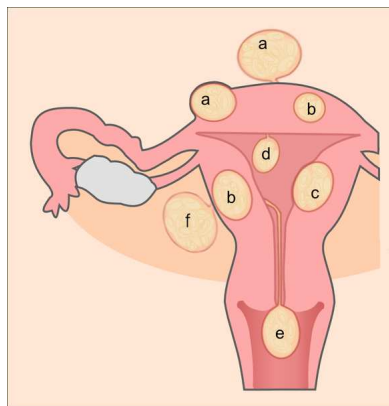
After any change or modification done in a specific file, one of the makefiles should be used to generate new master file and the executable. As indicated, the file<sup>22</sup> the model, and accordingly the boundary conditions can be changed and run under Linux-environment. In the next, some examples will be presented.

### 1.8.2 A Numerical Scenario: Growth of Uterine Fibroids

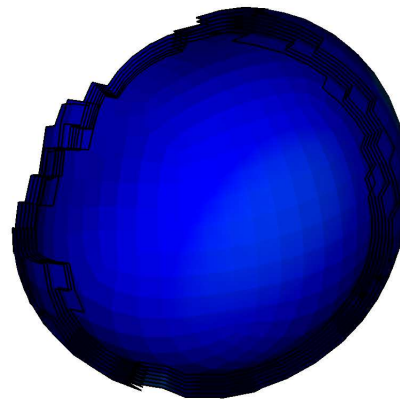
The first example stands only for the growth of an initially spherical-shaped abstract tissue. The abstract scenario together with the next one, can be analogously linked to some real

---

<sup>22</sup>Only nodes, coordinates, elements, solid sections materials and laminar lay-up informations are parsed. Caution, the complete list of parameters or header that follows the well known Abaqus<sup>©</sup> format. Abaqus<sup>©</sup> is not used as finite element analysis software, only the necessary part (compiler, API) is used as an aid for the implementation.



(a) This study mimics likely the variation a,c:subserosal or submucosal fibroid growth [Hic.et.nunc 2012](#)



(b) The spherical layer-wise structured initial fibroid geometry taken for this study

Figure 1.3: Schematic Drawing of various types of uterine fibroids and initial fibroid geometry

biomechanical phenomena, for instance fibroid growth as shown in the left side of the *Figure 1.3*<sup>23</sup>. In this case, some artificial hot points, or fluid supply network is preassigned, namely the pore-pressure is to be predefined. The tracing paths of the pressure supply nodes can be seen in the results of next pages, for instance fourth picture of *Figure 1.5*.

The scenario of growth is however a novel one, and not based on any other phenomenological or theoretical postulates done by pioneers of the field. It should be noted here that, the theory and numerics of the growth in the field of biomechanics is already postulated and significant amount of very valuable work is delivered to the science and engineering publicity. Among many of them, Menzel Ref.[\[A.Menzel 2004\]](#) postulated a general theoretical and numerical framework of remodeling and growth of fiber reinforced material. Garikipati Ref.[\[K.Garikipati 2005\]](#), has discussed stationary strain energy and thermodynamic aspects of remodeling with the realization of cell-traction experiments. Kuhl Ref.[\[E.Kuhl 2008\]](#) and Holzapfel Ref.[\[G.Holzapfel 2006\]](#) have showed that gradual alignment of unit-cell can represent collagen network orientation of an engineered tendon-like tissue. Hariton & Holzapfel Ref.[\[I.Hariton 2007\]](#) and Driessen Ref.[\[N.J.Driessen 2003\]](#) have recently used stress-driven reorientation of collagen fibers of arterial walls and porcine aortic valve leaflet. Wilson Ref.[\[W.Wilson 2006\]](#) has predicted the collagen orientation of depth dependent collagen orientation of AC with remodeling. These are all examples of modeling of growth, some of which will be re-visited in this treatise. In this stage, growth is assumed to be strictly depending on the selected pressure (or Darcy velocity) supply of fluid, or blood.

<sup>23</sup>picture:By Hic et nunc Own work CC-BY-SA-3.0, via [Wikimedia Commons](#)

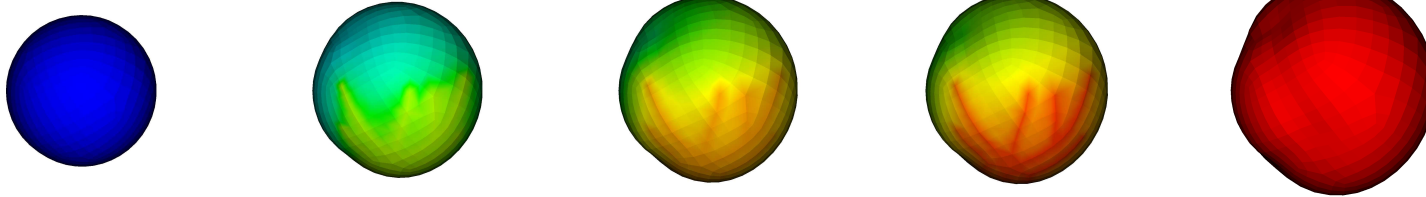


Figure 1.4: The development of the pore pressure distribution on the xy plane; time steps 1-20

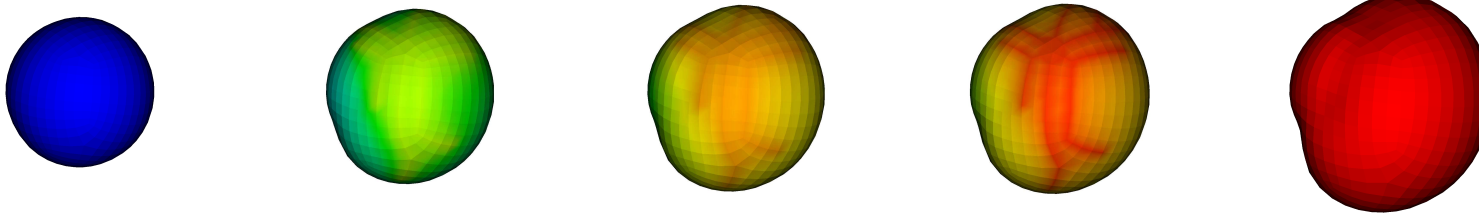


Figure 1.5: The development of the pore pressure distribution on the xz plane; time steps 1-20

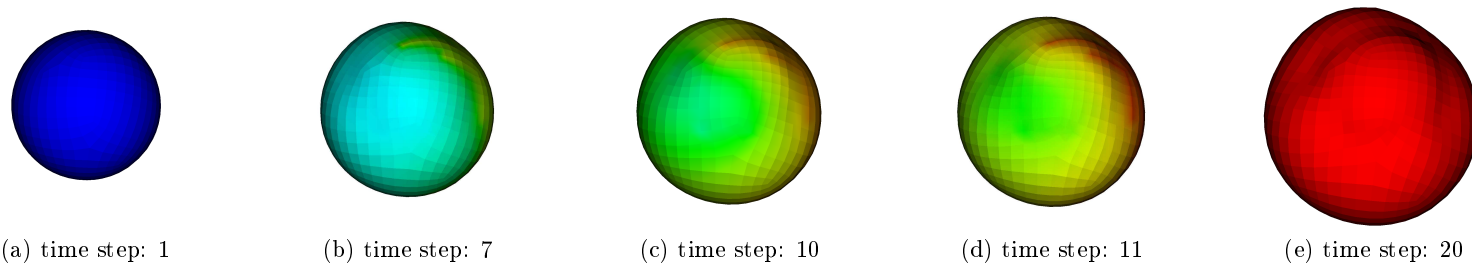
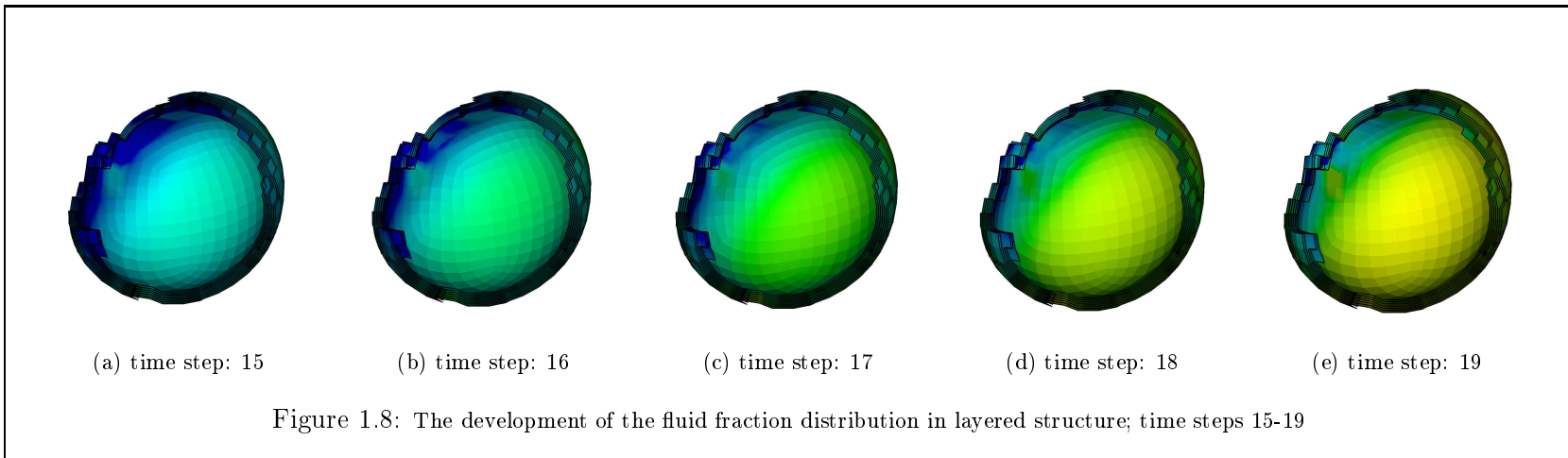
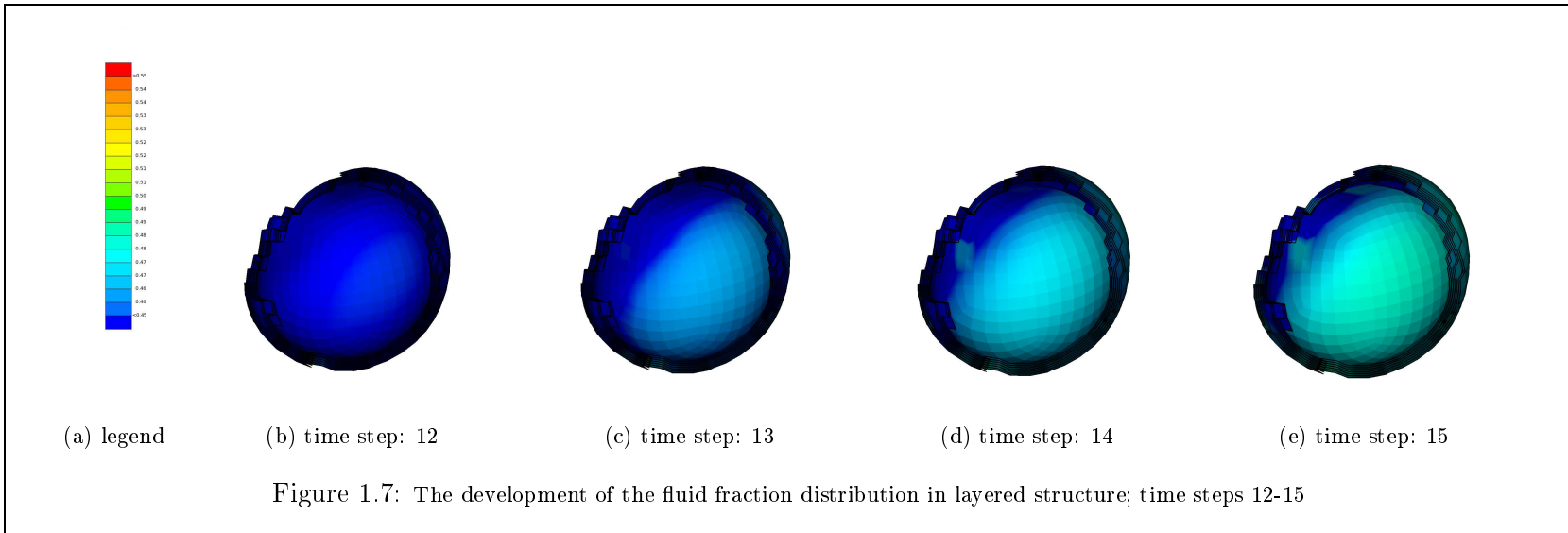


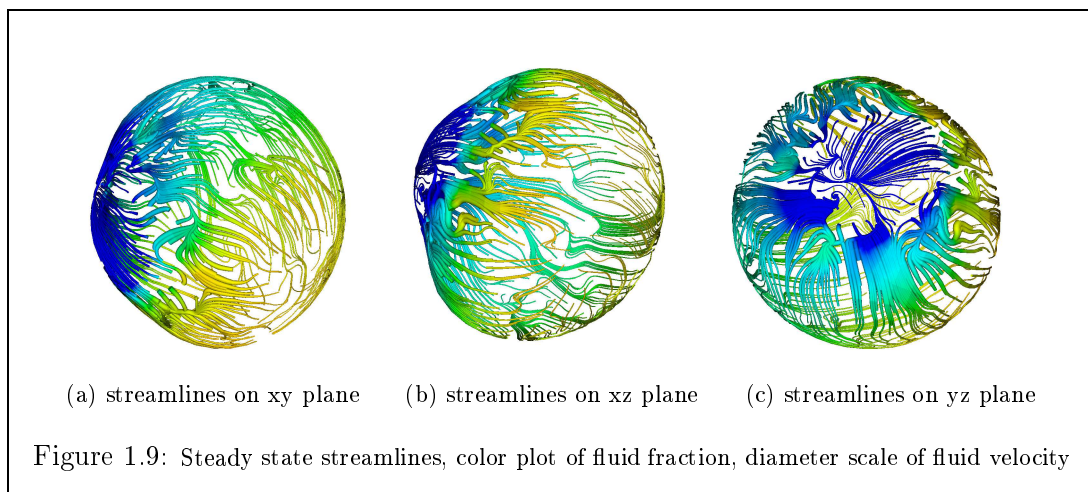
Figure 1.6: The development of the pore pressure distribution on the yz plane; time steps 1-20





The model has in total 2190 nodes, and 1143 elements. The model has been built to consist of two hexahedral rows, and the fiber direction is to be assigned randomly, but lying on the ground of the element row layers. Each element is assumed to contain 4 layers, thus 16 integration points each, means that the functions of element stiffness matrix and computing of internal forces are called 18288 times for each iteration, if one implements the typical Newton-Rhapson algorithm for the solution. As stated before, the pore-pressure is given as input, and the internal-most layer of the structure is assigned with very low permeability values, such that the tissue does not dehydrates from inside, and thus one can not observe the deterministic form of the growth over the pseudo time. According to the formulation given in the previous pages, the pore-pressure driven analysis corresponds to a natural boundary condition type of analysis, and thus shows better convergence characteristics.

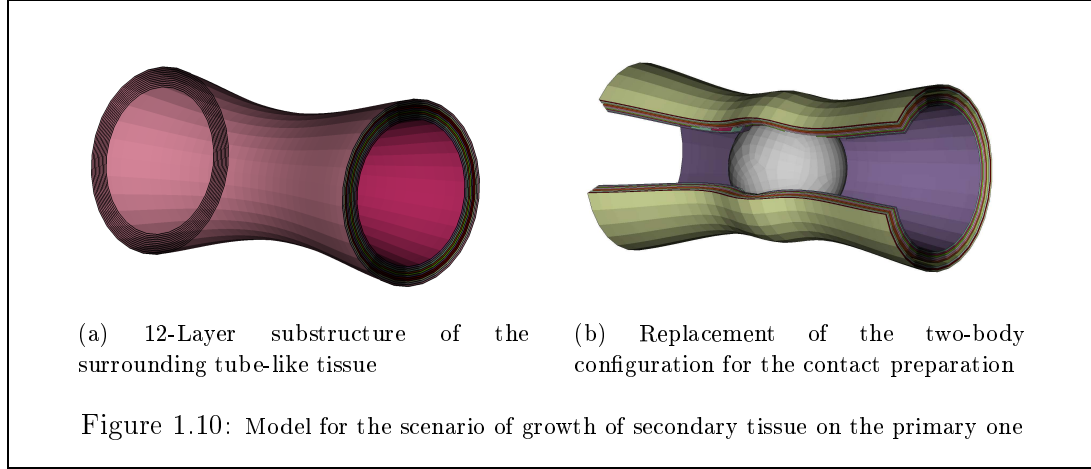
The results of pore pressure with the deformed (or grown) tissue can be seen in *figures of 1.4 to 1.6*. The results of fluid fraction distribution can be seen in the *figures of 1.7 and 1.8*. Initially forty percent of the tissue is assumed to contain fluid. The maximum fluid fraction gains around twenty percent of fluid for the given example. Before showing the results of this scenario of tissue growth on the surrounding primary tissue, the steady state streamlines of the growth on one layer (where the fiber directions are determined to be random), visualized as beneath,



### 1.8.3 A Numerical Scenario: Impact on the Surrounding Tissue

For modeling the impact of the tissue growth on the primary tissue, which is placed anatomically right next to the growing one, penalty type of contact is formulated, modeled and implemented. Besides, for the proper definition of the permeability, the anisotropic permeability behavior is implemented also, which is visited in this section. In this case, along-fiber permeability coefficient is taken to be significantly high, whereby the inter-fiber permeability is taken to be considerably small, but finite. Beneath in *Figure 1.10*, the 12-layer structure of the surrounding tissue and the placement of the healthy tissue inside

of it before the start of inflation is shown.



In the next page in *figures 1.11 to 1.13*, the quasi-isotropic layer-up structure are shown illustratively. *This type of layup fiber orientation is not only quite frequently exist in soft living tissues, but also has very common industrial applications, such as carbon fiber reinforced thermoplast composites or similar. But this type of industrial applications are kept to be completely out of the scope of this thesis.* Returning and recalling back the final definition of the seepage velocity in terms of the impermeability coefficient, fluid fraction, pore-pressure and more,

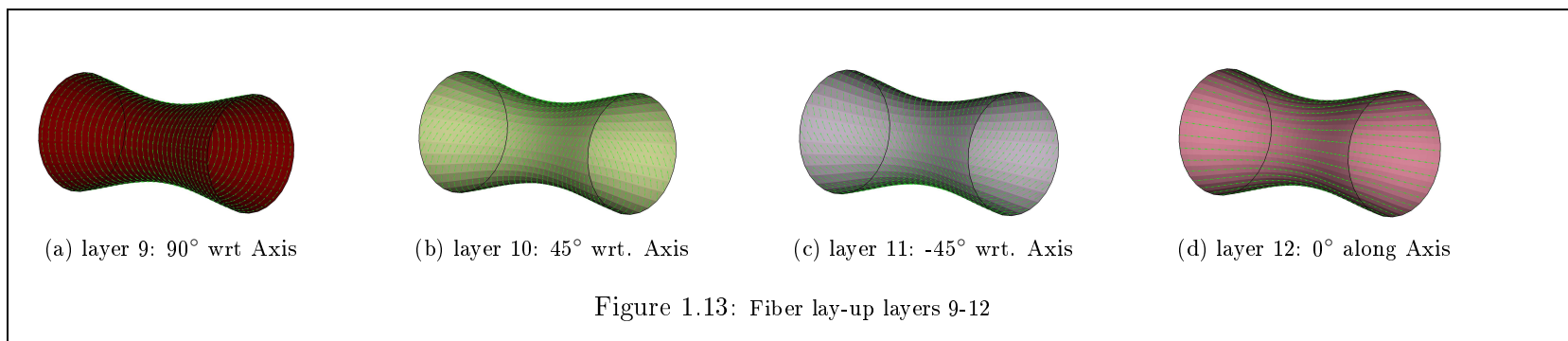
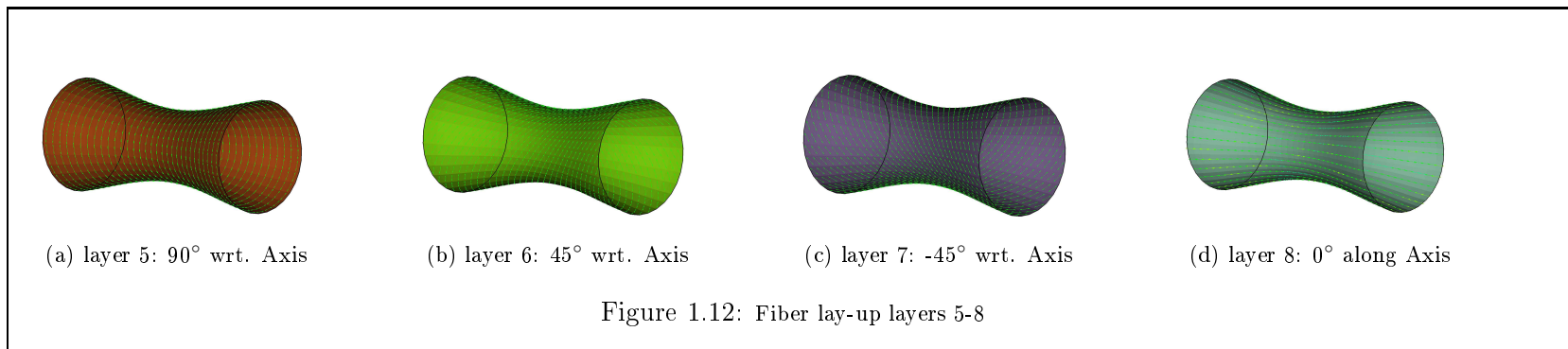
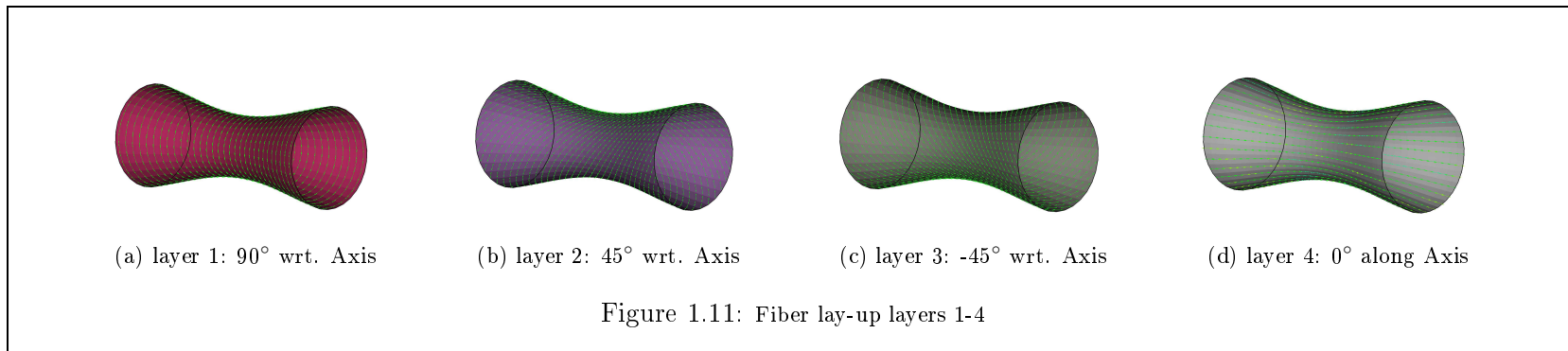
$$\mathbf{w}^{fs} = \beta^{-1} \left( \varrho^f \check{\mathbf{f}}_b^f - n^f \text{grad}(\lambda) \right) \quad (1.213)$$

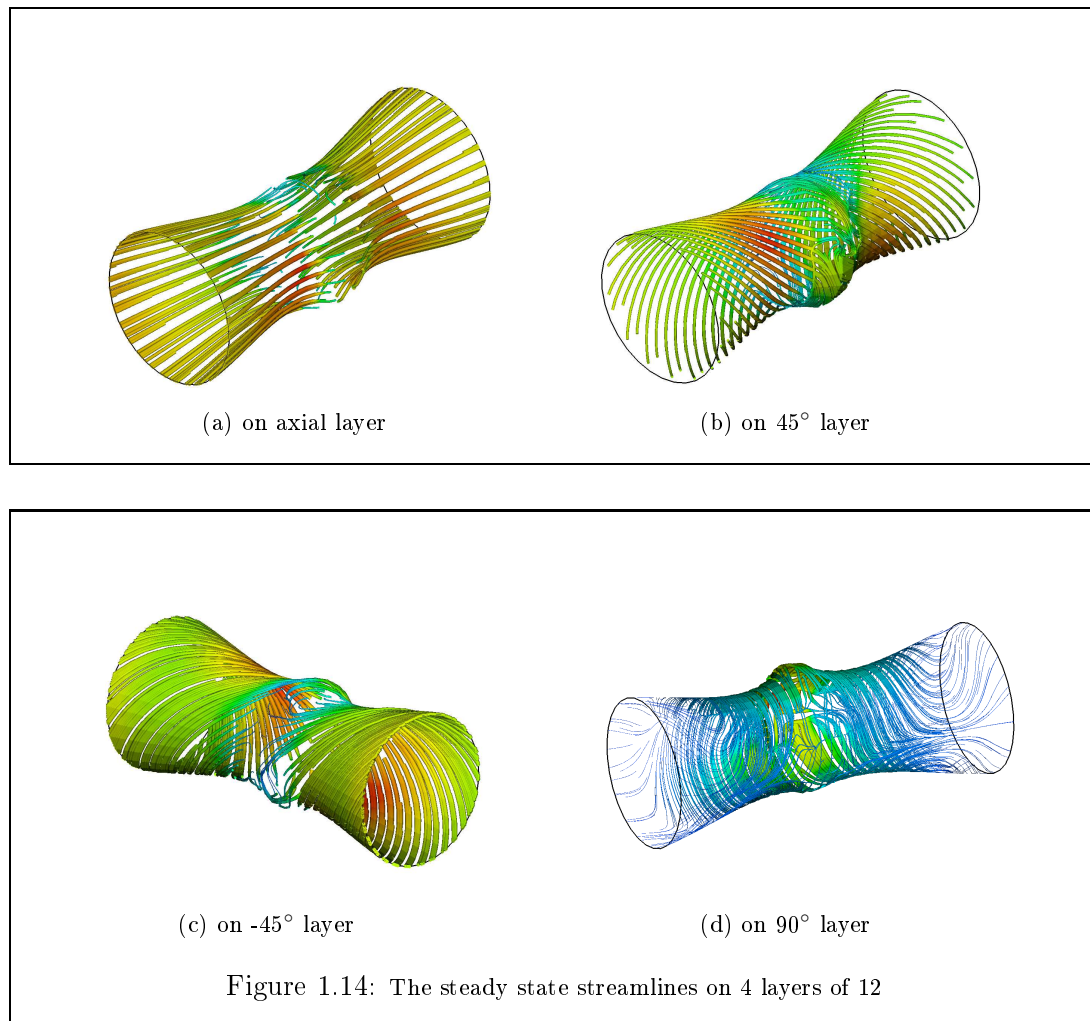
The effect of permeability on the seepage velocity can be divided into fiber-parallel and fiber-perpendicular components as follows,

$$\begin{aligned} \mathbf{w}^{fs} = & \beta_{\parallel}^{-1} (\mathbf{M} \otimes \mathbf{M}) \left( \varrho^f \check{\mathbf{f}}_b^f - n^f \text{grad}(\lambda) \right) \\ & + \beta_{\perp}^{-1} (\mathbf{I} - \mathbf{M} \otimes \mathbf{M}) \left( \varrho^f \check{\mathbf{f}}_b^f - n^f \text{grad}(\lambda) \right) \end{aligned} \quad (1.214)$$

Even though quantitative information about the permeability values are missing, one can state that the along-fiber resistance against flow is significantly less than perpendicular to the plane of fiber, or layup.

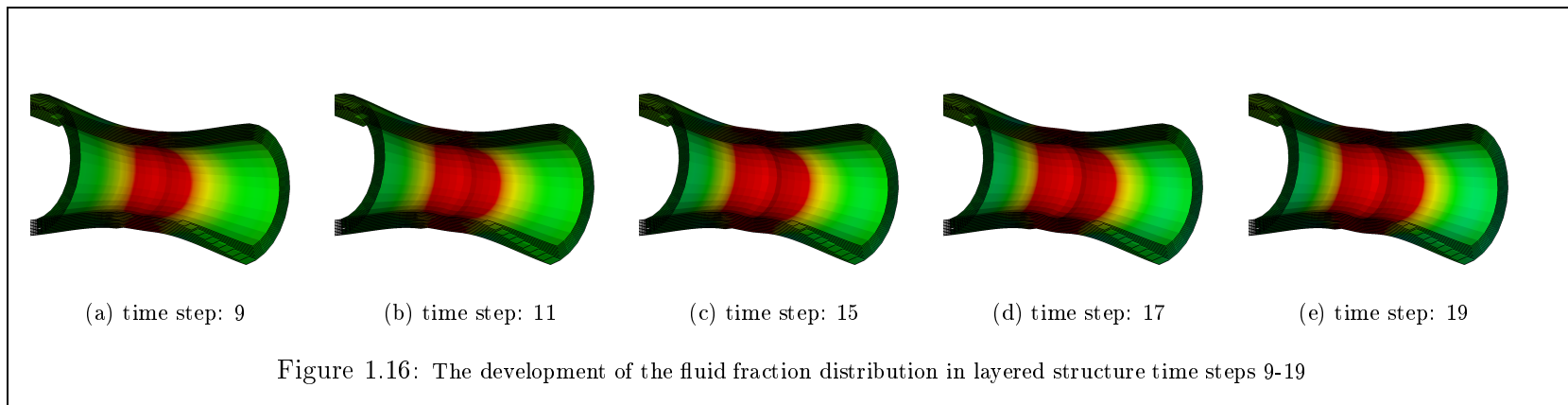
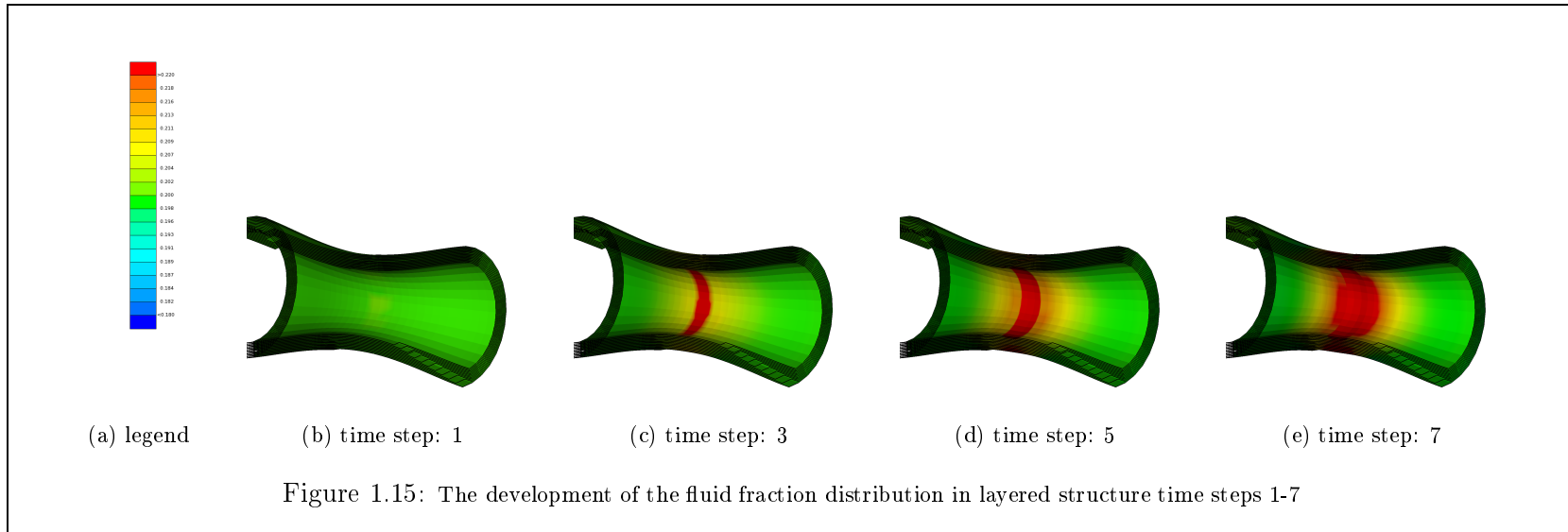
$$\beta_{\parallel} \leq \beta_{\perp} \quad (1.215)$$

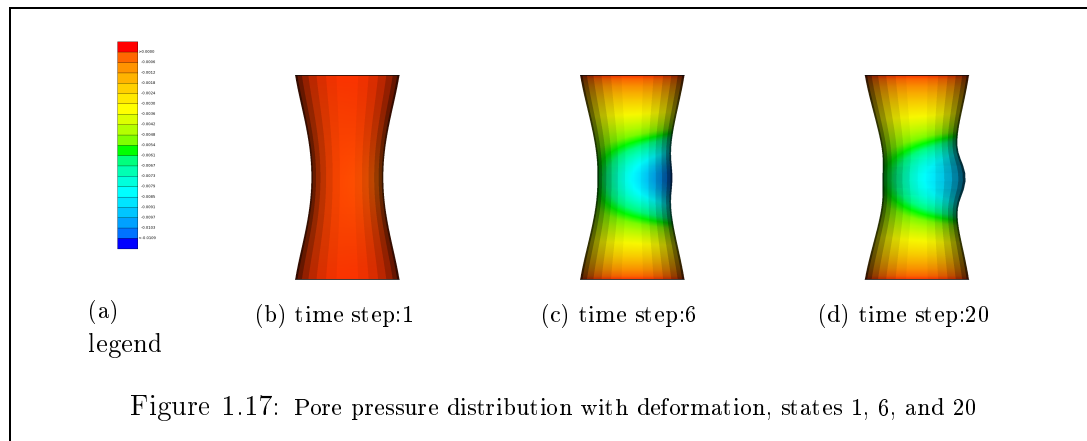




The model consists of three rows of hexahedral element, each of which contains 4 layers. The layup structure is illustrated in *figures 1.11 to 1.13*. According to the defined anisotropic permeability condition, for each individual layup, as long as the permeability ratio is given to be quite dominantly different in along and perpendicular directions, one expects to see streamlines following the pattern of layup fiber directions. As shown in *Figure 1.14*, the expectation is completely fulfilled, at least qualitatively quite satisfactory.

Concluding with some quantitative information about the model, is that the model consists of 2190 nodes, 4 degree of freedom at each node, 1456 elements, with 16 integration points at each. The case is loaded only at three kinematic degrees of freedoms per Node by means of contact displacements, which was supplied from the numerical scenario of deterministic tumor growth. At the free edges, the pore-pressure is forced to stay zero, considered as natural boundary condition. The initial fluid fraction is given to be only twenty percent, representing a dry thus an extraordinary case, as shown in the *figures of 1.15 to 1.16*.

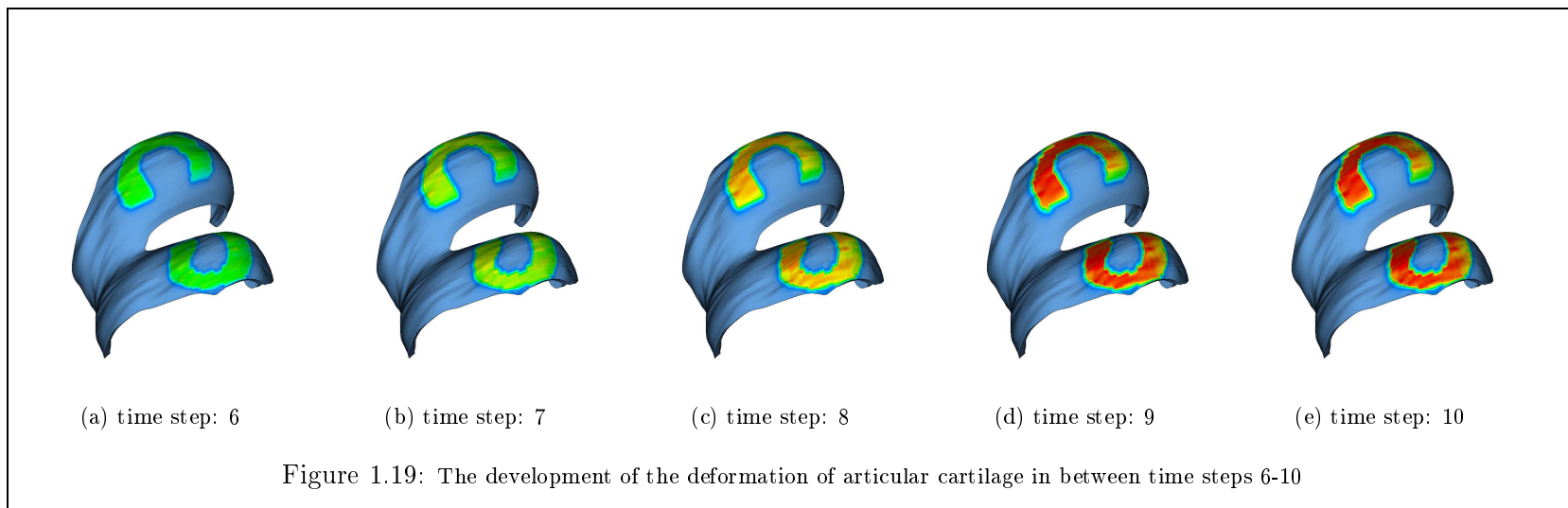
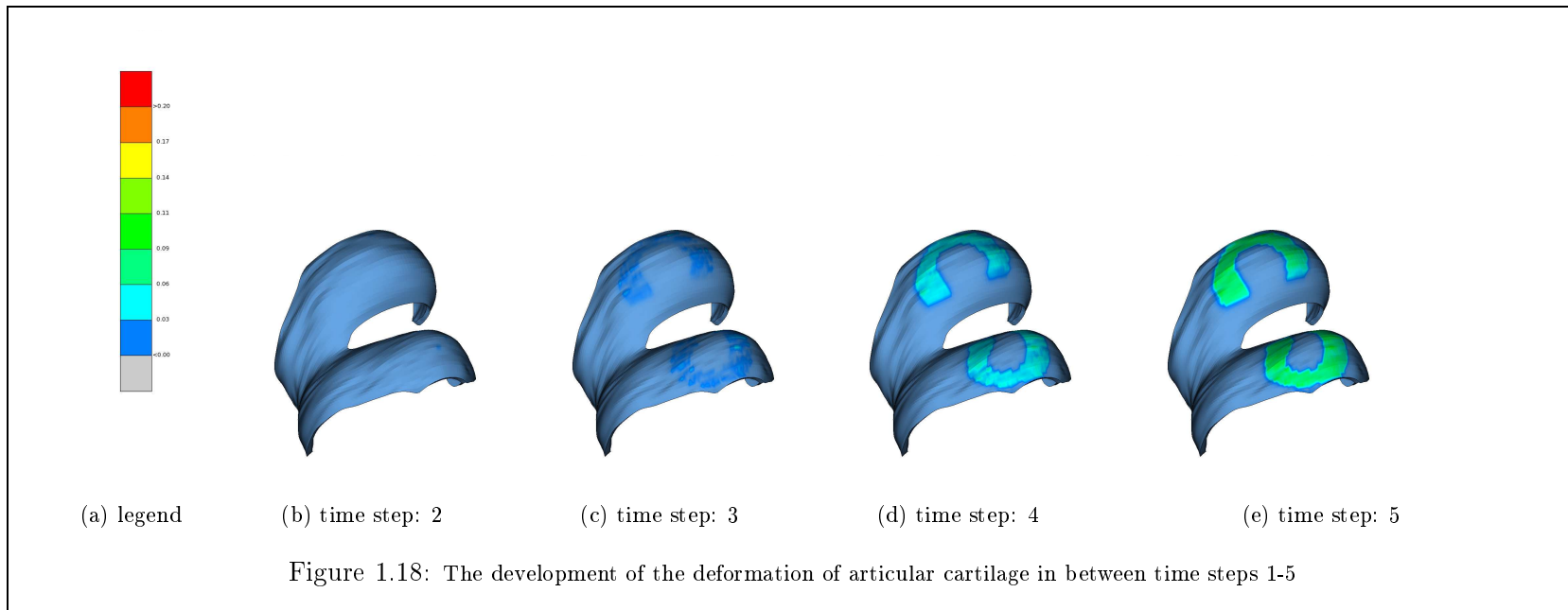


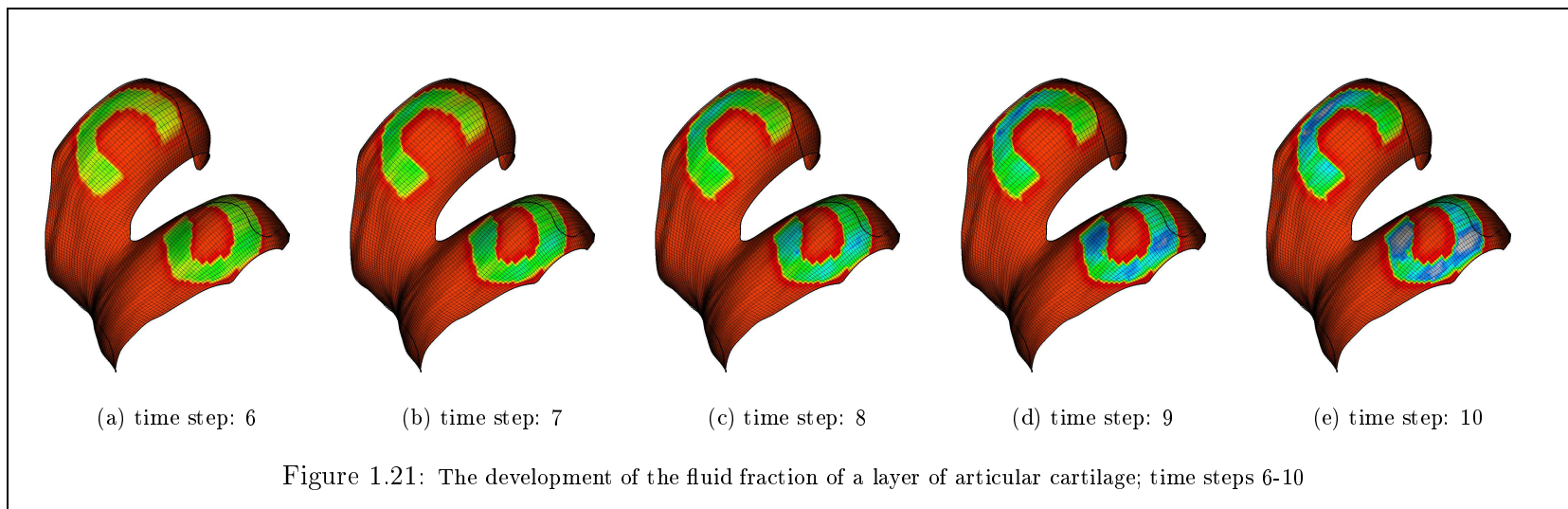
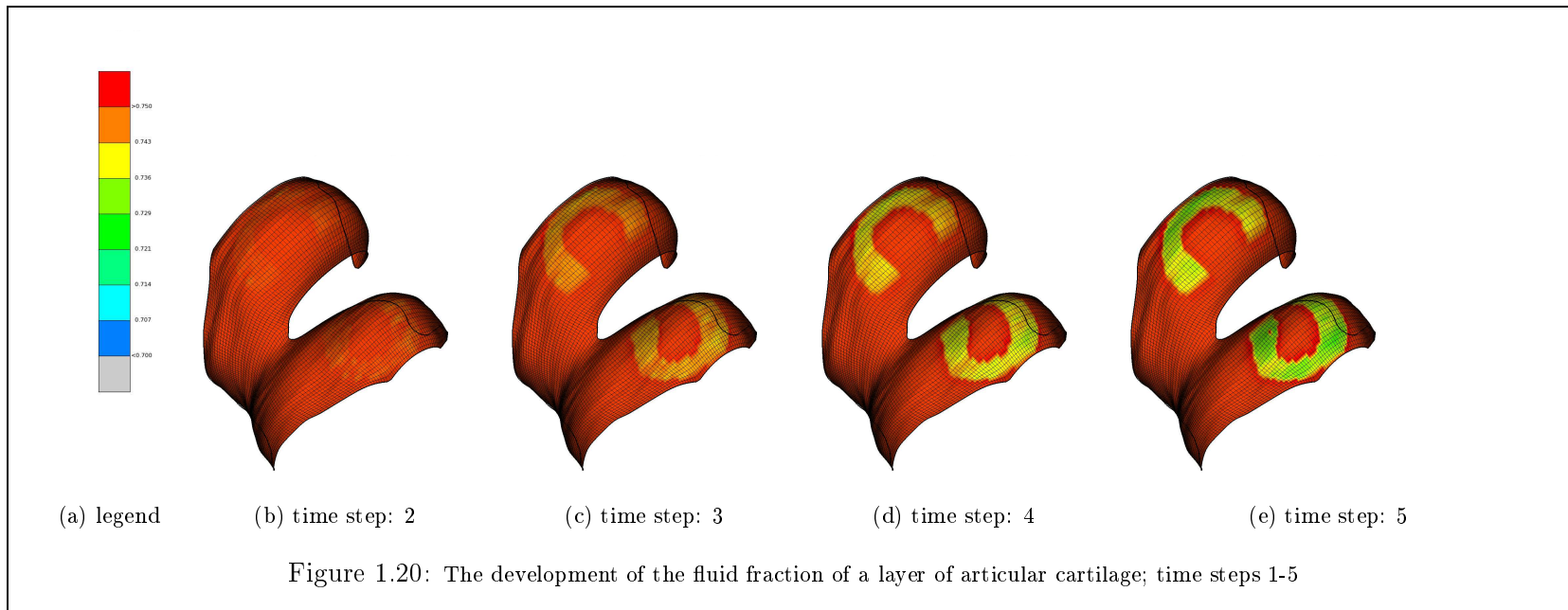


#### 1.8.4 A Numerical Scenario: Cartilage under Compression

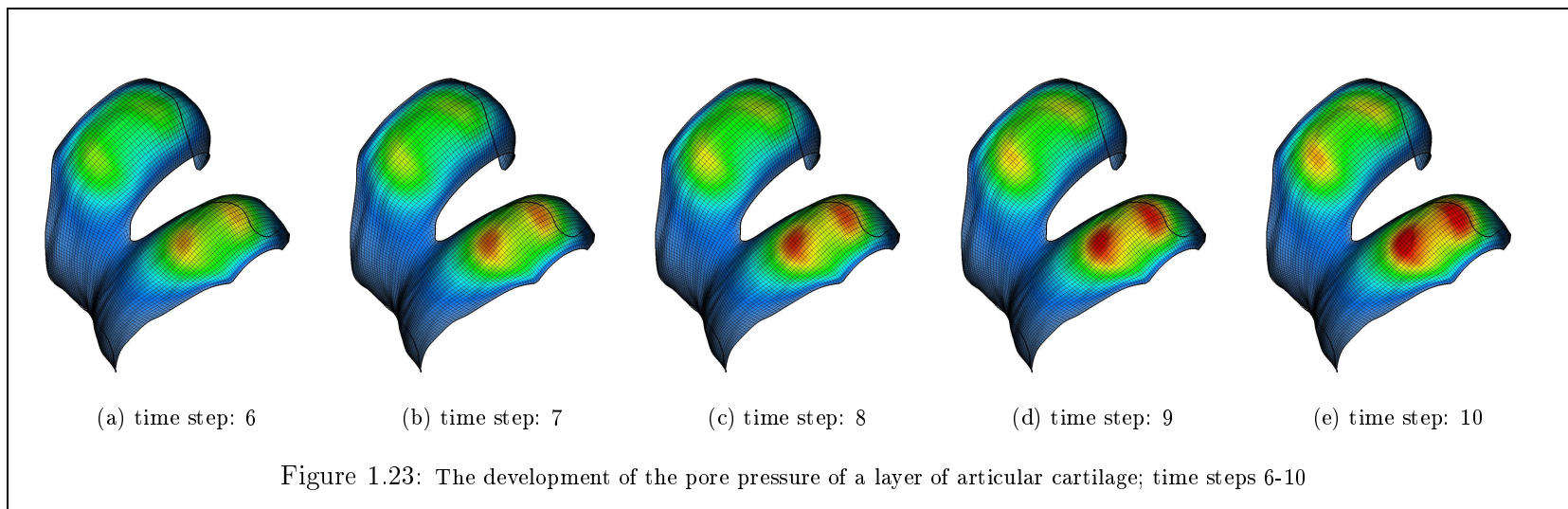
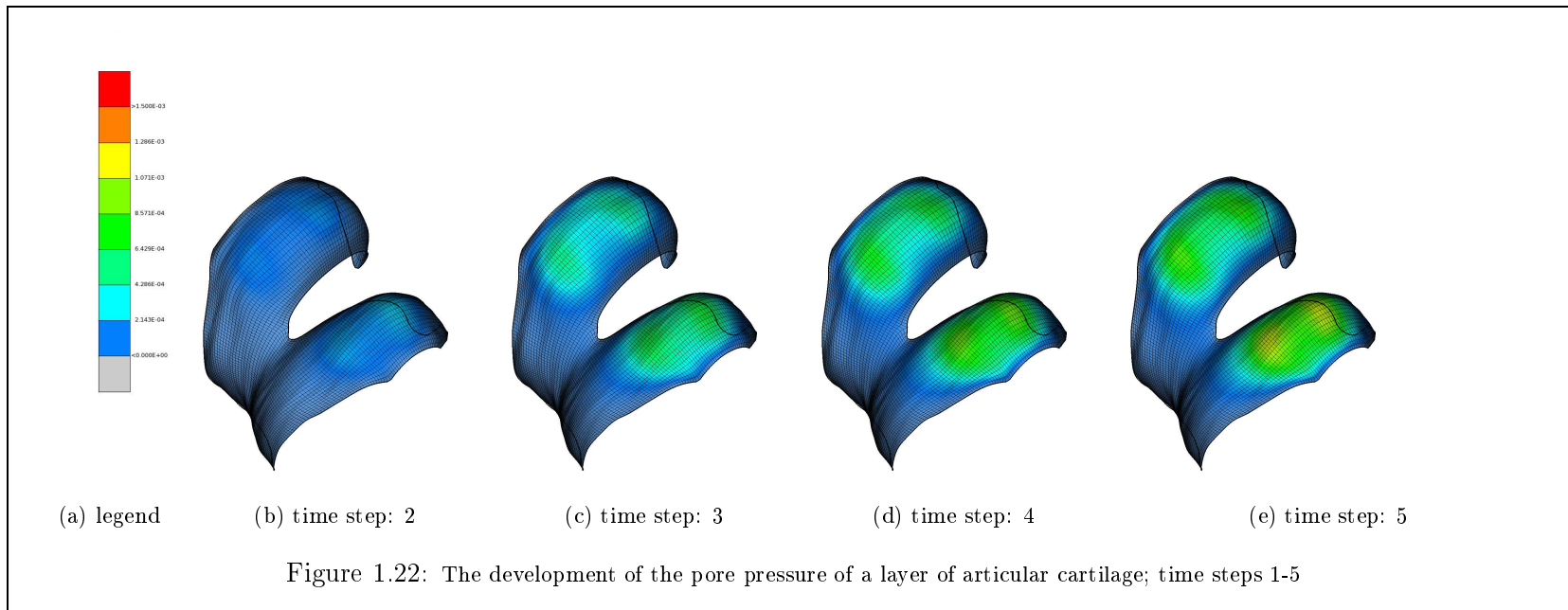
For the third scenario a rather realistic geometry and loading condition is taken. The finite element mesh-tree was obtained from a very appreciated source of Ref. [Erdemir 2014]. The case consist of a porous media of cartilage with 25274 nodes and 18546 elements. There are four element rows and 4 layups at each element considered, which results in 296736 integration points in total. In this scenario, the master surface with 1320 elements closures to the slave cartilage surface linearly with the pseudo time. The master surface is taken to be rigid, and the contact is of type kinematic. Realistic values are assumed for the fluid fraction of the cartilage, the composition consists of 80% fluid and 20% fibrous ground structure. As defined previously, the fiber orientation is modelled fo be quasi-isotropic and is visited via illustration in this chapter.

Since it is difficult and meantime might be misleading to reach solid upshots on the results, the conclusions based on these results are intepreted cursorily. As can be seen in *Figure 1.19*, for the given parameters and boundary conditions the deformation field seems to effect only contact region of solid part and the very near neighborhood of it. The same conclusion can be also done for the distribution of the fluid fraction as one can see from *Figure 1.21*. As opposite to the previous example of surrounding tissue of the growing spherical tumor, one can see here that, the contact region dehydrates significantly rapidly then anywhere else. . This numerical phenomena might be explainable if one consideres that the superficial zone permeability in the case of articular cartilage was given excessively low as in reality, therefore, the fluid is forced to flow apart from the contact region to the other regions of the tissue, whereby in the previous example the surrounding fluid was allowed to enter the superficial layers from outside. The pore pressure in *Figure 1.23* is more smoothly distributed, and significant difference in medial and lateral surfaces is observable. This observation draws the attention of importance of loading boundary conditions as well, it may be the wrong approximation to steer the simulation with vertical displacement only and for reliable solutions of finite element simulation some macro-scale musculoskeletal analysis and the output of it might be necessary.









# Hyperkinematics

---

## Contents

---

<b>2.1</b>	<b>Introduction</b>	<b>61</b>
<b>2.2</b>	<b>Theory: Kinematics</b>	<b>63</b>
2.2.1	Reference to Spatial: From Reference Lines to Spatial Curves . . .	63
2.2.2	Spatial to Reference: From Spatial Curves to Reference Lines . . .	67
2.2.3	Material to Spatial: From Reference Curves to Spatial Curves . . .	70
<b>2.3</b>	<b>Verification: Numerical Examples</b>	<b>72</b>
2.3.1	Push Forward: From straight Reference to the curved Spiral . . .	72
2.3.2	Pull Back: From curved Spiral to the straight Reference . . . . .	73
<b>2.4</b>	<b>Conclusion</b>	<b>75</b>

---

## 2.1 Introduction

Kinematics is the initial building block of continuum solid mechanics in matter and manner. Kinematics, which define the spatial and pseudo-temporal change of *'motion'* of a continuum, is historical and essential prologue. Therefore, any placement of postulates, extensions, suffix, annex, corrections or redefinitions, which deepens the subject of continuum mechanics, should be initiated at the stage of Kinematics.

The necessary reasoning of consideration of strain-gradient effects is in fact very crucial and a matter of scale problem. Irrespective of scale of interest, in many cases, the notion of material point and the size of its neighborhood might be quite comparable of the scale of interest itself. In other words, one may find itself quite on a border line, at the scale of grain, where unique material parameters can not be accepted to be generally valid. These parameters would be even not valid for the near next of point of interest, as obvious from *Figure 2.1* in Ref.[[J.M.Clark 1990](#)]. Considering the focus of interest of this thesis, namely fibrous biological soft-tissues, the previously mentioned scale-phenomenon is so clear that one can not deny the presence of it.

The scale problem forces the observer to stack in a borderline, where parametrization of significant quantities having an impact on energy density function, is no longer negligibly sensitive to little changes of the size of focus, and thus loses robustness. Reconsidering the example given in *Figure 2.1*, the selection of the material size as on the left hand size would indicate of inclusion of voids or porosity filler matrix excessively (or other way

around). Meanwhile, it may also indicate of ignoring some forms of kinematics (for instance bending and twisting of space curves), if the matter of concern, that one deals with, consists of significantly "long fibers" as in the case of *Figure 2.1*. The deviation of the material standard can be reduced, and some objectivity can be gained by moving towards to the middle form of *Figure 2.1*, however the second problem stated above would still persist to exist. The full fiber length can (for instance) be achieved by the selection of the size as suggested in the rightmost picture, however this would throw one out of to the stability limit and consistency radius of the method of solution for the partial differential equations. The least closing door is obviously defining a borderline from top, therefore one reaches back to the initial problem statement, namely the scale problem, if the characteristic material dimension is comparably near to the dimension of geometry. One improvement that is suggested here in this thesis is considering the strain gradient effects which enables one to get smaller in the size of the material and meanwhile preserving to stay in the consistency radius of solution method of PDE.<sup>1</sup>

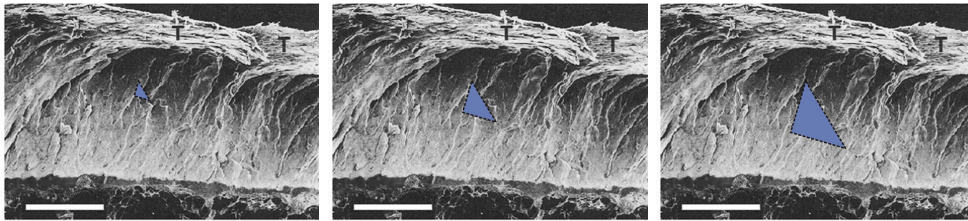


Figure 2.1: Material size subjectivity illustrated on real Human biological specimen (SEM Image taken from Ref.[[J.M.Clark 1991](#)]). The original image does not contain the blue triangle. Bar=1mm)

The scanning electron microscopy result of *Figure 2.1* is not a single evidence, which is selected specifically. Several other can be given here such as; Hughes et. all. Ref.[[L.C.Hughes 2005](#)], Clark Ref.[[J.M.Clark 1990](#)] again, and Kurogouchi et. all. Ref.[[S.Kobayashiv 1995](#)] present similar pictures, where similar conclusions can be driven from.

Keeping the introductory statement given above in mind, which is assembled in the following section, the necessary non-linear strain gradient kinematics is defined here. It is shown in a novel way that, quite unusual to classical kinematics, strain gradient kinematics forces the tangent maps of different configurations both additively and multiplicatively. Following, the straight reference to curved spatial tangent mappings and the inverse, as well as the tangent mappings in between two arbitrary curved configurations are numerically shown to be fully consistent with each other along the theory presented here. As mentioned above, the impact of the predictions on the balance is visited and assembled then in the subsection of numerical examples (see Ch.[[2.3](#)]).

Hereby, initially the kinematics of continua with hypergradient effects, present in their motion, is defined. The parametric reference to curved system tangential mapping, as well as the curved current to straight reference tangential mapping are defined. In order to

<sup>1</sup>Please refer to Zienkiewicz Ref.[[O.C.Zienkiewicz 2000a](#)] for the relationship of element size to stability, consistency and convergence of FEM as a method of solving PDE's

support and show the reversibility of tangential motion, the tangential mapping of arbitrarily curved configuration into another arbitrarily curved configuration is mentioned shortly.

The validity of the presented kinematical relationships are shown to be consistent with the given numerical examples. The drifting errors of classical kinematics and strain-gradient kinematics are compared with each other by considering a smooth motion.

## 2.2 Theory: Kinematics

In this section, the necessary kinematics and its components are introduced. In the next context, the *reference configuration* is taken to be as an accumulation of infinitely many, infinitely small straight line increments. Whereby the *spatial and material configurations* are defined to be the forward and reverse mappings of that reference configuration respectively. With these definitions in hand<sup>2</sup>, in three main subsections, reference to spatial, material to reference and finally material to spatial point and tangent mappings are introduced.

### 2.2.1 Reference to Spatial: From Reference Lines to Spatial Curves

The reference to spatial mapping of the '*continuous motion*', and the inverse spatial to reference '*reverse continuous motion*' are assumed to exist and be bijective, and thus continuum preserving and penetration averting.

$$\psi: \Omega_{\mathbf{X}} \subset \mathbb{R}^3 \mapsto \Omega_{\mathbf{x}} \subset \mathbb{R}^3, \quad \mathbf{x} = \psi(\mathbf{X}) \quad (2.1a)$$

$$\psi^{-1}: \Omega_{\mathbf{x}} \subset \mathbb{R}^3 \mapsto \Omega_{\mathbf{X}} \subset \mathbb{R}^3, \quad \mathbf{X} = \psi^{-1}(\mathbf{x}) \quad (2.1b)$$

The material coordinates  $\mathbf{X}$  and spatial coordinates  $\mathbf{x}$  are assumed to be  $C^r$  diffeomorphic. Thus, the bijective mapping  $\psi$  and its inverse  $\psi^{-1}$  are  $r$  times differentiable, but not necessarily smooth. Besides, it is assumed that, at least in the neighborhood of the infinite domain, the mapping and its inverse are analytic.

With the assumptions above, the material to spatial mapping at locus  $\mathbf{X}^* + d\mathbf{X}^*$  converges to the Taylor series expansion of the mapping  $\psi$  around  $\mathbf{X}^*$  with an infinite neighborhood director of  $d\mathbf{X}^*$ . In general, for  $r > 2$  for a  $C^r$  diffeomorphic analytic mapping the following

---

<sup>2</sup>In short, in this section and in the followings, if not otherwise stated, the reference and material configurations would not collide anymore, those will be taken to be different.

can be written,

$$\begin{aligned}
\boldsymbol{x} + d\boldsymbol{x} = \psi(\boldsymbol{X} + d\boldsymbol{X}) &= \frac{1}{0!} \left( \frac{\partial^0 \psi}{\partial \boldsymbol{\Upsilon}^0} \Big|_{\boldsymbol{\Upsilon}=\boldsymbol{X}} \right) (\boldsymbol{X} + d\boldsymbol{X} - \boldsymbol{X})^{\otimes 0} \\
&+ \frac{1}{1!} \left( \frac{\partial^1 \psi}{\partial \boldsymbol{\Upsilon}^1} \Big|_{\boldsymbol{\Upsilon}=\boldsymbol{X}} \right) \cdot (\boldsymbol{X} + d\boldsymbol{X} - \boldsymbol{X})^{\otimes 1} \\
&+ \frac{1}{2!} \left( \frac{\partial^2 \psi}{\partial \boldsymbol{\Upsilon}^2} \Big|_{\boldsymbol{\Upsilon}=\boldsymbol{X}} \right) : (\boldsymbol{X} + d\boldsymbol{X} - \boldsymbol{X})^{\otimes 2} \quad (2.2) \\
&+ \dots \\
&+ \frac{1}{r!} \left( \frac{\partial^r \psi}{\partial \boldsymbol{\Upsilon}^r} \Big|_{\boldsymbol{\Upsilon}=\boldsymbol{X}} \right) \cdot^r (\boldsymbol{X} + d\boldsymbol{X} - \boldsymbol{X})^{\otimes r}
\end{aligned}$$

As shown subsequently, even though it is not stated explicitly in many textbooks, the series expansion given in equation (2.2) is fully consistent with the classical deformation gradient kinematics. Before moving on, the first three powers of the first order tensor directors in terms of binary tensor operator  $(\boldsymbol{A})^{\otimes i}$  is defined. For  $i \in \mathbb{N}_0$  being a nonnegative integer and  $\boldsymbol{A} \in \mathbb{R}^3$  being a first order tensor, dyad power operator can be defined with  $i=1$  being the identity operator. The power of zero is not the absorbing element, since it has to be scalar unity to be consistent with the equation (2.2). The remaining powers are  $i$  times dyadic foldings of the vector  $\boldsymbol{A}$ . The first three powers read;

$$\begin{aligned}
[\boldsymbol{A}]^{\otimes i}: (\boldsymbol{A} \in \mathbb{R}^{3 \times 1}, i \in \mathbb{N}_0) &\mapsto \boldsymbol{B} \in \mathbb{R}^{3 \times i} \\
(\boldsymbol{A})^{\otimes 0} &= 1 \\
(\boldsymbol{A})^{\otimes 1} &= \boldsymbol{A} \\
(\boldsymbol{A})^{\otimes 2} &= \boldsymbol{A} \otimes \boldsymbol{A}
\end{aligned} \quad (2.3)$$

Using the definitions above, for instance, the truncated series expansion of scalar valued vector function  $x_2 = x_2(X_1, X_2, X_3)$  at an instant is written in tensor-off form as follows,

$$\begin{aligned}
x_2 + dx_2 &= x_2(\mathbf{X} + d\mathbf{X}) \\
&= x_2(X_1 + dX_1, Y + dY, Z + dZ) \\
&\approx \left( \frac{\partial^0 x_2}{\partial \alpha^0} \Big|_{\alpha=\mathbf{X}} \right) + \left( \frac{\partial^1 x_2}{\partial \alpha^1} \Big|_{\alpha=\mathbf{X}} \right) \cdot (d\mathbf{X}) + \left( \frac{1}{2} \frac{\partial^2 x_2}{\partial \alpha^2} \Big|_{\alpha=\mathbf{X}} \right) : (d\mathbf{X})^{\otimes 2} \\
&= x_2(\mathbf{X}) + \frac{\partial x_2}{\partial X_1} dX_1 + \frac{\partial x_2}{\partial Y} dY + \frac{\partial x_2}{\partial Z} dZ \\
&\quad + \frac{1}{2} \left( \frac{\partial^2 x_2}{(\partial X_1)^2} (dX_1)^2 + \frac{\partial^2 x_2}{(\partial X_2)^2} (dX_2)^2 + \frac{\partial^2 x_2}{(\partial X_3)^2} (dX_3)^2 + \right) \\
&\quad + \frac{1}{2} \left( 2 \frac{\partial^2 x_2}{\partial X_1 \partial X_2} dX_1 dX_2 + 2 \frac{\partial^2 x_2}{\partial X_3 \partial X_1} dX_3 dX_1 + 2 \frac{\partial^2 x_2}{\partial X_2 \partial X_3} dX_2 dX_3 \right)
\end{aligned} \tag{2.4}$$

Of course, similar tensor-off form can be written for other scalar valued components of mapping (2.1). Having truncated the series one term earlier, one gets the directional derivative of the point mapping, towards the direction of  $d\mathbf{X}$ . This specific type of linearization gives the backbone identity of the classical kinematics.

$$d\mathbf{x} = \mathbf{F} \cdot d\mathbf{X} \quad d\mathbf{X} = \mathbf{F}^{-1} \cdot d\mathbf{x} \tag{2.5}$$

As obvious, the forward tangent mapping of linearization  $\mathbf{F}$  in equation (2.5) preserves finite line segments as rotated and stretched line segments. Defining the gradient of the deformation gradient in tensor and indicial notations;

$$\mathbf{G} = \nabla_{\mathbf{X}} \mathbf{F} \quad G_{ijk} = \frac{\partial x_i}{\partial X_j \partial X_k} \tag{2.6}$$

With this definition of (2.6), equations (2.2) & (2.4) are shown in tensor notations<sup>3</sup> beneath.

$$d\mathbf{x} = \mathbf{F} \cdot d\mathbf{X} + \frac{1}{2} \nabla_{\mathbf{X}} \mathbf{F} :^r (d\mathbf{X} \otimes d\mathbf{X}) \tag{2.7}$$

The illustrative hypermatrix-matrix-vector notation shown in *Figure 2.2* gives a better understanding of the equation above. The linearized tangent mapping (2.5) is homogeneous of order 1, whereby equation (2.7) is not, and thus nonlinear. To show this, parameter  $\alpha$  is introduced and scale the infinite reference director in the parametric interval of alpha.

$$[-1, 1] = \{\alpha \in \mathbb{R} \mid -1 \leq \alpha \leq 1\} \tag{2.8}$$

$$\mathbf{F} \cdot \alpha d\mathbf{X} = \alpha \mathbf{F} \cdot d\mathbf{X} \quad \Rightarrow \quad \alpha d\mathbf{x} = (\nabla_{\mathbf{X}} \psi) |_{\mathbf{X}, \alpha d\mathbf{X}}$$

<sup>3</sup>Left, Right and Mid double contractions  $\binom{l}{:}$ , *beneath*  $\binom{:}{:}$ ,  $\binom{m}{:}$  are named according to the repeated indices, i.e. for the  $\binom{l}{:}$  contraction the leftmost two indices are repeated.

This statement obviously does not hold for equation (2.7). To move on, the sharp, flat and neutral reference directors ( $d\mathbf{X}^\sharp, d\mathbf{X}^b, d\mathbf{X}^\natural$ )<sup>4</sup> are defined by choosing alpha extremities as 1, -1 and again 1 respectively. As can be noted, sharp and neutral reference directors indicate the same and depending on the context, will be used from this point on interchangeably.

The spatial sharp and flat directors are defined via mapping, not via parametrization. Using (2.8) and the obvious identity of the equality of sharp and flat dyadic squares, i.e.  $(d\mathbf{X}^\sharp \otimes d\mathbf{X}^\sharp) = (d\mathbf{X}^b \otimes d\mathbf{X}^b)$ , one obtains the following tensor-algebraic equalities;

$$\begin{aligned} d\mathbf{x}^\sharp &= \mathbf{F} \cdot d\mathbf{X}^\sharp + \frac{1}{2} \mathbf{G}^r : (d\mathbf{X}^\sharp \otimes d\mathbf{X}^\sharp) = -\mathbf{F} \cdot d\mathbf{X}^b + \frac{1}{2} \mathbf{G}^r : (d\mathbf{X}^b \otimes d\mathbf{X}^b) \\ d\mathbf{x}^b &= \mathbf{F} \cdot d\mathbf{X}^b + \frac{1}{2} \mathbf{G}^r : (d\mathbf{X}^b \otimes d\mathbf{X}^b) = -\mathbf{F} \cdot d\mathbf{X}^\sharp + \frac{1}{2} \mathbf{G}^r : (d\mathbf{X}^\sharp \otimes d\mathbf{X}^\sharp) \end{aligned} \quad (2.9)$$

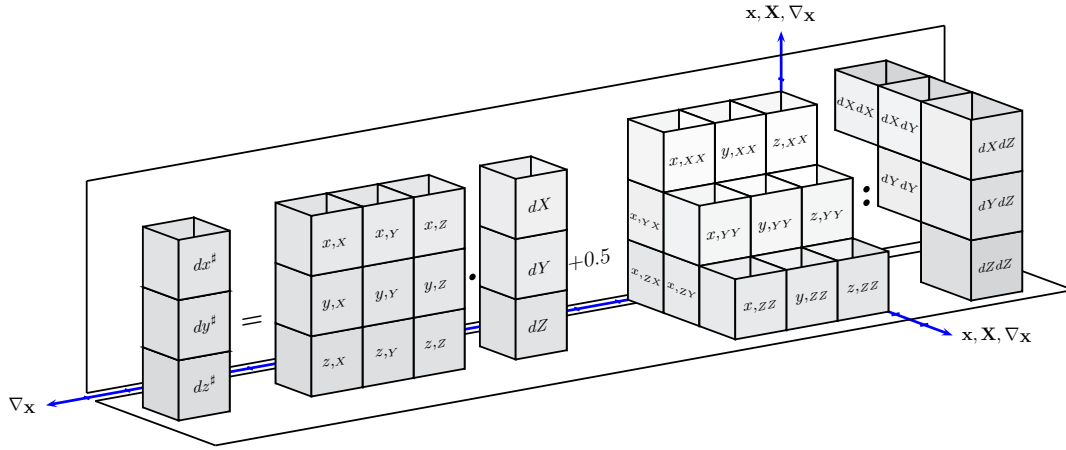


Figure 2.2: Hypermatrix-matrix-vector form of mapping of the sharp spatial tangent with the neutral reference tangent and its metric.

In the absence of contraction of gradient of deformation gradient with the dyadic square, equation (2.9) is homogeneous of order 1. Thus, it was essential to have sharp, neutral and flat definitions of the directors.

$$d\mathbf{x}^\sharp = -d\mathbf{x}^b \iff \mathbf{G}^r : (d\mathbf{X}^b \otimes d\mathbf{X}^b) = \mathbf{0} \quad (2.10)$$

Since the sharp and flat reference directors are linearly dependent, it is implied that the reference configuration is an *only straight* configuration. Correspondingly, since the sharp and flat spatial directors are not necessarily linearly dependent, it should be admitted that the current configuration is *curved & straight*.

<sup>4</sup>Instead of algebraic symbols, symbols of musical harmony is chosen, interchangeable usage of algebraic symbols may cause confusion in this context.

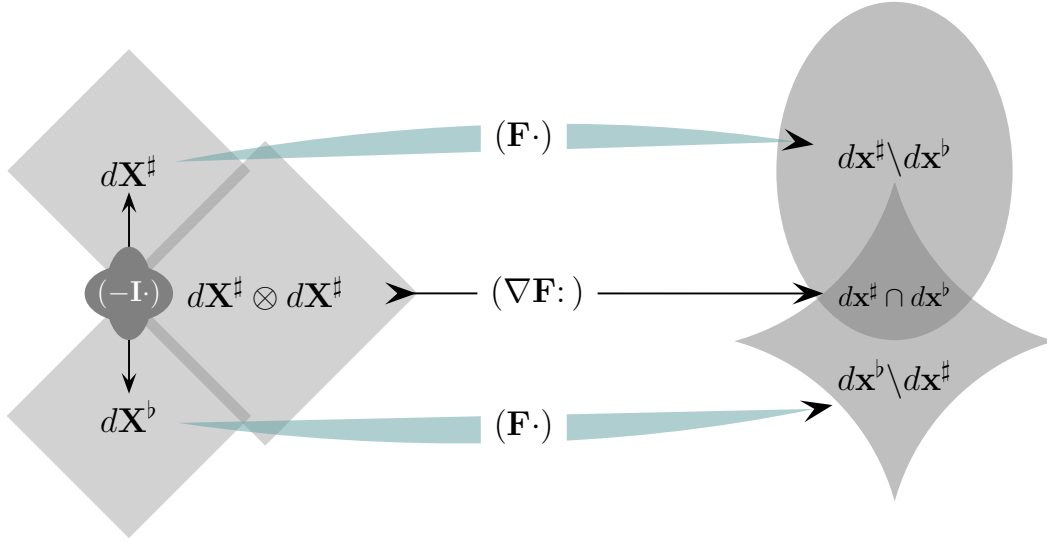


Figure 2.3: Kinematics of reference tangents to spatial tangents

### 2.2.2 Spatial to Reference: From Spatial Curves to Reference Lines

The differential behavior of the reverse kinematics is to be analyzed in this subsection. To do it so, it will not be tried to reverse the tangential mappings from the truncated approximations. Similar to the previous subsection, the (are) reference coordinates around the neighborhood of (were) current coordinates will be expanded, however this time via inverse motion.

$$\begin{aligned}
 \mathbf{X} + d\mathbf{X} &= \psi^{-1}(\mathbf{x} + d\mathbf{x}) \approx \frac{1}{0!} \left( \left. \frac{\partial^0 \psi^{-1}}{\partial \mathbf{v}^0} \right|_{\mathbf{v}=\mathbf{x}} \right) (d\mathbf{x})^{\otimes 0} \\
 &+ \frac{1}{1!} \left( \left. \frac{\partial^1 \psi^{-1}}{\partial \mathbf{v}^1} \right|_{\mathbf{v}=\mathbf{x}} \right) \cdot (d\mathbf{x})^{\otimes 1} \\
 &+ \frac{1}{2!} \left( \left. \frac{\partial^2 \psi^{-1}}{\partial \mathbf{v}^2} \right|_{\mathbf{v}=\mathbf{x}} \right) : (d\mathbf{x})^{\otimes 2}
 \end{aligned} \tag{2.11}$$

The reverse tangent mapping in the form of (2.7), without using sharp and flat director definitions.

$$d\mathbf{X} = \mathbf{F}^{-1} \cdot d\mathbf{x} + \frac{1}{2} \nabla_{\mathbf{x}} \mathbf{F}^{-1} : (d\mathbf{x} \otimes d\mathbf{x}) \tag{2.12}$$

The first term in equation (2.12) is well-known. For further evaluation of the higher order part, remember the fact that, the spatial gradient of the spatial deformation gradient is the spatial gradient of the inverse reference deformation gradient. Denoting this as  $\mathbf{H}$  and following the derivation in indicial notation leads into;

$$H_{ijk} = \frac{\partial F_{ij}^{-1}}{\partial x_k} = \frac{\partial F_{ij}^{-1}}{\partial X_l} \frac{\partial X_l}{\partial x_k} = \frac{\partial F_{ij}^{-1}}{\partial X_l} F_{lk}^{-1} \tag{2.13}$$



As obvious of equation (2.13) the reverse higher order gradient  $\mathbf{H}$  (from spatial to reference) is not the *inverse*<sup>5</sup> of the forward higher order gradient  $\mathbf{G}$ . For reformulation of the reference gradient of the inverse reference deformation gradient appearing in equation (2.13), the following identities are used;

$$\begin{aligned}
0_{mj} &= \frac{\partial}{\partial X_l} \left( F_{mi} F_{ij}^{-1} \right) = \frac{\partial F_{mn}}{\partial X_l} F_{nj}^{-1} + F_{mi} \frac{\partial F_{ij}^{-1}}{\partial X_l} \iff \\
F_{km}^{-1} F_{mi} \frac{\partial F_{ij}^{-1}}{\partial X_l} &= -F_{km}^{-1} \frac{\partial F_{mn}}{\partial X_l} F_{nj}^{-1} \iff \\
\delta_{ki} \frac{\partial F_{ij}^{-1}}{\partial X_l} &= -F_{km}^{-1} \frac{\partial F_{mn}}{\partial X_l} F_{nj}^{-1} \iff \\
\frac{\partial F_{ij}^{-1}}{\partial X_l} &= -F_{im}^{-1} \frac{\partial F_{mn}}{\partial X_l} F_{nj}^{-1}
\end{aligned} \tag{2.14}$$

Inserting it back into the equation (2.13) the reverse higher order gradient in indicial and tensor notations, one gets;

$$H_{ijk} = -G_{mnl} F_{im}^{-1} F_{nj}^{-1} F_{lk}^{-1} \quad \mathbf{H} = - \left[ \mathbf{F}^{-1} \cdot \left( \mathbf{G}^m \cdot \mathbf{F}^{-1} \right) \right]^r \cdot \mathbf{F}^{-1} \tag{2.15}$$

Since this identity is obtained from the point motion only, it should be shown that it holds for the tangential reverse mappings too. To show it, the push forwarded tangents are pulled back. In the following, the index notation is used. Because the proof is straightforward but lengthy, not to squander the indices, and hinder index crash, index and infix notations are applied together.

$$dX_i = F_{ij}^{-1} dx_j + \frac{1}{2} H_{ijk} dx_j dx_k = F_{ij}^{-1} dx_j - \frac{1}{2} G_{mnl} F_{im}^{-1} F_{nj}^{-1} F_{lk}^{-1} dx_j dx_k \tag{2.16}$$

The push forward components at the rhs of equation (2.16) are,

$$dx_j = F_{jo} dX_o + \frac{1}{2} G_{jop} dX_o dX_p \tag{2.17a}$$

$$dx_k = F_{kr} dX_r + \frac{1}{2} G_{krs} dX_r dX_s \tag{2.17b}$$

The first addend of the rhs infix of equation (2.16) reads then,

$$\begin{aligned}
F_{ij}^{-1} dx_j &= F_{ij}^{-1} F_{jo} dX_o + \frac{1}{2} G_{jop} F_{ij}^{-1} dX_o dX_p = \delta_{io} dX_o + \frac{1}{2} G_{jop} F_{ij}^{-1} dX_o dX_p \\
&= dX_i + \frac{1}{2} G_{jop} F_{ij}^{-1} dX_o dX_p
\end{aligned} \tag{2.18}$$

---

<sup>5</sup>So far, the writer could not find in the literature general definitions for hyperdeterminants and hyperinverses in  $\mathbb{R}^{3 \times 3 \times 3}$

Dyadic square  $dx_j dx_k$  in the second addend in equation (2.16) in index and infix notations are shown below,

$$\begin{aligned} dx_j dx_k &= F_{jo} F_{kr} dX_o dX_r + \frac{1}{2} G_{krs} F_{jo} dX_r dX_s dX_o \\ &+ \frac{1}{2} G_{jop} F_{kr} dX_o dX_p dX_r + \frac{1}{4} G_{jop} G_{krs} dX_o dX_p dX_r dX_s \end{aligned} \quad (2.19)$$

The second and third terms are the dyads of gradient push-forwards, with the hypergradient push-forwards. The last addend is the dyad square of the hypergradient push-forward. Dropping the last three addends of equation (2.19) is conform with the second order truncation of the mappings and reverse mappings. Inserting the first addend push-forwarded dyadic square of equation (2.19) into the second addend of equation (2.16), one gets,

$$\begin{aligned} -\frac{1}{2} G_{mnl} F_{im}^{-1} F_{nj}^{-1} F_{lk}^{-1} F_{jo} F_{kr} dX_o dX_r &= -\frac{1}{2} \delta_{no} \delta_{lr} G_{mnl} F_{im}^{-1} dX_o dX_r \\ &= -\frac{1}{2} G_{mnl} F_{im}^{-1} dX_n dX_l \end{aligned} \quad (2.20)$$

In the final version of equation (2.16) it can be seen that the reverse hypergradient of (2.15) together with the inverse of deformation gradient, maps push-forwarded sharp and flat directors into the reference sharp and flat directors.

$$dX_i = \left( dX_i + \frac{1}{2} G_{jop} F_{ij}^{-1} dX_o dX_p \right) - \frac{1}{2} G_{mnl} F_{im}^{-1} dX_n dX_l = dX_i \quad (2.21)$$

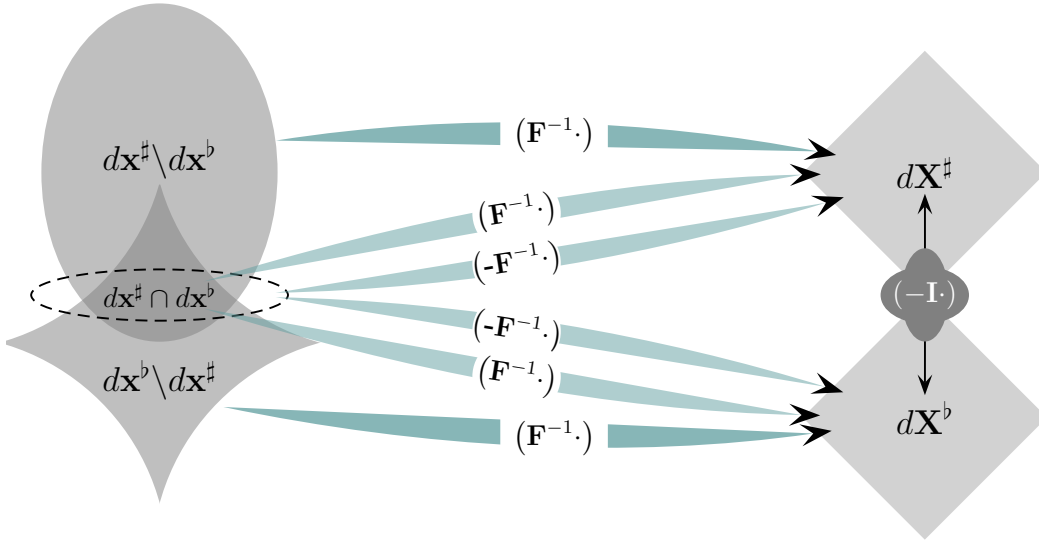


Figure 2.4: Kinematics of spatial tangents to reference tangents

In *Figure (2.4)* as well as in *Figure 4.1* the parallel tensor operators are additively acting. Deformation gradients are the same, standing for the reference to spatial mapping in those

two illustrations. As can be seen from the *Figure 2.4*, since the straight reference tangents are mapped only by inverse deformation gradient acting on the *complements* of curved spatial tangents from each other, which is apparent from equation (2.20), it can be agreed upon the necessity of defining sharp and flat directors.

### 2.2.3 Material to Spatial: From Reference Curves to Spatial Curves

A tangential mapping with hypergradient terms and its *arbitrariness* makes it mandatory that the kinematics coexists in between two geometrical manifolds of dimension, where both possess finite radius of curvatures. This notion of finite radius of curvature of two configurations, i.e. *spatial and material*, is quantified with respect to some *reference* configuration of infinitely large radius of curvature. Having defined a tangential reference directors and parameter  $\alpha$  as in equation (2.8), the existence of some intermediate configuration is implied. With respect to to this configuration, an *allowable parametric representation* of reference and material curves in the sections of Ch.[2.2.1] and Ch.[2.2.2] are defined. This is crucial for the progression of the kinematics towards to the balance equations, since the arbitrariness of the motion denies that *any stress-free configuration* is strictly identical to the straight reference one.

In the following, both reference and material coordinates are represented by capital letters. For the mapping tensors and material, reference and spatial coordinate vectors, the subscript letters  $m, r$ , and  $s$  are used respectively.

The *complement of sharp material director* relative to the flat material director, which is illustrated on the left side of *Figure 4.1*, according to the equation (2.9) is,

$$d\mathbf{X}_m^\# \setminus d\mathbf{X}_m^b = \frac{1}{2} \left( d\mathbf{X}_m^\# - d\mathbf{X}_m^b \right) = \mathbf{F}_{mr}^{-1} \cdot d\mathbf{X}_r^\# \quad (2.22)$$

Finally, the tangent mapping from the curved material into the curved spatial have the form,

$$\begin{aligned} d\mathbf{x}_s^\# &= \mathbf{F}_{rs} \cdot \left( \mathbf{F}_{mr} \cdot \left( d\mathbf{X}_m^\# \setminus d\mathbf{X}_m^b \right) \right) \\ &+ \frac{1}{2} \mathbf{G}_{rs}^r \left[ \left( \mathbf{F}_{mr} \cdot \left( d\mathbf{X}_m^\# \setminus d\mathbf{X}_m^b \right) \right) \otimes \left( \mathbf{F}_{mr} \cdot \left( d\mathbf{X}_m^\# \setminus d\mathbf{X}_m^b \right) \right) \right] \end{aligned} \quad (2.23)$$

As stated above, the double subscripts of tensors do not define the components, but the directions. Accordingly, the subscript of the forward hypergradient of motion can be omitted, since it's reverse is not to be interpreted as it's inverse (inverse of the hypermatrix form). As stated in equation (2.15), the hypergradient of the reverse motion (from straight reference to curved spatial or material) is depending on the inverse of *integral potential* of hypergradient of forward motion. In this sense, the forward deformation gradient (from reference to spatial or material) can be interpreted as the integral potential of the hypergradient of forward point mapping.

A good question as a consequence of the remarks done above would be, why the

hypergradient of the motion of -from material to reference- is not seen in equation (2.23)? The answer would be that, -it is in fact implicitly placed in equation (2.23)- otherwise the material configuration would not earn the abbreviation of being *curved*. In fact, the *complement* of sharp material director relative to the flat material director, and similarly the *complement* of flat material director relative to the sharp material director can be alternatively written as beneath.

$$\begin{aligned} d\mathbf{X}_m^\sharp \setminus d\mathbf{X}_m^b &= d\mathbf{X}_m^\sharp - \frac{1}{2} \mathbf{G}_{rm} :^r (d\mathbf{X}_r^\sharp \otimes d\mathbf{X}_r^\sharp) \\ d\mathbf{X}_m^b \setminus d\mathbf{X}_m^\sharp &= d\mathbf{X}_m^b - \frac{1}{2} \mathbf{G}_{rm} :^r (d\mathbf{X}_r^b \otimes d\mathbf{X}_r^b) \end{aligned} \quad (2.24)$$

Thus, the curvature of the material configuration with respect to the reference configuration is involved in the complete schema. Figure 2.5<sup>6</sup> shows illustratively the

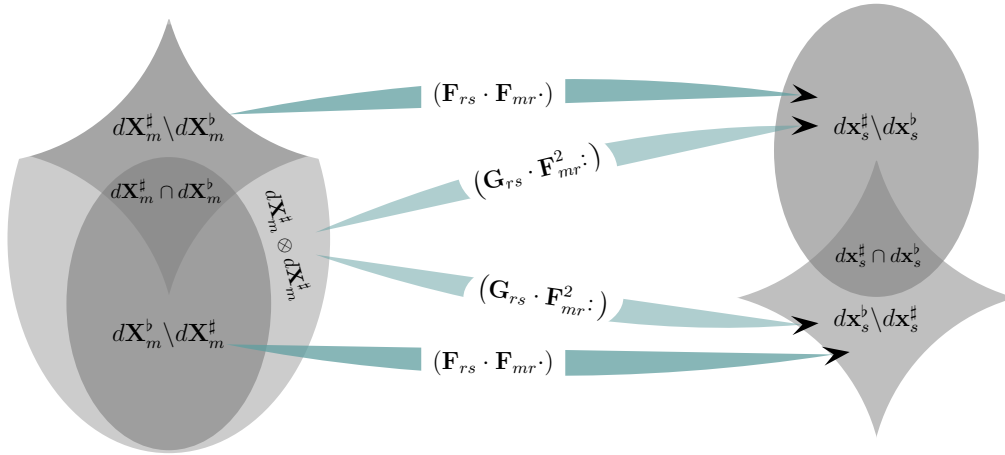


Figure 2.5: Kinematics of material tangents to current tangents

mapping in between arbitrarily curved material and spatial spaces. Even though the motion does not really visit the fictitious reference state, this state is considered as the common origin of the motion of different pseudo-times. From the material to reference, and from reference to spatial circuits of kinematics, additive splits are applied in the parallel elements of the circuit, and multiplicative splits in the serial elements of the circuit.

<sup>6</sup>In the figure, the replacement below is done with a similar argument which is used to simplify (2.19).

$$(d\mathbf{X}_m^\sharp \setminus d\mathbf{X}_m^b) \otimes (d\mathbf{X}_m^\sharp \setminus d\mathbf{X}_m^b) = (d\mathbf{X}_m^\sharp) \otimes (d\mathbf{X}_m^\sharp) \quad (2.25)$$

### 2.3 Verification: Numerical Examples

The given strain gradient kinematics will be verified and compared in this section with the classical one by means of a nonlinear smooth function<sup>7</sup>. The postulated mapping has been chosen to be called as *the spiral beam* and has mainly two parts, namely mid surface and the thickness contribution. The mid surface equation with respect to the time parameter  $\alpha$  is written as,

$$\begin{aligned} x_1^m &= \left[ \frac{2\alpha}{\pi} \cos \left( (1 - X_1) \frac{\pi}{2} \right) + \left( 1 - \frac{2\alpha}{\pi} \right) X_1 \right] \cos(\alpha + \alpha X_1) \\ x_2^m &= \left[ \frac{2\alpha}{\pi} \cos \left( (1 - X_1) \frac{\pi}{2} \right) + \left( 1 - \frac{2\alpha}{\pi} \right) X_1 \right] \sin(\alpha + \alpha X_1) \end{aligned} \quad (2.26)$$

For the thickness contribution, the Piola transformation of the derivatives of the mid curve is taken into account. These mid-curve-off contributions are called to be deviatoric, and depending on the derivatives of the mid-curve.

$$\begin{aligned} x_1^d &= \frac{\partial x_2}{\partial X_1} \Big|_m X_2 \left( \left( \frac{\partial x_1}{\partial X_1} \Big|_m \right)^2 + \left( \frac{\partial x_2}{\partial X_1} \Big|_m \right)^2 \right)^{-1/2} \\ x_2^d &= - \frac{\partial x_1}{\partial X_1} \Big|_m X_2 \left( \left( \frac{\partial x_1}{\partial X_1} \Big|_m \right)^2 + \left( \frac{\partial x_2}{\partial X_1} \Big|_m \right)^2 \right)^{-1/2} \end{aligned} \quad (2.27)$$

These contributions result a nonlinear Bernoulli kinematics, since the curvature through the thickness is punished (penalty) by the constant coefficient of  $X_2$ . In the next, the direct effect of the strain gradients through the thickness is neglected. The total mapping is then,

$$\begin{aligned} x_1 &= x_1^m + x_1^d \\ x_2 &= x_2^m + x_2^d \end{aligned} \quad (2.28)$$

For the corresponding deformation gradient and deformation hypergradient terms, please refer to *Appendix-A*.

#### 2.3.1 Push Forward: From straight Reference to the curved Spiral

In this subsection, the performances of the backbone identity of classical nonlinear kinematics (2.5) and the backbone identity of the strain-gradient kinematics (2.6) are compared with each other numerically. The comparison depends mainly on the discretization and the excession of the spiral beam *from the forth and towards to back*. The pseudo time parameter  $\alpha$  has also an influence on the total drifting error, since it is the main parameter driving the curvature of the deformation.

As apparent from *Figure 2.6*, for rough discretization and beginning time increments, the strain-gradient kinematics represents the deformation better then classical tangential mapping, however the difference is not significant. With enough number of sampling

<sup>7</sup>The details of derivatives of this smooth function can be found in *Appendix-A*

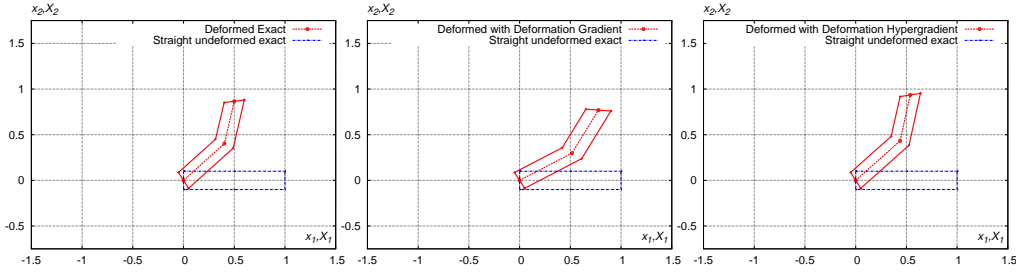


Figure 2.6: From straight reference to the curved spiral beam.  $\alpha = \pi/6, n = 2$

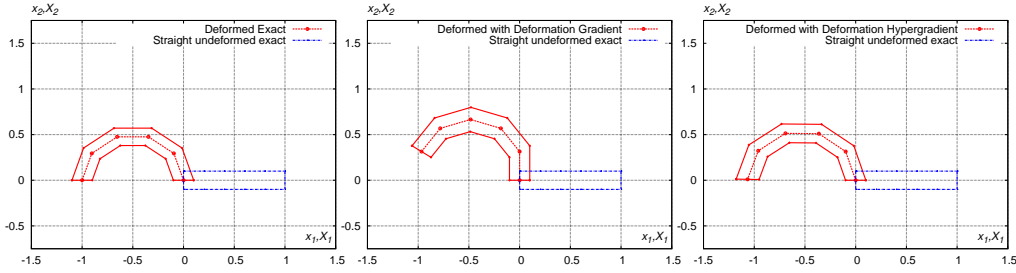


Figure 2.7: From straight reference to the curved spiral beam.  $\alpha = \pi/2, n = 5$

points as illustrated in *Figure 2.7*, the deformation gradient propagates some drifting error. The erroneous landing of the tip point of the deformation gradient representation and meanwhile the successive capture of the deformation hypergradient representation are comparably obvious. As can be noted from the  $\alpha = 3\pi/2$  parametrization of *Figure 2.8*, the

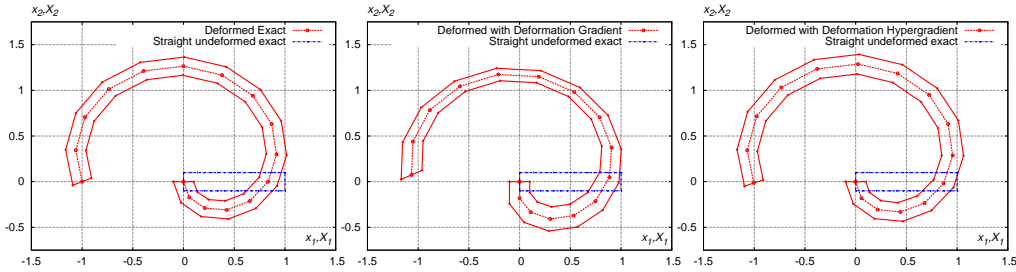


Figure 2.8: From straight reference to the curved spiral beam.  $\alpha = 3\pi/2, n = 15$

drifting error of deformation gradient representation of the tip displacement can be reduced if one increases the space parametrization with the time parametrization simultaneously. However, the deformation behavior through the thickness direction still remains arbitrary, and thus might be agreed upon the insufficient representation capacity of classical first order kinematics.

### 2.3.2 Pull Back: From curved Spiral to the straight Reference

Analogous to the previous subsection, the reverse tangent of the backbone equation (2.5) and the reverse strain gradient kinematics (2.12) are compared with each other either. The results are supporting the expectations significantly stronger as the previous example. The expectation has reasons, mainly the fact that the connection of the two successor locus of the curved structure is not necessarily tangent to the path. Such a problem may be

encountered in the case that the physical increment is drastically large in comparison with the idealization, in other words, the mathematical assumption of occupying *infinitely small* space. In other words, if the scale effects are present, the strain gradient kinematics performs far beyond better than the classical kinematics. For the reverse motion, the straightness of

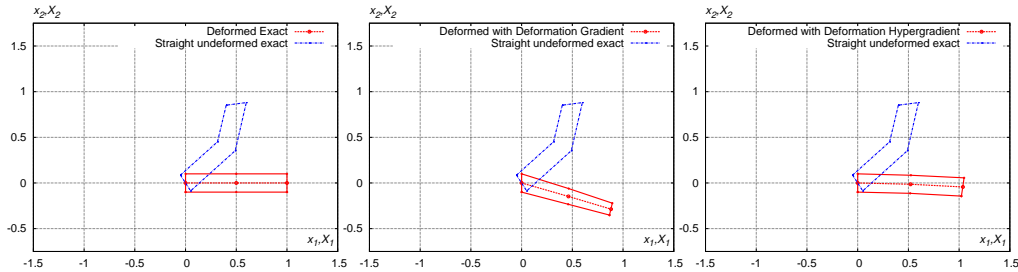


Figure 2.9: From curved spiral beam reference to the straight rod.  $\alpha = \pi/6, n = 2$

the current configuration is a measure of quality. For the case of  $\alpha = \pi/6$  parametrization, the deformation gradient exceeds the limits of acceptance, reaches to be a compromise as can be stated by *Figure 2.9*. As the pseudo time parameter and the discretization are

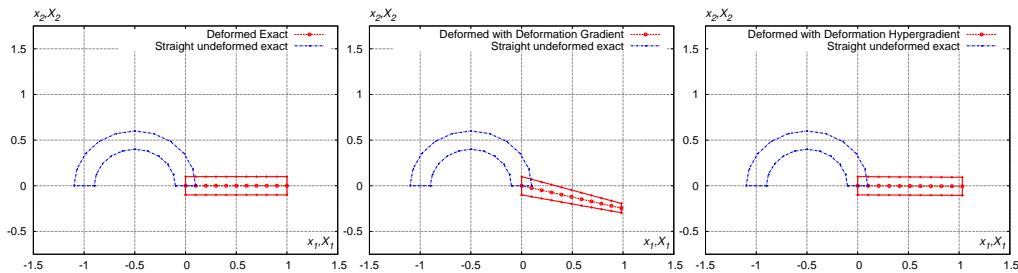


Figure 2.10: From curved spiral beam reference to the straight rod.  $\alpha = \pi/2, n = 10$

kept to be increased, as in *Figure 2.10*, one can only talk about a slight betterment of both tangent mappings, however, the deformation gradient mapping is still far beyond of limits of correctness. As one increases the parameters on more time as in *Figure 2.11*, analogously to

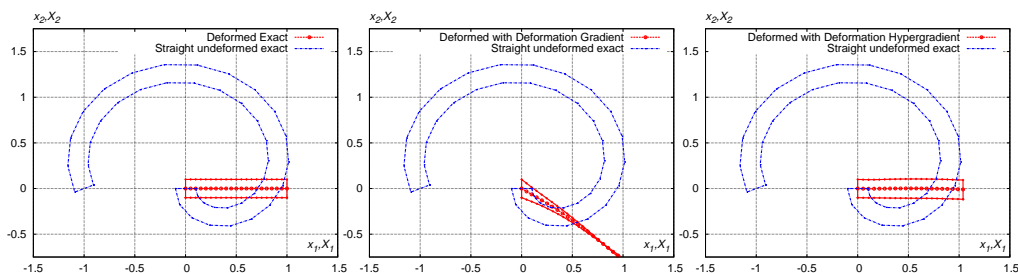


Figure 2.11: From curved spiral beam reference to the straight rod.  $\alpha = 3\pi/2, n = 20$

the straight reference to the curved spatial tangent mapping case, the deformation gradient mapping is disappointing with propagative drifting, whereby the reverse kinematics of the deformation hypergradient tangent mapping shows only slight betterment of the previous case, which might be already considered to be in the radius of qualitative acceptance. Yet the measure of this acceptance is of subjective nature.

## 2.4 Conclusion

Biophysically, it may or may not be *true* or weakly stating *evident* that the fibers do exist as space curves in their *initial*, or *reoriented* state. Independent of any claim, evidence or statement regarding to the existence of initially curved fibers, for the sake of convergence towards completeness of the kinematics, and since this kinematic contains additional information which might be essential for a better understanding of some phenomena, it is presented here in detail. Most probably<sup>8</sup> the first time definition of the strain gradient kinematics has been shown to capture and model excessive deformations precesively. However, the main advantage of the theory is not limited here, and first attempt of defining inextensible anisotropic materials is achieved in this scope, which are the subjects of the remaining parts (see Ch.[3]) of the work.

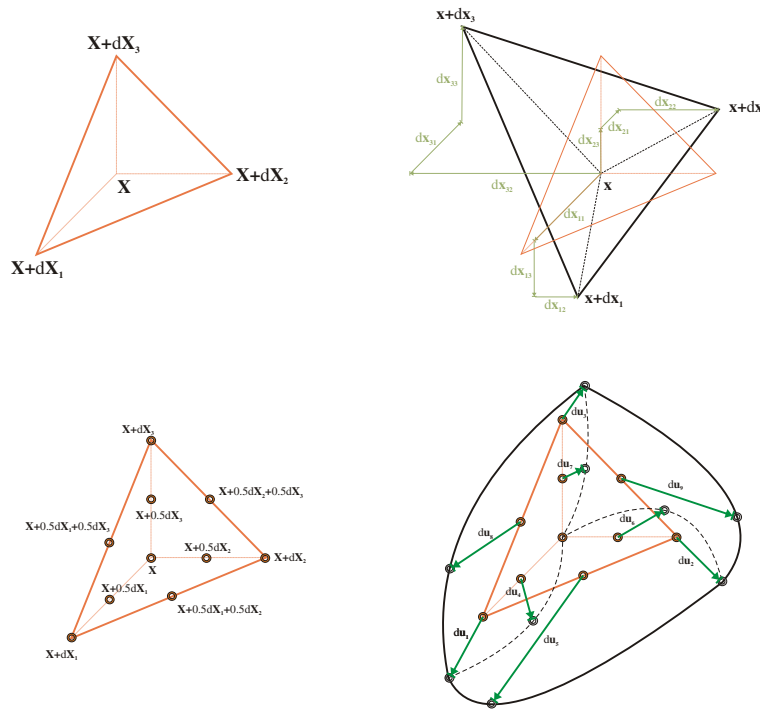


Figure 2.12: An example of Cauchy Tetrehedron, which demonstrates the difference in between first and second order kinematics

<sup>8</sup>The writer of the treatise could not locate during the literature survey any attempt of defining the strain gradient kinematics as a comprehensive treatise as presented in this thesis. . There are works defining the balance equations in the presence of strain gradient effects, however, those also omit the initial step, namely the *Strain Gradient Kinematics*.





# Nonlinear Strain-gradient Balance

---

## Contents

---

<b>3.1</b>	<b>Introduction</b>	<b>77</b>
<b>3.2</b>	<b>Hyper-Cauchy Equation-OM: The Governing Local Form</b>	<b>80</b>
<b>3.3</b>	<b>Curved Anisotropy</b>	<b>84</b>
3.3.1	Curvature Invariant with Euler Bernoulli Ansatz	84
3.3.2	Anisotropic Strain and Strain-gradient Energy Function - EB Ansatz	87
<b>3.4</b>	<b>FEM Implementation with Strain-gradient Effects</b>	<b>90</b>
3.4.1	Discrete Form for Finite Element Formulation	91
3.4.2	Strain-gradient Displacement Matrix	92
3.4.3	Numerical Examples	96

---

## 3.1 Introduction

In the previous chapter, the backbone identity of the strain gradient kinematics is introduced. Any experimental solid proof of existence of those effects are omitted, the strain gradient kinematics is assumed to present, and even higher kinematics are behold as natural as the very strains and deformation field itself. The immediately following discussion is the impact of those kinematic effects on the mechanical behavior, in other words the further existence of those presumably existing kinematic effects on the balance state of a control volume. In order to solidify the arguments, an example is stated here, namely the effective density of the energy depending on bending and stretch stiffness of a unit length profile per unit kinematic quantities (unit invariants). Consider the fractional profile given in *Figure 3.1*. Assuming that the kinematics is negligibly varying on the plane of thickness, and thus a single quantity for curvature 'c' is valid for all points in the plane, the effective energy density per square of invariant<sup>1</sup> is,

---

<sup>1</sup>The invariant is analogously defined to the concept of *stretch in the fiber direction*, known as the fourth invariant in the study of fiber reinforced biological tissue. The proof that the curvature can be analogously represented in terms of invariants, is omitted in this step.

$$\psi_{bending}^{eff} = \frac{\int_{r,t} \rho EI^0 c^2 dr dt}{A^a c^2} \quad (3.1a)$$

$$A^e = \int_{r,t} \text{sign}(\rho) dr dt \neq \int_{r,t} dr dt = A^a \quad (3.1b)$$

The density represents the density of the imaginary primitive substructure with no vacuum at all, and thus is valid as an abstract assumption. The second equation (3.1b) clarifies the evaluation condition of the quantities. This type of homogenization, even though with almost no applicable physical notion, might be still applicable in some abstract fractional structures as shown in the left picture of *Figure 3.1*<sup>2</sup>.

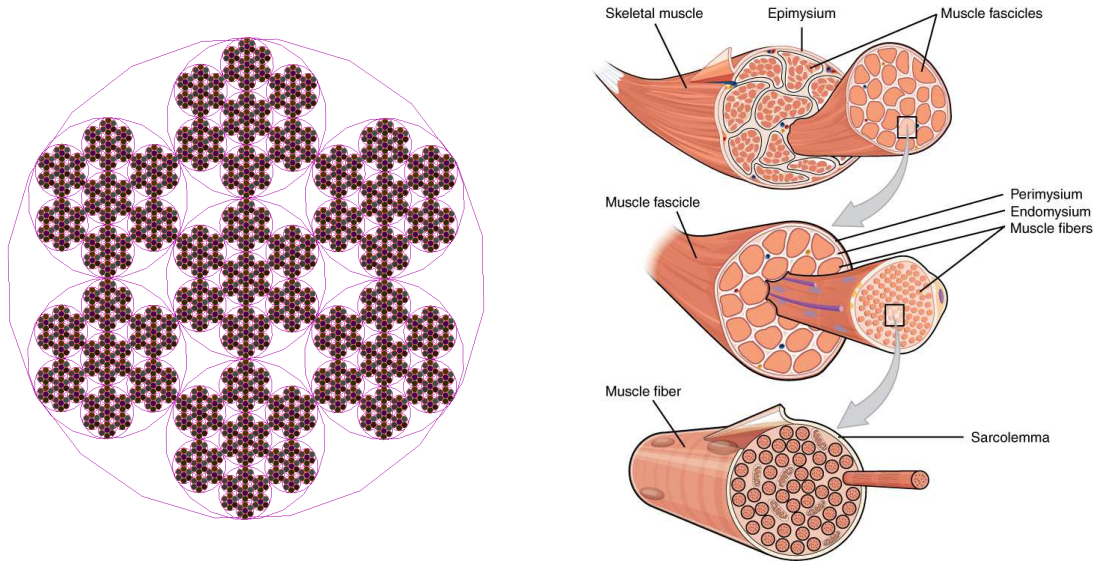


Figure 3.1: Left: An abstract profile with fractional characteristics; Right(Ref.[[OpenStax 2016](#)]) :Illustration of the reality of partially fractional Muscle-Hierarchy

The soft biological structures are known to be assembled in a fractional hierarchical structure Ref.[[C.L.Stanfield 2012](#)]. In this structure, collagen fibrils, which represent the fundamental but not necessarily the most primitive component of the collagenous tissues, determine the rigidity and anisotropy of the solid component by means of energy-converting deformation modes and orientations. That the collagen network determines the rigidity of the structure, is many times agreed upon by many researchers (Ref.[[R.Shirazi 2008](#)]), the consequences of the absence of healthy micro-structure of the collagen network, -again as taking cartilage as an example-, is addressed (Ref.[[R.A.Bank 2000](#)]) as a hot-topic as well. The idea that the collagen network is not the most primitive component which determines the rigidity of the structure (or the origin of rigidity is not achieved in the fibril level) was gaining more attraction and support by early experimental works (Ref.[[N.Sasaki 1996](#)]), and recent molecular dynamics numerical studies (Ref.[[M.J.Buehler 2006](#)]) quantifying the entropic elasticity of tropocollagen

<sup>2</sup>The right picture is taken from online sources Ref.[[OpenStax 2016](#)]

chains. All these works and similar -independent of each other- insist of existence of hierarchy of the tissue structure, and try to define and quantify the main fundamental actors of the phenomenon.

The radially packed structure of fibrils may account significant thickness and jointly resist against bending modes. In the presence of scale effects, those energy modes of the fibers which enable the structure to carry and undergo bending and under circumstances compression types of loadings, are driven by the higher order kinematics and governed by the corresponding extended balance laws.

For a straightforward numerical demonstration of the evolution of material parameters with

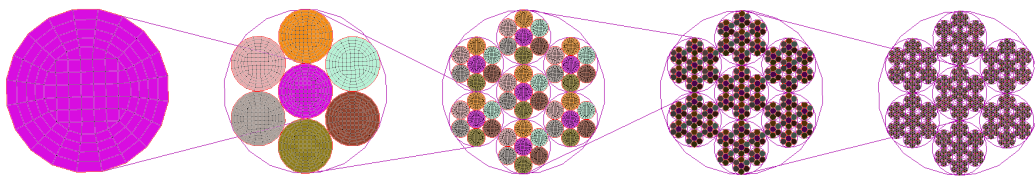


Figure 3.2: Left: An abstract fractional profile chain with depth of 5

respect to the selection of the size of continuum, an abstract fractional chain of depth 5 is chosen. As evident from *Figure 3.1* and equation (3.1b), the effective quantities of 'Area' which drives the stretch type energy, and 'Moment of Area' about the main axis, which drives the bending type of energy, would vary from one scale into another. Therefore, as apparent, the material objectivity<sup>3</sup> will be lost in this sense. The dilemma is, if the decrease (or increase) of bending and stretch type of quantities do develop compensable with each other or not. Otherwise ignoring one while keeping other would be a logical violation and philosophically inconsistent.

In *Diagram 3.3*, the values of effective area and the second moment of inertia around the mid axis with respect to the levels of hierarchy are demonstrated. Quite clear is that, both values do tendentiously condense towards smaller quantities. Apart from the initial decline, one can even state that the declination rate is almost equal for the case of Area and second moment of inertia. The quantities however, might be preserved in quite different scales, this however would not be consistent measure, since the elements of kinematics is quite arbitrary. For instance, by only considering stretch, or a mapping which results only in stretch type of formation, one may fallaciously conclude on the absence of bending effects. To avoid this type of misleading interpretation, one should focus on the rate of declination if one enlarges the frame of the continuum as shown in the example above. The result is not as obvious as one expects, since for any circular and fully filled vacuum-free cross section, one awaits that the effective second moment of inertia declines quadratically faster as the effective area. As shown in the illustration above, this expectation may disappoint one, if

<sup>3</sup>This material *objectivity* is considered under the *subject* of the size of the locus. In other words, the strain energy density and the effective parameters, strictly depend on the scale chosen.

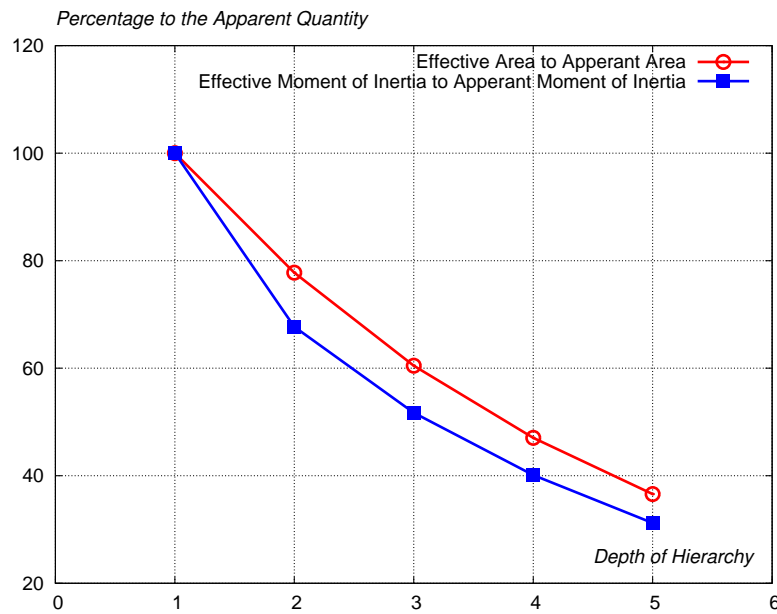


Figure 3.3: Development of the effective Area and Second Moment of Area values with respect to the selection of hierarchy levels of *Figure 3.2*

the matter of concern has a fractional characteristic. Despite this conclusion, this example should not be esteemed generically and used in commonplace, the rate of decline may show a totally different profile, if one chooses another type of fractional expansion and shrinkage. Quite familiarly, in engineering applications, bending effects are introduced into numerics by using theories of Bernoulli, Euler, Timoshenko, or relatively newer geometrically exact or higher order formulations. As the above argument states, any attempt of considering the impact of curvature in the balance equations in macro-scale is as valid as considering the curvature effects in smaller scales. Since these curvature effects may gain or loose as the effects of stretch do. In the next parts, the inclusion and implementation of those effects into strain gradient and strain energy functions will be discussed and clarified.

### 3.2 Hyper-Cauchy Equation-OM: The Governing Local Form

In this section the local form of the balance equation on the kinematics given in Ch.[2.2.1] is presented. The method applied by Steinmann et. all. Ref.[P.Fischer 2010] is traced mainly, but with some diversities. In opposite to Steinmann et. all. (Ref.[P.Fischer 2010]), the derivations of *normal gradient and surface divergence operators* are defined. By doing so, it is possible to show the geometrical extensions and the dimensions of those geometrical manifolds in the integral weak form of the governing equation. Additionally, the principle geometrical manifold(s), where hyperstress as the internal energy conjugate of hyperstrain is acting on -according to the writer- are interesting topics to visit. Subsequently, the volume and shell contra-internal forces and the surface and edge contra-internal tractions are to be exposed as well.

Since the time rates at the stage of hyper-kinematics were not defined (they were visited in the first chapter of biphasic media C.[1]), hereby, the virtual work form instead of virtual power form is preferred. Analogous to classical linear momentum balance, those two equations should have identical outcome, as soon as one states and argues on the assumptions done, for example no rate dependent damping or no inertial effects.

To start with, as Steinmann and Fischer (Ref.[P.Fischer 2010]) stated recently that, since internal energy depends on deformation gradient and hyper-deformation gradient, additive partition as a result of chain rule is obtained.

$$\delta\Pi_{int} = \int_{\Omega} \left[ \frac{\delta\Psi}{\delta\mathbf{F}} : \delta\mathbf{F} + \frac{\delta\Psi}{\delta\mathbf{G}} \cdot\cdot \delta\mathbf{G} \right] dV = \int_{\Omega} [\mathbf{P} : \delta\mathbf{F} + \mathbf{Q} \cdot\cdot \delta\mathbf{G}] dV = \delta\Pi_{int}^{PF} + \delta\Pi_{int}^{QG} \quad (3.2)$$

In addition to Gauss' Divergence Theorem and Green's theorem, additional tensor equalities to resolve and sunder the virtual work equation into smaller dimensions of integrations, are required. For arbitrary tensors of order three and two, (abbreviated here with  $\mathbf{T}$ ,  $\mathbf{D}$ ) and tensors of order one, (abbreviated here with  $\mathbf{u}$  and  $\mathbf{N}$ ), it is trivial to show that the following tensor identities hold;

$$Div(\mathbf{D}^T \cdot \delta\mathbf{u}) = (Div\mathbf{D}) \cdot \delta\mathbf{u} + \mathbf{D} : Grad(\delta\mathbf{u}) \quad (3.3a)$$

$$Div(\mathbf{T}^r : \delta\mathbf{D}) = (Div_l\mathbf{T}) : \delta\mathbf{D} + \mathbf{T} \cdot\cdot Grad(\delta\mathbf{D}) \quad (3.3b)$$

$$Div\left[(Div_l\mathbf{T})^T \cdot \delta\mathbf{u}\right] = [Div(Div_l\mathbf{T})] \cdot \delta\mathbf{u} + (Div_l\mathbf{T}) : Grad(\delta\mathbf{u}) \quad (3.3c)$$

$$Div\left[\left(\mathbf{T}^l \cdot \mathbf{N}\right)^T \cdot \delta\mathbf{u}\right] = \left[Div\left(\mathbf{T}^l \cdot \mathbf{N}\right)\right] \cdot \delta\mathbf{u} + \left(\mathbf{T}^l \cdot \mathbf{N}\right) : Grad(\delta\mathbf{u}) \quad (3.3d)$$

Applying (3.3a) and Gauss' divergence theorem after each other on the deformation gradient and first Piola-Kirchhoff driven virtual internal energy term, i.e. the first addend of equation (3.2), one gets the classical virtual energy form,

$$\delta\Pi_{int}^{PF} = \int_S (\mathbf{P}^T \cdot \mathbf{n}) \cdot \delta\mathbf{u} dA - \int_{\Omega} (\nabla_{\mathbf{X}} \cdot \mathbf{P}) \cdot \delta\mathbf{u} dV \quad (3.4)$$

In the following, the divergence and gradient operator notations ( $\nabla_{\mathbf{X}}^*$ ,  $\nabla_{\mathbf{X}}$ ) are replaced with literal type notations ( $Div_*$ ,  $Grad$ ). This is done for sake of clearness. Inserting (3.3b) and applying Gauss' divergence theorem after each other on the hyper-deformation gradient and hyperstress driven virtual internal energy partition, i.e. the second addend of equation (3.2), one gets the extensions caused by the higher order kinematic,

$$\begin{aligned} \delta\Pi_{int}^{QG} &= \int_{\Omega} [\mathbf{Q} \cdot\cdot \delta\mathbf{G}] dV \\ &= \int_{\Omega} Div(\mathbf{Q}^r : \delta\mathbf{F}) dV - \int_{\Omega} (Div_l\mathbf{Q}) : \delta\mathbf{F} dV \\ &= \int_S (\mathbf{Q}^l \cdot \mathbf{n}) : \delta\mathbf{F} dA - \int_{\Omega} (Div_l\mathbf{Q}) : \delta\mathbf{F} dV \end{aligned} \quad (3.5)$$

In which  $\mathbf{n}$  denotes the outer surface normal in reference coordinates of the control volume. The last term on the right hand side of equation (3.5), after inserting the identity of (3.3c) and gauss diverging once more time with surface normal  $\mathbf{n}$ , leads into,

$$\begin{aligned} - \int_{\Omega} (Div_l \mathbf{Q}) : \delta \mathbf{F} dV &= - \int_{\Omega} Div \left[ (Div_l \mathbf{Q})^T \cdot \delta \mathbf{u} \right] dV + \int_{\Omega} [Div(Div_l \mathbf{Q})] \cdot \delta \mathbf{u} dV \\ &= - \int_S \left[ (Div_l \mathbf{Q}) \cdot \mathbf{n} \right] \cdot \delta \mathbf{u} dA + \int_{\Omega} [Div(Div_l \mathbf{Q})] \cdot \delta \mathbf{u} dV \end{aligned} \quad (3.6)$$

The first addend of equation (3.5) can be transformed into the form beneath, by using the identity (3.3d), where Green's theorem can be applied next,

$$\int_S \left( \mathbf{Q}^l \cdot \mathbf{n} \right) : \delta \mathbf{F} dA = \int_S Div \left[ \left( \mathbf{Q}^l \cdot \mathbf{n} \right)^T \cdot \delta \mathbf{u} \right] dA - \int_S \left[ Div \left( \mathbf{Q}^l \cdot \mathbf{n} \right) \right] \cdot \delta \mathbf{u} dA \quad (3.7)$$

Applying the Green's theorem on to the first addend of equation (3.7) with the *surface frontier* normal  $\mathbf{m}$ ,

$$\int_S Div \left[ \left( \mathbf{Q}^l \cdot \mathbf{n} \right)^T \cdot \delta \mathbf{u} \right] dA = \int_{\Gamma} \left[ \left( \mathbf{Q}^l \cdot \mathbf{n} \right)^T \cdot \delta \mathbf{u} \right] \cdot \mathbf{m} dL = \int_{\Gamma} \left[ \mathbf{Q}^m \cdot (\mathbf{n} \otimes \mathbf{m}) \right] \cdot \delta \mathbf{u} dL \quad (3.8)$$

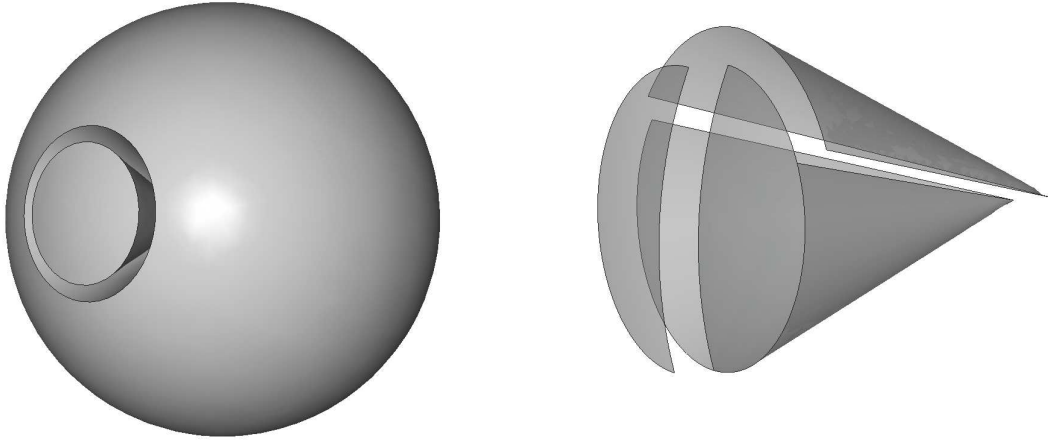
The *surface frontier* here represents the *edge* as a location, where the  $C^1$  continuity of the surface manifolds is not valid anymore. This is not a violation, in fact it is essential for filling the discontinuity gaps in between higher dimensional manifolds with lower ones. Since -for the local form-, the infinite control volume is taken to be arbitrary, it may be surrounded by patches of surfaces, and thus include edges. At the end, the total virtual work equation is formulated as below;

$$\begin{aligned} \delta \Pi_{int} &= \delta \Pi_{int}^{PF} + \delta \Pi_{int}^{QG} = \int_S (\mathbf{P}^T \cdot \mathbf{n}) \cdot \delta \mathbf{u} dA - \int_{\Omega} (Div \mathbf{P}) \cdot \delta \mathbf{u} dV \\ &\quad - \int_S \left[ (Div_l \mathbf{Q}) \cdot \mathbf{n} \right] \cdot \delta \mathbf{u} dA + \int_{\Omega} [Div(Div_l \mathbf{Q})] \cdot \delta \mathbf{u} dV \\ &\quad + \int_{\Gamma} \left[ \mathbf{Q}^m \cdot (\mathbf{n} \otimes \mathbf{m}) \right] \cdot \delta \mathbf{u} dL - \int_S \left[ Div \left( \mathbf{Q}^l \cdot \mathbf{n} \right) \right] \cdot \delta \mathbf{u} dA \end{aligned} \quad (3.9)$$

Rearranging the terms of equation (3.9) in the specific way, results into the final version of the variation of the internal work as below;

$$\begin{aligned} \delta \Pi_{int} &= \int_{\Omega} [Div((Div_l \mathbf{Q}) - \mathbf{P})] \cdot \delta \mathbf{u} dV + \int_{Su} \left[ (\mathbf{P}^T - Div_l \mathbf{Q}) \cdot \mathbf{n} \right] \cdot \delta \mathbf{u} dA \\ &\quad + \int_{Sh} \left[ -Div \left( \mathbf{Q}^l \cdot \mathbf{n} \right) \right] \cdot \delta \mathbf{u} dA + \int_{\Gamma} \left[ \mathbf{Q}^m \cdot (\mathbf{n} \otimes \mathbf{m}) \right] \cdot \delta \mathbf{u} dL \end{aligned} \quad (3.10)$$

In this final form, one obtains four integration domains two of which is dimensionally overlapping with each other. Respecting the different natures of the integration kernels,

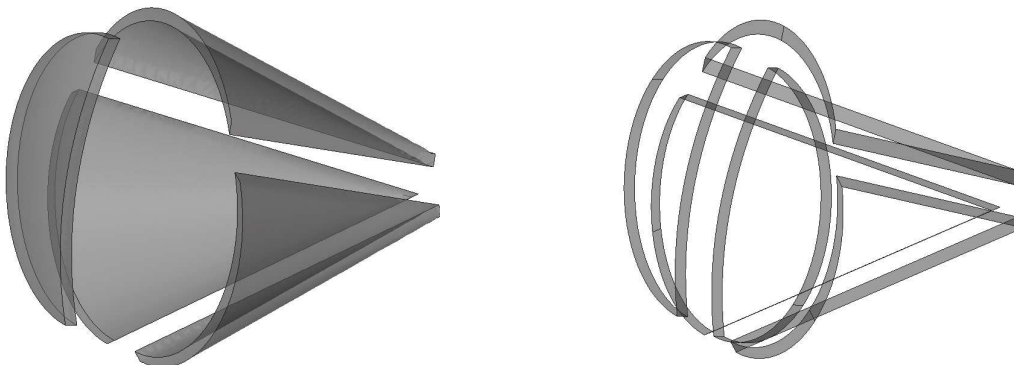


(a)  $Div(Div\mathbf{Q}^{T_2}) - \mathbf{P}$  on  $\Omega$

(b)  $(\mathbf{P}^T - Div\mathbf{Q}^{T_2}) \cdot \mathbf{n}$  on  $S_u$

Figure 3.4: Integration domains on which first and second order effects are acting

those two are kept apart. The first two domains (volume and surface) are the ones driven by the gradient effects, and thus familiar and well known ones. The hypergradient effects do act also on the first two manifolds and those effects generate remaining integral domains (shell and curve). The fact that, without any integrand, the integral can neither be defined nor exist, construes that the integral domain under discussion is a nonentity. In other words, the absence of *actor*, designates the absence of *space*. By keeping this logic in mind, from the integration kernel of the third domain, one can conclude that there are not only first order stress tractions, but also divergences of second order tensors (tractions of hyperstresses) acting on the surfaces. By respecting the two properties of the third integral, the first one being that the integrand acts contra to some body forces, and the second one being that the integral domain is a surface, this domain is called as *shell* domain. In fact,



(a)  $-Div(\mathbf{Q}^{T_2} \cdot \mathbf{n})$  on  $Sh$

(b)  $\mathbf{Q}^{T_3} : (\mathbf{n} \otimes \mathbf{m})$  on  $\Gamma$

Figure 3.5: Integration domains on which first and second order effects are acting



in conjunction with the notion of *shell*, a surface frontier (not only normal) and thickness of it are defined. This can be viewed as a further division of interface surfaces (of previously divided volumes) into patches. And the patch frontiers and interfaces as a result of the second division do generate infinite *curves* which constitute mainly the last integral domain of equation (3.10).

For the translational equilibrium, the complement effect applied by the remaining part of the system on the control volume has to be taken into account. The external virtual work should balance the internal one,

$$\delta\Pi_{ext} = \int_{\Omega} \mathbf{b}^{\Omega} \cdot \delta\mathbf{u}dV + \int_{Su} \mathbf{t}^{Su} \cdot \delta\mathbf{u}dA + \int_{Sh} \mathbf{b}^{Sh} \cdot \delta\mathbf{u}dA + \int_{\Gamma} \mathbf{t}^{\Gamma} \cdot \delta\mathbf{u}dA \quad (3.11)$$

Figure 3.4 represents illustratively the concepts of volume( $\Omega$ ) and surface( $Su$ ), whereby Figure 3.5 demonstrates the concepts of shell( $Sh$ ) and edge( $\Gamma$ ), which were declared as a result of equation (3.10).

### 3.3 Curved Anisotropy

In this section, the backbone invariant of the kinematics for building bending type of internal energy formulation is postulated first. In the next, the energy function and its consistency with the tangent tensor is demonstrated depending on a given mapping. The section is followed by problems and suggestions which will enable a finite element implementation of all-together. First, the novel concept of curvature is to be defined as an invariant.

#### 3.3.1 Curvature Invariant with Euler Bernoulli Ansatz

Even though it is concurrently pointless and difficult to describe the concept of *material point curvature*, it will be tried here to emphasize the approach on a script, formally and visually. Apprehension of the Figure C.2 during reading the next is strongly suggested by the writer of the treatise.

The bending energy formulations -irrespective of which theory will be used- require the estimation of the radius of curvature. The theory of kinematic assumptions of Euler-Bernoulli postulations will be applied here, namely the tangent of the profile will remain perpendicular to the profile at space and in pseudo time of deformation. Where the "geometrically exact" approach would require the cofactor of profile planes to determine the real curvature. For the curvature formulation this additional effect will be ignored. In short, for the next, the following assumptions hold,

$$\mathbf{F}^{\sharp} \cdot \mathbf{M}^{\sharp} \parallel \text{cof}(\mathbf{F}^{\sharp}) \cdot \mathbf{M}^{\sharp} \quad \mathbf{F}^{\flat} \cdot \mathbf{M}^{\flat} \parallel \text{cof}(\mathbf{F}^{\flat}) \cdot \mathbf{M}^{\flat} \quad (3.12)$$

The radius of curvature is estimated according to the angles of curvatures, where there is no reason that those to be equal. The radius of curvature is taken to be common in *sharp and flat* length changes, formally;

$$\sin(\alpha^{\sharp}) = \frac{|\mathbf{m}^{\sharp}|}{r} \quad \sin(\alpha^{\flat}) = \frac{|\mathbf{m}^{\flat}|}{r} \quad (3.13)$$

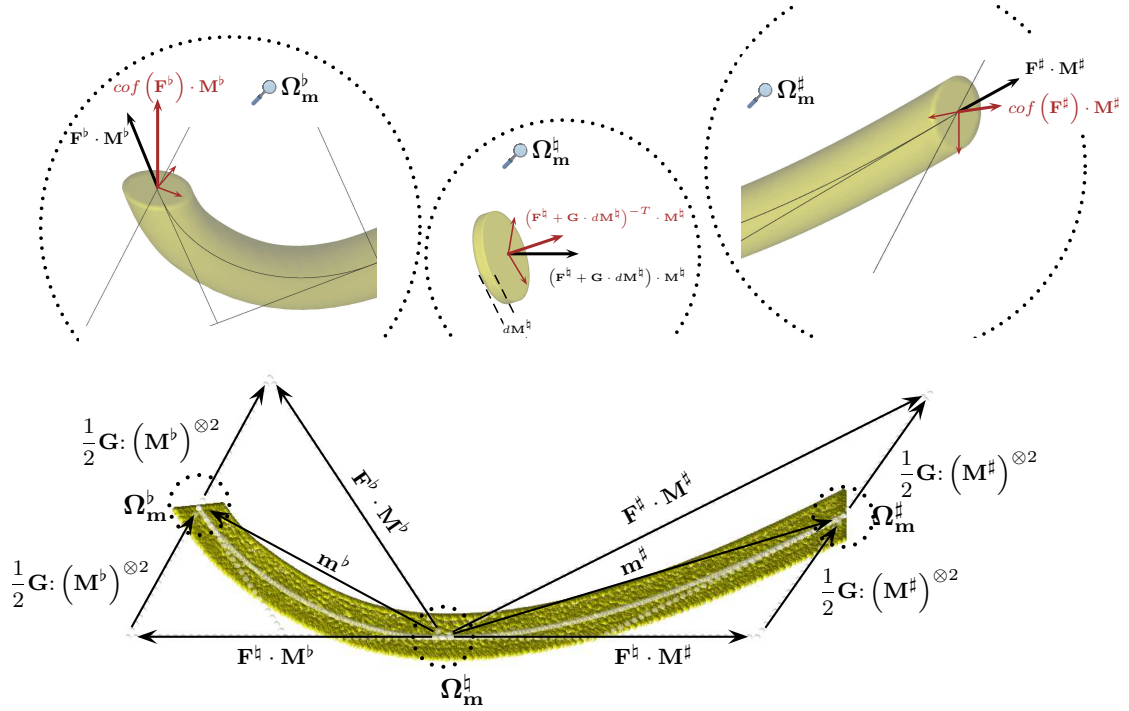


Figure 3.6: Kinematics of a single fiber with convecting and moving coordinates at the flat, natural and sharp sections

In order to take both effects into account, the following trigonometric identity and estimation can be done,

$$\begin{aligned}
 c = r^{-1} &= \frac{\sin(\alpha^\sharp) + \sin(\alpha^b)}{|\mathbf{m}^\sharp| + |\mathbf{m}^b|} \\
 &= \frac{2\sin((\alpha^\sharp + \alpha^b)/2) \cos((\alpha^\sharp - \alpha^b)/2)}{|\mathbf{m}^\sharp| + |\mathbf{m}^b|} \\
 &\approx \frac{2\sin((\alpha^\sharp + \alpha^b)/2)}{|\mathbf{m}^\sharp| + |\mathbf{m}^b|}
 \end{aligned} \tag{3.14}$$

The cosine of the rotation can be computed by at best with the dot product of *flat* and *sharp* deformed vectors. Alternatively, the cross product might be used, however it may cause some singularities in the initial stress and hyperstress terms, which have to be dealt with repulsive terms. In order to avoid dealing with numerical work-arounds, the dot product version of the estimation is used;

$$\cos(\alpha^\sharp + \alpha^b) = \frac{(-\mathbf{m}^\sharp \cdot \mathbf{m}^b)}{|\mathbf{m}^\sharp| |\mathbf{m}^b|} \tag{3.15}$$

The minus sign indicates that the *sharp* tangent to be rotated, since some positive notation for the dot projection is desired. The members which are used to compute the invariants

then,

$$\begin{aligned} -\mathbf{m}^\sharp &= \mathbf{F} \cdot \mathbf{M} - \frac{1}{2} \mathbf{G} : \mathbf{M}^{\otimes 2} \\ \mathbf{m}^\flat &= \mathbf{F} \cdot \mathbf{M} + \frac{1}{2} \mathbf{G} : \mathbf{M}^{\otimes 2} \end{aligned} \quad (3.16)$$

Even though the determined invariants are also stretch related, as indicated above, they have an impact in the bending energy either. The three invariants<sup>4</sup> required for defining Euler-Bernoulli type of radius of curvature are then;

$$\begin{aligned} I_4^\kappa &= (\mathbf{F}^T \cdot \mathbf{F}) : \mathbf{M}^{\otimes 2} = F_{kl} F_{km} M_l M_m \\ I_5^\kappa &= (\mathbf{F}^T \cdot (\mathbf{G} \cdot \mathbf{M})) : \mathbf{M}^{\otimes 2} = ((\mathbf{G} \cdot \mathbf{M})^T \cdot \mathbf{F}) : \mathbf{M}^{\otimes 2} = F_{kl} (\mathbf{G} \cdot \mathbf{M})_{km} M_l M_m \\ I_6^\kappa &= ((\mathbf{G} \cdot \mathbf{M})^T \cdot (\mathbf{G} \cdot \mathbf{M})) : \mathbf{M}^{\otimes 2} = (\mathbf{G} \cdot \mathbf{M})_{kl} (\mathbf{G} \cdot \mathbf{M})_{km} M_l M_m \end{aligned} \quad (3.17)$$

The second and third contractions above are identical since the contracted tensors are transpose of each other,

$$\mathbf{F}^T \cdot (\mathbf{G} \cdot \mathbf{M}) = ((\mathbf{G} \cdot \mathbf{M})^T \cdot \mathbf{F})^T \quad (3.18)$$

Analogous to the full length in the current curved coordinates as the sum of sharp and flat lengths, the values of the curvature of equation (3.15) can also be formulated. The full length for instance;

$$|\mathbf{m}| = |\mathbf{m}^\sharp| + |\mathbf{m}^\flat| = \sqrt{(I_4^\kappa + I_5^\kappa + 0.25I_6^\kappa)} + \sqrt{(I_4^\kappa - I_5^\kappa + 0.25I_6^\kappa)} \quad (3.19)$$

Together with the definitions above and the introduced invariants, the following invariant formulation for the curvature can be achieved;

$$\cos(\alpha^\sharp + \alpha^\flat) = \frac{(I_4^\kappa - 0.25I_6^\kappa)}{(I_4^\kappa - I_5^\kappa + 0.25I_6^\kappa)^{1/2} (I_4^\kappa + I_5^\kappa + 0.25I_6^\kappa)^{1/2}} \quad (3.20)$$

Accordingly, a scalar value for the curvature is determined and formulated with respect to some novel invariants. The independence of these invariants with respect to the post-deformation rotations can be proved smoothly, which is omitted here.

The obligatory question is, if this curvature definition can capture the whole evolute of a given mapping or not. In order to seek and provide an answer to this question, the analytical example of the spiral beam, which was introduced in the previous chapter (Ch.[2.3]) is revisited here. As shown previously, using the strain gradient kinematics, the forward mapping of straight to curved spatial configuration and the backward mapping of curved to straight reference configuration works far better than by only considering the deformation

<sup>4</sup>The invariance of the postulated variables is self evident, the parameters are independent of the pre-rotations of the reference fiber directions

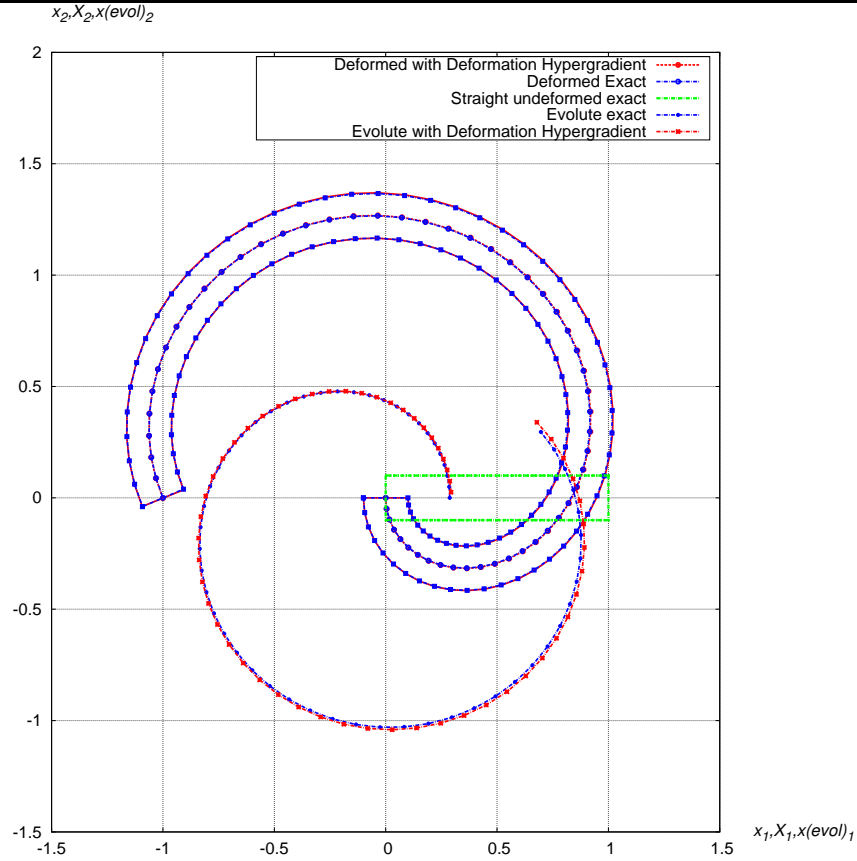


Figure 3.7: The deformation and the evolute of the spiral beam,  $\alpha = 3\pi/2$ ,  $n = 60$

gradient effects. As seen in the *Figure 3.7*, not only the mapping is almost with high accuracy captured, but also the connecting curve of the center of curvatures, namely the evolute is estimated quite nearby to the semi-analytical solution. It should be noted here that, the evaluation of an evolute in this case, is not possible to be extracted from the deformation gradient approach, since the neighborhood information is missing and thus obsolete in the latter case. In the example of *Figure 3.7*, apart from the fact that there is a slight drifting, one can conclude that curvature approximations such as equation (3.15) or similar variations, can capture the form of differential geometry satisfactorily, and therefore can be used for the formulation of novel formulations of material internal energy.

### 3.3.2 Anisotropic Strain and Strain-gradient Energy Function - EB Ansatz

In the next, the formulation of the Euler-Bernoulli based strain and strain gradient energy density function are presented (EB Ansatz). Having the approximation for the radius of curvature in hand, the energy density function is depending on the elastic modulus, and the

effective second moment of inertia can be introduced.

$$\begin{aligned}\psi^\kappa &= EI \frac{(2 - 2\cos(\alpha^\sharp + \alpha^b))}{(|\mathbf{m}^\sharp| + |\mathbf{m}^b|)^2} = EI \frac{2 - 2a}{|\mathbf{m}|^2} \\ a &= \cos(\alpha^\sharp + \alpha^b) = \frac{b}{d} \\ b &= (I_4^\kappa - 0.25I_6^\kappa) \\ d &= (I_4^\kappa - I_5^\kappa + 0.25I_6^\kappa)^{1/2} (I_4^\kappa + I_5^\kappa + 0.25I_6^\kappa)^{1/2} \\ |\mathbf{m}| &= (|\mathbf{m}^\sharp| + |\mathbf{m}^b|)\end{aligned}\tag{3.21}$$

The replacements are done for simplicity, and further trigonometric identities are used for the sake of evaluation of derivatives for finite element or natural element implementation. This energy function is tested on a simple representative abstract material point mapping. Quite purposely, some excessive mapping is chosen here, to comment on the convexity of the energy function without seeking any further mathematical proof. The chosen mapping enforces an exponential vertical displacement of initially straight horizontal line element, fixed at its origin (see *Figure 3.8*). The current coordinates of the mapping with respect to the reference coordinates and the pseudo time parameter reads;

$$x(X, Y, Z, t) = X \quad y(X, Y, Z, t) = Y + \exp(Xt) - 1 \quad z(X, Y, Z, t) = Z\tag{3.22}$$

The deformation in pseudo time is illustrated in the left part of *Figure 3.8*. In the right

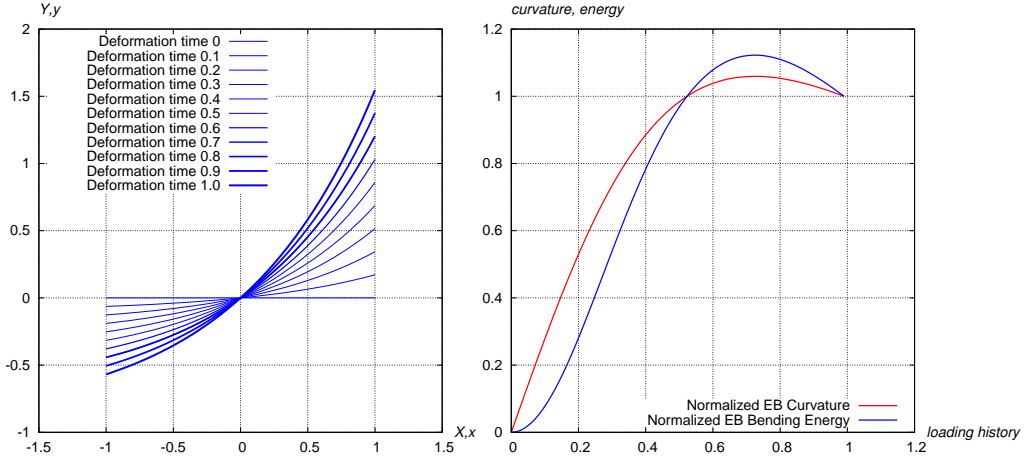


Figure 3.8: Left: The exponential material formation in 10 time steps; Right: The normalized curvature and normalized EB bending energy of the exponential mapping

diagram, the normalized (wrt. the final curvature) curvature and the normalized bending energy (wrt. to the final bending energy) based on equation (3.21) are shown. The curvature is to be decreasing after a degree of formation, which is required completely based upon the nature of the given kinematics, and may cause some non-convexity of the density function. This is a quite natural fact, and tendentious monolithic increase is quested for the purpose

of numerical convergence. According to the writer, the formulation should not be altered fallaciously, rather the numerical scenario for solving this type of softening shall be improved, than the result of a trail of arguments listed above are manipulated. Another issue which should not be forgotten is the existence of third order remainder of this approximation. This means that, the evaluated curvature and stretch deviates from the analytical one. However, it is the self-consistency what is intended here, for comparison of the power of kinematics, please refer to the arguments of hyperkinematics (Ch.[2]).

Before moving ahead, the definitions of the first Piola Kirchoff stress tensor, and hyperstress tensor should be introduced here. By taking the first derivatives of the energy function of equation (3.21), with respect to the deformation gradient and deformation hypergradient results into;

$$\begin{aligned}\mathbf{P}^\kappa &= \frac{\partial \psi^\kappa}{\partial \mathbf{F}} = -2EI \frac{\partial a}{\partial \mathbf{F}} |\mathbf{m}|^{-2} - 2EI |\mathbf{m}|^{-3} \frac{\partial |\mathbf{m}|}{\partial \mathbf{F}} (2 - 2a) \\ \mathbf{Q}^\kappa &= \frac{\partial \psi^\kappa}{\partial \mathbf{G}} = -2EI \frac{\partial a}{\partial \mathbf{G}} |\mathbf{m}|^{-2} - 2EI |\mathbf{m}|^{-3} \frac{\partial |\mathbf{m}|}{\partial \mathbf{G}} (2 - 2a)\end{aligned}\quad (3.23)$$

The necessary three tangent terms have to be also evaluated and the consistence of the integration with the stress and hyperstress should be checked. This is performed to demonstrate the softening behavior primarily, and second, it is done to ensure the correctness. The detailed extraction of the derivatives can be found in the list of *Appendix-B*. The tangent tensors can be evaluated as beneath;

$$\begin{aligned}\mathbf{D}_{\mathbf{F}}^{\mathbf{P}^\kappa} &= \frac{\partial \mathbf{P}^\kappa}{\partial \mathbf{F}} = -2EI \frac{\partial^2 a}{\partial \mathbf{F}^2} |\mathbf{m}|^{-2} + 4EI |\mathbf{m}|^{-3} \frac{\partial |\mathbf{m}|}{\partial \mathbf{F}} \otimes \frac{\partial a}{\partial \mathbf{F}} \\ &+ 6EI |\mathbf{m}|^{-4} \frac{\partial |\mathbf{m}|}{\partial \mathbf{F}} \otimes \frac{\partial |\mathbf{m}|}{\partial \mathbf{F}} (2 - 2a) - 2EI |\mathbf{m}|^{-3} \frac{\partial^2 |\mathbf{m}|}{\partial \mathbf{F}^2} (2 - 2a) \\ &+ 4EI |\mathbf{m}|^{-3} \frac{\partial a}{\partial \mathbf{F}} \otimes \frac{\partial |\mathbf{m}|}{\partial \mathbf{F}}\end{aligned}\quad (3.24)$$

$$\begin{aligned}\mathbf{D}_{\mathbf{G}}^{\mathbf{P}^\kappa} &= \frac{\partial \mathbf{P}^\kappa}{\partial \mathbf{G}} = -2EI \frac{\partial^2 a}{\partial \mathbf{G} \partial \mathbf{F}} |\mathbf{m}|^{-2} + 4EI |\mathbf{m}|^{-3} \frac{\partial |\mathbf{m}|}{\partial \mathbf{G}} \otimes \frac{\partial a}{\partial \mathbf{F}} \\ &+ 6EI |\mathbf{m}|^{-4} \frac{\partial |\mathbf{m}|}{\partial \mathbf{G}} \otimes \frac{\partial |\mathbf{m}|}{\partial \mathbf{F}} (2 - 2a) - 2EI |\mathbf{m}|^{-3} \frac{\partial^2 |\mathbf{m}|}{\partial \mathbf{G} \partial \mathbf{F}} (2 - 2a) \\ &+ 4EI |\mathbf{m}|^{-3} \frac{\partial a}{\partial \mathbf{G}} \otimes \frac{\partial |\mathbf{m}|}{\partial \mathbf{F}}\end{aligned}\quad (3.25)$$

$$\begin{aligned}\mathbf{D}_{\mathbf{G}}^{\mathbf{Q}^\kappa} &= \frac{\partial \mathbf{Q}^\kappa}{\partial \mathbf{G}} = -2EI \frac{\partial^2 a}{\partial \mathbf{G}^2} |\mathbf{m}|^{-2} + 4EI |\mathbf{m}|^{-3} \frac{\partial |\mathbf{m}|}{\partial \mathbf{G}} \otimes \frac{\partial a}{\partial \mathbf{G}} \\ &+ 6EI |\mathbf{m}|^{-4} \frac{\partial |\mathbf{m}|}{\partial \mathbf{G}} \otimes \frac{\partial |\mathbf{m}|}{\partial \mathbf{G}} (2 - 2a) - 2EI |\mathbf{m}|^{-3} \frac{\partial^2 |\mathbf{m}|}{\partial \mathbf{G}^2} (2 - 2a) \\ &+ 4EI |\mathbf{m}|^{-3} \frac{\partial a}{\partial \mathbf{G}} \otimes \frac{\partial |\mathbf{m}|}{\partial \mathbf{G}}\end{aligned}\quad (3.26)$$

Two comments can be done about the consistency of the material points result, first one

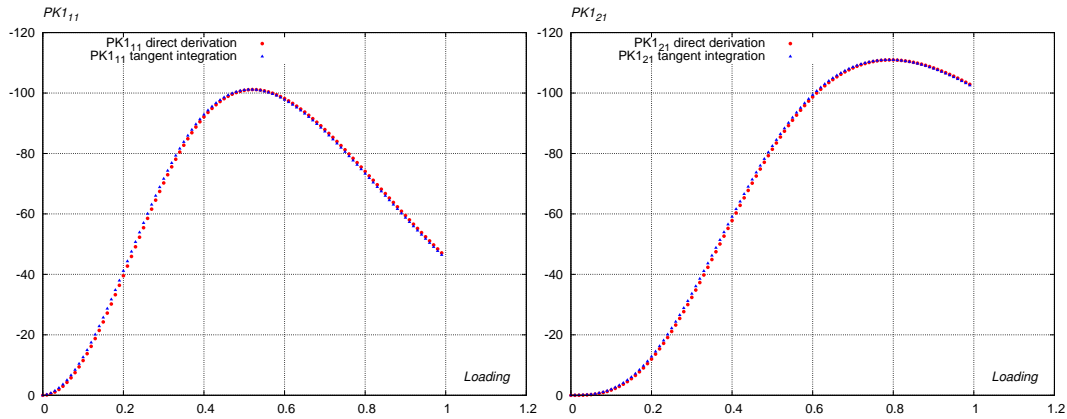


Figure 3.9: Left: First Piola Kirchoff Stress tensor traction on the reference X plane and current x direction. Right: First Piola Kirchoff Stress tensor traction on the reference X plane and current y direction

is the conformity of the tangent values with the direct derived tractions, second one is the expected capture of the non-zero tractions for the given deformation. Since there is no dependency of the reference Y coordinate was given in the mapping, no thickness change may be evaluated, by recalling the fact that the kinematics is only applied around the fixed origin. Another interesting but foreseen phenomena is that the traction on the reference X-normal plane in the current x-parallel direction coexist with the shear traction, indicating that bending energy may enforce also axial forces on straight lines of reference. As can be

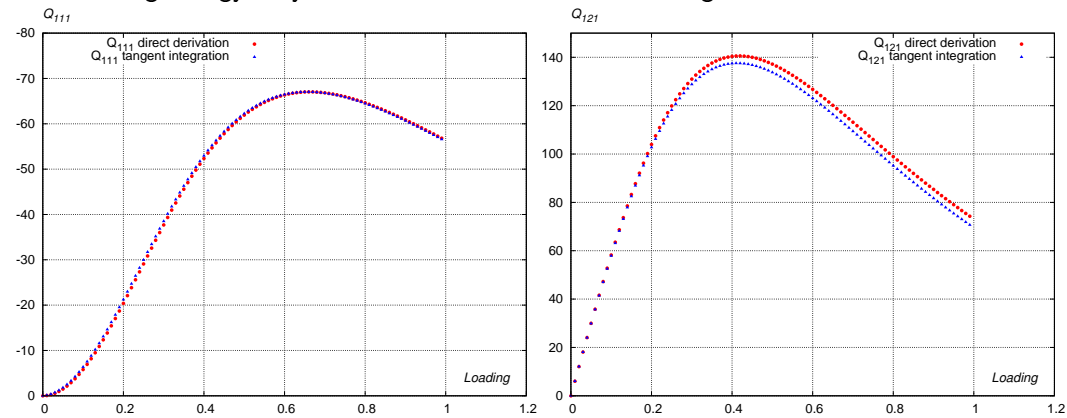


Figure 3.10: Left: First Piola Kirchoff Hypertress tensor traction on the reference X plane and xX First Piola Stress-Space. Right: First Piola Kirchoff Hypertress tensor traction on the reference X plane and xY First Piola Stress-Space

seen in *Figure 3.10*, the consistence of the tangent and the directly derived terms are also well satisfied. The details of the derivation can be found in *Appendix-B*. It can be now moved on with the problems concerning any possible finite element implementation.

### 3.4 FEM Implementation with Strain-gradient Effects

The previously in this section defined material model with bending internal energy can be well embedded into a finite element implementation. As will be seen, there is no special

element type for this purpose is suggested, nor the consequences are discussed. There might be several problems arising quite analogous to the strain element library of total accumulated knowledge of finite element method, but these all are taken out of the concern of the thesis. In this section, the discrete form, and one schema of achieving the destination are presented.

### 3.4.1 Discrete Form for Finite Element Formulation

The energy split proposed before is repeated here, and shape function interpolation on the virtual energy integrals is applied. In order to be consistent with the ongoing chapters, the general gradient notation which is similar to mainstream interpolation schemes is used, such as natural element shape value interpolation, which is visited in the next chapters (see Ch.[5.3.2]). At the end, the notation is converted to the generally accepted matrix-voigt form, to keep the well known standards of finite element jargon. To start with, the nonlinear internal virtual energy divisions are,

$$\begin{aligned}\delta\Pi_{int}^{PF} &= \int_{\Omega} [\mathbf{P} : \nabla_{\mathbf{X}} \delta \mathbf{u}] dV \approx \int_{\Omega} [\mathbf{P} \cdot \nabla_{\mathbf{X}} (\sum N^I)] \cdot \delta \tilde{\mathbf{u}} dV = \mathbf{f}_{int}^{PF} \cdot \delta \tilde{\mathbf{u}} \\ \delta\Pi_{int}^{QG} &= \int_{\Omega} [\mathbf{Q} : \nabla_{\mathbf{X}}^{\otimes 2} \delta \mathbf{u}] dV \approx \int_{\Omega} [\mathbf{Q}^T : \nabla_{\mathbf{X}}^{\otimes 2} (\sum N^I)] \cdot \delta \tilde{\mathbf{u}} dV = \mathbf{f}_{int}^{QG} \cdot \delta \tilde{\mathbf{u}}\end{aligned}\quad (3.27)$$

Where the first one can be interpreted as pure virtual strain energy of internals, the second one is the pure virtual strain gradient energy of internals. It should be kept in mind that, the virtual energy of bending is not straightly or ideally equal to the virtual strain gradient energy of internals. As shown previously, the bending energy can only be formulated at the locus of material if one has the hyperstrain information in hand, and this accounts to the strain energy as well. Correspondingly, the tangent matrices of the non-mixed residuum internal forces can be repeated here to be,

$$\mathbf{K}_{\mathbf{P}(\mathbf{F})}^{IJ} = \int_{\Omega} \left[ \nabla_{\mathbf{X}} N^I \cdot \frac{\partial \mathbf{P}^T}{\partial \mathbf{F}} \cdot \nabla_{\mathbf{X}} N^J \right] dV \quad (3.28a)$$

$$\mathbf{K}_{\mathbf{Q}(\mathbf{G})}^{IJ} = \int_{\Omega} \left[ \nabla_{\mathbf{X}}^{\otimes 2} N^I : \frac{\partial \mathbf{Q}^{T_2}}{\partial \mathbf{G}} : \nabla_{\mathbf{X}}^{\otimes 2} N^J \right] dV \quad (3.28b)$$

And the mixed-residuals of the internal forces cause the following contributions in the tangent stiffness matrices,

$$\mathbf{K}_{\mathbf{P}(\mathbf{G})}^{IJ} = \int_{\Omega} \left[ \nabla_{\mathbf{X}} N^J \cdot \frac{\partial \mathbf{Q}^{T_2}}{\partial \mathbf{G}} : \nabla_{\mathbf{X}}^{\otimes 2} N^I \right] dV \quad (3.29a)$$

$$\mathbf{K}_{\mathbf{Q}(\mathbf{F})}^{IJ} = \int_{\Omega} \left[ \nabla_{\mathbf{X}}^{\otimes 2} N^I : \frac{\partial \mathbf{Q}^{T_2}}{\partial \mathbf{F}} \cdot \nabla_{\mathbf{X}} N^J \right] dV \quad (3.29b)$$

The assumed strain displacement, and assumed hyperstrain displacement matrices as consistent definitions to finite element method are,

$$\begin{aligned}\tilde{\mathbf{B}}^I &= \frac{1}{V} \int_{\Omega} [\nabla_{\mathbf{X}} N^I] dV \\ \tilde{\mathbf{B}}_{\nabla}^I &= \frac{1}{V} \int_{\Omega} [\nabla_{\mathbf{X}}^{\otimes 2} N^I] dV\end{aligned}\quad (3.30)$$



Before moving ahead with the promised strain gradient finite element formulation, one claim has to be cleared here numerically. In general, irrespective of total Lagrange or Euler formulations, or any incremental formulation, the finite element solution at the level of computer numerics is always taken to be based on symmetric tensors. The very well understood reason of it is the coherence and applicability of the symmetric tensors to Voigt notation or similar. In this way, the major and minor symmetries for instance, does allow one to represent fourth order tensors in plane matrix format. Considering the nonsymmetric characteristics of the deformation gradient and the first Piola Kirchoff stress tensor, the notation can not bring any value, since significant symmetry properties are lost. Beside, there might be still a benefit of formulation (3.28a), since it involves both the geometrical and the material tangent values in one, thus is programmer-friendly. However the correctness is to be tested, if the conjugacy of energy works well or not. The start is the representation of the First Piola-Kirchoff stress to deformation gradient tangent with respect to the second Piola-Kirchoff stress to Cauchy-Green strain tensor as formulated beneath.

$$\begin{aligned}
P_{ij} &= F_{im}S_{mj} \\
\mathbb{C}_{ijkl}^{PF} &= \frac{\partial P_{ij}}{\partial F_{kl}} = \frac{\partial F_{im}}{\partial F_{kl}}S_{mj} + F_{im}\frac{\partial S_{mj}}{\partial F_{kl}} \\
&= \delta_{ik}\delta_{ml}S_{mj} + F_{im}\frac{\partial S_{mj}}{\partial C_{no}}\frac{\partial C_{no}}{\partial F_{kl}} \\
&= \delta_{ik}\delta_{ml}S_{mj} + \frac{1}{2}F_{im}\mathbb{C}_{mjno}^{SE}(\delta_{nl}F_{ko} + F_{kn}\delta_{ol})
\end{aligned} \tag{3.31}$$

Where the last identity comes from the derivation of the Cauchy-Green strain tensor with respect to the deformation gradient as shown below,

$$\frac{\partial C_{no}}{\partial F_{kl}} = \frac{\partial}{\partial F_{kl}}(F_{pn}F_{po}) = \delta_{pk}\delta_{nl}F_{po} + F_{pn}\delta_{pk}\delta_{ol} \tag{3.32}$$

In index notation, the conversion of two tangents in index notation is well developed and tested as can be seen next. For this purpose, a spring-like sinusoidal geometry is chosen, clamped at the left edge in elongation direction, pulled on the right edge in the elongation direction. The main purpose is to unbend the geometry, and prove the conjugacy condition is well satisfied with equation (3.31) The constructed model has 5604 nodes with two degrees of freedom each, 1143 quadratic quadrilaterals with 8 nodes and 9 integration points each. The scenario is tested by St. Venant-Kirchoff material, results can be found below. As obvious from the results shown in *Figures 3.11* and *3.12*, two formulations result the same deformation field. Thus, further consideration can be discussed next.

### 3.4.2 Strain-gradient Displacement Matrix

The evaluation of strain gradient displacement matrix can be generalized, however the formulation presented here is based on one element type, namely 8-noded quadrilateral element with 9-integration points. The shape functions, the derivatives of the shape functions can be found elsewhere, writer recommends Zienkiewicz (Ref.[O.C.Zienkiewicz 2000a]) for this purpose. In this stage, the first Piola-Kirchoff/Deformation-gradient consistent

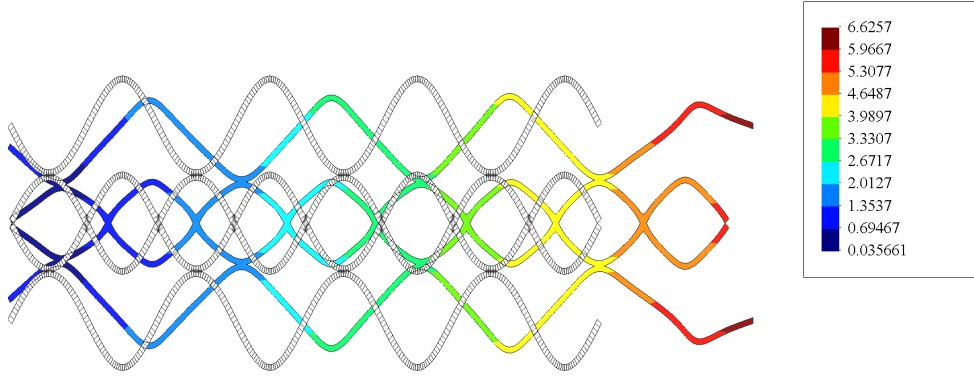


Figure 3.11: Extending the sinusoidal spiral, undeformed Grey, deformed color plot, Legend: Deformation magnitude

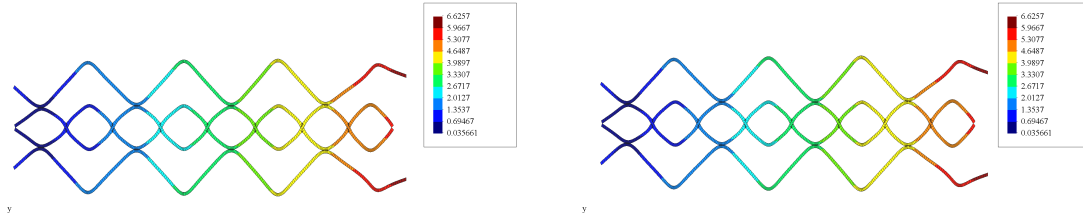


Figure 3.12: Extending the sinusoidal spiral, Left: PF formulation, Right:SE formulation

Strain-Displacement matrix and Strain gradient-Displacement matrix are presented. The arising problems and the solution suggestions of those are presented here. Given 8 Shape functions in this case, to compute a derivative matrix with respect to the local coordinates (evaluated at integration points) can be written as;

$$\begin{aligned}
 \left. \begin{matrix} (4 \times 16) \\ [\mathbf{N}, \boldsymbol{\xi}] \end{matrix} \right|_{(\boldsymbol{\xi}=\boldsymbol{\xi}^*)} &= \left. \begin{bmatrix} N^1_{,\xi} & 0 & N^2_{,\xi} & 0 & N^3_{,\xi} & 0 & N^4_{,\xi} & 0 & \dots \\ N^1_{,\eta} & 0 & N^2_{,\eta} & 0 & N^3_{,\eta} & 0 & N^4_{,\eta} & 0 & \dots \\ 0 & N^1_{,\xi} & 0 & N^2_{,\xi} & 0 & N^3_{,\xi} & 0 & N^4_{,\xi} & \dots \\ 0 & N^1_{,\eta} & 0 & N^2_{,\eta} & 0 & N^3_{,\eta} & 0 & N^4_{,\eta} & \dots \end{bmatrix} \right|_{(\boldsymbol{\xi}=\boldsymbol{\xi}^*)} \quad (3.33)
 \end{aligned}$$

Besides of this, a modified jacobian inverse matrix can be formulated,

$$\left. [\mathbf{J}^{-1}] \right|_{(\boldsymbol{\xi}=\boldsymbol{\xi}^*)} = \left. \begin{bmatrix} \xi_{,X} & \eta_{,X} & 0 & 0 \\ \xi_{,Y} & \eta_{,Y} & 0 & 0 \\ 0 & 0 & \xi_{,X} & \eta_{,X} \\ 0 & 0 & \xi_{,Y} & \eta_{,Y} \end{bmatrix} \right|_{(\boldsymbol{\xi}=\boldsymbol{\xi}^*)} \quad (3.34)$$

These both result in the strain-displacement matrix at a location,

$$\begin{aligned} \left. [\mathbf{B}^{PF}] \right|_{(\xi=\xi^*)}^{(4 \times 16)} &= [\mathbf{J}^{-1}] \Big|_{(\xi=\xi^*)} \cdot \left. [\mathbf{N}, \xi] \right|_{(\xi=\xi^*)}^{(4 \times 16)} \\ &= \left[ \begin{array}{cccccccc} N^1_{,X} & 0 & N^2_{,X} & 0 & N^3_{,X} & 0 & N^4_{,X} & 0 & \dots \\ N^1_{,Y} & 0 & N^2_{,Y} & 0 & N^3_{,Y} & 0 & N^4_{,Y} & 0 & \dots \\ 0 & N^1_{,X} & 0 & N^2_{,X} & 0 & N^3_{,X} & 0 & N^4_{,X} & \dots \\ 0 & N^1_{,Y} & 0 & N^2_{,Y} & 0 & N^3_{,Y} & 0 & N^4_{,Y} & \dots \end{array} \right] \Big|_{(\xi=\xi^*)} \end{aligned} \quad (3.35)$$

As a very well known fact, this matrix is used to obtain strains at the integration points from nodal displacements. In short, the following relation holds;

$$\left. (\mathbf{u}, \mathbf{X}) \right|_{(\xi^*)}^{4 \times 1} = \left. [\mathbf{B}^{PF}] \right|_{(\xi=\xi^*)}^{(4 \times 16)} \cdot \left. (\tilde{\mathbf{u}}) \right|_{(\xi=\xi^*)}^{16 \times 1} \quad (3.36)$$

One may think in the first step, quite analogous to this method, a second derivative matrix format of the shape functions with respect to the global coordinates can be realized. This is however, not as trivial as it sounds at first glance. To show the claim, the index notation can be taken under consideration. Consider the derivative of one degree of freedom with respect to one global reference coordinate,

$$(u, X) \Big|_{(\xi=\xi^*)} = \sum_i \frac{\partial N^i}{\partial X} \Big|_{(\xi=\xi^*)} \tilde{u}^i = \sum_i \left( \frac{\partial N^i}{\partial \xi} \frac{\partial \xi}{\partial X} + \frac{\partial N^i}{\partial \eta} \frac{\partial \eta}{\partial X} \right) \Big|_{(\xi=\xi^*)} \tilde{u}^i \quad (3.37)$$

The computation of the second derivatives results into,

$$\begin{aligned} (u, XX) &= \sum_i \frac{\partial}{\partial X} \left( \frac{\partial N^i}{\partial \xi} \frac{\partial \xi}{\partial X} + \frac{\partial N^i}{\partial \eta} \frac{\partial \eta}{\partial X} \right) \tilde{u}^i \\ &= \sum_i \left[ \left( \frac{\partial^2 N^i}{\partial \xi^2} \frac{\partial \xi}{\partial X} + \frac{\partial^2 N^i}{\partial \xi \partial \eta} \frac{\partial \eta}{\partial X} \right) \frac{\partial \xi}{\partial X} \right. \\ &\quad \left. + \left( \frac{\partial^2 N^i}{\partial \eta \partial \xi} \frac{\partial \xi}{\partial X} + \frac{\partial^2 N^i}{\partial \eta^2} \frac{\partial \eta}{\partial X} \right) \frac{\partial \eta}{\partial X} \right. \\ &\quad \left. + \frac{\partial N^i}{\partial \xi} \frac{\partial^2 \xi}{\partial X^2} + \frac{\partial N^i}{\partial \eta} \frac{\partial^2 \eta}{\partial X^2} \right] \tilde{u}^i \end{aligned} \quad (3.38)$$

The first two addends are easy to obtain, however the third component is simply elements of inverse of the third order Jacobian matrix. Since such an inverse is not found to be defined in the literature, this version of defining strain gradient-displacement matrix is omitted. For this purpose, a element-wise global strain displacement matrix is defined, which includes the strain-displacement matrices evaluated at all nodes,

$$\left. [\mathbf{B}^{PF}] \right|_{nodal}^{(32 \times 16)} = \left[ \left. [\mathbf{B}^{PF}] \right|_{(-1,-1)}^{(4 \times 16)}, \left. [\mathbf{B}^{PF}] \right|_{(1,-1)}^{(4 \times 16)}, \left. [\mathbf{B}^{PF}] \right|_{(1,1)}^{(4 \times 16)}, \left. [\mathbf{B}^{PF}] \right|_{(-1,1)}^{(4 \times 16)}, \dots \right]^T \quad (3.39)$$

The purpose of the matrix above is to get *assumed nodal deformation gradients*, in order to evaluate integration point deformation-hypergradients conjunctively. For that purpose, a larger shape function derivative matrix is to be defined, which is to be evaluated again at the integration locations.

$$\left[ \mathbf{GB}^{PF} \right] \Big|_{(\xi=\xi^*)}^{(8 \times 32)} = \begin{bmatrix} N^1_{,X} & 0 & 0 & 0 & N^2_{,X} & 0 & 0 & 0 & \dots \\ N^1_{,Y} & 0 & 0 & 0 & N^2_{,Y} & 0 & 0 & 0 & \dots \\ 0 & N^1_{,X} & 0 & 0 & 0 & N^2_{,X} & 0 & 0 & \dots \\ 0 & N^1_{,Y} & 0 & 0 & 0 & N^2_{,Y} & 0 & 0 & \dots \\ 0 & 0 & N^1_{,X} & 0 & 0 & 0 & N^2_{,X} & 0 & \dots \\ 0 & 0 & N^1_{,Y} & 0 & 0 & 0 & N^2_{,Y} & 0 & \dots \\ 0 & 0 & 0 & N^1_{,X} & 0 & 0 & 0 & N^2_{,X} & \dots \\ 0 & 0 & 0 & N^1_{,Y} & 0 & 0 & 0 & N^2_{,Y} & \dots \end{bmatrix} \Big|_{(\xi=\xi^*)} \quad (3.40)$$

Finally the strain gradient-displacement matrix, which can be evaluated in any location of the element can be obtained by multiplying the last two defined matrices,

$$\left[ \mathbf{G}^{PF} \right] \Big|_{(\xi=\xi^*)}^{(8 \times 16)} = \left[ \mathbf{GB}^{PF} \right] \Big|_{(\xi=\xi^*)}^{(8 \times 32)} \cdot \left[ \mathbf{B}^{PF} \right] \Big|_{nodal}^{(32 \times 16)} \quad (3.41)$$

Therefore, the desired relationship is obtained and can be further used for the construction of finite element strain-gradient stiffness matrix.

$$(\mathbf{u}, \mathbf{XX}) \Big|_{(\xi^*)}^{8 \times 1} = \left[ \mathbf{G}^{PF} \right] \Big|_{(\xi=\xi^*)}^{(8 \times 16)} \cdot (\tilde{\mathbf{u}}) \Big|_{(\xi=\xi^*)}^{16 \times 1} \quad (3.42)$$

According to the writers opinion, the plane strain formulation given here which suits for 8-node quadrilateral with 9 integration points, is definitely applicable for the 3 dimensional case trivially. One challenge might be here to show the performance in the case of elements with bi- or tri-linear shape functions are used. For instance the second method which is omitted here, namely the equation (3.38), would lack of the first two terms in such an attempt. On the other hand, the suggested method here would be fine adapted to any type of element, however the performance is another topic which was not regarded as the main focus of this work. In the priory step, one has to show the impact of the bending energy on the solution path, and if this is convincing, one may look for improving the other issues, including a diversity of elements and way of integrating the field equations.

### 3.4.3 Numerical Examples

In this section a simple academic example is chosen. The model consist of 88 quadrilateral elements and 317 nodes. The beam is modeled with four layers of elements, each of them consisting of 9 integration points. Therefore, 12 layers of fibrous structure are modeled. In the undeformed reference configuration, the fibers are taken to be straight and aligned in the horizontal direction. The beam is left clamped and a unit force is applied on the right tip. The solution is force controlled. There are in total 3 numerical scenarios shown

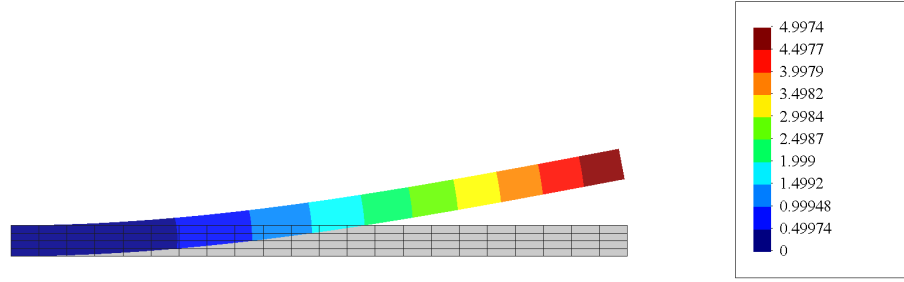


Figure 3.13: Case1; Bending a simple beam, undeformed Grey, deformed color plot, Legend:Deformation Magnitude

here, for all of them the boundary conditions are kept to be the same. The only parameter regarded here is the type and inclusion of the material models. In the first case only a Sn-Venant-Kirchoff material model is chosen. For the second case, additional to the first isotropic energy function, the stretch energy is considered (see *Appendix-B*). For the final case, additional to the stretch energy and isotropic energy, the bending energy is also considered. The stretch and bending energy functions are shown beneath,

$$\psi^s = \frac{1}{2}EA \left( |\mathbf{m}^\#|^2 - 1 \right)^2 + \frac{1}{2}EA \left( |\mathbf{m}^b|^2 - 1 \right)^2 \quad \psi^\kappa = EI \frac{(2 - 2\cos(\alpha^\# + \alpha^b))}{(|\mathbf{m}^\#| + |\mathbf{m}^b|)^2} \quad (3.43)$$

The expectation is that the overall deformation decreases from case one to case three, since the structure is supported with more sources of elastic energy. The amount of influence is another question to be answered. A clear conclusion of the result states that as expected,



Figure 3.14: Deformation plots of beam bending, Left: Case2; Isotropic strain energy density function and Stretch energy density function, Right: Case3; Istropic strain energy density, Stretch energy density and Bending energy density functions

the deformation gets smaller if one considers more energy terms. The deformation under the action of the same force for the case of isotropic, stretch and bending effects is smaller

and thus stiffer than the remaining two scenarios. The amount or the direction of the difference is another discussion topic, but more interesting is the observation of impact on the result, and the convergent behaviour of the numerical implementation itself.



Figure 3.15: Energy distribution plots of beam bending, Left: Stretch energy distribution, Right: Case3; Bending energy distribution



# Reorientation with Strain and Gradient Effects

---

## Contents

---

<b>4.1</b>	<b>Introduction</b>	<b>99</b>
<b>4.2</b>	<b>Orthotropic Hyperelasticity</b>	<b>100</b>
4.2.1	Worm-like Chain Model	100
4.2.2	Mechanics of the Chain Network	101
4.2.3	Structural Tensors	102
4.2.4	Energy Split, Stress at Integration Point and Tangent Modulus	108
4.2.5	Simple Tension and Shear on the Orthotropic 8-chain Model	110
<b>4.3</b>	<b>Material Point Reorientation</b>	<b>113</b>
4.3.1	Strain based Reorientation	113
4.3.2	Curvature Reorientation	118
4.3.3	Reorientation based on the EB Material Model	119

---

## 4.1 Introduction

The macroscopic mechanical function of the soft tissue depends on anisotropy and local homogenized orientations of load bearing fibrous network. The indications of early wear damage (Ref.[[W.Wilson 2003](#)]) of AC have been associated with the local network damage of collagen mesh. The depth dependent local anisotropy and fiber orientation of AC have been studied recently under theoretical, numerical and experimental frameworks (see Wilson Ref.[[W.Wilson 2005](#)] , Quinn Ref.[[T.M.Quinn 2005](#)]). Mechanical and material functionality of AC are investigated frequently by taking the complicated microscopic behavior into account also, refer to the works for instance by; (Federico Ref.[[Federico 2008](#)] , Schinagl Ref.[[Schinagl 1997](#)] , and Buckley Ref.[[Buckley 2008](#)]). The macroscopic mechanical function of the soft tissue depends on anisotropy and local homogenized orientations of load bearing fibrous network. The indications of early wear damage (Ref.[[W.Wilson 2003](#)]) of AC have been associated with the local network damage of collagen mesh. The depth dependent local anisotropy and fiber orientation of AC have been studied recently under theoretical, numerical and experimental frameworks (see Wilson Ref.[[W.Wilson 2005](#)] , Quinn Ref.[[T.M.Quinn 2005](#)]). Mechanical and material functionality of AC are investigated frequently



by taking the complicated microscopic behavior into account also, refer to the works for instance by; (Federico Ref.[Federico 2008] , Schinagl Ref.[Schinagl 1997] , and Buckley Ref.[Buckley 2008]).

Remodeling by Menzel (Ref.[A.Menzel 2004]) is defined as the evolution of microstructure or variations in the configuration of the underlying manifold. Many novel and recent recognitions of remodeling definitions with various applications are present. The current local microstructure of soft tissues like tendons, ligaments, AC, arterial walls, or cell traction experiments, engineered soft tissues and even abstract-type materials are investigated with the present remodeling strategies cited here. Without proof, in these works, it is assumed that the soft tissue takes its evaluated microform with the postulated biomechanical continuum setting.

Menzel (Ref.[A.Menzel 2004]) has postulated a general theoretical and numerical framework of remodeling and growth of fiber reinforced material. Garikipati (Ref.[K.Garikipati 2005]), has discussed stationary strain energy and thermodynamic aspects of remodeling with the realization of cell-traction experiments. Kuhl (Ref.[E.Kuhl 2008]) and Holzapfel (Ref.[G.Holzapfel 2006]) have showed that gradual alignment of unit-cell can represent collagen network orientation of an engineered tendon-like tissue. Holzapfel (Ref.[I.Hariton 2007]) and Driessen (Ref.[N.J.Driessen 2003]) have recently used stress-driven reorientation of collagen fibers of arterial walls and porcine aortic valve leaflet. Wilson (Ref.[W.Wilson 2006]) has predicted the depth dependent collagen orientation of AC with remodeling.

In this work, the comprehensive formulation of orthotropic hyperelasticity of eight-chain network model with the full set of structural invariants are presented first. The strain energy density function of the unit-cell, with orthonormal reference bases depending on irreducible set of invariants are introduced. The reorientation of unit cell depending on the strain energy density function are presented thereafter. Small academic examples and illustrations of quasi-static cyclic remodeling using nonlinear finite element method are presented. Finally, comments on the spatial local architecture of AC are left.

Analogous to the strain dependent reorientation, two types of strain gradient dependent reorientation methods are postulated here too. Comments are left, and the comparison of the strain and strain gradient reorientations and their effects on AC-alike geometry are investigated in next sections.

## 4.2 Orthotropic Hyperelasticity

### 4.2.1 Worm-like Chain Model

The hyperelastic strain energy density function developed here, is applicable to any kind of given force-displacement relationship. For the sake of relevancy, the wormlike chain model is reintroduced. It is a simple but generally accepted one for the remodeling of biological tissue (Garikipati Ref.[K.Garikipati 2005] , Kuhl Ref.[E.Kuhl 2008]Ref.[G.Holzapfel 2006]). The wormlike chain model considers the persistence length of the chain (which can be measured experimentally) as a measure of unbending stiffness.

$$\psi(|\mathbf{r}|) = \frac{\gamma k T l}{4A} \left( 2 \frac{|\mathbf{r}|^2}{L^2} + \frac{1}{(1 - |\mathbf{r}|/L)} - \frac{|\mathbf{r}|}{L} \right) \quad (4.1)$$

For missing fundamental knowledge, please refer to the references in the given order. For the statistical approach of basic thermodynamics refer to Baierlein (Ref.[R.Baierlein 2010]), for gathering undergraduate knowledge about physics of polymer chains to Boal (Ref.[David Boal 2010]), and for a clean derivation of wormlike chain force-displacement behavior to MacKintosh (Ref.[F.C.MacKintosh 2009]).

## 4.2.2 Mechanics of the Chain Network

### 4.2.2.1 Essential Kinematics

The nonlinear deformation map  $\mathbf{x} = \varphi(\mathbf{X}, t)$  defines the quasi-static (Ogden-Ref.[R.W.Ogden 2008]) (kinematic) motion of material coordinates of a particle with coordinates  $\mathbf{X} \in \Omega_0$  at  $t = 0$  to the spatial coordinates of that particle  $\mathbf{x} \in \Omega$  at a subsequent time  $t > 0$ . The two point tensor deformation gradient  $\mathbf{F}$  maps the material tangent space  $d\mathbf{X} \in T\Omega_0$  to the spatial tangent space  $d\mathbf{x} \in T\Omega$  subsequent time  $t > 0$ . In this first order kinematics<sup>1</sup>, the coordinates  $\theta^i$  are assumed to convect with the linear

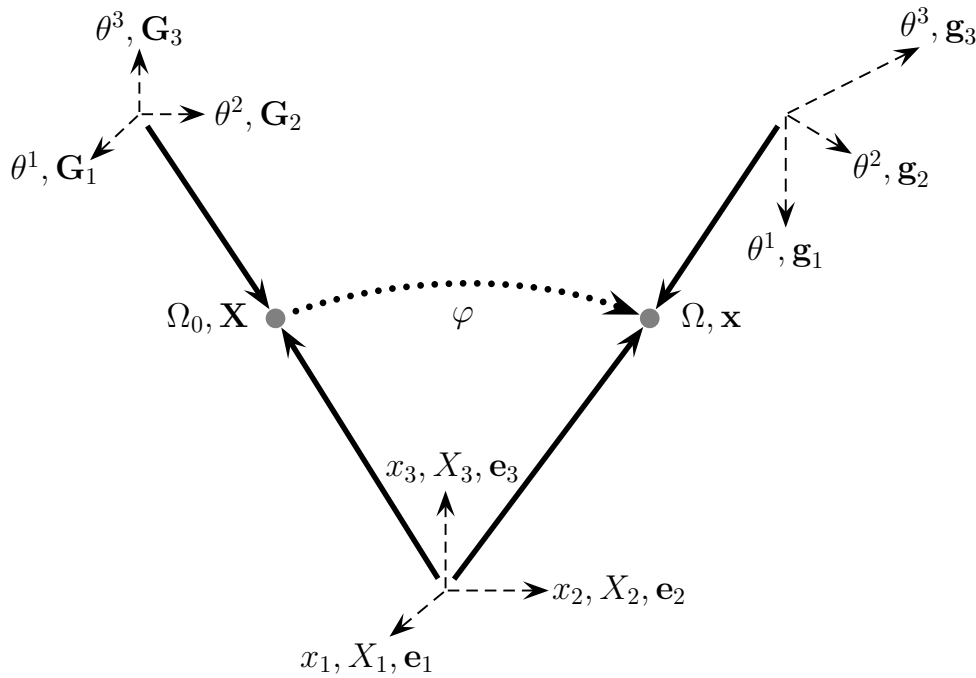


Figure 4.1: Nonlinear deformation map with convective coordinates

<sup>1</sup>For the second order kinematics, please refer to the chapter of Hyperkinematics(Ch.[2])

tangent map  $F$ .

$$\begin{aligned}\mathbf{X} &= X_i \hat{\mathbf{e}}_i = \theta^i \mathbf{G}_i \\ \mathbf{x} &= x_i \hat{\mathbf{e}}_i = \theta^i \mathbf{g}_i\end{aligned}\quad (4.2)$$

Where the following well known relations between the material and spatial bases and the tangent map are valid here.

$$\mathbf{G}_j = \frac{\partial X^m}{\partial \theta^j} \hat{\mathbf{e}}_m \quad (4.3a)$$

$$\hat{\mathbf{e}}_j = \frac{\partial X^j}{\partial \theta^m} \mathbf{G}^m \quad (4.3b)$$

$$\mathbf{g}_j = \frac{\partial x^i}{\partial \theta^j} \hat{\mathbf{e}}_i \quad (4.3c)$$

$$\hat{\mathbf{e}}_i = \frac{\partial \theta^m}{\partial x^i} \mathbf{g}_m \quad (4.3d)$$

Besides, the two point tensor deformation gradient in terms of the base vectors of convecting coordinates can be evaluated as the following. These convected coordinates and metrics will be used next for the derivation of the orthotropic hyperelastic 8-chain unit-cell model.

$$\mathbf{F} = \frac{\partial x_i}{\partial X_j} (\hat{\mathbf{e}}_i \otimes \hat{\mathbf{e}}_j) = \frac{\partial x_i}{\partial X_j} \left( \frac{\partial \theta^m}{\partial x^i} \mathbf{g}_m \otimes \frac{\partial X^j}{\partial \theta^m} \mathbf{G}^m \right) = \mathbf{g}_m \otimes \mathbf{G}^m \quad (4.4)$$

### 4.2.3 Structural Tensors

To define the orthotropic free energy function, the structural invariants<sup>2</sup> are used. The structural tensors are defined by material or spatial covariant bases given as;

$$\mathbf{G}_{ij} = \mathbf{G}_i \otimes \mathbf{G}_j \quad (4.5a)$$

$$\mathbf{g}_{ij} = \mathbf{g}_i \otimes \mathbf{g}_j = \mathbf{F} \cdot \mathbf{G}_i \otimes \mathbf{F} \cdot \mathbf{G}_j \quad (4.5b)$$

With the indexes no summation is implied. It is taken such that the unit scalars are convected with the deformation, thus the material and spatial base vectors are not necessarily defined as unit vectors. The traces of these dyadic products can be interpreted as the lengths of the basis vectors in the reference and deformed configurations if the indexes are equal, otherwise; the scalar projections on each other should be taken as the interpretation. By considering that the lengths and scalar projections being unaffected under any kind of *post or pre-rotations*<sup>3</sup> (the length or projection of a convecting frame is unchanged if rotated), the trace operators generate so called structural invariants. The

<sup>2</sup>For a better understanding of the structural tensors please refer to the beautiful treatise written by Bohler (Ref.[[Boehler 1979](#)]) almost a half a decade ago

<sup>3</sup>post/pre rotation: orthogonal type of deformation acting after and before motion accordingly

invariants as entries of covariant spatial metric have the following relations;

$$\begin{aligned}
\begin{pmatrix} \mathbf{g}_1 \\ \mathbf{g}_2 \\ \mathbf{g}_3 \end{pmatrix} &= \begin{bmatrix} \mathbf{g}_1 \cdot \mathbf{g}_1 & \mathbf{g}_1 \cdot \mathbf{g}_2 & \mathbf{g}_1 \cdot \mathbf{g}_3 \\ \mathbf{g}_2 \cdot \mathbf{g}_1 & \mathbf{g}_2 \cdot \mathbf{g}_2 & \mathbf{g}_2 \cdot \mathbf{g}_3 \\ \mathbf{g}_3 \cdot \mathbf{g}_1 & \mathbf{g}_3 \cdot \mathbf{g}_2 & \mathbf{g}_3 \cdot \mathbf{g}_3 \end{bmatrix} \cdot \begin{pmatrix} \mathbf{g}^1 \\ \mathbf{g}^2 \\ \mathbf{g}^3 \end{pmatrix} \\
&= \begin{bmatrix} tr(\mathbf{g}_{11}) & tr(\mathbf{g}_{12}) & tr(\mathbf{g}_{13}) \\ tr(\mathbf{g}_{21}) & tr(\mathbf{g}_{22}) & tr(\mathbf{g}_{23}) \\ tr(\mathbf{g}_{31}) & tr(\mathbf{g}_{32}) & tr(\mathbf{g}_{33}) \end{bmatrix} \cdot \begin{pmatrix} \mathbf{g}^1 \\ \mathbf{g}^2 \\ \mathbf{g}^3 \end{pmatrix} \\
&= \begin{bmatrix} tr(\mathbf{G}_{11} \cdot \mathbf{C}) & tr(\mathbf{G}_{12} \cdot \mathbf{C}) & tr(\mathbf{G}_{13} \cdot \mathbf{C}) \\ tr(\mathbf{G}_{21} \cdot \mathbf{C}) & tr(\mathbf{G}_{22} \cdot \mathbf{C}) & tr(\mathbf{G}_{23} \cdot \mathbf{C}) \\ tr(\mathbf{G}_{31} \cdot \mathbf{C}) & tr(\mathbf{G}_{32} \cdot \mathbf{C}) & tr(\mathbf{G}_{33} \cdot \mathbf{C}) \end{bmatrix} \cdot \begin{pmatrix} \mathbf{g}^1 \\ \mathbf{g}^2 \\ \mathbf{g}^3 \end{pmatrix}
\end{aligned} \tag{4.6}$$

Where  $\mathbf{C} = \mathbf{F}^T \cdot \mathbf{F}$  is the right Cauchy-Green deformation tensor.

There can be nine dependent structural tensors present, whereas six of them being transpose of each other. The set of covariant material base vectors are chosen to be orthonormal. Therefore, the matrix form of the covariant material metric is a diagonal square. Because the deformation is arbitrary, the covariant spatial metric has not necessarily zero off-diagonal terms. However, the covariant material structural tensors are trace-wise dependent on each other.

For an orthotropic hyperelastic material formulation, the strain energy function is established based on the basic invariants of Cauchy-Green deformation tensor and the six structural invariants with unit bases given beneath. For other examples please refer to Boehler Ref.[[Boehler 1979](#)], Park Ref.[[H.C.Prk 1997](#)] and Sansour Ref.[[C.Sansour 2007](#)].

$$J_1 = \mathbf{G}_{11} : \mathbf{C} \tag{4.7a}$$

$$J_2 = \mathbf{G}_{22} : \mathbf{C} \tag{4.7b}$$

$$J_3 = \mathbf{G}_{33} : \mathbf{C} \tag{4.7c}$$

$$J_4 = \mathbf{G}_{11} : \mathbf{C}^2 \tag{4.7d}$$

$$J_5 = \mathbf{G}_{22} : \mathbf{C}^2 \tag{4.7e}$$

$$J_6 = \mathbf{G}_{33} : \mathbf{C}^2 \tag{4.7f}$$

The concepts of objectivity<sup>4</sup> (invariance of strain energy for post rotations, observations), material symmetry<sup>5</sup> (invariance of strain energy for pre rotations) and convexity of strain energy function are out of scope of this work. With all of the assumptions, the strain energy density takes the following form;

$$\psi = \psi(I_1, I_2, I_3, J_1, J_2, J_3, J_4, J_5, J_6) \tag{4.8}$$

There are many phenomenological models fitting with the theoretical form given above. The intent is to find the relation between the invariants, network structure, deformed chain

<sup>4</sup>A post-rotation can be interpreted as the rotation of the observer of the deformed body. This type of observer motion can not manipulate the strain energy, since the action has already taken place, indicating the term *objective material depending on invariants*

<sup>5</sup>An isotropic material would be insensitive to the pre-rotations and thus symmetric

length and strain energy density function for the unit cell. The geometrical approach given by Kuhl (Ref.[[E.Kuhl 2008](#)]) (transversely isotropic 8-chain model) will be followed and extended here. The lengths of the chains in the undeformed configuration become;

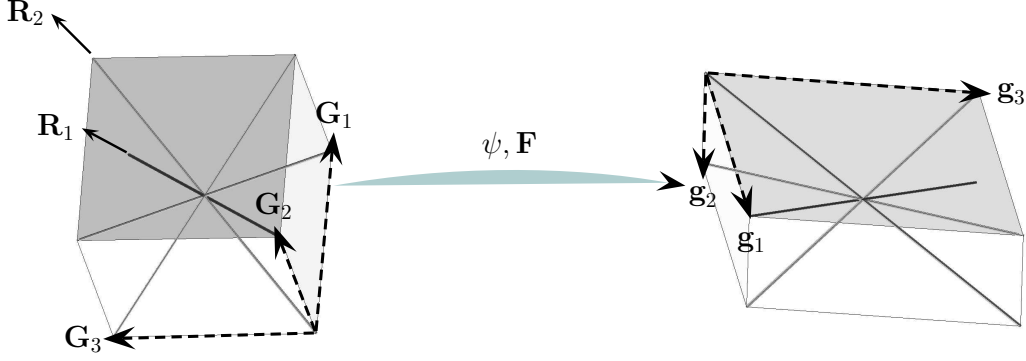


Figure 4.2: undeformed and deformed coordinates of the unit cell

$$\begin{aligned} |\mathbf{R}_0| &= |\mathbf{R}_{0\parallel}| = |\mathbf{R}_1| = |\mathbf{R}_{1\parallel}| = |\mathbf{R}_2| = |\mathbf{R}_{2\parallel}| = |\mathbf{R}_3| = |\mathbf{R}_{3\parallel}| = \\ |\mathbf{R}| &= \sqrt{\mathbf{G}_{11} : \mathbf{I} + \mathbf{G}_{22} : \mathbf{I} + \mathbf{G}_{33} : \mathbf{I}} \end{aligned} \quad (4.9)$$

The lengths of chains in the deformed configuration are;

$$\begin{aligned} |\mathbf{r}_0| &= |\mathbf{r}_{0\parallel}| = \sqrt{(\mathbf{G}_1^T \cdot \mathbf{F}^T + \mathbf{G}_2^T \cdot \mathbf{F}^T + \mathbf{G}_3^T \cdot \mathbf{F}^T) \cdot (\mathbf{F} \cdot \mathbf{G}_1 + \mathbf{F} \cdot \mathbf{G}_2 + \mathbf{F} \cdot \mathbf{G}_3)} \\ &= \sqrt{(\mathbf{G}_1^T \cdot \mathbf{F}^T \cdot \mathbf{F} \cdot \mathbf{G}_1) + (\mathbf{G}_2^T \cdot \mathbf{F}^T \cdot \mathbf{F} \cdot \mathbf{G}_2) + (\mathbf{G}_3^T \cdot \mathbf{F}^T \cdot \mathbf{F} \cdot \mathbf{G}_3) +} \\ &\quad 2(\mathbf{G}_1^T \cdot \mathbf{F}^T \cdot \mathbf{F} \cdot \mathbf{G}_2) + 2(\mathbf{G}_3^T \cdot \mathbf{F}^T \cdot \mathbf{F} \cdot \mathbf{G}_1) + 2(\mathbf{G}_2^T \cdot \mathbf{F}^T \cdot \mathbf{F} \cdot \mathbf{G}_3) \\ &= \sqrt{\mathbf{G}_{11} : \mathbf{C} + \mathbf{G}_{22} : \mathbf{C} + \mathbf{G}_{33} : \mathbf{C} + 2\mathbf{G}_{12} : \mathbf{C} + 2\mathbf{G}_{31} : \mathbf{C} + 2\mathbf{G}_{23} : \mathbf{C}} \end{aligned} \quad (4.10)$$

Similarly, the other deformed lengths become,

$$\begin{aligned} |\mathbf{r}_1| &= |\mathbf{r}_{1\parallel}| = \sqrt{\mathbf{G}_{11} : \mathbf{C} + \mathbf{G}_{22} : \mathbf{C} + \mathbf{G}_{33} : \mathbf{C} - 2\mathbf{G}_{12} : \mathbf{C} + 2\mathbf{G}_{31} : \mathbf{C} - 2\mathbf{G}_{23} : \mathbf{C}} \\ |\mathbf{r}_2| &= |\mathbf{r}_{2\parallel}| = \sqrt{\mathbf{G}_{11} : \mathbf{C} + \mathbf{G}_{22} : \mathbf{C} + \mathbf{G}_{33} : \mathbf{C} + 2\mathbf{G}_{12} : \mathbf{C} - 2\mathbf{G}_{31} : \mathbf{C} - 2\mathbf{G}_{23} : \mathbf{C}} \\ |\mathbf{r}_3| &= |\mathbf{r}_{3\parallel}| = \sqrt{\mathbf{G}_{11} : \mathbf{C} + \mathbf{G}_{22} : \mathbf{C} + \mathbf{G}_{33} : \mathbf{C} - 2\mathbf{G}_{12} : \mathbf{C} - 2\mathbf{G}_{31} : \mathbf{C} + 2\mathbf{G}_{23} : \mathbf{C}} \end{aligned} \quad (4.11)$$

These simple derivations are supported by the statement of Boehler (Ref.[[Boehler 1979](#)]); "All the invariants of general anisotropy can be expressed as single valued functions of the six independent invariants". The invariants that Boehler mentioned are nothing but the ones given in the deformed chain lengths formulas above, which is chosen on purpose in this way,

to be consistent with the historical terminology of the invariant algebra.

The remaining part of the work is, reformulation of structural tensors. The aim is, to catch consistency with the common orthotropic hyperelastic energy functions in the literature, which are usually given in terms of the invariants above. Another reason beyond the seek of consistency is to establish a strain energy density functions using the given derivatives of standard structural invariants with respect to the Right Cauchy-Green deformation tensor.

$$\mathbf{G}_{ij} : \mathbf{C} = \mathbf{G}_{ij} : \mathbf{C} = (J_1, J_2, J_3, J_4, J_5, J_6) \quad (4.12)$$

For further reductions, the next equalities which are valid for non-unit<sup>6</sup> orthonormal bases are used.

$$\mathbf{I} : \mathbf{I} = \frac{\mathbf{G}_{11} : \mathbf{I}}{\mathbf{G}_{11} : \mathbf{I}} + \frac{\mathbf{G}_{22} : \mathbf{I}}{\mathbf{G}_{22} : \mathbf{I}} + \frac{\mathbf{G}_{33} : \mathbf{I}}{\mathbf{G}_{33} : \mathbf{I}} \quad (4.13a)$$

$$\mathbf{I} : \mathbf{C} = \frac{\mathbf{G}_{11} : \mathbf{C}}{\mathbf{G}_{11} : \mathbf{I}} + \frac{\mathbf{G}_{22} : \mathbf{C}}{\mathbf{G}_{22} : \mathbf{I}} + \frac{\mathbf{G}_{33} : \mathbf{C}}{\mathbf{G}_{33} : \mathbf{I}} \quad (4.13b)$$

$$\mathbf{I} : \mathbf{C}^2 = \frac{\mathbf{G}_{11} : \mathbf{C}^2}{\mathbf{G}_{11} : \mathbf{I}} + \frac{\mathbf{G}_{22} : \mathbf{C}^2}{\mathbf{G}_{22} : \mathbf{I}} + \frac{\mathbf{G}_{33} : \mathbf{C}^2}{\mathbf{G}_{33} : \mathbf{I}} \quad (4.13c)$$

$$\text{tr}(\mathbf{G}_{11} \cdot \mathbf{C}^2) = \frac{(\mathbf{G}_{11} : \mathbf{C})^2}{\mathbf{G}_{11} : \mathbf{I}} + \frac{(\mathbf{G}_{12} : \mathbf{C})^2}{\mathbf{G}_{22} : \mathbf{I}} + \frac{(\mathbf{G}_{13} : \mathbf{C})^2}{\mathbf{G}_{33} : \mathbf{I}} \quad (4.13d)$$

$$\text{tr}(\mathbf{G}_{22} \cdot \mathbf{C}^2) = \frac{(\mathbf{G}_{21} : \mathbf{C})^2}{\mathbf{G}_{11} : \mathbf{I}} + \frac{(\mathbf{G}_{22} : \mathbf{C})^2}{\mathbf{G}_{22} : \mathbf{I}} + \frac{(\mathbf{G}_{23} : \mathbf{C})^2}{\mathbf{G}_{33} : \mathbf{I}} \quad (4.13e)$$

$$\text{tr}(\mathbf{G}_{33} \cdot \mathbf{C}^2) = \frac{(\mathbf{G}_{31} : \mathbf{C})^2}{\mathbf{G}_{11} : \mathbf{I}} + \frac{(\mathbf{G}_{32} : \mathbf{C})^2}{\mathbf{G}_{22} : \mathbf{I}} + \frac{(\mathbf{G}_{33} : \mathbf{C})^2}{\mathbf{G}_{33} : \mathbf{I}} \quad (4.13f)$$

The first three equations can be seen or found by simple tensor calculus. For the derivation of the last three equations, please refer to *Appendix-D*. By using these six equations the mixed invariants can be represented as;

$$\begin{aligned} 2(\mathbf{G}_{12} : \mathbf{C})^2 &= (\mathbf{G}_{11} : \mathbf{I})(\mathbf{G}_{22} : \mathbf{I}) \left[ \mathbf{I} : \mathbf{C}^2 - 2 \frac{(\mathbf{G}_{33} : \mathbf{C})^2}{\mathbf{G}_{33} : \mathbf{I}} \right] \\ &+ \left[ -\frac{\mathbf{G}_{22} : \mathbf{I}}{\mathbf{G}_{11} : \mathbf{I}} (\mathbf{G}_{11} : \mathbf{C})^2 - \frac{\mathbf{G}_{11} : \mathbf{I}}{\mathbf{G}_{22} : \mathbf{I}} (\mathbf{G}_{22} : \mathbf{C})^2 + \frac{(\mathbf{G}_{11} : \mathbf{I})(\mathbf{G}_{22} : \mathbf{I})}{(\mathbf{G}_{33} : \mathbf{I})^2} (\mathbf{G}_{33} : \mathbf{C})^2 \right] \\ &= (\mathbf{G}_{11} : \mathbf{I})(\mathbf{G}_{22} : \mathbf{I}) \left[ \left( \mathbf{I} : \mathbf{C}^2 - 2 \frac{(\mathbf{G}_{33} : \mathbf{C})^2}{\mathbf{G}_{33} : \mathbf{I}} \right) \right. \\ &\quad \left. + \left( -\frac{(\mathbf{G}_{11} : \mathbf{C})^2}{(\mathbf{G}_{11} : \mathbf{I})^2} - \frac{(\mathbf{G}_{22} : \mathbf{C})^2}{(\mathbf{G}_{22} : \mathbf{I})^2} + \frac{(\mathbf{G}_{33} : \mathbf{C})^2}{(\mathbf{G}_{33} : \mathbf{I})^2} \right) \right] \end{aligned} \quad (4.14a)$$

<sup>6</sup>The base vectors do not have to be necessarily of unit size, so that the undeformed invariants may represent the finite space occupied by a fundamental biological unit -and the mechanical correspondent of it-.

Similarly, the second mixed invariant becomes,

$$\begin{aligned}
2(\mathbf{G}_{13} : \mathbf{C})^2 &= (\mathbf{G}_{11} : \mathbf{I})(\mathbf{G}_{33} : \mathbf{I}) \left[ \mathbf{I} : \mathbf{C}^2 - 2 \frac{(\mathbf{G}_{22} : \mathbf{C})^2}{\mathbf{G}_{22} : \mathbf{I}} \right] \\
&+ \left[ -\frac{\mathbf{G}_{33} : \mathbf{I}}{\mathbf{G}_{11} : \mathbf{I}} (\mathbf{G}_{11} : \mathbf{C})^2 + \frac{(\mathbf{G}_{11} : \mathbf{I})(\mathbf{G}_{33} : \mathbf{I})}{(\mathbf{G}_{22} : \mathbf{I})^2} (\mathbf{G}_{22} : \mathbf{C})^2 - \frac{\mathbf{G}_{11} : \mathbf{I}}{\mathbf{G}_{33} : \mathbf{I}} (\mathbf{G}_{33} : \mathbf{C})^2 \right] \\
&= (\mathbf{G}_{11} : \mathbf{I})(\mathbf{G}_{33} : \mathbf{I}) \left[ \left( \mathbf{I} : \mathbf{C}^2 - 2 \frac{(\mathbf{G}_{22} : \mathbf{C})^2}{\mathbf{G}_{22} : \mathbf{I}} \right) \right. \\
&\quad \left. + \left( -\frac{(\mathbf{G}_{11} : \mathbf{C})^2}{(\mathbf{G}_{11} : \mathbf{I})^2} + \frac{(\mathbf{G}_{22} : \mathbf{C})^2}{(\mathbf{G}_{22} : \mathbf{I})^2} - \frac{(\mathbf{G}_{33} : \mathbf{C})^2}{(\mathbf{G}_{33} : \mathbf{I})^2} \right) \right] \tag{4.15a}
\end{aligned}$$

And the last mixed invariant for clearance,

$$\begin{aligned}
2(\mathbf{G}_{23} : \mathbf{C})^2 &= (\mathbf{G}_{22} : \mathbf{I})(\mathbf{G}_{33} : \mathbf{I}) \left[ \mathbf{I} : \mathbf{C}^2 - 2 \frac{(\mathbf{G}_{11} : \mathbf{C})^2}{\mathbf{G}_{11} : \mathbf{I}} \right] \\
&+ \left[ +\frac{(\mathbf{G}_{22} : \mathbf{I})(\mathbf{G}_{33} : \mathbf{I})}{(\mathbf{G}_{11} : \mathbf{I})^2} (\mathbf{G}_{11} : \mathbf{C})^2 - \frac{\mathbf{G}_{33} : \mathbf{I}}{\mathbf{G}_{22} : \mathbf{I}} (\mathbf{G}_{22} : \mathbf{C})^2 - \frac{\mathbf{G}_{22} : \mathbf{I}}{\mathbf{G}_{33} : \mathbf{I}} (\mathbf{G}_{33} : \mathbf{C})^2 \right] \\
&= (\mathbf{G}_{22} : \mathbf{I})(\mathbf{G}_{33} : \mathbf{I}) \left[ \left( \mathbf{I} : \mathbf{C}^2 - 2 \frac{(\mathbf{G}_{11} : \mathbf{C})^2}{\mathbf{G}_{11} : \mathbf{I}} \right) \right. \\
&\quad \left. + \left( +\frac{(\mathbf{G}_{11} : \mathbf{C})^2}{(\mathbf{G}_{11} : \mathbf{I})^2} - \frac{(\mathbf{G}_{22} : \mathbf{C})^2}{(\mathbf{G}_{22} : \mathbf{I})^2} - \frac{(\mathbf{G}_{33} : \mathbf{C})^2}{(\mathbf{G}_{33} : \mathbf{I})^2} \right) \right] \tag{4.16a}
\end{aligned}$$

To check or ensure the correctness of these reductions please refer to *Appendix-D*. According to the calculations, the complete set of new invariants are to be redefined;

$$I_2 = \mathbf{I} : \mathbf{C}^2 \quad (4.17a)$$

$$J_1 = \frac{\mathbf{G}_{11} : \mathbf{C}}{\mathbf{G}_{11} : \mathbf{I}} \quad (4.17b)$$

$$J_2 = \frac{\mathbf{G}_{22} : \mathbf{C}}{\mathbf{G}_{22} : \mathbf{I}} \quad (4.17c)$$

$$J_3 = \frac{\mathbf{G}_{33} : \mathbf{C}}{\mathbf{G}_{33} : \mathbf{I}} \quad (4.17d)$$

$$J_4 = \frac{\mathbf{G}_{11} : \mathbf{C}^2}{\mathbf{G}_{11} : \mathbf{I}} \quad (4.17e)$$

$$J_5 = \frac{\mathbf{G}_{22} : \mathbf{C}^2}{\mathbf{G}_{22} : \mathbf{I}} \quad (4.17f)$$

$$J_6 = \frac{\mathbf{G}_{33} : \mathbf{C}^2}{\mathbf{G}_{33} : \mathbf{I}} \quad (4.17g)$$

The new set of structural invariants can be considered as the normalizations of the standard ones. The mixed invariants in terms of the new integrity basis;

$$(\mathbf{G}_{12} : \mathbf{C})^2 = (\mathbf{G}_{11} : \mathbf{I}) (\mathbf{G}_{22} : \mathbf{I}) \left[ (I_2 - 2J_6) \left( -(J_1)^2 - (J_2)^2 + (J_3)^2 \right) \right] \quad (4.18a)$$

$$(\mathbf{G}_{13} : \mathbf{C})^2 = (\mathbf{G}_{11} : \mathbf{I}) (\mathbf{G}_{33} : \mathbf{I}) \left[ (I_2 - 2J_5) \left( -(J_1)^2 + (J_2)^2 - (J_3)^2 \right) \right] \quad (4.18b)$$

$$(\mathbf{G}_{23} : \mathbf{C})^2 = (\mathbf{G}_{22} : \mathbf{I}) (\mathbf{G}_{33} : \mathbf{I}) \left[ (I_2 - 2J_4) \left( (J_1)^2 - (J_2)^2 - (J_3)^2 \right) \right] \quad (4.18c)$$

And the deformed chain length of one of the chains in terms of the new integrity basis;

$$\begin{aligned} |r| &= \sqrt{\frac{tr(\mathbf{G}_{11} : \mathbf{C}) + tr(\mathbf{G}_{22} : \mathbf{C}) + tr(\mathbf{G}_{33} : \mathbf{C})}{+tr(\mathbf{G}_{12} : \mathbf{C}) + tr(\mathbf{G}_{31} : \mathbf{C}) + tr(\mathbf{G}_{23} : \mathbf{C})}} \\ &= \sqrt{\frac{(\mathbf{G}_{11} : \mathbf{I}) J_1 + (\mathbf{G}_{22} : \mathbf{I}) J_1 + (\mathbf{G}_{33} : \mathbf{I}) J_1}{+ \sqrt{2(\mathbf{G}_{11} : \mathbf{I}) (\mathbf{G}_{22} : \mathbf{I}) \left[ (I_2 - 2J_6) \left( -(J_1)^2 - (J_2)^2 + (J_3)^2 \right) \right]} \\ &\quad + \sqrt{2(\mathbf{G}_{11} : \mathbf{I}) (\mathbf{G}_{33} : \mathbf{I}) \left[ (I_2 - 2J_5) \left( -(J_1)^2 + (J_2)^2 - (J_3)^2 \right) \right]} \\ &\quad + \sqrt{2(\mathbf{G}_{22} : \mathbf{I}) (\mathbf{G}_{33} : \mathbf{I}) \left[ (I_2 - 2J_4) \left( (J_1)^2 - (J_2)^2 - (J_3)^2 \right) \right]}}}{+ \sqrt{2I_{12}} + \sqrt{2I_{31}} + \sqrt{2I_{23}}} \quad (4.19) \end{aligned}$$



Where, to reduce the complexity, the mixed invariants can be formulated as;

$$I_{12} = (\mathbf{G}_{11} : \mathbf{I}) (\mathbf{G}_{22} : \mathbf{I}) \left[ (I_2 - 2J_6) \left( -(J_1)^2 - (J_2)^2 + (J_3)^2 \right) \right] \quad (4.20a)$$

$$I_{31} = (\mathbf{G}_{11} : \mathbf{I}) (\mathbf{G}_{33} : \mathbf{I}) \left[ (I_2 - 2J_5) \left( -(J_1)^2 + (J_2)^2 - (J_3)^2 \right) \right] \quad (4.20b)$$

$$I_{23} = (\mathbf{G}_{22} : \mathbf{I}) (\mathbf{G}_{33} : \mathbf{I}) \left[ (I_2 - 2J_4) \left( (J_1)^2 - (J_2)^2 - (J_3)^2 \right) \right] \quad (4.20c)$$

Finally, with this explained frame, the chain strain energy density function is defined depending on six structural and one basic invariant of the first order kinematics unit-cell based on worm-like chains.

$$\psi^{chain} = \psi^{chain} (I_2, J_1, J_2, J_3, J_4, J_5, J_6) \quad (4.21)$$

The invariants of the transverse isotropy  $I_2, J_1$  and  $J_4$  account for the stretch of the fiber coincidentally parallel to the first covariant material base vector (a physical interpretation), and  $J_5$  and  $J_6$  account indirectly to the strain energy of shear modes. It is commented by Ogden (Ref.[[R.W.Ogden 2008](#)]) that there is no straightforward interpretation of the last two invariants, however the relation in between finite strain and the dependency on  $J_5$  and  $J_6$  holds. Among the microstructure based models in the literature, the kinematics defined by Kuhl (Ref.[[E.Kuhl 2008](#)]) and Holzapfel (Ref.[[G.Holzapfel 2006](#)]) represent the chain strain energy density function for transverse isotropy depending on stretch invariant  $J_4$  by neglecting  $J_5$  and  $J_6$ . Bischoff (Ref.[[J.E.Bischoff 2002](#)]) on the other side, formulated the orthotropic hyperelasticity of eight-chain model by principle stretches along the material axes. There are several other similar approaches in the literature. By admitting that, finite shear strains exist in biological tissue with arbitrary geometry and boundary conditions (including AC), their contribution into the strain energy density function should be involved either. Otherwise, one can speak about an incompleteness in between the given unit-cell morphology and strain energy density function formulation.

#### 4.2.4 Energy Split, Stress at Integration Point and Tangent Modulus

For the finite element or natural element implementation of remodeling and orthotropic hyperelasticity, the tangent modulus has to be evaluated. There are generally accepted procedures of iterative solution methods for finding tangent moduli (by Miehe Ref.[[C.Miehe 1996](#)] for instance). Here, it is preferred to calculate the tangent moduli analytically by following the current state formulation of Zienkiewicz (Ref.[[O.C.Zienkiewicz 2000b](#)]). The physically motivated split of strain energy density function into the bulk energy and chain energy parts is applied. For the chain energy, the strain energy density function defined in the previous section is used. Following the other researchers in the field, Menzel (Ref.[[A.Menzel 2004](#)]) for example, an additional term on the chain energy is defined, to prevent the shrinkage of the chains into the stable end-to-end length, which is being zero. This repulsive term is defined so that, the chain strain energy has stress-free reference configuration for a given Cauchy-Green deformation tensor.

$$\psi = \psi^{chain} (I_2, J_1, J_2, J_3, J_4, J_5, J_6) + \psi^{rep} + \psi^{bulk} \quad (4.22)$$

This formulation with the bulk strain energy density accounting for the surrounding compressible fluid in the biological tissue includes the complete set of integrity bases. This set includes 9 parameters defining the orthotropy, corresponding one Young's modulus and two Poisson's ratio in each direction in analogy with the linear elasticity. In nonlinear elasticity, the underlying physical interpretation of invariants is not so straightforward. Next, the chain and repulsive terms of second Piola-Kirchoff stresses and current state tangent moduli are shown. The energetically conjugate stress measure of Cauchy-Green deformation tensor is the symmetric Piola-Kirchoff stress tensor. The chain second Piola-Kirchoff stress tensor is evaluated by taking the derivative of energy function once. In tensor-index mixed notation;

$$S_{IJ}^{chain} = 2 \left( \frac{\partial \psi^{chain}}{\partial \mathbf{C}} \right)_{IJ} = 2 \frac{\partial \psi^{chain}}{|\mathbf{r}|} \left[ \frac{\partial |\mathbf{r}|}{\partial I_2} \left( \frac{\partial I_2}{\partial \mathbf{C}} \right)_{IJ} + \sum_{k=1}^6 \frac{\partial |\mathbf{r}|}{\partial J_k} \left( \frac{\partial J_k}{\partial \mathbf{C}} \right)_{IJ} \right] \quad (4.23)$$

In indicial-matrix-tensor mixed notation proposed by Zienkiewicz (Ref. [O.C.Zienkiewicz 2000b]);

$$\begin{aligned} S_{IJ}^{chain} = & 2 \left[ 2C_{ij} \frac{(\mathbf{G}_{11})_{IJ}}{tr(\mathbf{G}_{11})} \frac{(\mathbf{G}_{22})_{IJ}}{tr(\mathbf{G}_{22})} \frac{(\mathbf{G}_{33})_{IJ}}{tr(\mathbf{G}_{33})} \right] \\ & \cdot \left[ \frac{\partial \psi}{\partial |\mathbf{r}|} \frac{\partial |\mathbf{r}|}{\partial I_2} \quad \frac{\partial \psi}{\partial |\mathbf{r}|} \frac{\partial |\mathbf{r}|}{\partial J_1} \quad \frac{\partial \psi}{\partial |\mathbf{r}|} \frac{\partial |\mathbf{r}|}{\partial J_2} \quad \frac{\partial \psi}{\partial |\mathbf{r}|} \frac{\partial |\mathbf{r}|}{\partial J_3} \right]^T \\ & + 2 \left[ \frac{(\mathbf{G}_{11} \cdot \mathbf{C} + \mathbf{C} \cdot \mathbf{G}_{11})_{IJ}}{tr(\mathbf{G}_{11})} \quad \frac{(\mathbf{G}_{22} \cdot \mathbf{C} + \mathbf{C} \cdot \mathbf{G}_{22})_{IJ}}{tr(\mathbf{G}_{22})} \quad \frac{(\mathbf{G}_{33} \cdot \mathbf{C} + \mathbf{C} \cdot \mathbf{G}_{33})_{IJ}}{tr(\mathbf{G}_{33})} \right] \\ & \cdot \left[ \frac{\partial \psi}{\partial |\mathbf{r}|} \frac{\partial |\mathbf{r}|}{\partial J_4} \quad \frac{\partial \psi}{\partial |\mathbf{r}|} \frac{\partial |\mathbf{r}|}{\partial J_5} \quad \frac{\partial \psi}{\partial |\mathbf{r}|} \frac{\partial |\mathbf{r}|}{\partial J_6} \right]^T \end{aligned} \quad (4.24)$$

And the repulsive chain term of the second Piola-Kirchoff stress tensor is;

$$S_{IJ}^{rep} = - \frac{\partial \psi}{\partial |\mathbf{r}|} \Big|_{\mathbf{R}} \left[ \frac{(\mathbf{G}_{11})_{IJ}}{tr(\mathbf{G}_{11})J_1} \quad \frac{(\mathbf{G}_{22})_{IJ}}{tr(\mathbf{G}_{22})J_2} \quad \frac{(\mathbf{G}_{33})_{IJ}}{tr(\mathbf{G}_{33})J_3} \right] \cdot \left[ \frac{\partial |\mathbf{r}|}{\partial J_1} \Big|_{\mathbf{R}} \quad \frac{\partial |\mathbf{r}|}{\partial J_2} \Big|_{\mathbf{R}} \quad \frac{\partial |\mathbf{r}|}{\partial J_3} \Big|_{\mathbf{R}} \right]^T \quad (4.25)$$

The material tangent matrix term in reference coordinates is,

$$\begin{aligned} \mathbb{C}_{IJKL}^{chain} = & 4 \left[ 2C_{IJ} \frac{(\mathbf{G}_{11})_{IJ}}{tr(\mathbf{G}_{11})} \frac{(\mathbf{G}_{22})_{IJ}}{tr(\mathbf{G}_{22})} \frac{(\mathbf{G}_{33})_{IJ}}{tr(\mathbf{G}_{33})} \frac{(\mathbf{G}_{11} \cdot \mathbf{C} + \mathbf{C} \cdot \mathbf{G}_{11})_{IJ}}{tr(\mathbf{G}_{11})} \frac{(\mathbf{G}_{22} \cdot \mathbf{C} + \mathbf{C} \cdot \mathbf{G}_{22})_{IJ}}{tr(\mathbf{G}_{22})} \frac{(\mathbf{G}_{33} \cdot \mathbf{C} + \mathbf{C} \cdot \mathbf{G}_{33})_{IJ}}{tr(\mathbf{G}_{33})} \right] \cdot \\ & \mathbb{H} \cdot \\ & \left[ 2C_{KL} \frac{(\mathbf{G}_{11})_{KL}}{tr(\mathbf{G}_{11})} \frac{(\mathbf{G}_{22})_{KL}}{tr(\mathbf{G}_{22})} \frac{(\mathbf{G}_{33})_{KL}}{tr(\mathbf{G}_{33})} \frac{(\mathbf{G}_{11} \cdot \mathbf{C} + \mathbf{C} \cdot \mathbf{G}_{11})_{KL}}{tr(\mathbf{G}_{11})} \frac{(\mathbf{G}_{22} \cdot \mathbf{C} + \mathbf{C} \cdot \mathbf{G}_{22})_{KL}}{tr(\mathbf{G}_{22})} \frac{(\mathbf{G}_{33} \cdot \mathbf{C} + \mathbf{C} \cdot \mathbf{G}_{33})_{KL}}{tr(\mathbf{G}_{33})} \right]^T \\ & + 4 \left[ 2(\mathbf{I} \otimes \mathbf{I})_{IJKL} \quad 0 \quad 0 \quad 0 \quad \frac{[\mathbf{G}_{11} \otimes \mathbf{C} + \mathbf{C} \otimes \mathbf{G}_{11}]_{IJKL}}{tr(\mathbf{G}_{11})_{IJKL}} \quad \frac{[\mathbf{G}_{22} \otimes \mathbf{C} + \mathbf{C} \otimes \mathbf{G}_{22}]_{IJKL}}{tr(\mathbf{G}_{22})_{IJKL}} \quad \frac{[\mathbf{G}_{33} \otimes \mathbf{C} + \mathbf{C} \otimes \mathbf{G}_{33}]_{IJKL}}{tr(\mathbf{G}_{33})_{IJKL}} \right] \cdot \\ & \left[ \frac{\partial \psi}{\partial |\mathbf{r}|} \frac{\partial |\mathbf{r}|}{\partial I_2} \quad \frac{\partial \psi}{\partial |\mathbf{r}|} \frac{\partial |\mathbf{r}|}{\partial J_1} \quad \frac{\partial \psi}{\partial |\mathbf{r}|} \frac{\partial |\mathbf{r}|}{\partial J_2} \quad \frac{\partial \psi}{\partial |\mathbf{r}|} \frac{\partial |\mathbf{r}|}{\partial J_3} \quad \frac{\partial \psi}{\partial |\mathbf{r}|} \frac{\partial |\mathbf{r}|}{\partial J_4} \quad \frac{\partial \psi}{\partial |\mathbf{r}|} \frac{\partial |\mathbf{r}|}{\partial J_5} \quad \frac{\partial \psi}{\partial |\mathbf{r}|} \frac{\partial |\mathbf{r}|}{\partial J_6} \right]^T \end{aligned} \quad (4.26)$$

Where the dyadic products of the second order tensors and the Hessian matrices are defined as;

$$[\mathbf{A} \otimes \mathbf{B}]_{IJKL} = 0.5 ([\mathbf{A}]_{IK} [\mathbf{B}]_{JL} + [\mathbf{A}]_{IL} [\mathbf{B}]_{JK}) \quad (4.27a)$$

$$\mathbb{H}_{ij} = \frac{\partial}{\partial J_i} \left( \frac{\partial \psi}{\partial |\mathbf{r}|} \frac{\partial |\mathbf{r}|}{\partial J_i} \right) = \frac{\partial^2 \psi}{\partial |\mathbf{r}|^2} \frac{\partial |\mathbf{r}|}{\partial J_i} \frac{\partial |\mathbf{r}|}{\partial J_i} + \frac{\partial \psi}{\partial |\mathbf{r}|} \frac{\partial}{\partial J_i} \frac{\partial |\mathbf{r}|}{\partial J_i} \quad (4.27b)$$

The derivatives of the strain gradient energy of the worm-like chain given in equation (4.1) with respect to the deformed length is straightforward and is omitted in this stage. The repulsive tangent material tensor in reference coordinates is following the same procedure becomes,

$$\mathbb{C}_{IJKL}^{rep} = -4 \frac{\partial \psi}{\partial |\mathbf{r}|} \bigg|_{\mathbf{R}} \left[ -\frac{(\mathbf{G}_{11})_{IJ}(\mathbf{G}_{11})_{KL}}{(\text{tr}(\mathbf{G}_{11})J_1)^2} - \frac{(\mathbf{G}_{22})_{IJ}(\mathbf{G}_{22})_{KL}}{(\text{tr}(\mathbf{G}_{22})J_2)^2} - \frac{(\mathbf{G}_{33})_{IJ}(\mathbf{G}_{33})_{KL}}{(\text{tr}(\mathbf{G}_{33})J_3)^2} \right]. \quad (4.28)$$

$$\left[ \frac{\partial |\mathbf{r}|}{\partial J_1} \bigg|_{\mathbf{R}} \quad \frac{\partial |\mathbf{r}|}{\partial J_2} \bigg|_{\mathbf{R}} \quad \frac{\partial |\mathbf{r}|}{\partial J_3} \bigg|_{\mathbf{R}} \right]^T$$

As indicated in the formulations, some derivatives should be evaluated at the reference tip to tail length of the worm-like chains. For demonstration, two different examples with two different deformation gradient-histories are developed and plotted. Comparisons of the six independent entries of second Piola-Kirchoff stresses calculated with the first derivatives, with the ones calculated with the tangent maps are done. The first example is simple unconstrained tension test to one integration point, the second one is simple unconstrained shear test to one integration point. For each test, 50 time steps are applied, and the covariant material base vectors are chosen to be coincident with Cartesian bases and have equal size. The applied deformation gradients are given priorily. The same tests can be compared with publications of similar demonstrations; such as in Ref. [J.E. Bischoff 2002].

#### 4.2.5 Simple Tension and Shear on the Orthotropic 8-chain Model

After each other, two examples are presented here. The first one is a given deformation gradient of a pure stretch without potential mapping. Time time parameter of Figure 4.6 is chosen in a way that the maximum stretch of the unit-cell reaches around fifty percent.

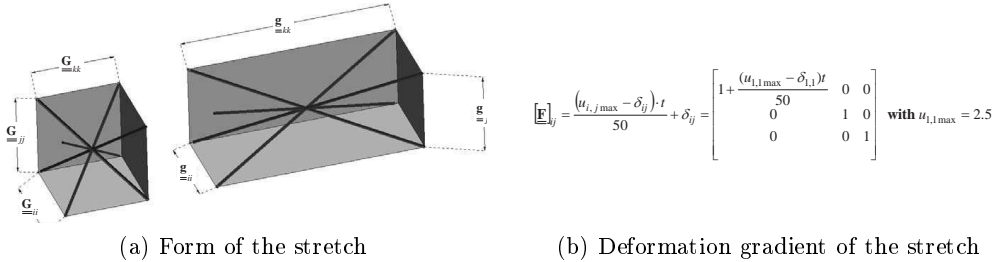


Figure 4.3: Form and the formula of the stretch on 8-chain model

As expected, for this type of first order kinematics, the shear stresses all vanish. In Figure 4.4 two of the three non-zero components of the stretch tensor are plotted against the stretch parameter. Those two are clearly equal to each other. Additionally, the correlation of the second Piola-Kirchoff tensor computation with the tangent moduli is verified to be correct. This had to be performed to show the reliability of the lengthy expressions presented in the previous section of Ch.[4.2.4].

The stress values along the loading direction can be seen in Figure 4.5. The exponential

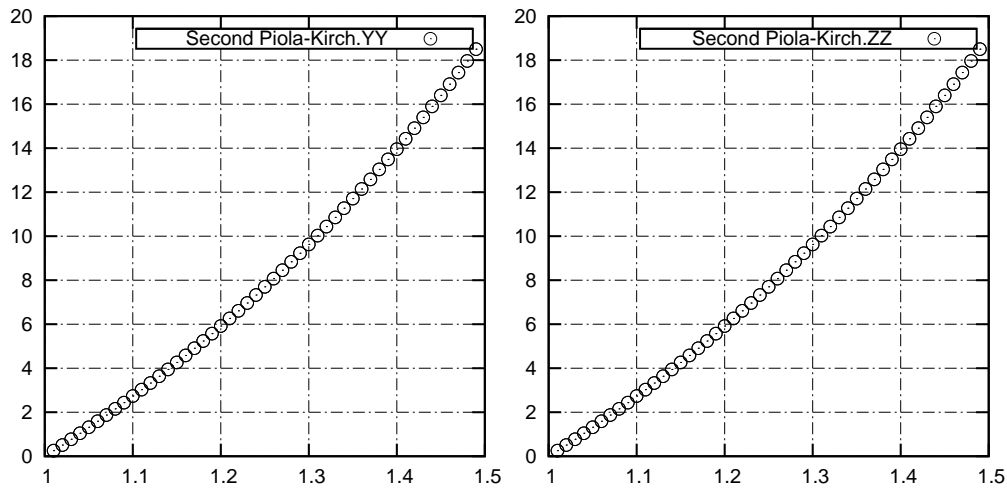
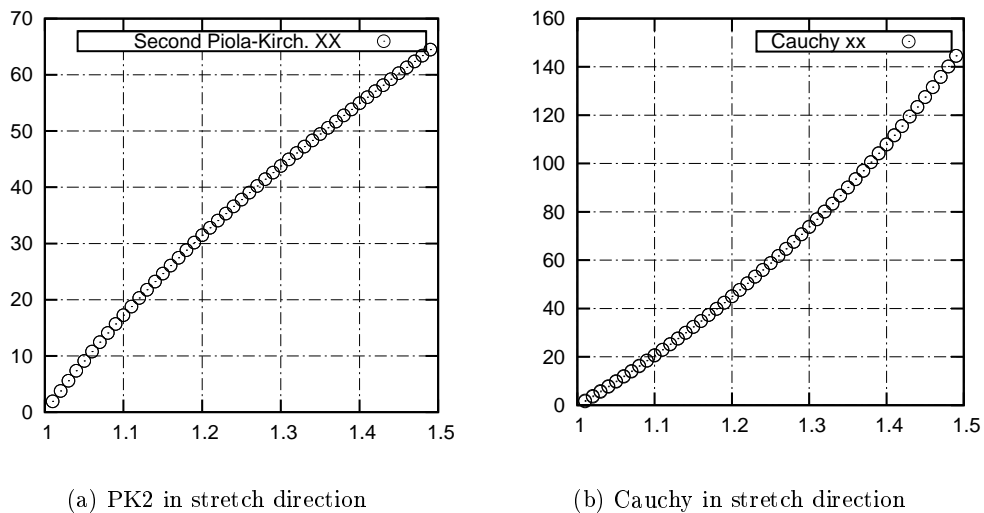


Figure 4.4: Second Piola Kirchoff Stress tensor components

behavior of the true stress component can be observed to be ascending with the stretch value.



(a) PK2 in stretch direction

(b) Cauchy in stretch direction

Figure 4.5: Comparison of second Piola Kirchoff and Cauchy stress component in stretch direction

This is expected either, since the surface with the normal of direction of stretch is getting significantly smaller. On the other side, the other normal stresses are observed to be staying with the same order of quantity, since those surfaces undergo area-preserving type of deformation. After being convinced about the consistency of the formulation based on the stretch type of deformation, the pure-shear type of deformation can be investigated as well.

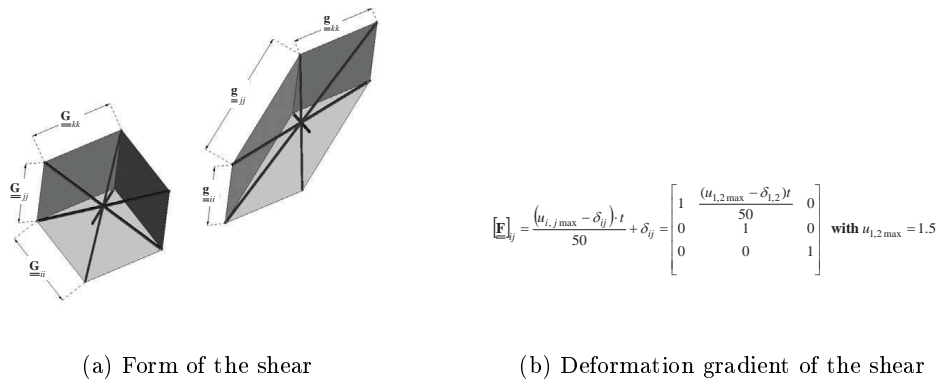


Figure 4.6: Form and the formula of the shear on 8-chain model

The given deformation gradient and the mapping on the eight chain model is given in Figure 4.6. All three normal stress values are expected to be quantitatively finite.

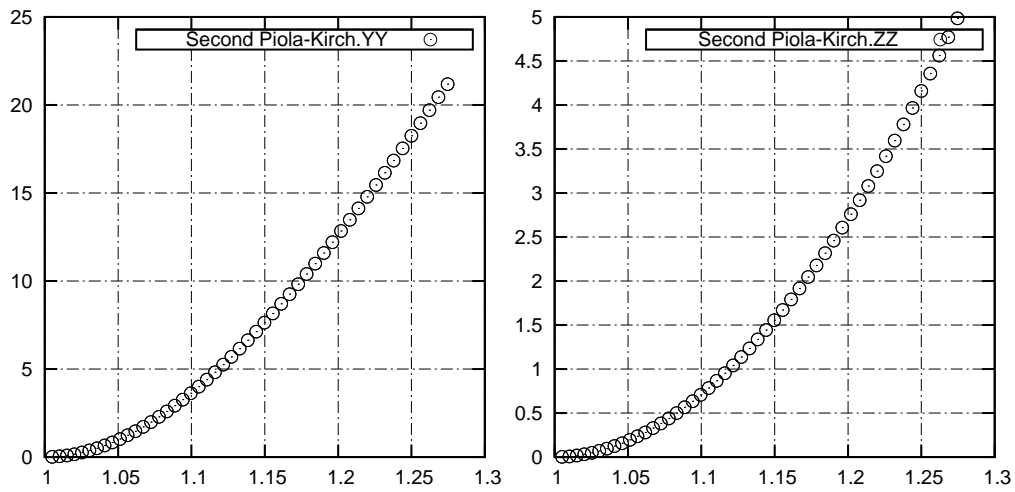


Figure 4.7: Second Piola Kirchoff Stress tensor components

As predicted, one normal component is equal to another one, and the third one is significantly smaller than the other two, as can be seen in Figure 4.7. The largest component on the other side, is noticed to be the single shear component, again as expected, the other two shear components are the only non-zero values for the example of pure-shear.

After showing the reliability and completeness of the proposed material model, one can give a look to the main topic of the chapter, namely the reorientation with strain and strain gradient effects. For the case of reorientation with strain effects, the aforementioned orthotropic material model is used.

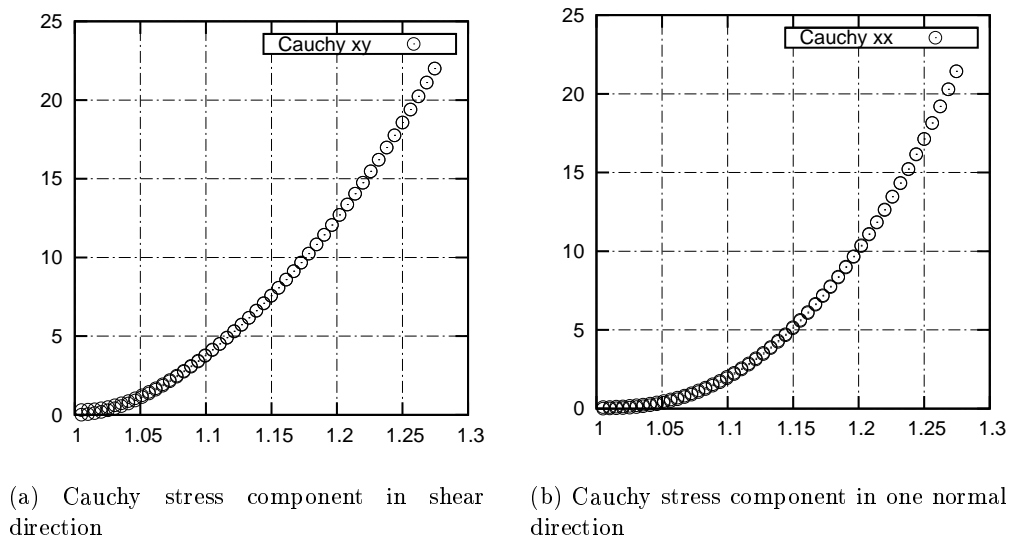


Figure 4.8: Comparison of second Piola Kirchoff and Cauchy stress component in stretch direction

## 4.3 Material Point Reorientation

### 4.3.1 Strain based Reorientation

A fiber reorientation scheme can be defined as the evolution of reference configuration (Ref.[K.Garikipati 2005]). This successive updating procedure suggests pre-rotations and translations on the material point. Therefore, the multiplicative split of the deformation gradient into the rotation and elastic part is applicable. In this work, the rotation tensor in *Figure 4.9* is introduced as an internal variable as investigated in other works, for instance in Ref.[Himpel 2007]. Similarly, it is preferred to modify previous configuration in the quasi-static iterative procedure gradually. Even though the given kinematics is of type first order, it is still valid and can be applied to gradient reorientation.

The steering causality of remodeling is certainly not a trivial question with a simple answer. Some works suggest strain driven reorientation<sup>7</sup> whereas some prefer stress driven<sup>8</sup> one. There is certainly a difference, since the strain and stress tensors for anisotropic media is arbitrarily non-coaxial. However, the strain driven reorientation is certainly motivated with the stationary strain energy criteria, for mathematical proof, please refer to the *Appendix-D*.

This proof is fully motivated by the works of Norris (Ref.[Norris 2005]) and Vianello (Ref.[Vianello 1996a]), who have proved that for anisotropic linear materials the optimal orientation of the material is achieved if stress and corresponding strain measures are parallel with the coaxial. This coaxiality requirement is only fulfilled if the material axes are parallel with the eigenvectors of strains. Again Vianello had showed in two separate works ( Ref.[Vianello 1995] ,

<sup>7</sup>strain driven works: Ref.[K.Garikipati 2005] , Ref.[A.Menzel 2004] , Ref.[E.Kuhl 2008] , Ref.[W.Wilson 2006] , Ref.[A.Menzel 2006]

<sup>8</sup>stress driven works: Ref.[I.Hariton 2007] , Ref.[N.J.Driessen 2003] , Ref.[Hariton 2007]

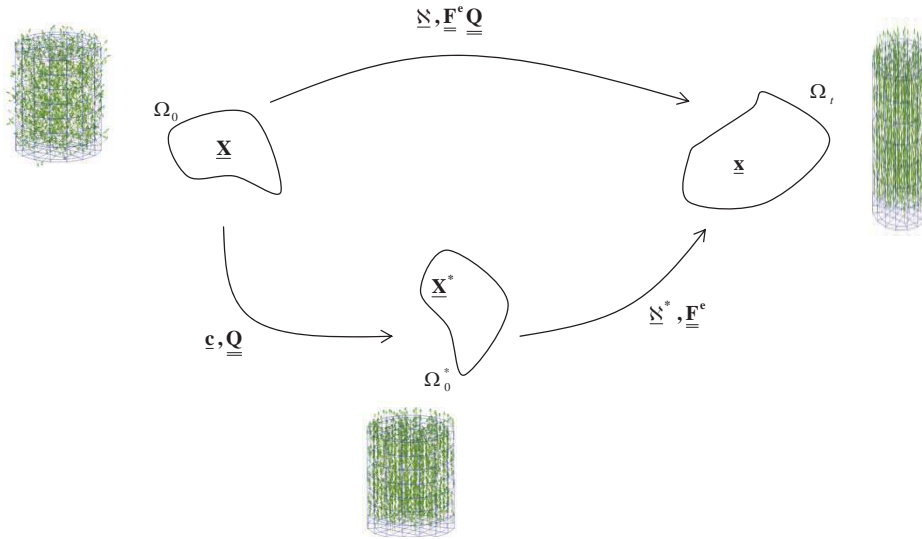


Figure 4.9: Kinematics of updating the reference configuration with rotation tensor

Ref.[Vianello 1996b]) that the same argument holds also for the finite elasticity. The procedure in appendix section uses the same line of action which were previously proposed, but applies another terminology, which fits better to the form of this treatise.

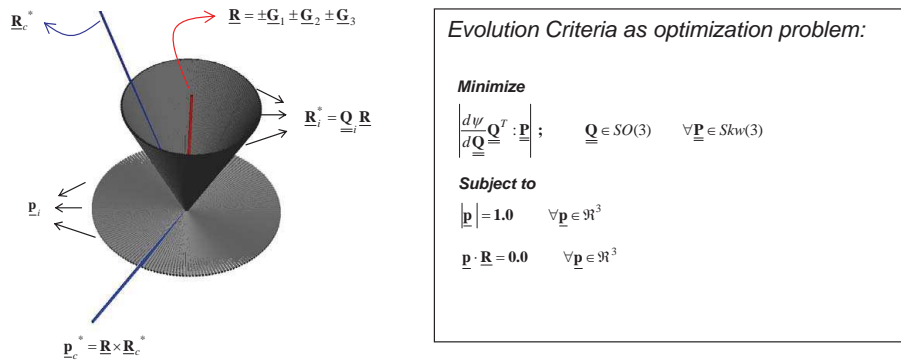


Figure 4.10: The definition of the evolution as an optimization set problem

The given Figure 4.10 describes the evolution criteria in terms of an optimization problem set, and gives a set-up for the numerical validation. The left illustration of Figure 4.10 includes two sets of vectors, as the first one being the vector set of all possible target reference configurations  $R_c^t$ . The first set is separated from the initial fiber direction  $R$  with an angle of  $\beta$ , and thus forms a conical shape. The second set is determined according to the reference fiber direction and the set of target fiber direction. Consequently, the second set defines the set of rotation axis.

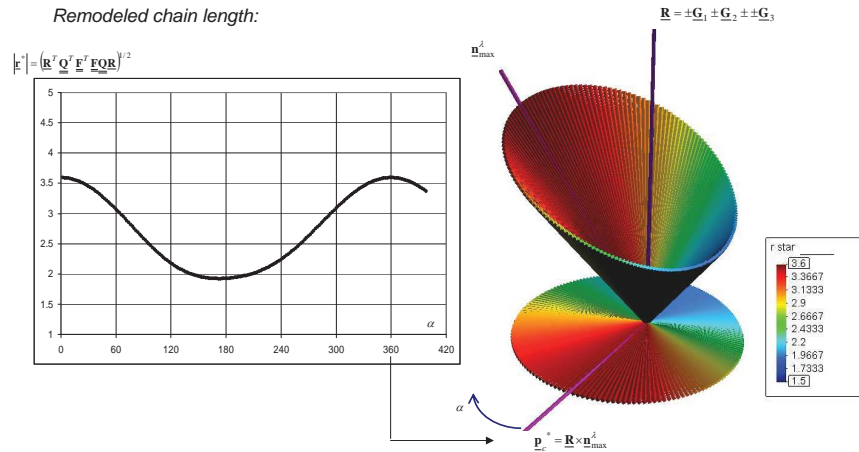


Figure 4.11: Numerical verification of maximizing the stretch in one step

As can be seen from the *Figure 4.11*, by selecting the successive location of target in terms of the eigenvector of Cauchy-Green strain tensor with the maximum positive eigenvalue, one receives the maximum stretch at the location.

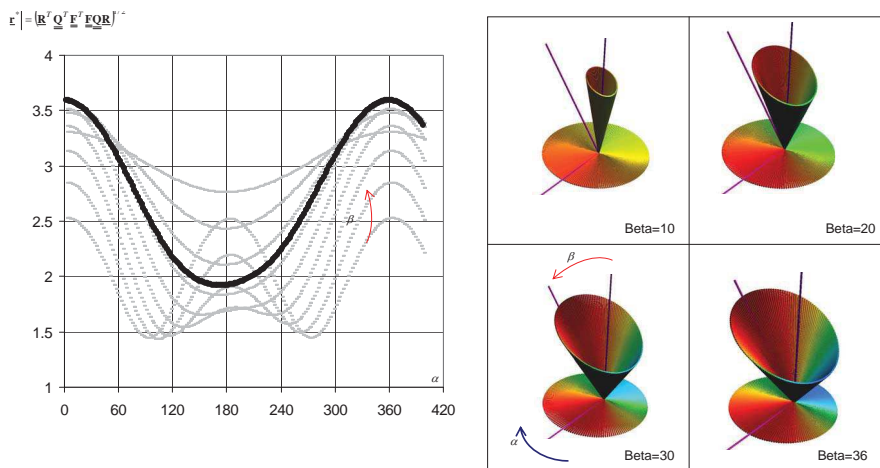


Figure 4.12: Numerical verification of maximizing the stretch stepwise

As stated, the situation is numerically shown to be holding for a one-step, sudden adaptation, namely closing the angle ' $\beta$ ' all of a sudden. Additional remark to that can be made accordingly, by admitting that the number of critical locations is not necessarily unique, as can be seen from this single example. Comments around this observation will be made in the next sections. In *Figure 4.12*, it is clear that the stepwise approaching to the target is also well established and preserves the maximum stretch and thus maximum strain energy criteria. However, for some lower angle of rotations of ' $\beta$ ', another stable energy location for ' $\alpha$ ' can be preferably selected by the actor of adaptivity.

Further comments on this subject can be done by stating the coaxiality requirement as the



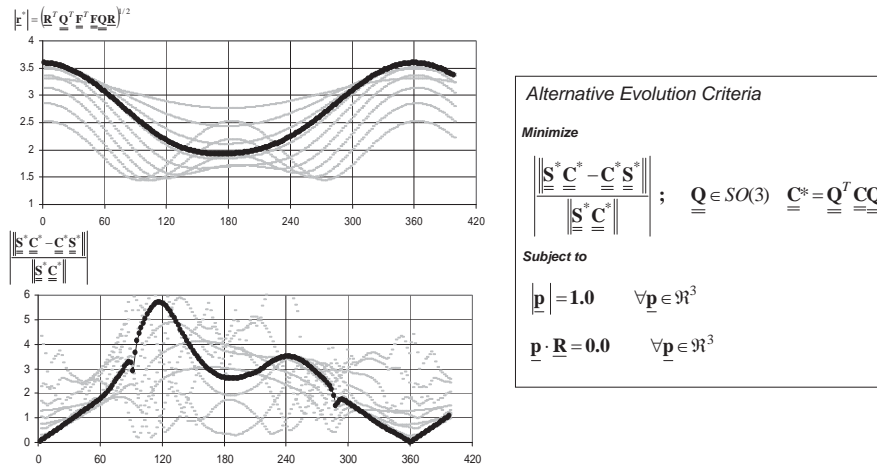


Figure 4.13: Comparison of stretch maximizing and coaxiality optimization manifolds

optimization manifest, as done in *Figure 4.13*. As can be seen from the diagrams on the left, at the maximum location the coaxiality requirement is comprehensively fulfilled, however, for the alternative local maximum of stretch at the half angle of rotation of ' $\alpha = 0.5\pi$ ' for the initial attempts of reorientation (for small  $\beta$ ) the same conclusion can not be done. Even though the coaxiality function is not as smooth as the fourth invariant<sup>9</sup>, it is still a better candidate for searching the optimum reference fiber directions. One drawback is, as one can observe from the *Figure 4.13*, the fact that the coaxiality has a local minimum value for the minimum locations of the strain energy function, for instance the location of  $\alpha = 0.5\pi$ . If one has the intent of using numerical optimization algorithms for solving the problem in hand, should consider this phenomenon. This point will not be visited again, since the treatise preferably follows in fact the semi-analytical methods, thus searching the perfect location for a given manifest.

To compare the strain driven reorientation with the strain gradient driven one, a more realistic example is taken as basis, namely an abstract cross-section, which represents articular cartilage. The geometry is generated by hand-free methods, mainly by mimicking the scanning electron microscopy pictures of cartilage cross sections. This gives one also the opportunity of comparing the reorientation results with the reality.

Some specifications of the model should be cleared here as well. The model is simply based on three rows of 8-noded hexahedral elements. The geometry is fixed only from the bottom, the nodal consistent force step is applied until reaching a certain level of deformation. There is no contact algorithm applied, as done previously in the chapter of mixed field theory (Ch.[1]). As can be seen from the *Figure 4.15*, the recently presented eight-chain model is used for the simulations.

<sup>9</sup>according to the given numerical examples

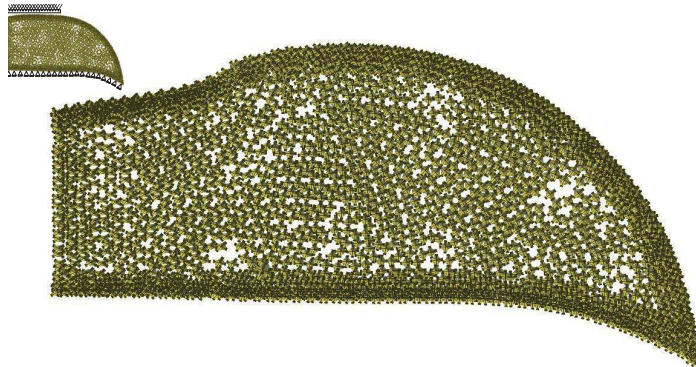


Figure 4.14: Pressing the Cartilage-alike profile with uniform force

The self-consistency and correctness of the results are interpreted based on the coaxiality requirement, as obvious from the previous comments done in this section. As one can see, the stress, strain and the fictitious target spaces all overlap with each other. However, turning back to the consistency of the results with comparison of reality, one can obviously see that the expectation in some regions are not satisfying. The superficial zone is consistent with the reality, consist of fibers along the surface, In the depth zone rather perpendicular fibers are anticipated being consistent with experimental observations.

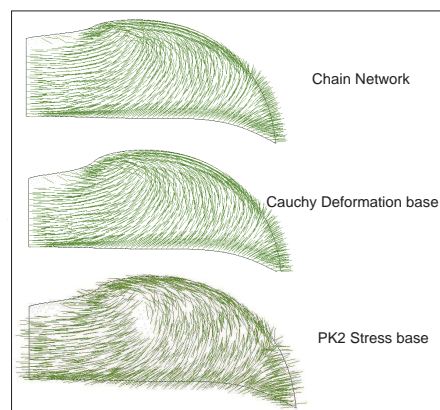


Figure 4.15: The coaxiality requirement

However, the mid and depth zones in the middle region are anticipated to be perpendicular to the surface, where the opposite is observed here.

Furthermore, the side-facets of the system are not constrained at all, therefore the problem is in 3D scale in fact a plane stress problem, rather than plane strain. This scenario would represent rather a quasi-static type of vertical loading. On the other side, an impact type of loading would most probably cause the fluid constituent smear away from the solid abruptly, and thus increase the effect of locality. Such a case, is according to the opinion of the writer of the treatise is rather a case for plane strain. The focus in this case is for normal loading conditions, thus plane strain.

Hereby, the strain gradient reorientation suggestions will be presented next. A finalizing conclusion will be done in the next chapters.

### 4.3.2 Curvature Reorientation

Claiming that any proposed energy function is an increasing function of hyperstrains is not necessarily true. The strain gradient effects can be acting along the stretch, and thus may have a cumulative effect. However, a simple assumption of presupposing that the curvature effects are proportional with hyperstrains, can facilitate a use of simple energy function for definition and usage of semi-analytical methods similar to strain-driven reorientation.

$$\psi^\kappa \simeq \exp\left(\hat{M}^{\natural\otimes 2} : \mathbb{K} : \hat{M}^{\natural\otimes 2}\right) \quad (4.29)$$

Where the fourth order Cauchy-Green correspondence of Hypergradient is defined as,

$$\mathbb{K} = \mathbf{G}^{\cdot l} \cdot \mathbf{G} \quad K_{ijkl} = G_{nij}G_{nkl} \quad (4.30)$$

According to the Schwarz integrability condition, the hypergradient tensor possess one-plane symmetry. As a result of this, the Cauchy-Green Hypergradient has major and minor symmetry properties. The fourth order contraction stays under the following actions invariant<sup>10</sup> ;

$$M_i M_j K_{ijkl} M_k M_l = M_i M_j K_{jikl} M_k M_l = M_i M_j K_{ijkl} M_l M_k = M_i M_j K_{klij} M_k M_l \quad (4.31)$$

The first two equalities indicate minor symmetries, where the last one represents major symmetry. To move on, a so called *scatter* transformation is defined, which transforms the fourth order tensors with major and minor symmetries by reducing the order of the tensor and increasing the dimension of the vector space with no loss of information.

$$\mathbb{K}^{3^4} \in \mathbb{R}^{3 \times 3 \times 3 \times 3} \xrightarrow{\text{Scatter}} \mathbb{K}^{9^2} \in \mathbb{R}^{9 \times 9} \quad (4.32)$$

Because of the major symmetry, the transformed form of  $\mathbb{K}$  is symmetric in tensor order directions. The eigen-decomposition of the transformed form generates therefore 9 linearly independent eigenvectors.

$$\mathbb{K}^{9^2} = \sum_i^9 \lambda_i^K \left( \mathbf{N}_i^{9^1} \otimes \mathbf{N}_i^{9^1} \right) \quad (4.33)$$

Referring to the comments done about the coaxiality and stable energy configurations, the eigenvector with the maximum corresponding eigenvalue can be *gathered* into a lower order vector space dimension with higher tensor order. Again this transformation does not cause any information loss.

$$\mathbf{N}_{max}^{9^1} \in \mathbb{R}^9 \xrightarrow{\text{Gather}} \mathbf{N}_{max}^{3^2} \in \mathbb{R}^{3 \times 3} \quad (4.34)$$

The Gathered matrix of eigenvector of scattered Cauchy-Green strain tensor can be further decomposed into linearly independent eigenvectors.

$$\mathbf{N}_{max}^{3^2} = \sum_i^3 \lambda_i^N \left( \mathbf{n}_i^{3^1} \otimes \mathbf{n}_i^{3^1} \right) \quad (4.35)$$

---

<sup>10</sup>The invariancy is not trivial to prove, to be consistent with the previous definitions of the strain energy density functions, the term is accepted to be valid

The Scattered matrix can be in fact further reduced into  $\mathbb{K}^{6^2} \in \mathbb{R}^{6 \times 6}$  by imposing the minor symmetries. By doing so, it becomes evident that the eigenvectors of nonzero eigenvalues  $N_i^{91}$  are linearly independent. The eigenvector of the eigenvalue with the maximum absolute value is chosen to be the reorientation target. It is straightforward to build a spin-free incremental orthonormal tensor for the evolution towards to the desired direction. In opposite to the usual (strain driven-only) reorientation manifolds, where only the eigenvectors with positive eigenvalues are considered, in this case the one with the absolutely largest eigenvalue is taken to be the ideal orientation of that instant.

To prove the validity of the proposed semi-analytical analogy, the following strain-gradient contribution is tested;

$$\begin{aligned} \mathbf{G} &= \mathbf{G}_x \otimes \mathbf{G}_y \otimes \mathbf{G}_z \\ &= \begin{pmatrix} 1.3 & 0.2 & -2.8 \\ 0.2 & 0.9 & -2.1 \\ -2.8 & -2.1 & 1.3 \end{pmatrix} \otimes \begin{pmatrix} 0.2 & 1 & 1.8 \\ 1 & 0.6 & 2.7 \\ 1.8 & 2.7 & -2.1 \end{pmatrix} \otimes \begin{pmatrix} -1.6 & -2.4 & -0.5 \\ -2.4 & 0.9 & -1.45 \\ -0.5 & -1.45 & 2.3 \end{pmatrix} \quad (4.36) \end{aligned}$$

For the construction of this hyperstrain tensor, no special investigation is performed concerning the potential of the tensor. There is neither a mapping or deformation gradient, thus there is no warranty of any property of the potential is provided. But, the minor symmetry is preserved. In order to show that the verification done above is not a coincidence,

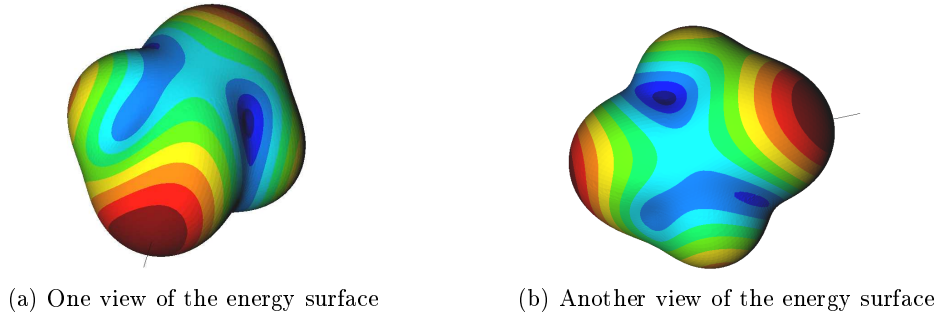


Figure 4.16: Maximizing of equation (4.29) under the action of hypergradient of equation (4.36). The maximum location is found correctly and marked with a line.

more examples are presented in *figures 4.16 and 4.17*. The given reorientation postulate based on a simple material invariant, namely the curvature correspondent of the fourth invariant of first order kinematics anisotropy, is well established and verified with numerical examples. In order to investigate the complete effect of bending/stretch relationships, one additional reorientation manifest will be introduced next.

### 4.3.3 Reorientation based on the EB Material Model

Since the previous reorientation manifest is accepted to be a practical alternative, and enables one to allow semi-analytical type of solution methods, a more realistic approach will be introduced here. The difference is mainly based on the used energy function. Namely, the

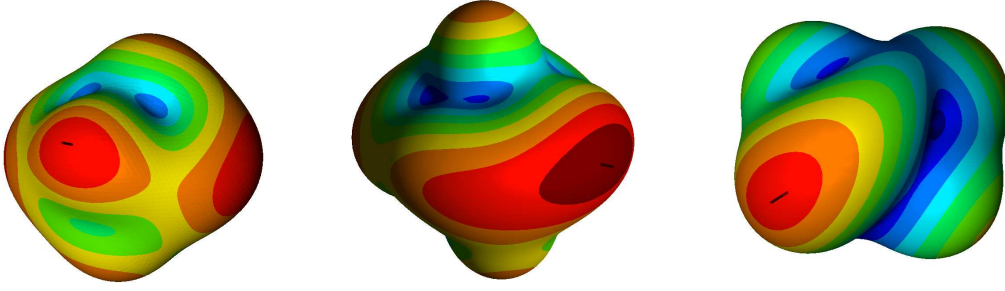


Figure 4.17: Arbitrary surfaces of  $(\hat{\mathcal{M}}^{\mathfrak{h}\otimes 2} : \mathbb{K} : \hat{\mathcal{M}}^{\mathfrak{h}\otimes 2})$  and the location of reorientation target. The maximum overlaps with scattered-gathered eigenvector result.

Euler-Bernoulli type of material model, introduced in the chapter of Hyperbalance (Ch.[3]).

$$\psi = \frac{EA}{4} (|\mathbf{m}|^2 - 1)^2 + E I c^2 \quad (4.37)$$

Any split which divides the terms driven only by strain and only by strain-gradient effects is not trivial to apply here. This is a consequence of additive nature of the strain-gradient truncation of the spatial/reference mapping of the second order continuum locations. Accordingly, this makes it cumbersome to find basic invariants to apply eigenvalue decomposition methods, prove the stability of the energy function around those directions and implement numerics for it.

It had been mentioned in the previous sections that the strain energy function and the reorientation manifests have non-convex nature. By considering that any search candidate  $\mathbf{R}^*$  in the reference configuration should preserve unit vector property, the problem can not be considered as a case of unconstrained optimization. Therefore, any solution of non-convex constrained optimization problem had been considered (relatively) to be not only non-trivial and also quite excessive for the main intent of this treatise. As a result of this argumentation, for finding critical locations of the energy function of equation (4.37), direct numerical methods are applied.

The following mapping, deformation gradient and hyperdeformation gradient components are used for demonstration;

$$y = 0.5tX^2 \quad FyX = tX \quad GyXX = t \quad (4.38)$$

For this example, the values (ratios) for the area and second moment of inertia are taken from the example of fractional profiles introduced in the previous chapter of Hyperbalance equations. The ratio is  $l/A$  is accordingly taken to be 12. In equation (4.38), only the non-zero terms are given.

In the right picture of *Figure 4.18* the undefined bending/stretch energy ratio is simply marked by zero. On the left picture it is quite evident that the trivial direct numeric search is working well around the given discrete set of rays generated by spherical coordinates. In the right picture it is quite evident that there is another stable region, where the bending

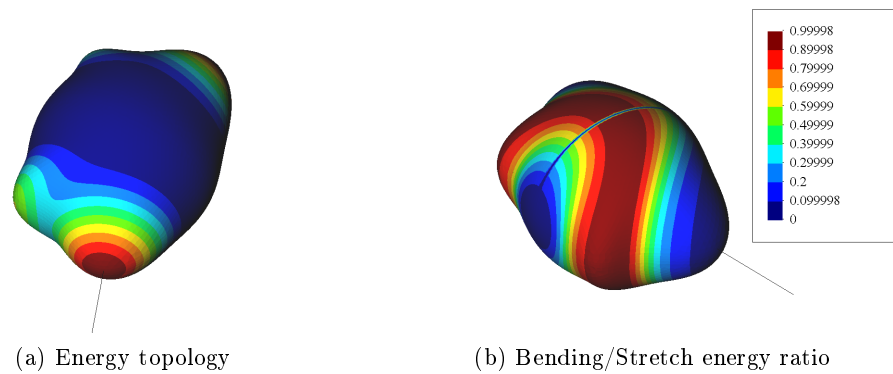


Figure 4.18: Maximizing of equation (4.37) under the action of hypergradient of equation (4.38). The maximum location is found correctly and marked with a line.

energy dominates the total energy. As a regard of that, for the fiber network it is logical to consider other benefits, such as permeability and wear resistance, then trying to reach the ultimate maximum. This is of course only a comment, not an absolute conclusive statement of this study.

The comparison on a specific model of articular cartilage is let to be a topic of the following sections, and omitted here.



# Natural Element Method

---

## Contents

---

<b>5.1</b>	<b>Introduction</b>	<b>123</b>
<b>5.2</b>	<b>Clustered and Constrained Delaunay-Voronoi Dual</b>	<b>125</b>
5.2.1	Clustering the Delaunay Triangulation	125
5.2.2	Constrained Voronoi Tessellation	129
<b>5.3</b>	<b>Non-sequential Nodal Integration</b>	<b>135</b>
5.3.1	Evaluation of Shape Value Matrix	138
5.3.2	Nature of Shape Value Matrix	143
<b>5.4</b>	<b>Implementation and Examples</b>	<b>146</b>
<b>5.5</b>	<b>Comparison of Different Reorientation Manifests</b>	<b>150</b>

---

## 5.1 Introduction

Natural element method falls into the category of particle-based methods for solving PDE's. Particle based methods are diversified in many significant topics, including discretization, interpolation, problem type, and solution method. Among many different examples, meshless finite element method Ref.[[S.R.Idelsohn 2002](#)] (MFEM), particle finite element method Ref.[[E.Onate 2004](#)] (PFEM), discrete element method Ref.[[N.Bicanic 2004](#)] (DEM), smoothed particle hydrodynamics Ref.[[Monaghan 1992](#)] (SPH) and natural element method Ref.[[N.Sukumar 1998](#)] (NEM) are widely revisited genuine examples of particle based methods.<sup>1</sup>

NEM, as the method under consideration, requires a dual mesh similar to MFEM and PFEM. These methods are certainly not free of mesh, but free of any other mesh dependent definitions, i.e. local coordinates, jacobians or conservative element connectivities. Through NEM, the continuum neighborhood of a infinite point and the integration of the differentials are naturally-i.e.geometrically approximated.

As indicated presently, the method includes *meshes*, which needs to be clarified from the point of view of the writer of this treatise. In fact, many researchers noticed this, and introduced deviations from the list of above, namely "*truly meshless methods*" (Ref.[[M.DufLOT 2002](#)]), intending to put the emphasis on the occurrence or absence of a *mesh*.

---

<sup>1</sup>the citations do not necessarily indicate the first founders of the individual methods, but widely accepted writers of the topics of interest



However, the primary difference outlined by means of many meshless methods is sometimes the line of action through the mesh, especially, in between classical finite element method and the postulated one. The best practice of the meshless methods focus not only to the geometry, but also to the action. Meshless methods often used to simulate crack openings and propagations (Ref.[Y.Chen 2006]), without requiring a re-meshing procedure. Or, it was used in quite early times, to simulate Eulerian motion on Lagrangian mesh (Ref.[J.Braun 2006]), where the main advantage is stressed to be; "*highly irregular evolving grids*". Applications in statistical physics, for instance to define fluid motion using Voronoi cells (Ref.[M.Serrano 2005]), or to quantify entropic elasticity of worm-like chains using molecular dynamics based particle simulations (Ref.[M.J.Buehler 2006]), are strengthening the idea, that the motivation of meshless methods are rather to simulate complicated *actions*, then represent a geometry. Further readings such as Ref.[S.R.Idelshon 2006] and more examples on the notion of *meshless*, can be too excessive for this treatise.

The focus of *action* as a motivation of using NEM for the thesis is however none of the layouts pointed<sup>2</sup> above. The main attempt was to generate a procedure to realize networks which can be extracted from clinical data (usually a point cloud), and to be able to consider the strain-gradient effects in three dimensions in an efficient way.

The content of this chapter has three main divisions. The first one (Ch.[5.2]) covers constraining the Delaunay-Voronoi dual of arbitrary geometries. The constrain is driven by frequency sampling of alpha-shapes (Ref.[Edelsbrunner 1983]), and eliminating unfeasible Delaunay volumes. In the first section, a method for enforcing the Voronoi region to overlap with the integration domain is presented. This method bases on boundary detection and *sharp featuring* of the point cloud. The constrained Delaunay triangulation and sharp featuring algorithms are going to be shown to accomplish robust results for densely packed, or homogeneously distributed point clouds.

In the second section (Ch.[5.3]), a novel extension to stabilized conforming nodal integration will be presented. In opposite to the earlier interpolation schemata, which suggest local-  $2^{nd}$  order Voronoi regions around gauss points, the defined method detects the nodal-quadrature interpolaters non-sequentially. The *non-sequential interpolation* schema does not only improves the speed, but also produces denser, and thus smoother interpolating matrices.

In the third part (Ch.[5.4]), numerical academic tests will be presented. Convergence of the method by seeking for the fundamental solution of the Laplace's equation are shown in this chapter. In adjacent to that, examples of finite deformation and fiber reorientation are covered too. Especially the last, is considered by the writer of the document an application of biomechanics. In order to preserve the main objective of the work, relevant examples are chosen and presented.

---

<sup>2</sup>neither cracks and molecular dynamics, nor Eulerian motions

## 5.2 Clustered and Constrained Delaunay-Voronoi Dual

Delaunay triangulation and Voronoi tessellation are in general usage of many weakly related fields, such as image processing, computational geometry, terrain modeling and computational mechanics. Depending on the application and corresponding distinctive geometry in hand, constrained triangulation or tessellation may differ<sup>3</sup> in meaning. The constrained meshing is defined here as "*the post-elimination of unfeasible discrete domains from the raw outcome*". By this definition of mesh constraining, betterment of the bad-conditioned mesh sub-domains is not esteemed to be notable. The quality of mesh, concerning the convergence characteristics, is left to be an issue of formulation and solution. The main intent is to uncover non-convex properties of the shapes with domain discretization and *post-clustering*.

### 5.2.1 Clustering the Delaunay Triangulation

It is possible to eliminate undesired triangles or tetrahedrons or disregard from the integration domain by defining threshold values or feasibility intervals for Delaunay primitives (alpha-shape method in Ref.[Edelsbrunner 1983]). However, a Delaunay triangle or tetrahedron owns several size and shape dependent properties, which are adherent on geometry and number of sites representing this geometry. Thus, alpha-shape thresholds would be as arbitrary as geometrical variations. Besides, in case an intermediate meshing is necessary (PFEM-Laplace mesh fluid dynamics), one has to consider that the threshold canon may alter during the runtime drastically. The iffy selection of proper parameters, as well as their uncertain intervals (even the parameters are normalized), are according to the writer valid excuses to seek systematic and pragmatic post-filtering methods.

#### 5.2.1.1 Definition of Clustered Delaunay Triangulation, CDT

Let 'P' be a finite point set with cardinality 'm' in 'n' dimensions.

$$\bar{\mathbb{P}} = \{p_1, p_2, p_3, \dots, p_m : \forall p_i \in \mathbb{R}^n\} \quad (5.1)$$

In 3d, the collection of 4 apart members of P is the union of 4-combinations of tetrahedrons in P with cardinality of;

$$c = \binom{n}{k} \quad (5.2a)$$

$$\mathbb{C}_i = \{p_{i1}, p_{i2}, p_{i3}, p_{i4} : (\forall p_{ij} \in \mathbb{P}) \wedge (p_{ij} = p_{ik} \iff j = k)\} \quad (5.2b)$$

$$\bigcup_{i=1}^c \mathbb{C}_i = \{\{p_{11}, p_{12}, p_{13}, p_{14}\}, \{p_{21}, p_{22}, p_{23}, p_{24}\}, \dots : \forall p_{ij} \in \mathbb{P}\} \quad (5.2c)$$

A primitive 'C' in the union(5.2b) is say, *Delaunay feasible* and thus a *Delaunay simplex*, if there is an equidistant point 'o' to the vertices of the primitive (5.2c), if no points in

---

<sup>3</sup>therefore, any citation of the initial statement is purposely avoided, not to cause any confusion of the definitions. Here, the application is obviously continuum mechanics.

the relative complement set of 'C' in ' $\bar{\mathbb{P}}$ ' occur in the hemisphere around 'o' (5.3d), and if the point set of the primitive combination is not coplanar (5.3d). The union of simplices following these clauses is called here the Delaunay triangulation ' $\mathbb{DT}$ ' (5.3a).

$$\mathbb{DT} = \bigcup_{\substack{i_{df} < c \\ i_{df} \geq 1}} C_i \quad (5.3a)$$

$$C_i = \mathbb{DT}_i \iff \exists ! o \in \mathbb{R}^3 : \quad (5.3b)$$

$$\left( r = d(o, p_{i1}) = d(o, p_{i2}) = d(o, p_{i3}) = d(o, p_{i4}) \right) \wedge \quad (5.3c)$$

$$\forall p_* \in (\mathbb{P} \setminus C_i) \quad r < d(o, p_*) \quad \wedge \quad (5.3d)$$

$$\left( (p_{i1} - p_{i2}) \times (p_{i1} - p_{i3}) \right) \cdot (p_{i1} - p_{i4}) \neq 0 \quad (5.3e)$$

A simplex might be Delaunay, but any other point in that simplex may not be desired in the domain representation. Increasing the number of points for the domain representation does not assist in to lay off simplices, which are filling semi or exact exclusions.

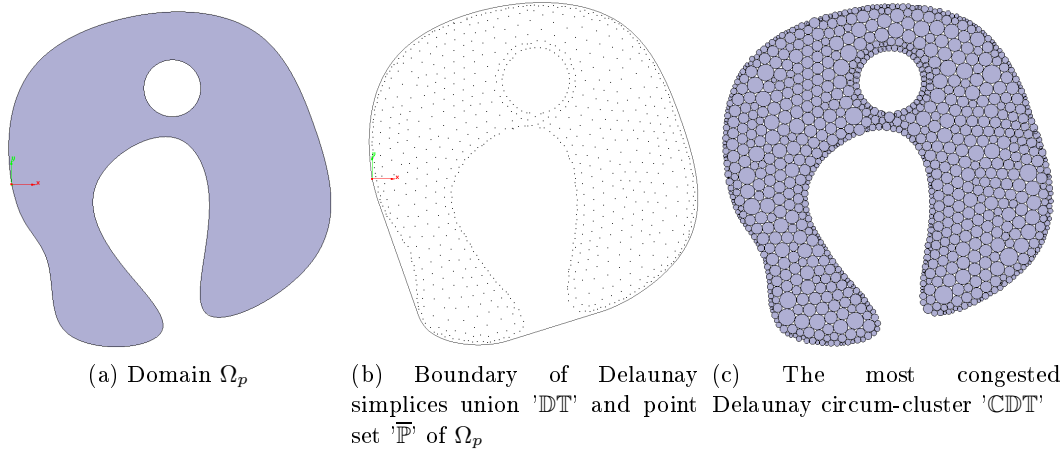


Figure 5.1: An example where ' $\mathbb{DT}$ ' condition set does not represent challenging geometries

Therefore, a further partitioning term through k-means clustering is suggested. The final reduced form of the Delaunay triangulation through clustering is designated as *Clustered Delaunay Triangulation* ' $\mathbb{CDT}$ '. For initiation, a property representation for each ' $\mathbb{DT}_i$ ' is founded. Any common property of the primitives which can lead a certain discrepancy between desired cluster and undesired cluster(s) should enter this list. In brief, volume, smallest face angle, distance between Delaunay hemisphere center and Delaunay geometric-center, summation of longest two edges, can be candidates for the attribute list. The attribute list parametric representation is not a unique representation of the primitive itself. With respect to the attribute coordinates, two or more primitives might appear to be same.

$$\mathbb{DT}_i = \{att_{i1}, att_{i2}, att_{i3}, \dots, att_{ik} : (\forall att_{ij} \in \mathbb{R})\} \quad (5.4)$$

It is assumed that the set of Delaunay simplices of a non-convex geometry can be clustered into finite number of 'K' disjoint subsets-(5.5a).

$$\mathbb{DT} = \bigcup_{C=0}^K \mathbb{DT}^{Cl_C} = \bigcup_{C=0}^K \bigcup_{i=0}^{\#Cl_C} \mathbb{DT}_i^{Cl_C} \quad (5.5a)$$

$$\mathbb{DT}^{Cl_M} \cap \mathbb{DT}^{Cl_N} = \emptyset \quad \iff M \neq N \quad (5.5b)$$

A *Cluster* union is defined as the collection of Delaunay primitives with a mean attribute value-(5.6a), where the *distance* of the each member attributes to the mean attribute is smaller then to any other cluster mean attribute (5.6b).

$$\overline{\mathbb{DT}}^{Cl_M} = \frac{\sum_{i=0}^{\#Cl_M} \mathbb{DT}_i}{\#Cl_M} \quad (5.6a)$$

$$\mathbb{DT}^{Cl_M} = \{\mathbb{DT}_i : \|\mathbb{DT}_i - \overline{\mathbb{DT}}^{Cl_M}\| < \|\mathbb{DT}_i - \overline{\mathbb{DT}}^{Cl_N}\| \quad \forall N \neq M\} \quad (5.6b)$$

This partition is not a violation of the conservation of simplex cardinality-(5.7a), because the subsets do not have intersections. In other words, there is no gain or loss of tetrahedrons. Additionally, for arbitrary point distributions representing non-convex geometries, the number of clusters can be at least 2, at most 'm' in (5.7b), i.e. the cardinality of initial point set P in equation-(5.1).

$$i_{dl} = \sum_{C=0}^K \#Cl_C \quad (5.7a)$$

$$2 \leq K \leq m \quad (5.7b)$$

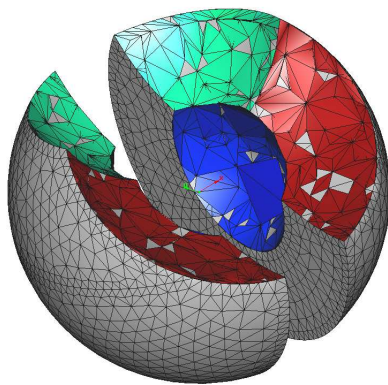
The cluster with the largest cardinality, i.e. with the largest Delaunay primitive population is called clustered Delaunay triangulation, 'CDT'.

$$\mathbb{DT}^{Cl_M} = \text{CDT} \iff \#Cl_M > \#Cl_N : \forall N \in (\mathbb{DT} \setminus \mathbb{DT}^{Cl_M}) \quad (5.8)$$

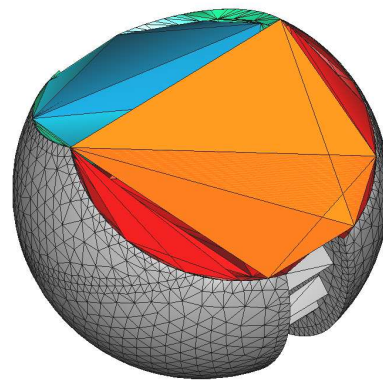
### 5.2.1.2 K-means Property Clustering for Delaunay Simplices

In k-means clustering breaks apart 'k' numbers of observations from a single global dataset. The hierarchical structure between the individual subsets is not of interest. The main concern is the clean-cut division of the global. Therefore, it is considered as a partitioned type clustering. In this frame, a division for a single feasible set (CDT) and a union of unfeasible subsets ( $\mathbb{DT} \setminus \text{CDT}$ ) are searched. The details of the algorithm can be found elsewhere (Ref.[G.Bradoski 2008]), however the individual steps will be repeated here for fluent reading.

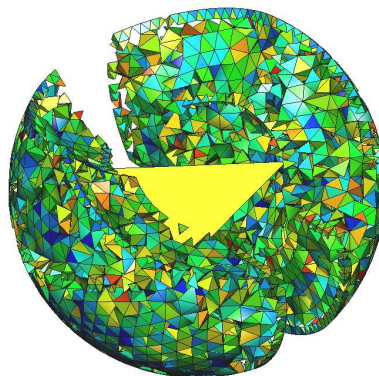
1. State precisely an attribute list for each Delaunay primitive. Normalize each attribute according to the global maximum and minimum values of  $\mathbb{DT}$  and orient/reverse them towards to the feasible or ill-conditioned direction. Define norms for cluster build.
2. Designate a  $k \geq 2$ . Make an shrewd estimation in the feasible direction for the initial feasible cluster origin, and predict remaining  $(k-1)$  origins randomly in the unfeasible directions.
3. Construct clusters according to the norms defined.
4. Compute new cluster centers by a mean norm.
5. Repeat steps (3) and (4) until convergence is satisfied, e.g. via the change of cluster centers, or via the change of set element list, or their cardinality.



(a) Insufficient number of clusters



(b) Inadequate attribute list



(c) Conflicting attribute list

Figure 5.2: Plausible cases of erroneous CDT

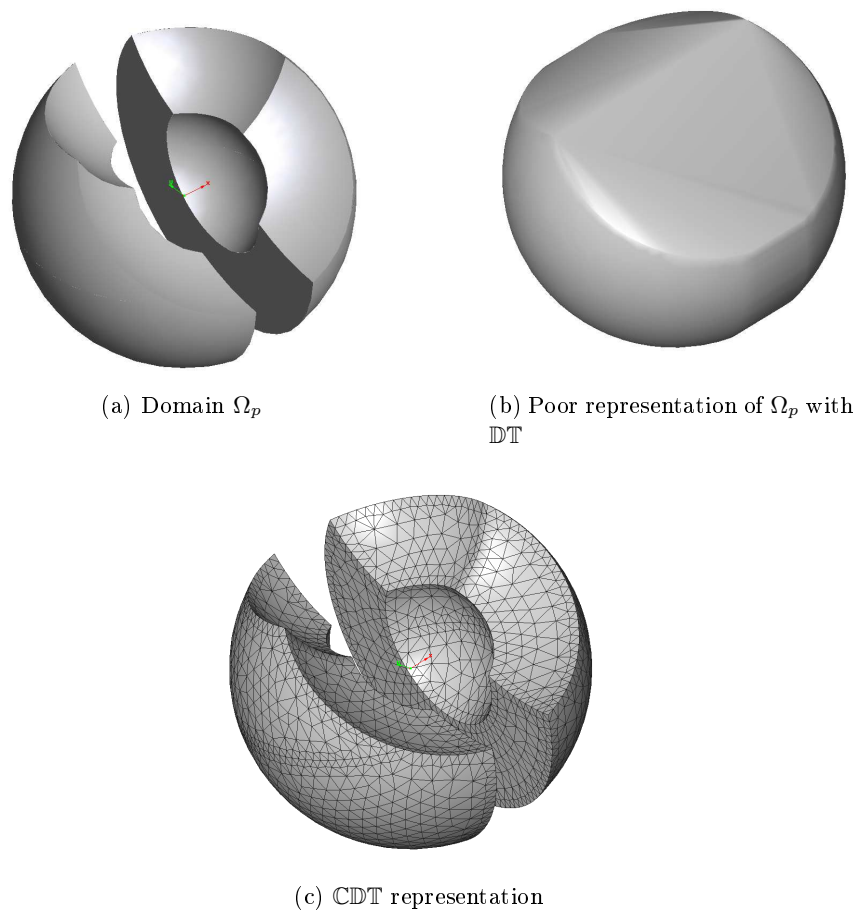


Figure 5.3: 3-means clustering of an object

## 5.2.2 Constrained Voronoi Tessellation

The integration schema of a bunch of particle based methods is based on Voronoi tessellation motivated interpolation methods. It is of fundamental importance to fulfill the interpolation requirements. The primary enlisted demand is the correct representation of the discrete domain which determines the interpolators.

In fact, the clustering was an initial attempt of fulfilling this requirement. The persecuting process can be defined as constraining Voronoi tessellation according to the clustered Delaunay triangulation, CDT. This procedure has been proven to be able to deal with complicated geometries as given in *Figure 5.4*<sup>4</sup>.

At this stage, first some dissonant characteristics of Voronoi diagram will be delineated, which appear to be trivial to deal with, and probably therefore, rarely mentioned in the texts. Immediately after, the way of dealing with this problem will be proposed, and exemplified.

<sup>4</sup>The model data was downloaded from the project AIM Shape-Visionair Ref. [P. Alliez 2006], the point cloud only is used for the demonstration of clustering

The Voronoi diagram of a number of points representing a domain (and domain boundaries) in a point-wise discrete manner, is a perfect candidate for focusing field parameters at an infinite locus, and meanwhile define gradients and fluxes around this locus. Voronoi Diagram is the union of disjoint locations, each of is them defined as given as in equation-(5.9a).

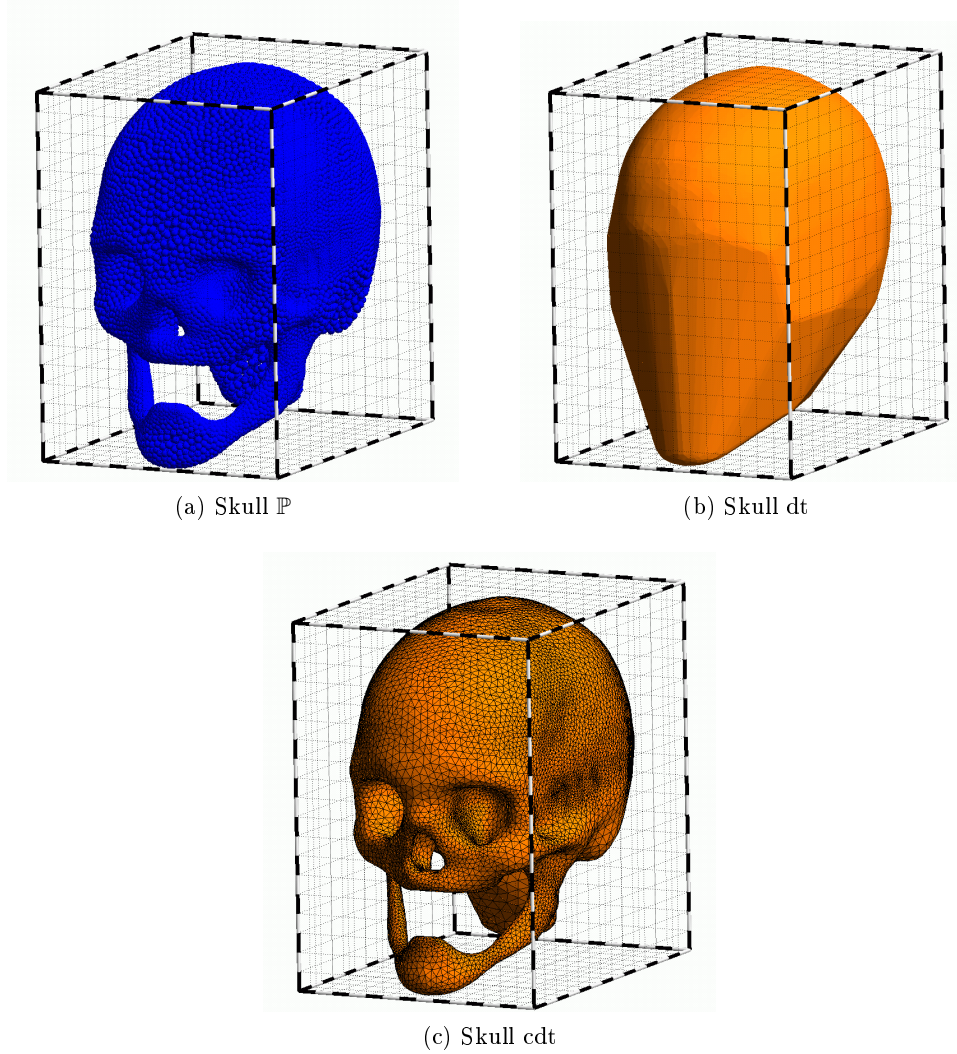


Figure 5.4: Clustering of complicated Skull geometry - Node Set is taken from AIM Shape-Visonair Ref.[<sup>P.Alliez 2006</sup>]

$$\mathbb{V}^{P_i} = \{r : \|x - p_i\| < \|x - p_j\| \quad \forall i \neq j \wedge x \in \mathbb{R} \wedge p_i, p_j \in \mathbb{P}\} \quad (5.9a)$$

$$\mathbb{V} = \bigcup_{p=1}^m \mathbb{V}^{P_i} \quad (5.9b)$$

One of the artifacts of Voronoi tessellation regarding to the interpolation schema is the existence of semi-infinite Lebesgue measures of the cells. Irrespective of the type of



geometry, there might be vertices present at infinity or far regions. Similarly, Voronoi cells with over or underestimated Lebesgue measures may be present, and thus shall be considered as artifacts disrupting the integration method.

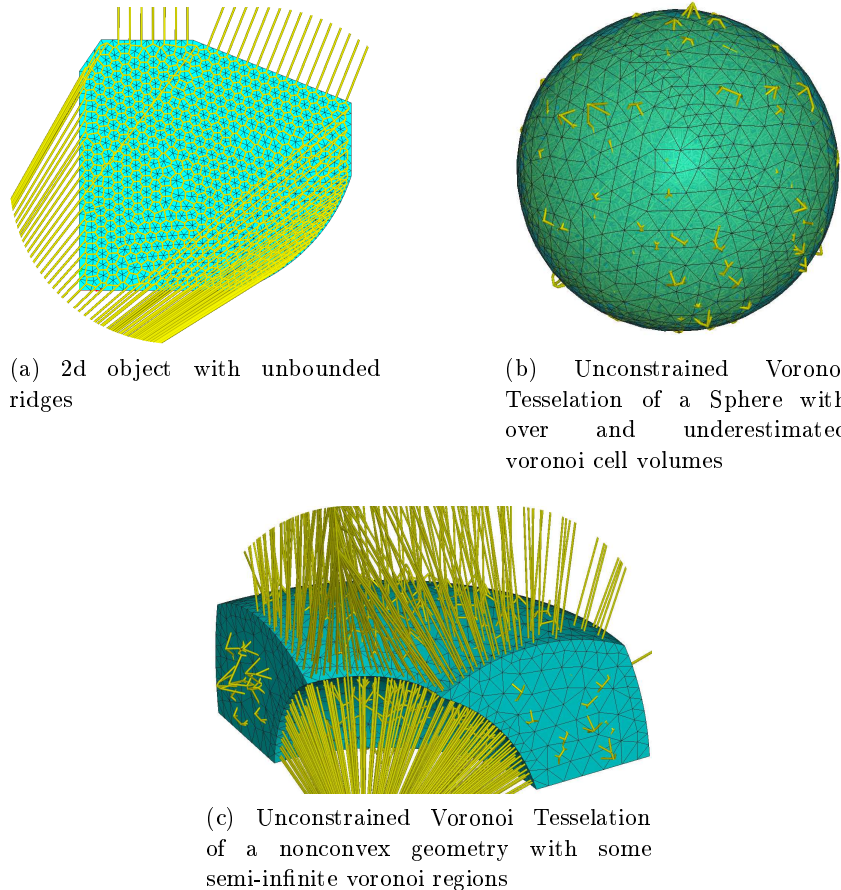


Figure 5.5: Unconstrained Voronoi Tessellations

Method of eliminating such artifacts is based on initially determining the boundary properties of the geometry, and then grading these properties quantitatively. Boundary detection for strictly concave geometries is trivial and intrinsically given by the unconstrained Voronoi tessellation. For instance, each boundary node -which is to be determined- in *figures 5.5* have an infinite Voronoi Lebesgue measure, whereby, bulk nodes have finite volumes or areas. Therefore, those ones can be stated to be *boundary nodes* immediately after unconstrained Voronoi tessellation. On the other hand, Voronoi tessellation -stand alone-, would not be enough to determine each and very boundary nodes for a non-convex geometry, as for example in *Figure 5.5*. In such a case, the connectivity nodes of the complement ' $DT \setminus CDT$ ' completes the missing list of boundary nodes.

In the scope of this thesis, for further grading of the boundary properties is necessary. To do it so, the surface nodes into its gradual details for a more stable Voronoi diagram constraining, are highlighted. A subdivision of the depiction of a *boundary* into a group of



surfaces, edges, and corners is suggested. This split is performed by the usual calculation and assembly of boundary normals, which is trivial if one has the boundary nodes in hand. Assembling of normals refers to grouping node normals gained from different primitives together.

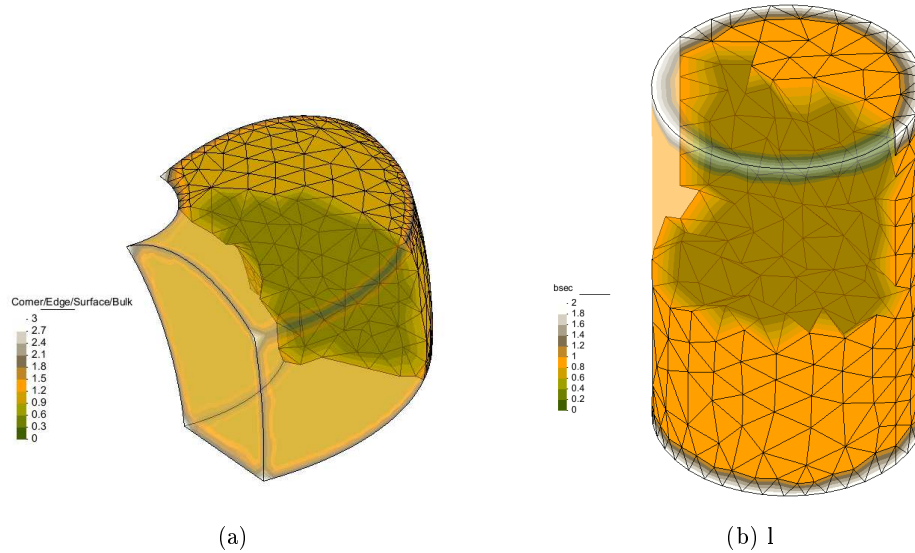


Figure 5.6: Bulk, Surface, Edge and Corner detection

As a result of assembling, bulk, surface, edge and corner nodes regain node normal sets with the cardinalities, 0,1,2 and 3 respectively, see *Figure 5.6*. This generalization would be violated in the absence of *conforming delaunay triangulation* is present, which is the case even for the latest and fastest convex hull algorithms such as *qhull* (Ref.[[B.Barber 1996](#)])). The conforming discretization is a necessity for Delaunay based interpolation methods. Since NEM interpolation and thereupon concluded integration outline is driven by Voronoi polyhedras, non-conforming Delaunay triangulation is a very passable problem for this content.

A certain *Lebesgue measure consistency* in between Delaunay tetrahedralization and Voronoi polyhedralization of a specific domain is inquired. To clarify, the discretization Lebesgue measure should close with increasing number of data points asymptotically towards to the desired Lebesgue measure of the original, i.e. of the domain. The Voronoi tessellation fulfilling this argument is called as constrained Voronoi tessellation, CV.

$$\lim_{m \rightarrow \infty} \text{vol}(\text{CDT}) = \lim_{m \rightarrow \infty} \text{vol}(\text{CV}) \quad (5.10)$$

Following this fundamental property of the constrained Voronoi tessellation, the *featured frontier* (featured boundary) set of the domain is defined. It is the intersection of domain set with the absolute complement set, and can be obtained by the extension of the

boundary set towards their normal direction. The boundary can be defined as,

$$\partial\mathbb{P} = \overline{\mathbb{P}} \setminus \mathbb{P}^o \quad (5.11)$$

Whereby the featured frontier has the following properties;

$$F(\mathbb{P}) \cup \mathbb{P}' = \mathbb{P}' \quad (5.12a)$$

$$F(\mathbb{P}) \cap \partial\mathbb{P} = \emptyset \quad (5.12b)$$

Accordingly, the featured frontier can be defined as a sequence as follows,

$$F(\mathbb{P}) = \{p_i + \varepsilon n_i\} \wedge (p_i \in \partial\mathbb{P}) \wedge (0 < \varepsilon \ll 1) \quad (5.13)$$

Where,  $n_i$  is denoting the normal vector at boundary point  $p_i$ . Epsilon ( $\varepsilon$ ) is a prescribed finite scale of the normal, which should be determined according to the size of the geometry, and the precision limits of the Voronoi constructor. According to the definitions above, the

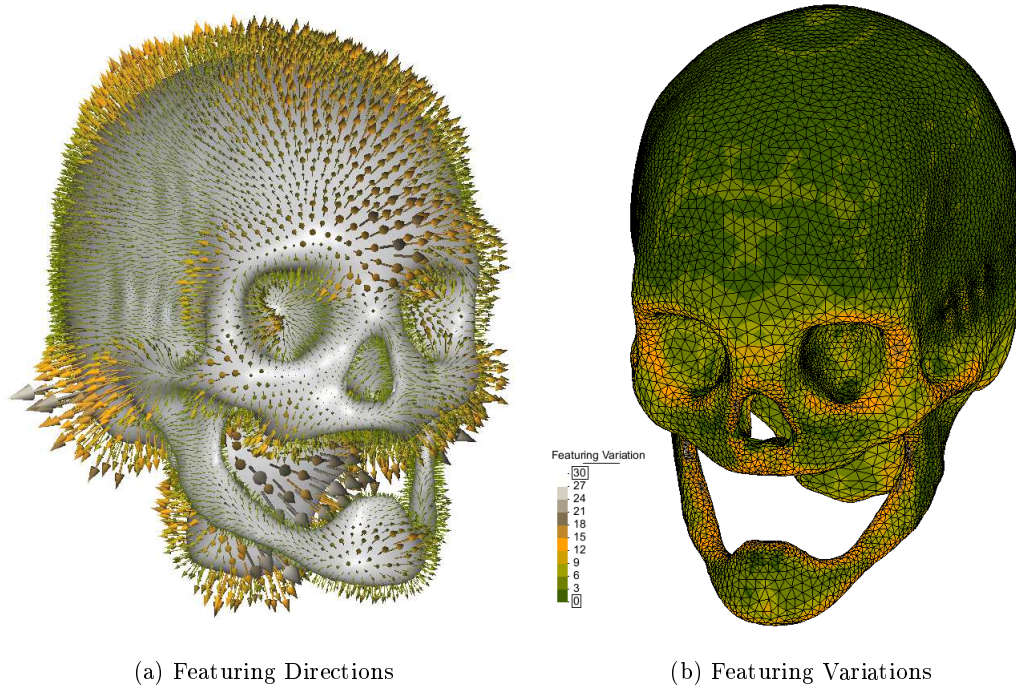


Figure 5.7: Sharp Featuring of the Skull geometry - Node Set is taken from AIM Shape-Visonair Ref.[<sup>P.Alliez 2006</sup>]

constrained Voronoi diagram is build on the following union of sets.

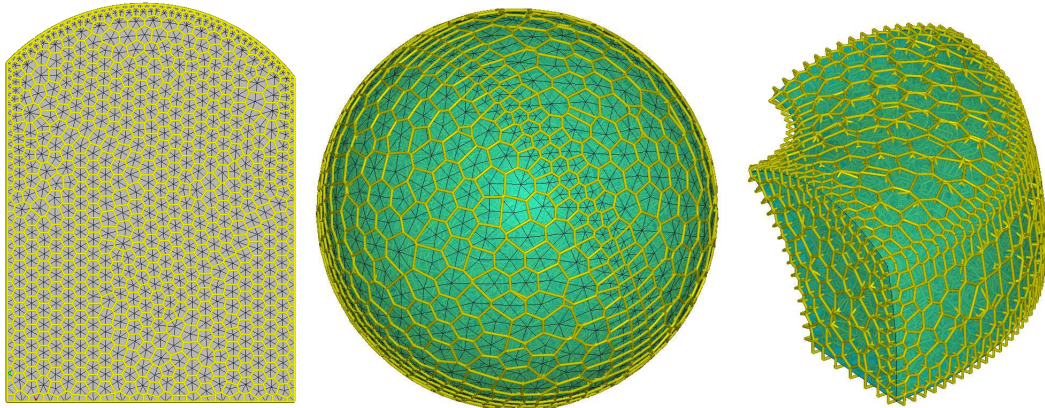
$$\overline{\mathbb{P}}_v = \mathbb{P}^o \cup \partial\mathbb{P} \cup F(\mathbb{P}) = \overline{\mathbb{P}} \cup F(\mathbb{P}) \quad (5.14)$$

The Voronoi cell definition is done by means of the following membership restrictions.

$$\mathbb{C}\mathbb{V}^{P_i} = \{r : \|x - p_i\| < \|x - p_j\| \quad (\forall i \neq j) \wedge (x \in \mathbb{R}) \wedge (p_i \in \overline{\mathbb{P}}) \wedge (p_j \in \overline{\mathbb{P}}_v)\} \quad (5.15a)$$

$$\mathbb{C}\mathbb{V} = \bigcup_{p=1}^m \mathbb{C}\mathbb{V}^{P_i} \quad (5.15b)$$

The constrains of Voronoi diagram are supplied in equation-(5.15a) based on the split given in eq(14). Similar to the raw Voronoi definition given in equation-(5.14), only the Voronoi regions of point set  $\overline{\mathbb{P}}$  are of interest. The significant change is the allowed and forbidden neighboring regions. The hyperplanes which divide two featuring frontier sequence points are strictly forbidden. The hyperplanes lying in between a boundary point ( $p_i \in \partial\mathbb{P}$ ) and a featured frontier point ( $p_j \in F(\mathbb{P})$ ) is allowed and define the boundary facets (ridges in 2d). The union of Voronoi polyhedras conforming these conditions is called here *constrained voronoi tessellation*,  $\mathbb{C}\mathbb{V}$ . The success of the suggested methodology can be



(a) Constrained 2d tessellation (b) Constrained Voronoi Tessellation of a sphere (c) Constrained Voronoi Tessellation of a nonconvex geometry

Figure 5.8: Constrained Voronoi Tessellations

well observed for shape featuring in *Figure 5.7* and for constrained Voronoi tessellation in *Figure 5.8*.

As stated before, the problems which are faced with, related to the dual construction, are considered to be general and fundamental, and exist in many in-use algorithms in public and commercial softwares. However, any solution suggestion for the corresponding problem of interest is unfortunately not spotted during the literature survey. In this stage, the issues concerning meshing are finalized, and into next step of natural element method can be entered.

### 5.3 Non-sequential Nodal Integration

Interpolators are mandatory for numerical techniques of solving PDE's. In general, algebraic functions which fulfill certain conditions are of fundamental importance for traditional FEM. Specifically, coefficients which are used to approximate field values at a certain location do not exist in NEM in means of algebraic functions with constant coefficients, i.e. polynomials. The interpolators of a locations are values, which depend subjectively on the distribution topology of the point set around this location. Additionally, Zienkiewicz Ref.[[O.C.Zienkiewicz 2000a](#)] states the general convergence criteria for shape functions used in Finite Element method as follows,

1. *"The continuity of the unknown only had to occur between elements (i.e., slope continuity is not required), or, in mathematical notation  $C_0$  continuity was needed;*
2. *The function has to allow any arbitrary linear form to be taken so that the constant strain (constant first derivative) criterion should be observed in each element*

For NEM, the correspondent of the element in FEM would be at best the Voronoi cell. Since a node is representing the center of that Voronoi cell, the ideas listed above for the convergece criteria are self-verified. In non-Sibsonian interpolation, the values of the interface of elements are directly evaluated by using the center values of the Voronoi cells, thus first condition is well satisfied. Since a local Voronoi construction<sup>5</sup> is necessary for the verification of second condition, and if done so, since it will be seen that another strain value be evaluated in the new location, the minimum requirement of point two is satisfied as well. These arguments let the definition of *meshless* to overlap with the concept of interpolating element-free (connectivity-free) domains.

For the sake of completeness, the non-Sibsonian (Ref.[[J.S.Chen 2001](#)]) form of the numerical interpolation summation will be repeated here. Some criteria such as, gradient-free (strain-free) constant field (rigid body) condition known as partition of unity and self (linear) reproducibility conditions should be fulfilled. These requirements, in opposite to the previously listed pre-requests, is of quantitative nature to be satisfied.

To start with, a vector field at a locus  $x$  can be approximated in terms of the nodal values

---

<sup>5</sup>i.e., inserting another point in the Voronoi cell of interest and investigating the value

of that vector field as shown next.

$$\mathbf{u}(\mathbf{x}) \approx \hat{\mathbf{u}}(\mathbf{x}) = \sum_{I \in N}^{\#support} \varphi_I(\mathbf{x}) \tilde{\mathbf{u}}_I \quad (5.16a)$$

$$\varphi_I(\mathbf{x}) = \frac{\mathcal{L}(V_{\mathbf{x}, \mathbf{x}_I}) / \|\mathbf{x}, \mathbf{x}_I\|}{\sum_J^{\#} \mathcal{L}(V_{\mathbf{x}, \mathbf{x}_J}) / \|\mathbf{x}, \mathbf{x}_J\|} \quad (5.16b)$$

$$\sum_{I \in N}^{\#support} \varphi_I(\mathbf{x}) = 1 \quad (5.16c)$$

$$\mathbf{x} = \sum_{I \in N}^{\#support} \varphi_I(\mathbf{x}) \mathbf{x}_I \quad (5.16d)$$

The support size is given as a priori in terms of element connectivities for FEM, or bounded by scaling parameters in meshfree methods with reproducing kernel particle<sup>a</sup> and element free Galerkin interpolators. For the case of nodal integration, based on the non-Sibsonian interpolation, the size of the support is assumed to be pre-determined by means of the primary Voronoi neighborhood. The underlying manifold allows partial inclusion of nearly equidistant points in the interpolation support of the locus of interest as can be seen in *Figure 5.9*.

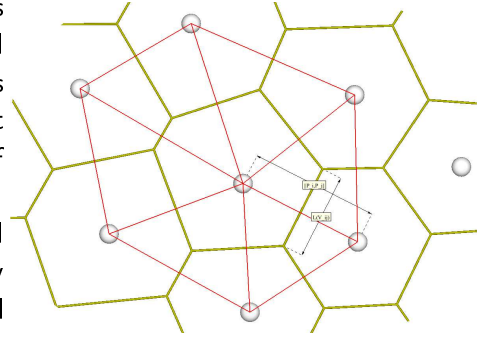


Figure 5.9: Non-sibsonian interpolation around a point. The right-most node is not included in the integration but the uppermost is.

<sup>a</sup>for more reading, refer Ref.[[Y.Chen 2006](#)]

The logical conflict clarified above is explored and significantly retrenched by the researchers of the field. Dolbow and Belytschko (Ref.[[Dolbow 1998](#)]) state that the *misalignment of the spatial coordinates and local supports is the (more) significant source of error* in meshfree methods. Chen et.al. (Ref.[[J.W.Yoo 2004](#)]) are consent to former developers of the method and call the result pertinent to the ambiguous determination of support size as *spatially instable and under-integrated*. Again Chen et al. (Ref.[[J.W.Yoo 2004](#)]) show that a significant betterment is possible if secondary Voronoi tessellations are done around the Voronoi cell of the locus of interest. The idea of interpolation summation around a point proposed by these writers is tangible if one considers it with the divergence of a differential around the point of interest. In fact, the method is named as *stabilized conforming nodal integration*, but not *interpolation*.

Considering a differential, for instance the gradient of a scalar field around a point  $\mathbf{x}$ , without referring to any homogeneous or in-homogeneous relationship. The integration of the mentioned gradient can be reduced in space by using the Gauss-divergence theorem as follows:

$$\int_{\Omega} \nabla \mathbf{u}(\mathbf{x}) dV = \int_{\Gamma} \mathbf{u}(\mathbf{x}) \mathbf{n} dS \quad (5.17)$$

If the aforementioned integration domain is taken to be a Voronoi polyhedra, the counter surface would consist of the set of polygon facets defining that Voronoi cell. Consequently, the integration of a gradient (or a differential) requires specific evaluation points on the counter polygons. The Dirichlet cells around the integration points are called in this thesis as *secondary voronoi cells*. The divergenced integral can be approximated on a Voronoi cell as the following:

$$\int_{\Gamma} (\mathbf{u}\mathbf{n})dS \approx \int_{\Gamma} (\hat{\mathbf{u}}\mathbf{n})dS = \sum_I^{\#PrimSupp} \left( \mathcal{L}(V_{\mathbf{x},\mathbf{x}_I}) \mathbf{n}_I \sum_J^{\#SecSupp} \varphi_J(\mathbf{x}_I) \tilde{\mathbf{u}}_J \right) \quad (5.18)$$

The preceding method is postulated as *stabilized conforming nodal integration*. The

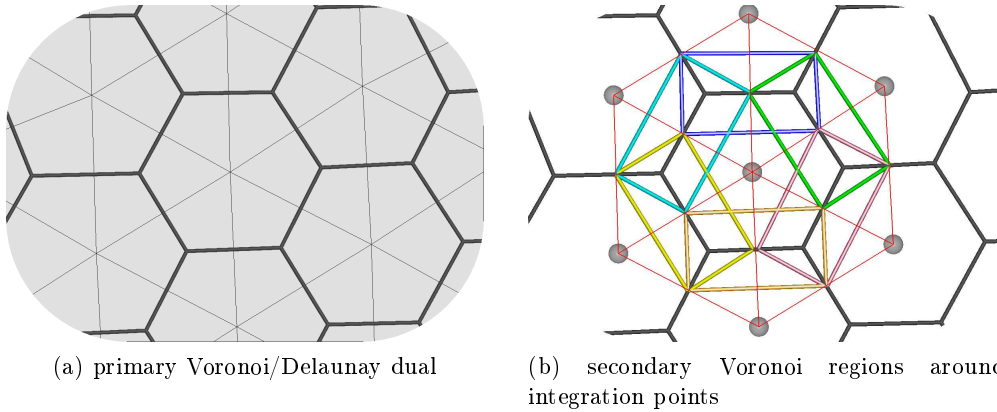


Figure 5.10: Primary and secondary Voronoi tessellation for the sequential integration of the differentials

method of integration developed for the current work differs from the former one in terms of the antagonism of *forming* and *outcome*. The previous method is established on a successive construction of secondary Voronoi cells. The contribution is done on the order of the tandem, which is ineffectual for the result. The posterior one is therefore renamed as *non-sequential nodal integration*, due to the unordered and sudden construction attribution of individual components of integration.

### 5.3.1 Evaluation of Shape Value Matrix

The method is founded on the idea of meshing nodal point set together with the evaluation, i.e. integration point set. The integration points are priorly known, or alternatively determinant (perfectly predictable), as long as initial constrained Voronoi tessellation is performed. For the Voronoi-based integration methods, it is difficult or incoherent to argue on the location as well as the number of (necessary or sufficient) integration points, because shape values are not resultants of functions. One difference stated as *forming* is obvious in comparing *Figure 5.10* with *Figure 5.11*. In non-sequential forming, the nodal and gaussian (integrating) points are combined into a single nodal/gaussian Delaunay/Voronoi dual. As a consequence of non-sequential forming, an explicit dependence of an arbitrary integrator point to another one is present. Whereby in sequential forming, secondary cells are non-overlapping and thus an explicit dependence (almost) of an arbitrary integrator point to *only* nodal points is present.

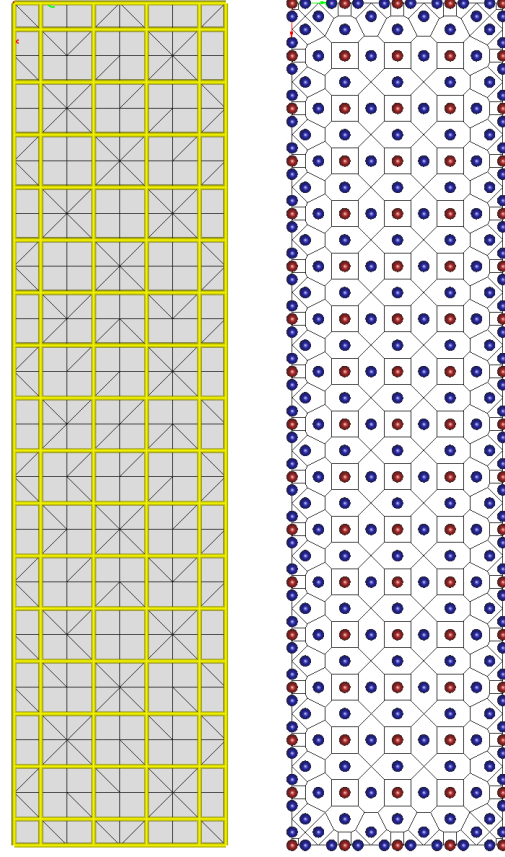


Figure 5.11: *Left*: Nodal Delaunay-Voronoi dual including only nodes. *Right*: Nodal/Gaussian Voronoi tessellation. Nodes in red, integrators (gauss points) in blue.

On the basis of the fast convex hull construction algorithms, non-sequential forming is observed to be faster<sup>6</sup> than sequential one. The second difference is the *outcome* of the postulated method. For this purpose, the sets of nodal and gaussian point coordinates  $\bar{\mathbf{N}}$  and  $\bar{\mathbf{G}}$  are defined, and their union with the disjoint nodal coordinate set  $\bar{\mathbf{N}\mathbf{G}}$ .

$$\bar{\mathbf{N}} = \{\mathbf{x}^{\bar{\mathbf{N}}_1}, \mathbf{x}^{\bar{\mathbf{N}}_2}, \mathbf{x}^{\bar{\mathbf{N}}_3}, \dots, \mathbf{x}^{\bar{\mathbf{N}}_m} : \forall \mathbf{x}^{\bar{\mathbf{N}}_i} \in \mathbb{R}^3\} \quad (5.19a)$$

$$\bar{\mathbf{G}} = \{\mathbf{x}^{\bar{\mathbf{G}}_1}, \mathbf{x}^{\bar{\mathbf{G}}_2}, \mathbf{x}^{\bar{\mathbf{G}}_3}, \dots, \mathbf{x}^{\bar{\mathbf{G}}_k} : \forall \mathbf{x}^{\bar{\mathbf{G}}_i} \in \mathbb{R}^3\} \quad (5.19b)$$

$$\bar{\mathbf{N}\mathbf{G}} = \bar{\mathbf{N}} \cup \bar{\mathbf{G}} \quad \wedge \quad \bar{\mathbf{N}} \cap \bar{\mathbf{G}} = \emptyset \quad (5.19c)$$

<sup>6</sup>The P or NP complexity of the problem, as well as any comparison is omitted in this treatise. The intent is a postulation of an alternative method without referring pragmatic arguments, yet the speed advantage is still a qualitative objective and advantage which is to be briefly mentioned.



The condition-(5.16d) written in matrix-vector form defined in the set of nodal coordinates and set of union of nodal\vegaussian coordinates are;

$$\mathbf{x}^{\bar{N}} = \Psi^{\bar{N}} \mathbf{x}^{\bar{N}} \quad (5.20a)$$

$$\mathbf{x}^{\bar{NG}} = \Psi^{\bar{NG}} \mathbf{x}^{\bar{NG}} \quad (5.20b)$$

Where,  $\Psi^{\bar{N}}$  and  $\Psi^{\bar{NG}}$  are shape value matrices settled on the nodal configuration *Figure 5.11(Left)* and nodal\vegaussian configuration *Figure 5.11(Right)* respectively.  $\Psi^{\bar{G}}$  is not of interest and therefore not given here.

Some properties of shape value matrices are important to follow on.  $\Psi^{\bar{N}}(m \times m)$  is a zero-diagonal square matrix, because self-inclusion is adverse to the definition of the non-Sibsonian interpolation scheme.  $\Psi^{\bar{NG}}$  is a  $(k+m) \times (k+m)$  zero-diagonal square matrix which includes at least 9 times (6 times in 2d) more zero or non-zero entries as  $\Psi^{\bar{N}}$  does. The cardinality of  $\bar{G}$  determines the size of the  $\Psi^{\bar{NG}}$  shape value matrix. The simple reason for this lower limit is that, each Voronoi cell should have support neighbors of 4 (3in 2d) such that the simplest enclosed primitive could be represented.

$$k = \frac{1}{2} \sum_{I=1}^m \#Support_I \geq \sum_{I=1}^m 2 \quad (5.21)$$

It is not immediately clear that one searches for the shape value matrix which re-produces gaussian coordinate vector from the nodal coordinate vector.

$$\mathbf{x}^{\bar{G}} = \Psi \mathbf{x}^{\bar{N}} \quad (5.22)$$

If one extends the size of the vectors to  $(k+m)$ ,

$$\mathbf{x}^{\bar{N}} = [\overbrace{\mathbf{x}^{\bar{N}_1}, \mathbf{x}^{\bar{N}_2}, \dots, \mathbf{x}^{\bar{N}_m}}^m, \overbrace{\mathbf{0}, \mathbf{0}, \dots, \mathbf{0}}^k] \quad (5.23a)$$

$$\mathbf{x}^{\bar{G}} = [\overbrace{\mathbf{0}, \mathbf{0}, \dots, \mathbf{0}}^m, \overbrace{\mathbf{x}^{\bar{G}_1}, \mathbf{x}^{\bar{G}_2}, \dots, \mathbf{x}^{\bar{G}_k}}^k] \quad (5.23b)$$

$$\mathbf{x}^{\bar{NG}} = [\overbrace{\mathbf{x}^{\bar{N}_1}, \mathbf{x}^{\bar{N}_2}, \dots, \mathbf{x}^{\bar{N}_m}}^m, \overbrace{\mathbf{x}^{\bar{G}_1}, \mathbf{x}^{\bar{G}_2}, \dots, \mathbf{x}^{\bar{G}_k}}^k] \quad (5.23c)$$

And similarly, if one extends the size of matrices to  $(k+m)$ ,

$$\Psi^{\bar{N}} = \begin{bmatrix} \overbrace{m \times m} & \overbrace{m \times k} \\ \psi_{nw}^{\bar{N}} & \psi_{ne}^{\bar{N}} \\ \psi_{sw}^{\bar{N}} & \psi_{se}^{\bar{N}} \\ \underbrace{k \times m} & \underbrace{k \times k} \end{bmatrix} \quad \Psi^{\bar{NG}} = \begin{bmatrix} \overbrace{m \times m} & \overbrace{m \times k} \\ \psi_{nw}^{\bar{NG}} & \psi_{ne}^{\bar{NG}} \\ \psi_{sw}^{\bar{NG}} & \psi_{se}^{\bar{NG}} \\ \underbrace{k \times m} & \underbrace{k \times k} \end{bmatrix} \quad (5.24)$$

The northeast, southwest and southeast sub-matrices of the nodal shape value matrix are zero-matrices, whereby the northwest is a zero-diagonal sparse matrix. Precisely, it is a



hollow row-stochastic matrix.

$$\boldsymbol{\psi}_{nw}^{\bar{N}} = \begin{pmatrix} \mathbf{0} & \cdots & \psi_{0m}^{\bar{N}} \\ \vdots & \mathbf{0} & \vdots \\ \psi_{m0}^{\bar{N}} & \cdots & \mathbf{0} \end{pmatrix}; \quad \boldsymbol{\psi}_{ne}^{\bar{N}} = \boldsymbol{\psi}_{sw}^{\bar{N}} = \boldsymbol{\psi}_{se}^{\bar{N}} = (\mathbf{0}) \quad (5.25)$$

Similarly, the southeast sub-matrix of nodal/gaussian shape value matrix is also a hollow row-stochastic matrix. The remaining sub-matrices are sparsely populated. Among them the northwest sub-matrix is almost zero matrix, because the nodal Voronoi regions are mostly surrounded by the gaussian regions.

$$\boldsymbol{\psi}_{se}^{\bar{NG}} = \begin{pmatrix} \mathbf{0} & \cdots & \psi_{(m)(m+k)}^{\bar{NG}} \\ \vdots & \mathbf{0} & \vdots \\ \psi_{(m+k)(m)}^{\bar{NG}} & \cdots & \mathbf{0} \end{pmatrix}; \quad \boldsymbol{\psi}_{nw}^{\bar{NG}} \approx (\mathbf{0}); \quad \boldsymbol{\psi}_{ne}^{\bar{NG}} \neq (\mathbf{0}); \quad \boldsymbol{\psi}_{sw}^{\bar{NG}} \neq (\mathbf{0}) \quad (5.26)$$

A row stochastic matrix may have eigenvalues with absolute values smaller or equal than one. The row stochastic matrices of equations (5.25) & (5.26), have at least one eigenvalue reaching their maximum of unity, which is self evident from self reproducibility conditions of equations (5.20a) & (5.20b). In any ways of getting the shape value matrix in equation (5.22) include infinite powers of these stochastic matrices, which diverge. Therefore, the existence of explicit inversion operations to reach a form of equation (5.22) should be discussed carefully. To start with, the gaussian vector can be written using the self reproducibility conditions of the shape value matrices,

$$\begin{aligned} \mathbf{x}^{\bar{G}} &= \mathbf{I}\mathbf{x}^{\bar{G}} = \mathbf{x}^{\bar{NG}} - \mathbf{x}^{\bar{N}} \\ &= \boldsymbol{\Psi}^{\bar{NG}}\mathbf{x}^{\bar{NG}} - \boldsymbol{\Psi}^{\bar{N}}\mathbf{x}^{\bar{N}} = \boldsymbol{\Psi}^{\bar{NG}}\mathbf{x}^{\bar{NG}} - \boldsymbol{\Psi}^{\bar{N}}\mathbf{x}^{\bar{NG}} \\ &= (\boldsymbol{\Psi}^{\bar{NG}} - \boldsymbol{\Psi}^{\bar{N}})\mathbf{x}^{\bar{NG}} = (\boldsymbol{\Psi}^{\bar{NG}} - \boldsymbol{\Psi}^{\bar{N}})(\mathbf{x}^{\bar{N}} + \mathbf{x}^{\bar{G}}) \end{aligned} \quad (5.27)$$

Reformulated in matrix-vector form for the sake of clearence,

$$\begin{aligned} \mathbf{x}^{\bar{G}} &= \begin{bmatrix} \mathbf{I}_{nw} & \mathbf{0} \\ \mathbf{0} & \mathbf{I}_{se} \end{bmatrix} \begin{bmatrix} \mathbf{0} \\ \mathbf{x}_s^{\bar{G}} \end{bmatrix} = \begin{bmatrix} -\boldsymbol{\psi}_{nw}^{\bar{N}} & \mathbf{0} \\ \boldsymbol{\psi}_{sw}^{\bar{NG}} & \mathbf{0} \end{bmatrix} \begin{bmatrix} \mathbf{x}_n^{\bar{N}} \\ \mathbf{0} \end{bmatrix} + \begin{bmatrix} \mathbf{0} & \boldsymbol{\psi}_{ne}^{\bar{NG}} \\ \mathbf{0} & \boldsymbol{\psi}_{se}^{\bar{NG}} \end{bmatrix} \begin{bmatrix} \mathbf{0} \\ \mathbf{x}_s^{\bar{G}} \end{bmatrix} \\ &= \begin{bmatrix} \mathbf{I}_{nw} & -\boldsymbol{\psi}_{ne}^{\bar{NG}} \\ \mathbf{0} & \mathbf{I}_{se} - \boldsymbol{\psi}_{se}^{\bar{NG}} \end{bmatrix}^{-1} \begin{bmatrix} -\boldsymbol{\psi}_{nw}^{\bar{N}} & \mathbf{0} \\ \boldsymbol{\psi}_{sw}^{\bar{NG}} & \mathbf{0} \end{bmatrix} \begin{bmatrix} \mathbf{x}_n^{\bar{N}} \\ \mathbf{0} \end{bmatrix} \\ &= \left( \begin{bmatrix} \mathbf{I}_{nw} & \mathbf{0} \\ \mathbf{0} & \mathbf{I}_{se} \end{bmatrix} - \begin{bmatrix} \mathbf{0} & \boldsymbol{\psi}_{ne}^{\bar{NG}} \\ \mathbf{0} & \boldsymbol{\psi}_{se}^{\bar{NG}} \end{bmatrix} \right)^{-1} \begin{bmatrix} -\boldsymbol{\psi}_{nw}^{\bar{N}}\mathbf{x}_n^{\bar{N}} \\ \boldsymbol{\psi}_{sw}^{\bar{NG}}\mathbf{x}_n^{\bar{N}} \end{bmatrix} \end{aligned} \quad (5.28)$$

The existence of this form depends on the invertibility of identity minus eastern nodal/gaussian shape value matrix. In fact, only a local existence of the inverse is necessary. By considering that gaussian coordinate vector in equation (5.23b) has only southern values

of interest, we require finite values only in the southern part of the inverse matrix as subscribed in the inverse term of the equation beneath;

$$\mathbf{x}^{\bar{e}} = \left( \mathbf{I} - \Psi_e^{\text{NG}} \right)^{-1} \left( \Psi_w^{\text{NG}} - \Psi_w^{\bar{N}} \right) \mathbf{x}^{\bar{N}} \quad (5.29a)$$

$$\Rightarrow \Psi = \left[ \left( \mathbf{I} - \Psi_e^{\text{NG}} \right)^{-1} \right]_s \left( \Psi_w^{\text{NG}} - \Psi_w^{\bar{N}} \right) \quad (5.29b)$$

The existence of finite southern part of the inverse given in equation (5.29b) can be investigated if one writes the infinite Neumann series of the inverse.

$$\begin{aligned} \left[ \left( \mathbf{I} - \Psi_e^{\text{NG}} \right)^{-1} \right]_s &= [\mathbf{I}_e]_s + \left[ \left( \Psi_e^{\text{NG}} \right) \right]_s + \left[ \left( \Psi_e^{\text{NG}} \right)^2 \right]_s + \dots + \left[ \left( \Psi_e^{\text{NG}} \right)^l \right]_s + \dots \\ &= \sum_{n=0}^{\infty} \left[ \left( \Psi_e^{\text{NG}} \right)^n \right]_s = \sum_{n=0}^{\infty} \left[ \begin{pmatrix} \mathbf{0} & \psi_{ne}^{\text{NG}} \\ \mathbf{0} & \psi_{se}^{\text{NG}} \end{pmatrix}^n \right]_s \\ &= \sum_{n=0}^{\infty} \left( \Psi_{se}^{\text{NG}} \right)^n \end{aligned} \quad (5.30)$$

Each and every member of this Neumann series, which consist of the powers of eastern part of the hollow stochastic matrix of nodal/gaussian shape values, have zero western part. As can be followed from equation (5.30), the zero-convergence of the southeastern powers is required for the equality of the form of equation (5.29b).

$$\lim_{n \rightarrow \infty} \left( \Psi_{se}^{\text{NG}} \right)^n = \mathbf{0} \iff \det \left( \mathbf{I} - \Psi_{se}^{\text{NG}} \right) \neq 0 \quad (5.31)$$

The nodal and gaussian coordinates are not self interpolated. Therefore, the southeastern matrix of equation (5.31) is also hollow. Regardless of the condition of partition of unity, the absolute values of each entry of this matrix is strictly smaller than unity. The supremum norm of the absolute sums of the rows, i.e. infinity norm is also smaller than unity as evident in block-wise representation of equation (5.31). The latter inequality is a result of the fact that, nodal/gaussian shape value matrix is row stochastic<sup>7</sup>, and each gauss point has at least one node point as neighbor. Thus, eastern/western split of the southern part of the nodal/gaussian matrix enforces the infinity norm under interest to be strictly less than unity.

$$\| \Psi_{se}^{\text{NG}} \|_{max} = \sup \left\{ \left| \left( \psi_{se}^{\text{NG}} \right)_{rc} \right| \right\} < 1; \quad (5.32a)$$

$$\| \Psi_{se}^{\text{NG}} \|_{\infty} = \sup_r \left\{ \sum_c^k \left| \left( \psi_{se}^{\text{NG}} \right)_{rc} \right| \right\} < 1 \quad (5.32b)$$

The condition (5.32a) alone is weak for the proof of convergence of geometric series in equation (5.30), because the maximum norm is not a sub-multiplicative norm. In order

<sup>7</sup>As a result of partition of unity and the arbitrariness of the geometry and system under consideration

to strengthen the arguments, first, the maximum norm of the square of the matrix and sub-multiplicative infinity norm should be compared with each other.

$$\begin{aligned}
\|(\Psi_{se}^{\overline{NG}})^2\|_{max} &= \sup \left\{ \left| \sum_l (\psi_{se}^{\overline{NG}})_{rl} (\psi_{se}^{\overline{NG}})_{lc} \right| \right\} \\
&\leq \sup \left\{ \sum_l |(\psi_{se}^{\overline{NG}})_{rl} (\psi_{se}^{\overline{NG}})_{lc}| \right\} \\
&\leq \sup \left\{ \|\Psi_{se}^{\overline{NG}}\|_{max} \sum_l |(\psi_{se}^{\overline{NG}})_{rl}| \right\} \\
&= \sup_r \left\{ \sum_l |(\psi_{se}^{\overline{NG}})_{rl}| \right\} \|\Psi_{se}^{\overline{NG}}\|_{max} \\
&= \|\Psi_{se}^{\overline{NG}}\|_{max} \|\Psi_{se}^{\overline{NG}}\|_{\infty}
\end{aligned} \tag{5.33}$$

Accordingly, the upper limit of the third power and any power of the matrix is predictable in the same way.

$$\begin{aligned}
\|(\Psi_{se}^{\overline{NG}})^3\|_{max} &= \|\Psi_{se}^{\overline{NG}} (\Psi_{se}^{\overline{NG}})^2\|_{max} \leq \|(\Psi_{se}^{\overline{NG}})^2\|_{max} \|\Psi_{se}^{\overline{NG}}\|_{\infty} \\
&\leq \|\Psi_{se}^{\overline{NG}}\|_{max} \|\Psi_{se}^{\overline{NG}}\|_{\infty}^2
\end{aligned} \tag{5.34a}$$

$$\Rightarrow \|\Psi_{se}^{\overline{NG}}\|_{max}^n \leq \|\Psi_{se}^{\overline{NG}}\|_{max} \|\Psi_{se}^{\overline{NG}}\|_{\infty}^n < \|\Psi_{se}^{\overline{NG}}\|_{\infty}^n \tag{5.34b}$$

Which says that the maximum norm of the powers are always smaller than the same powers of the infinity norm, for the matrices satisfying the condition set of (5.32a) & (5.32b). Having this information in hand and using the sub-additivity of norms in definition, one can argue on the upper border of the matrix to be inverted. The final equation below shows that the maximum norm of the Neumann series is smaller than the Neumann series of the infinity norms. Knowing that the infinity norm is finite and strictly smaller than one, it can be shown that the maximum entry of the inverse is finite, thus a shape value matrix in the form of (5.29b) does exist for arbitrary configurations.

$$\begin{aligned}
\|(I - \Psi_{se}^{\overline{NG}})^{-1}\|_{max} &= \left\| \sum_{n=0}^{\infty} (\Psi_{se}^{\overline{NG}})^n \right\|_{max} \leq \sum_{n=0}^{\infty} \|(\Psi_{se}^{\overline{NG}})^n\|_{max} \\
&< \sum_{n=0}^{\infty} \|\Psi_{se}^{\overline{NG}}\|_{\infty}^n = (1 - \|\Psi_{se}^{\overline{NG}}\|_{\infty})^{-1}
\end{aligned} \tag{5.35}$$

Finally, it can be concluded that finding a shape value matrix which maps nodal coordinates to the gaussian ones is achieved by a single explicit inversion and multiplication as below. Practically, there is no need of evaluation of nodal shape value matrix of (5.20a). However, nodal CDT&CV configurations are necessary for the determination of integration locations.

$$\Psi = (I_{se} - \Psi_{se}^{\overline{NG}})^{-1} (\Psi_{sw}^{\overline{NG}}) \tag{5.36}$$

### 5.3.2 Nature of Shape Value Matrix

In this section, some important properties of the shape value matrix will be stated. Together with the equations (5.20a), (5.24) and (5.26) one can conclude that the nodal coordinates are representable in terms of the gaussian coordinates, by means of the northeastern part of the nodal/gaussian shape value matrix.

$$\mathbf{x}_n^{\bar{N}} = \boldsymbol{\psi}_{ne}^{\bar{NG}} \mathbf{x}_s^{\bar{G}} \quad (5.37)$$

By remembering the inequality (5.21), a comment on the cardinality of the gaussian and nodal point sets can be done.

$$k \geq 2m \quad \Rightarrow \quad \#\bar{G} \geq 2\#\bar{N} \quad (5.38)$$

Depending on the identification of linear mapping direction, the system of equations given in equation (5.38) can be seen as an underestimated or an overestimated system. By considering the gaussian coordinates as unknowns -which is plausible considering that the geometry is defined initially in terms of the nodal coordinates-, the system would have more unknowns than equations, thus underestimated.

The matrix  $(\boldsymbol{\psi}_{ne}^{\bar{NG}})$  is size of  $m \times k$  with  $m < k$  as stated above. This type of matrix has the so-called pseudoinverse  $(\boldsymbol{\psi}_{ne}^{\bar{NG}})^+ \in \mathbb{R}^{k \times m}$ , which always  $(\forall (\boldsymbol{\psi}_{ne}^{\bar{NG}}) \in \mathbb{R}^{m \times k})$  uniquely exists. Under the definition of Penrose conditions (Ref.[A.Laub 2008]), the Moore-Penrose pseudoinverse of a matrix (a row independent matrix) can be evaluated by the following equality;

$$(\boldsymbol{\psi}_{ne}^{\bar{NG}})^+ = (\boldsymbol{\psi}_{ne}^{\bar{NG}})^T \left[ (\boldsymbol{\psi}_{ne}^{\bar{NG}}) (\boldsymbol{\psi}_{ne}^{\bar{NG}})^T \right]^{-1} \quad (5.39)$$

Solving the system of equations of (5.38) is equivalent of searching for a gaussian coordinates vector  $\tilde{\mathbf{x}}_s^{\bar{G}}$  which satisfies the equality constraint (5.38). One can further take on board an inequality condition, which can select one of the solutions among many other possibilities which do exist according to the underestimated nature of the statement. Linking the additional inequality as the least half of the Euclidian norm of the possible solution vector, the problem statement results in terms of an optimization set;

$$\begin{aligned} \text{minimize} \quad & 0.5 \|\mathbf{x}\|_2^2 \\ \text{:} \quad & -\boldsymbol{\psi}_{ne}^{\bar{NG}} \mathbf{x} + \mathbf{x}_n^{\bar{N}} = \mathbf{0} \end{aligned} \quad (5.40)$$

The minimization of the Lagrangian function below with a proper selection of Lagrangian multiplier vector  $\boldsymbol{\lambda}$  (Ref.[K.U.Bletzinger 2011]) is analogous to the problem set above.

$$\text{minimize} \quad L(\mathbf{x}, \boldsymbol{\lambda}) = 0.5 \|\mathbf{x}\|_2^2 + \boldsymbol{\lambda} \left( -\boldsymbol{\psi}_{ne}^{\bar{NG}} \mathbf{x} + \mathbf{x}_n^{\bar{N}} \right) \quad (5.41)$$

There are two sets of Kuhn-Tucker conditions (Ref.[K.U.Bletzinger 2011]) of equation (5.42b) & (5.42c) of the given Lagrangian to be satisfied at the optimum location. Written in the

indicial notation,

$$\text{minimize} \quad L(x_i, \lambda_j) = 0.5(x_i)^2 + \lambda_j \left( - \left( \psi_{ne}^{\overline{NG}} \right)_{ji} x_i + \left( x_n^{\overline{N}} \right)_j \right) \quad (5.42a)$$

$$\left. \frac{\partial L}{\partial x_i} \right|_{x_i = (\tilde{x}_s^{\overline{G}})_i} = \left( \tilde{x}_s^{\overline{G}} \right)_i - \lambda_j \left( \psi_{ne}^{\overline{NG}} \right)_{ji} = 0 \quad (5.42b)$$

$$\left. \frac{\partial L}{\partial \lambda_j} \right|_{x_i = (\tilde{x}_s^{\overline{G}})_i} = - \left( \psi_{ne}^{\overline{NG}} \right)_{ji} \left( \tilde{x}_s^{\overline{G}} \right)_i + \left( x_n^{\overline{N}} \right)_j = 0 \quad (5.42c)$$

The KT conditions state that,

$$\left( \psi_{ne}^{\overline{NG}} \right)^T \boldsymbol{\lambda} = \tilde{\boldsymbol{x}}_s^{\overline{G}} \quad (5.43a)$$

$$\left( \psi_{ne}^{\overline{NG}} \right) \tilde{\boldsymbol{x}}_s^{\overline{G}} = \boldsymbol{x}_n^{\overline{N}} \quad (5.43b)$$

Left multiplication of equation (5.43a) with  $\left( \psi_{ne}^{\overline{NG}} \right)$  and substituting into gives,

$$\left( \psi_{ne}^{\overline{NG}} \right) \left( \psi_{ne}^{\overline{NG}} \right)^T \boldsymbol{\lambda} = \boldsymbol{x}_n^{\overline{N}} \quad \Rightarrow \quad \boldsymbol{\lambda} = \left[ \left( \psi_{ne}^{\overline{NG}} \right) \left( \psi_{ne}^{\overline{NG}} \right)^T \right]^{-1} \boldsymbol{x}_n^{\overline{N}} \quad (5.44)$$

By back-substituting of the expression (5.44) into equation (5.43a), it is clarified that the optimization manifold given in (5.40) is satisfied with the Moore-Penrose type pseudo inverse given by the definition (5.39).

$$\begin{aligned} \tilde{\boldsymbol{x}}_s^{\overline{G}} &= \left( \psi_{ne}^{\overline{NG}} \right)^T \left[ \left( \psi_{ne}^{\overline{NG}} \right) \left( \psi_{ne}^{\overline{NG}} \right)^T \right]^{-1} \boldsymbol{x}_n^{\overline{N}} \\ &= \left( \psi_{ne}^{\overline{NG}} \right)^+ \boldsymbol{x}_n^{\overline{N}} \end{aligned} \quad (5.45)$$

By the definition, the gauss points do satisfy the equation (5.20b). The northeastern part of the equation indicates that there are many possible gauss point vectors (by keeping the number of gauss points constant) which satisfies the condition of (5.20b) and there is no strong argument that the correct one should have the least Euclidean norm.

It has been suggested to locate the integration points at the coordinates which tender geometrical symmetry, i.e. Voronoi facet centroids, and centroids of the triangles of Voronoi facet divisions. Some other set of location which satisfies the minimization problem (5.40) does not necessarily overlap with the geometrically symmetrical set of location. As a result, the least square Moore-Penrose inverse conflicts geometrically with the discrete divergence approximation (5.18), and thus it should stayed perfectly determinate way of evaluation (5.36).

The difference in between the determinate and Moore-Penrose inversion is observable if one back-updates the coordinates according to the shape-value matrix found, seen in Figure 5.12. Therefore, the Moore-Penrose type of inversion in non-sequential stabilized nodal integration should not be seen as an alternative, however, it should be noted here to

draw attention about the possible bottlenecks, one can possibly face with.

Differences in support sizes in between the classical FEM shape function interpolation, NFEM non-Sibsonian sequential interpolation spuort, and the presented non-sequential interpolation for NEM can be seen in *Figure 5.13*. As obvious, the support for the continuum can be extended to large radius of influence. However, since this may influence the sparsity of the global matrices, the writer of the treatise suggest to manipulate the density of the support. This can be achieved by determining threshold values for the minimum shape-value quantity, and the normalize the sum, so that the condition of partition of unity is satisfied.

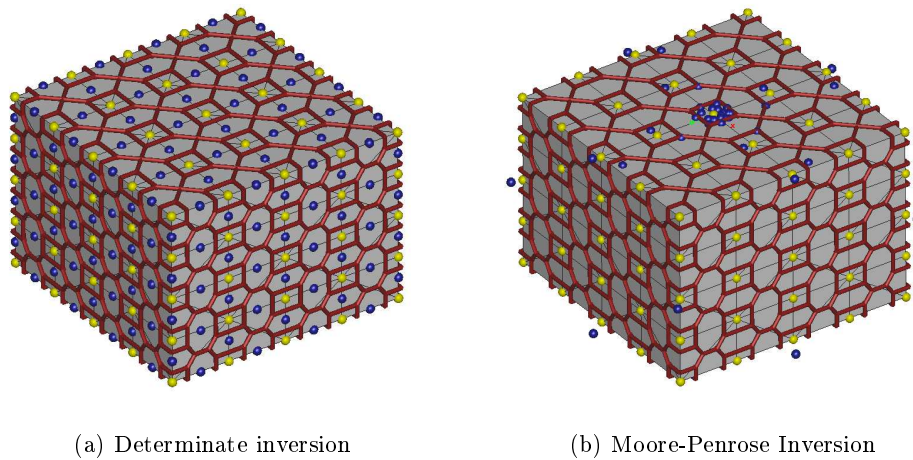


Figure 5.12: Location of gauss points (in blue) and nodal points (in orange) interpolated with two different linear mappings

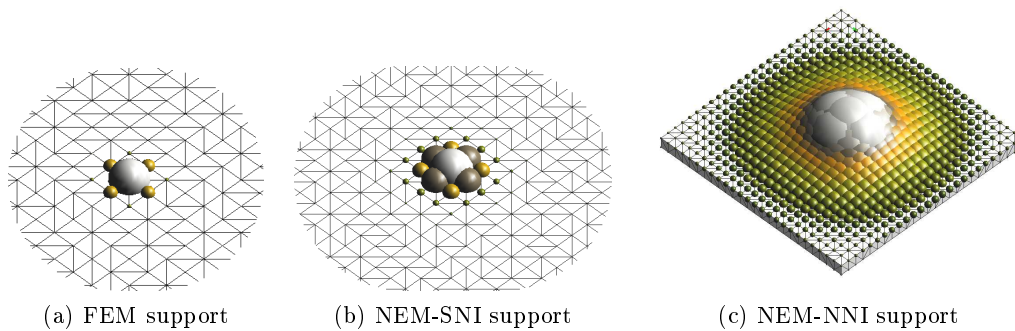


Figure 5.13: Support sizes of a surface node of a plate model

## 5.4 Implementation and Examples

In the implementations section, initially a short introduction is done for the application of Hypercauchy equation. Since this equation is almost the most complicated one, the other formulations can be extracted from it accordingly. Based on this formulation some demonstrative examples obtained by the execution of the written code are presented visually through illustrations.

To begin with, the energy split proposed is repeated here, and natural element shape value interpolation on the virtual energy integrals is applied. The nonlinear internal virtual energy divisions become,

$$\begin{aligned}\delta\Pi_{int}^{PF} &= \int_{\Omega} [\mathbf{P} : \nabla_{\mathbf{X}} \delta \mathbf{u}] dV \approx \int_{\Omega} [\mathbf{P} \cdot \nabla_{\mathbf{X}} \left( \sum N^I \right)] \cdot \delta \tilde{\mathbf{u}} dV = \mathbf{f}_{int}^{PF} \cdot \delta \tilde{\mathbf{u}} \\ \delta\Pi_{int}^{QG} &= \int_{\Omega} [\mathbf{Q} : \nabla_{\mathbf{X}}^{\otimes 2} \delta \mathbf{u}] dV \approx \int_{\Omega} [\mathbf{Q}^T \nabla_{\mathbf{X}}^{\otimes 2} \left( \sum N^I \right)] \cdot \delta \tilde{\mathbf{u}} dV = \mathbf{f}_{int}^{QG} \cdot \delta \tilde{\mathbf{u}}\end{aligned}\quad (5.46)$$

Correspondingly, the tangent matrices of the non-mixed residuum internal forces can be repeated here to be,

$$\mathbf{K}_{\mathbf{P}(\mathbf{F})}^{IJ} = \int_{\Omega} \left[ \nabla_{\mathbf{X}} N^I \cdot \frac{\partial \mathbf{P}^T}{\partial \mathbf{F}} \cdot \nabla_{\mathbf{X}} N^J \right] dV \quad \mathbf{K}_{\mathbf{Q}(\mathbf{G})}^{IJ} = \int_{\Omega} \left[ \nabla_{\mathbf{X}}^{\otimes 2} N^I \cdot \frac{\partial \mathbf{Q}^{T_2}}{\partial \mathbf{G}} \cdot \nabla_{\mathbf{X}}^{\otimes 2} N^J \right] dV \quad (5.47)$$

And the mixed-residuum's of the internal forces cause the following contributions in the tangent stiffness matrices,

$$\mathbf{K}_{\mathbf{P}(\mathbf{G})}^{IJ} = \int_{\Omega} \left[ \nabla_{\mathbf{X}} N^J \cdot \frac{\partial \mathbf{Q}^{T_2}}{\partial \mathbf{G}} \cdot \nabla_{\mathbf{X}}^{\otimes 2} N^I \right] dV \quad \mathbf{K}_{\mathbf{Q}(\mathbf{F})}^{IJ} = \int_{\Omega} \left[ \nabla_{\mathbf{X}}^{\otimes 2} N^I \cdot \frac{\partial \mathbf{Q}^{T_2}}{\partial \mathbf{F}} \cdot \nabla_{\mathbf{X}} N^J \right] dV \quad (5.48)$$

The assumed strain displacement, and assumed hyperstrain displacement matrices are,

$$\begin{aligned}\tilde{\mathbf{B}}^I &= \frac{1}{V} \int_{\Omega} [\nabla_{\mathbf{X}} N^I] dV = \frac{1}{V} \int_S N^I \mathbf{n} dA \\ \tilde{\mathbf{B}}_{\nabla}^I &= \frac{1}{V} \int_{\Omega} [\nabla_{\mathbf{X}}^{\otimes 2} N^I] dV = \frac{1}{V} \int_S [\mathbf{n} \otimes \nabla_{\mathbf{X}} N^I] dA\end{aligned}\quad (5.49)$$

The second term is an extension of stabilized conforming nodal integration to the higher order volume average derivatives of coordinate interpolaters. No analytic functions or patches for integration is implemented here, in fact, the integration is performed on natural neighbors of Voronoi polyhedrons, and therefore is truly natural element method.

This schema and simpler version of it can be applied to many differential equations. The first example chosen is the fundamental solution of the Laplace equation;

$$\nabla^2 \varphi = \delta(\mathbf{x} - \mathbf{x}_o) \quad (5.50)$$

Since the solution is fundamental, as indicated a Dirac delta type excitation is used. The phenomenological analogue of Laplace equation is the steady state heat conduction equation. The formulation is investigated on a quarter of 3D Mobius strip with rectangular

cross section and elliptical path way geometry, and a point source of heat flux in the origin of the ellipse. The result is satisfying and well overlapping with the analytical solution, which is omitted here.

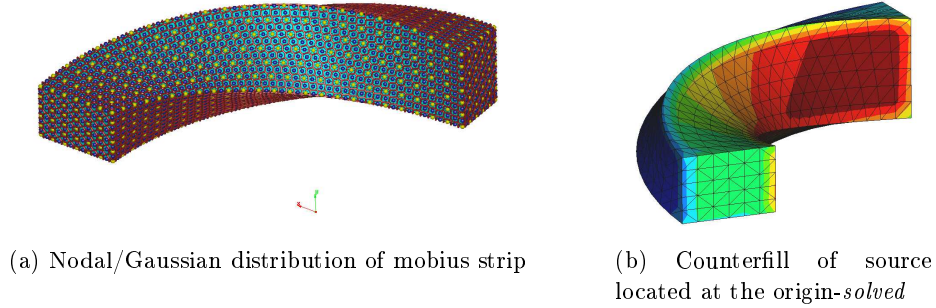


Figure 5.14: A piece from an infinitely large imaginary volume with a heat source located at the origin of the elliptical split pathway

This example represents also a cross-check of all the previous steps, namely the clustered triangulation, constrained Voronoi construction and non-sequential integration. As next example, one can move into solution of the linear momentum equation with first-order finite kinematics.

$$\operatorname{div}(\boldsymbol{\sigma}) + \mathbf{f} = \mathbf{0} \quad (5.51)$$

Any other validation more then checking the visual smoothness and convergence

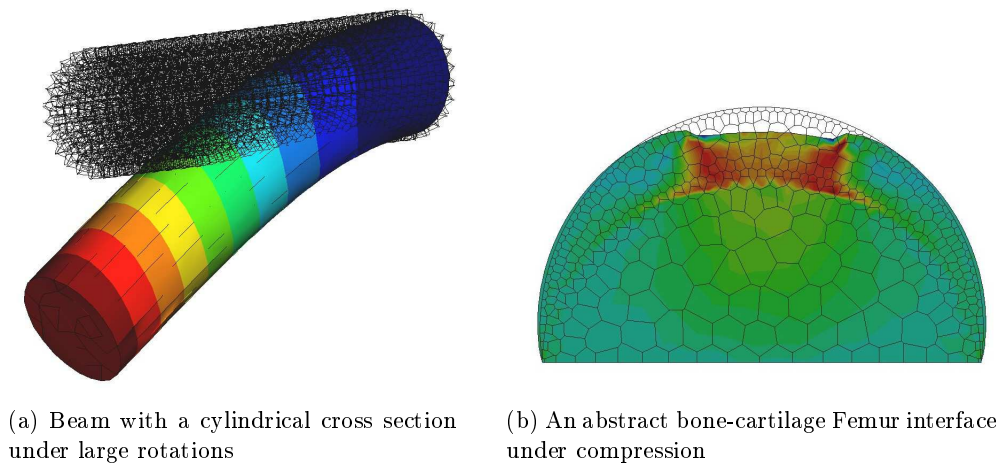


Figure 5.15: Two solutions of linear momentum equation for large deformations, considering geometrical nonlinear effects only

characteristics of examples similar to *Figure 5.15* are not performed for this treatise. To approach the final destination, an additional check for the correct evaluation of the curvature vector can be performed as well. For this purpose, a beam structure clamped on both sides



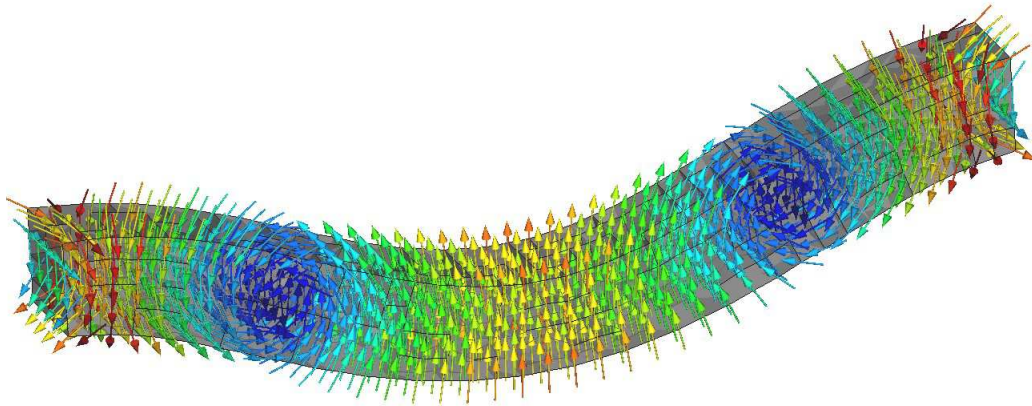


Figure 5.16: Bending directions as curvature vortexes of a beam.

loaded in the middle is taken as a candidate. The vector plot of *Figure 5.16* is quite satisfying and consistent with the anticipation. After getting all the necessary kinematic quantities ready, a more realistic example can be taken for comparison of different reorientation manifests. For the geometry a cartilage-like geometry in *Figure 5.17*, suffusing a spherical rigid grounding which represents the bone-cartilage interface, is constructed. For imposing the essential boundary conditions, an analytic-plate against cartilage model is taken for the contact implementation. As stated previously, particle based methods -NEM being one of

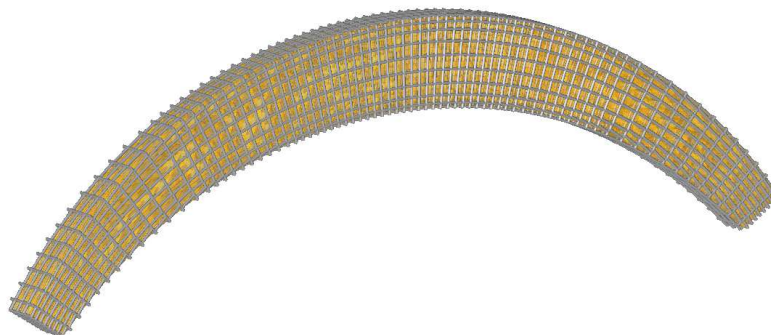


Figure 5.17: Constrained 3d Voronoi diagramm of the described cartilage-like geometry

them- can be alternatively quite attractive if it comes to the point of simulating challenging actions, contact being one of them. In the case of NEM, the evaluation of the contact search algorithms is significantly easier than FEM, as done in the first chapter of modeling AC as biphasic media. The nodal normals can be very uniquely and easily determined by summing up the polyhedral surface normals and inverting it. Accordingly, the current normal of the node can be very efficiently determined by applying Piola transformation or Nanson's

formula at <sup>8</sup> that location of interest. Accordingly, any complex contact formulation of penalty methods or Lagrangian multiplier methods can be applied for constraining the penetration of the surfaces. As can be seen from the *Figure 5.18*, the contact search in between an analytical surface and the cartilage-like plane strain system performs notably well. From the bottom picture of the *Figure 5.18* it can be concluded that the isotropic

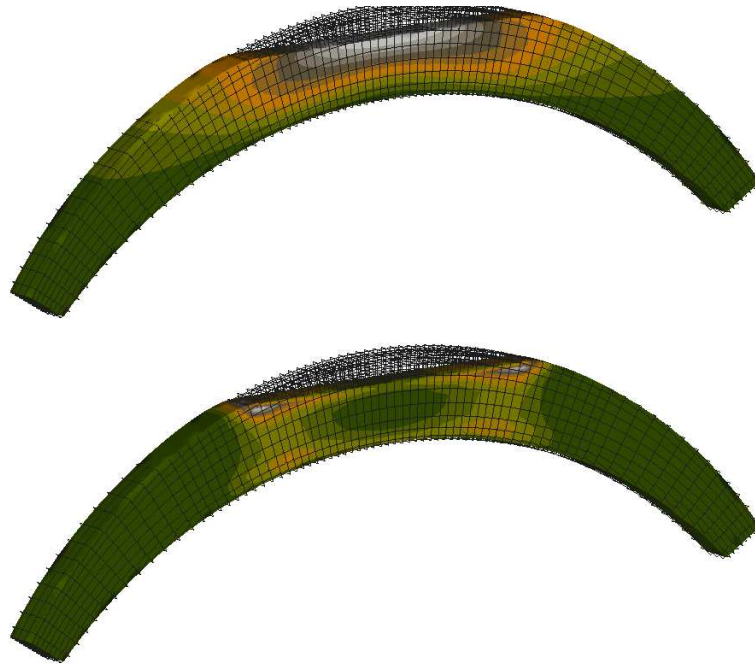


Figure 5.18: Top: Displacement result of plate cartilage contact. Bottom: Distribution of Isotropic strain gradient energy  $\mathbf{G} : \mathbf{G}$ .

strain energy is dominated under the loading surface, and propagating from middle to contact free zones. This monolithic increase can be observed by giving a look to the vortex development (*Figure 5.19*) through the history of the deformation. Based on this

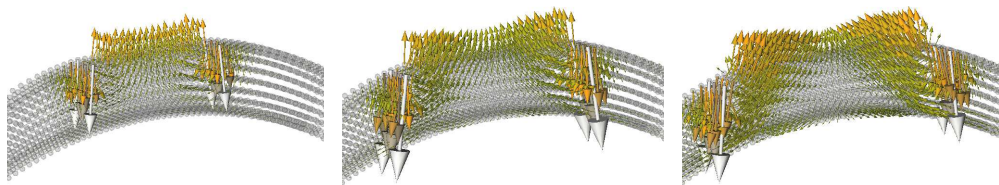


Figure 5.19: Development of  $\mathbf{G} : \hat{\mathbf{E}}_1^{\otimes 2}$  from the beginning, intermediate to the final stage of the imposed boundary condition.

<sup>8</sup>For natural element methods, remember that the nodes and evaluation points are overlapping

investigations and comments in hand, one can move into comparing the different types of reorientation manifests introduced in the previous chapter.

## 5.5 Comparison of Different Reorientation Manifests

In this final section a rough comparison in between the proposed reorientation manifests are compared on cartilage-alike plane strain scenario. The compared reorientation manifests are namely, the strain driven, curvature driven and the one which maximizes the Euler-Bernoulli type of material model, which is introduced in the chapter of Hyperbalance equations. The details about the manifests and their consistency can be checked by giving a look to the chapter of reorientation with strain and gradient effects.

The final results are presented in *Figure 5.20*. The first one is the result of reorientation with pure strain effects, second one as the maximization of simple curvature, and the third one as being maximizing combined stretch-bending effects.

The first result differs significantly from the one presented in the chapter of reorientation, even though the manifest is kept to be same. The reason beyond is obviously the given boundary conditions, in the previous one plane stress type of assumption is made, in the latter one plane strain assumption is used. The previous one giving accordingly tangential reorientations under the loading path through the depth, and perpendicular in the depth zone and parallel to the superficial zone away from the application of load. The current one which is presented here in the first *Figure* of *5.20* however, gives almost perpendicular type of fibers in the overall structure, which is certainly not representing the reality.

The second manifest with maximizing the curvature on the other side, suggests partially tangential fiber orientations on the surface, especially at the locations of contact release, as commented previously on *Figure 5.19*. This manifest was however suggested to be a work-around, but served practical advantages, like semi-analytical reorientation, developed analogous to the strain driven reorientation.

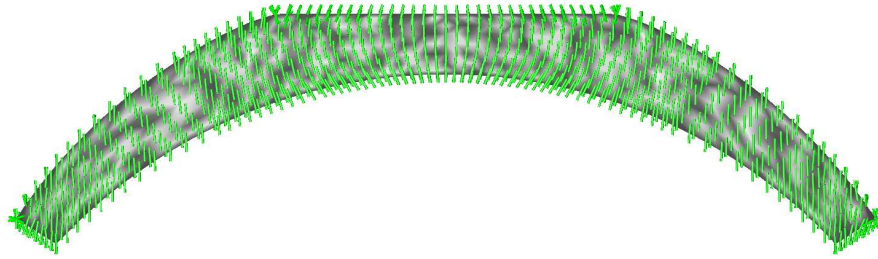
The third one represents the fiber orientation at the depth zone of the contact region nicely. The superficial zone and the depth zone far away the loading are captured the reality as well, as being tangential on the surface and perpendicular towards to the bone interface. The superficial zone beneath the contact interface however leads perpendicular fiber to the surface, which is the only drawback of the bending and stretch type combined reorientation manifest.

Based on these objective interpretations, several comments can be done. First the modeling artifacts should be taken under consideration. The flat punching or pressing the surface follows the assumption of that the master and slave bodies have almost comparable stiffness values. The other approach applied for the case of plane stress in the chapter of reorientation with strain and strain gradient effects, did not follow this assumption, thus only consistent nodal type of forces are applied. On the other side, the contact formulation presented in the first chapter of cartilage as biphasic media, took the geometry of the master surface into account, but not the stiffness. The modeling artifacts, and variations around those artifacts

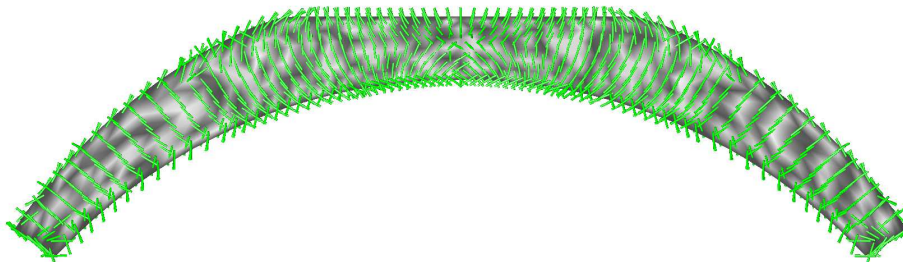
are a common problem in nonlinear mechanics, and leads in the absence of experimental evidence mostly to speculations.

A final and quite crucial comment can be done around the fundamental philosophy of the reorientation in this context. One can never assure that the tissue in the microlevel tries hard to improve the macroscopic mechanical properties. Besides, those macroscopic properties can not be always reduced to stiffness, or compliance. As experimentally evident, articular cartilage has the principle functionality of minimizing the tangential surface resistance in between two load carriers. This might be achieved by swelling, but in which rate and under which circumstances is still an unknown parameter. In short, the biological structure is extremely complicated, and one can only accumulate information segmentally, as tried to be done in this treatise. By learning this, the writer of the thesis has consciously avoided to reach solid statements, which can lead the reader under doubt, discourage or conduct generally wrong, specifically correct informations.

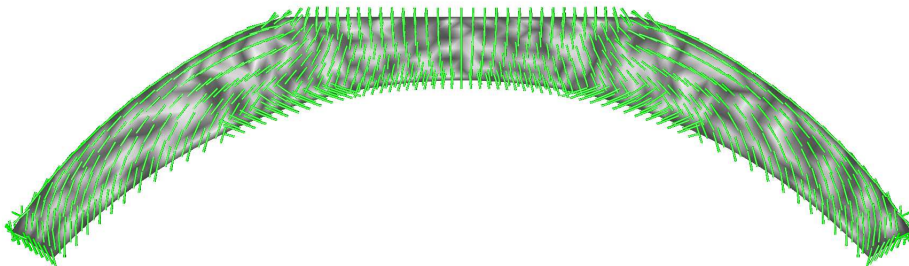
One clear statement is, that any improvement, novel formulation presented in this section had been shown to impact on the material properties and the remodeling manifests. Without specifically claiming one is better then the other one, it is but clear that, strain gradient effects do have an effect on reorientation.



(a) Strain based reorientation



(b) Curvature based reorientation



(c) Strain and strain gradient based reorientation

Figure 5.20: Comparisons of different reorientation manifests

# Summary

---

## Contents

---

<b>6.1</b>	<b>Introduction</b>	<b>153</b>
<b>6.2</b>	<b>Least Requirements</b>	<b>153</b>
<b>6.3</b>	<b>Hyperelasticity</b>	<b>154</b>
<b>6.4</b>	<b>Functional Adaptation, Abnormal Cell Growth</b>	<b>154</b>
<b>6.5</b>	<b>Methodical Development</b>	<b>155</b>

---

## 6.1 Introduction

This conclusion refers to the German word to *Zusammenfassung*, rather than *Fazit*, where the previous one represents a kind of summary, and the latter one refers to a solid upshot. Since the field of Biomechanics as a branch of continuum mechanics is actively developed, any concrete statement is avoided on purpose. In the ongoing subsections of this conclusion, the outcomes of the individual chapters of this work will be linked to each other, and some necessary brief interpretations will be summarized.

## 6.2 Least Requirements

One may find many recent PhD publications, where a long repetition of the generically accepted theory of continuum mechanics are presented as fundamental or as introduction. As in many others, this work takes advantage of the tradition, however in a one-step-front philosophy is still reconsidered.

The first chapter deals with the most simple formulation of bi-phasic media, presented by means of cited publications in the corresponding places of the chapter. According to the results given, namely the representative scenario of the tumor growth and the vertically loaded Articular cartilage do demonstrate the power and difference of using multiphase approach against the single-solid phase approach. To list it, the advantages may be listed as follows.

- Mixed field approach gives the opportunity to determine the manifests for solid and fluid phases of material, irrespective and independent of each other.
- Mixed field approach gives the opportunity to determine the respective effects of individual components, such as permeability

- The numerical effort for both programming and computing are comparable with one-phase approach
- Most of the Biological components are of multi-phase composites, thus the approach is realistic per definition, and more rational than empirical models based on viscoelasticity.

There are many ways of fulfilling this *least requirements*, in this work the re-introduction of bi-phase material formulation and numerics considered and shown to be sufficient.

### 6.3 Hyperelasticity

As stated above, the least requirement is considered to be necessary, however not sufficient for improvement. In this concern, in between the fundamental necessity and the superior limit, there are enough topics which worth to investigate. Hyperelasticity is considered to be one of them. As stated in the corresponding chapter, the Hyperelasticity should follow a fully developed *motion* of the Mechanic, namely Hyperkinematics. Accordingly, the work about Hyperkinematics can lead into these conclusions;

- Higher order terms in Kinematic motion do present, or existentially as natural as lower order terms (This is a biconditional statement)
- Higher order terms in Kinematic is taken into account in relatively older theories (Shell theory: Curvature dependent Energy terms Ref.[[Bischoff 2004](#)])
- Any objective function of the natural minimization processes may be triggered by higher order effects

The last claim is hard to prove, and equally hard to disprove. For comprehensive discussion of this argument, please visit the previous conclusion on this topic, namely Ch.[5.5]. However the difference in the presence and the absence of these higher order kinematic and thus elastic effects can be demonstrated. But first, a mathematically consistent framework for the theory is to be developed. This is partially done during the preparation of this work. The chapters Ch.[2] and Ch.[3] deal only with the specific topics concerning the higher order effects, and try to clarify the arising questions in a novel way.

### 6.4 Functional Adaptation, Abnormal Cell Growth

It is of crucial interest to understand the intermediate objective function beyond functional adaptation and abnormal cell growth. The better understanding brings one to the next practical step, estimating the time, the volume and the ongoing consequences. For this purpose, theoretically consistent growth models are postulated, which can be related to empirical observations of phenomena. As usual in the phenomenological theory, not enough attention might be paid into the fundamental significance Ref.[[Thewlis 1973](#)]. For practical purposes again, the intermediate significance might be of the main purpose. Any design of experiment can be performed to feed new parameters to broaden and deepen the number of significant figures into the list of parameters.

In this work, it has been shown that,

- For the generated geometry and boundary conditions, the existing remodeling algorithms do not always reveal the expected final form of evolution (thus of functional adaptation)
- For the generated geometry and boundary conditions, functional adaptation with higher order Kinematics does an effect on the solution, thus may play a role in metamorphosis

Which may mean that the generated geometry and boundary conditions do not represent the reality, or represent the main trigger of evolution. However, as method of design of experiments states, locking this discussion (geometry & BC) as unchanged, the effects caused by the higher order kinematics are still undeniable.

Apart from this short conclusion, an emphasis has been made on the importance of providing the abstract system with clear boundary conditions. Therefore, there is the attempt of deterministic way of growth is presented in the theory of porous media section. In this model, the hot points were predetermined (which can be provided by means of experimentation), and the empirical model and its consistency with the reality can be verified from this approach. This verification is not covered in this work.

## 6.5 Methodical Development

The methodical developments are generally done, in order to generally improve computation power in saving physical space and gaining speed. In the field of Biomechanics, if the developed method is generally accepted to be revealing pragmatic results, especially for patient specific applications, these types of developments are expected to be done. In this branch, one can give numerous works as examples.

Even though Finite Element Method has been the most widely used method of solving partial differential equations, there are countably many methods are still finding their fields of application. The obvious reason beyond this is the fact that, each individual method has its own core area, where no other can be as fast or as reliable. Among them, Natural Element Method has the advantage of solving a domain of a problem, which defined as a point cloud. This possibility enables one to omit the generation of the geometry, thus any raw data can be prepared directly ready for computation. The primary reason of developing Natural Element Solver is to serve this purpose. The indirect aim is to feedback to the field of computational mechanics. This is also done in this thesis, for instance by developing the non-sequential nodal integration technique, which is not of primary importance for Biomechanical applications. Those kind of side-outcomes shows a new perspective for the field of computational mechanics.





# Appendix A

## Contents

<b>A.1 The derivatives of the spiral beam . . . . .</b>	<b>157</b>
---	------------

### A.1 The derivatives of the spiral beam

Starting from this point, the derivatives for the spiral example will be given here in detail. The spiral beam has mainly two parts, namely mid surface and the thickness contribution,

$$\begin{aligned} x_1^m &= \left[ \frac{2\alpha}{\pi} \cos \left( (1 - X_1) \frac{\pi}{2} \right) + \left( 1 - \frac{2\alpha}{\pi} \right) X_1 \right] \cos(\alpha + \alpha X_1) \\ x_2^m &= \left[ \frac{2\alpha}{\pi} \cos \left( (1 - X_1) \frac{\pi}{2} \right) + \left( 1 - \frac{2\alpha}{\pi} \right) X_1 \right] \sin(\alpha + \alpha X_1) \end{aligned} \quad (\text{A.1})$$

For the thickness contribution, the Piola transformation of the derivatives of the mid curve is taken into account. These mid-curve-off contributions are called to be deviatoric, and depending on the derivatives of the mid-curve.

$$\begin{aligned} x_1^d &= \frac{\partial x_2}{\partial X_1} \Big|_m X_2 \left( \left( \frac{\partial x_1}{\partial X_1} \Big|_m \right)^2 + \left( \frac{\partial x_2}{\partial X_1} \Big|_m \right)^2 \right)^{-1/2} \\ x_2^d &= - \frac{\partial x_1}{\partial X_1} \Big|_m X_2 \left( \left( \frac{\partial x_1}{\partial X_1} \Big|_m \right)^2 + \left( \frac{\partial x_2}{\partial X_1} \Big|_m \right)^2 \right)^{-1/2} \end{aligned} \quad (\text{A.2})$$

These contributions will cause nonlinear Bernoulli kinematics, since the curvature through the thickness is punished by the constant coefficient of  $X_2$ . Additionally the strain gradient effects through the thickness are neglected. The total mapping is then,

$$\begin{aligned} x_1 &= x_1^m + x_1^d \\ x_2 &= x_2^m + x_2^d \end{aligned} \quad (\text{A.3})$$

The following derivatives are required,

$$\begin{aligned} \frac{\partial x_1^m}{\partial X_1} \quad \frac{\partial x_2^m}{\partial X_1} \quad \frac{\partial^2 x_1^m}{(\partial X_1)^2} \quad \frac{\partial^2 x_2^m}{(\partial X_1)^2} \\ \frac{\partial x_1^d}{\partial X_1} \quad \frac{\partial x_2^d}{\partial X_1} \quad \frac{\partial^2 x_1^d}{(\partial X_1)^2} \quad \frac{\partial^2 x_1^d}{(\partial X_2)^2} \quad \frac{\partial^2 x_1^d}{\partial X_1 \partial X_2} \quad \frac{\partial^2 x_2^d}{\partial X_1 \partial X_2} \end{aligned} \quad (\text{A.4})$$

First the first four set of derivatives will be given,

$$\begin{aligned} \frac{\partial x_1^m}{\partial X_1} &= \left[ \alpha \sin \left( (1 - X_1) \frac{\pi}{2} \right) + \left( 1 - \frac{2\alpha}{\pi} \right) \right] \cos(\alpha + \alpha X_1) \\ &\quad - \alpha \left[ \frac{2\alpha}{\pi} \cos \left( (1 - X_1) \frac{\pi}{2} \right) + \left( 1 - \frac{2\alpha}{\pi} \right) X_1 \right] \sin(\alpha + \alpha X_1) \end{aligned} \quad (\text{A.5a})$$

$$\begin{aligned} \frac{\partial x_2^m}{\partial X_1} &= \left[ \alpha \sin \left( (1 - X_1) \frac{\pi}{2} \right) + \left( 1 - \frac{2\alpha}{\pi} \right) \right] \sin(\alpha + \alpha X_1) \\ &\quad + \alpha \left[ \frac{2\alpha}{\pi} \cos \left( (1 - X_1) \frac{\pi}{2} \right) + \left( 1 - \frac{2\alpha}{\pi} \right) X_1 \right] \cos(\alpha + \alpha X_1) \end{aligned} \quad (\text{A.5b})$$

The second derivatives of the first set,

$$\begin{aligned} \frac{\partial^2 x_1^m}{(\partial X_1)^2} &= -\alpha \frac{\pi}{2} \cos \left( (1 - X_1) \frac{\pi}{2} \right) \cos(\alpha + \alpha X_1) \\ &\quad - 2\alpha \left[ \alpha \sin \left( (1 - X_1) \frac{\pi}{2} \right) + \left( 1 - \frac{2\alpha}{\pi} \right) \right] \sin(\alpha + \alpha X_1) \\ &\quad - \alpha^2 \left[ \frac{2\alpha}{\pi} \cos \left( (1 - X_1) \frac{\pi}{2} \right) + \left( 1 - \frac{2\alpha}{\pi} \right) X_1 \right] \cos(\alpha + \alpha X_1) \end{aligned} \quad (\text{A.6a})$$

$$\begin{aligned} \frac{\partial^2 x_2^m}{(\partial X_1)^2} &= -\alpha \frac{\pi}{2} \cos \left( (1 - X_1) \frac{\pi}{2} \right) \sin(\alpha + \alpha X_1) \\ &\quad + 2\alpha \left[ \alpha \sin \left( (1 - X_1) \frac{\pi}{2} \right) + \left( 1 - \frac{2\alpha}{\pi} \right) \right] \cos(\alpha + \alpha X_1) \\ &\quad - \alpha^2 \left[ \frac{2\alpha}{\pi} \cos \left( (1 - X_1) \frac{\pi}{2} \right) + \left( 1 - \frac{2\alpha}{\pi} \right) X_1 \right] \sin(\alpha + \alpha X_1) \end{aligned} \quad (\text{A.6b})$$

The second set requires a little more operations,

$$\begin{aligned} \frac{\partial x_1^d}{\partial X_1} &= \frac{\partial}{\partial X_1} \left( \left. \frac{\partial x_2}{\partial X_1} \right|_m \right) X_2 \left( \left( \left. \frac{\partial x_1}{\partial X_1} \right|_m \right)^2 + \left( \left. \frac{\partial x_2}{\partial X_1} \right|_m \right)^2 \right)^{-1/2} \\ &\quad - \left. \frac{\partial x_2}{\partial X_1} \right|_m X_2 \left( \left( \left. \frac{\partial x_1}{\partial X_1} \right|_m \right)^2 + \left( \left. \frac{\partial x_2}{\partial X_1} \right|_m \right)^2 \right)^{-3/2} \left. \frac{\partial x_1}{\partial X_1} \right|_m \frac{\partial}{\partial X_1} \left( \left. \frac{\partial x_1}{\partial X_1} \right|_m \right) \\ &\quad - \left. \frac{\partial x_2}{\partial X_1} \right|_m X_2 \left( \left( \left. \frac{\partial x_1}{\partial X_1} \right|_m \right)^2 + \left( \left. \frac{\partial x_2}{\partial X_1} \right|_m \right)^2 \right)^{-3/2} \left. \frac{\partial x_2}{\partial X_1} \right|_m \frac{\partial}{\partial X_1} \left( \left. \frac{\partial x_2}{\partial X_1} \right|_m \right) \end{aligned} \quad (\text{A.7})$$

$$\begin{aligned}
\frac{\partial x_2^d}{\partial X_1} &= -\frac{\partial}{\partial X_1} \left( \frac{\partial x_1}{\partial X_1} \Big|_m \right) X_2 \left( \left( \frac{\partial x_1}{\partial X_1} \Big|_m \right)^2 + \left( \frac{\partial x_2}{\partial X_1} \Big|_m \right)^2 \right)^{-1/2} \\
&+ \frac{\partial x_1}{\partial X_1} \Big|_m X_2 \left( \left( \frac{\partial x_1}{\partial X_1} \Big|_m \right)^2 + \left( \frac{\partial x_2}{\partial X_1} \Big|_m \right)^2 \right)^{-3/2} \frac{\partial x_1}{\partial X_1} \Big|_m \frac{\partial}{\partial X_1} \left( \frac{\partial x_1}{\partial X_1} \Big|_m \right) \quad (\text{A.8}) \\
&+ \frac{\partial x_1}{\partial X_1} \Big|_m X_2 \left( \left( \frac{\partial x_1}{\partial X_1} \Big|_m \right)^2 + \left( \frac{\partial x_2}{\partial X_1} \Big|_m \right)^2 \right)^{-3/2} \frac{\partial x_2}{\partial X_1} \Big|_m \frac{\partial}{\partial X_1} \left( \frac{\partial x_2}{\partial X_1} \Big|_m \right)
\end{aligned}$$

From time being the following replacement holds,

$$\left( \frac{\partial x_1}{\partial X_1} \Big|_m \right)^2 + \left( \frac{\partial x_2}{\partial X_1} \Big|_m \right)^2 = r \quad (\text{A.9})$$

The derivatives of this replacement are,

$$\frac{\partial r}{\partial X_1} = 2 \frac{\partial x_1}{\partial X_1} \Big|_m \frac{\partial}{\partial X_1} \left( \frac{\partial x_1}{\partial X_1} \Big|_m \right) + 2 \frac{\partial x_2}{\partial X_1} \Big|_m \frac{\partial}{\partial X_1} \left( \frac{\partial x_2}{\partial X_1} \Big|_m \right) \quad (\text{A.10a})$$

$$\begin{aligned}
\frac{\partial^2 r}{(\partial X_1)^2} &= 2 \left( \frac{\partial}{\partial X_1} \left( \frac{\partial x_1}{\partial X_1} \Big|_m \right) \right)^2 + 2 \frac{\partial x_1}{\partial X_1} \Big|_m \frac{\partial^2}{(\partial X_1)^2} \left( \frac{\partial x_1}{\partial X_1} \Big|_m \right) \\
&+ 2 \left( \frac{\partial}{\partial X_1} \left( \frac{\partial x_2}{\partial X_1} \Big|_m \right) \right)^2 + 2 \frac{\partial x_2}{\partial X_1} \Big|_m \frac{\partial^2}{(\partial X_1)^2} \left( \frac{\partial x_2}{\partial X_1} \Big|_m \right) \quad (\text{A.10b})
\end{aligned}$$

with this replacement the first derivatives of the second set become,

$$\frac{\partial x_1^d}{\partial X_1} = \frac{\partial}{\partial X_1} \left( \frac{\partial x_2}{\partial X_1} \Big|_m \right) X_2 r^{-1/2} - \frac{1}{2} \frac{\partial x_2}{\partial X_1} \Big|_m X_2 r^{-3/2} \frac{\partial r}{\partial X_1} \quad (\text{A.11a})$$

$$\frac{\partial x_2^d}{\partial X_1} = -\frac{\partial}{\partial X_1} \left( \frac{\partial x_1}{\partial X_1} \Big|_m \right) X_2 r^{-1/2} + \frac{1}{2} \frac{\partial x_1}{\partial X_1} \Big|_m X_2 r^{-3/2} \frac{\partial r}{\partial X_1} \quad (\text{A.11b})$$

$$\frac{\partial x_1^d}{\partial X_2} = \frac{\partial x_2}{\partial X_1} \Big|_m r^{-1/2} \quad (\text{A.11c})$$

$$\frac{\partial x_2^d}{\partial X_2} = -\frac{\partial x_1}{\partial X_1} \Big|_m r^{-1/2} \quad (\text{A.11d})$$

The second derivatives are,

$$\begin{aligned} \frac{\partial^2 x_1^d}{(\partial X_1)^2} &= \frac{\partial^2}{(\partial X_1)^2} \left( \frac{\partial x_2}{\partial X_1} \Big|_m \right) X_2 r^{-1/2} - \frac{1}{2} \frac{\partial}{\partial X_1} \left( \frac{\partial x_2}{\partial X_1} \Big|_m \right) X_2 r^{-3/2} \frac{\partial r}{\partial X_1} \\ &\quad - \frac{1}{2} \frac{\partial}{\partial X_1} \left( \frac{\partial x_2}{\partial X_1} \Big|_m \right) X_2 r^{-3/2} \frac{\partial r}{\partial X_1} + \frac{3}{4} \frac{\partial x_2}{\partial X_1} \Big|_m X_2 r^{-5/2} \left( \frac{\partial r}{\partial X_1} \right)^2 \\ &\quad - \frac{1}{2} \frac{\partial x_2}{\partial X_1} \Big|_m X_2 r^{-3/2} \frac{\partial^2 r}{(\partial X_1)^2} \end{aligned} \quad (\text{A.12a})$$

$$\begin{aligned} \frac{\partial^2 x_2^d}{(\partial X_1)^2} &= - \frac{\partial^2}{(\partial X_1)^2} \left( \frac{\partial x_1}{\partial X_1} \Big|_m \right) X_2 r^{-1/2} + \frac{1}{2} \frac{\partial}{\partial X_1} \left( \frac{\partial x_1}{\partial X_1} \Big|_m \right) X_2 r^{-3/2} \frac{\partial r}{\partial X_1} \\ &\quad + \frac{1}{2} \frac{\partial}{\partial X_1} \left( \frac{\partial x_1}{\partial X_1} \Big|_m \right) X_2 r^{-3/2} \frac{\partial r}{\partial X_1} - \frac{3}{4} \frac{\partial x_1}{\partial X_1} \Big|_m X_2 r^{-5/2} \left( \frac{\partial r}{\partial X_1} \right)^2 \\ &\quad + \frac{1}{2} \frac{\partial x_1}{\partial X_1} \Big|_m X_2 r^{-3/2} \frac{\partial^2 r}{(\partial X_1)^2} \end{aligned} \quad (\text{A.12b})$$

And the mixed second derivatives of the last set are,

$$\frac{\partial^2 x_1^d}{\partial X_2 \partial X_1} = \frac{\partial}{\partial X_1} \left( \frac{\partial x_2}{\partial X_1} \Big|_m \right) r^{-1/2} - \frac{1}{2} \frac{\partial x_2}{\partial X_1} \Big|_m r^{-3/2} \frac{\partial r}{\partial X_1} \quad (\text{A.13a})$$

$$\frac{\partial^2 x_2^d}{\partial X_2 \partial X_1} = - \frac{\partial}{\partial X_1} \left( \frac{\partial x_1}{\partial X_1} \Big|_m \right) r^{-1/2} + \frac{1}{2} \frac{\partial x_1}{\partial X_1} \Big|_m r^{-3/2} \frac{\partial r}{\partial X_1} \quad (\text{A.13b})$$

The mid-curve correlation and the first derivative of the mid-curve was in fact given before,

$$\begin{aligned} \frac{\partial x_1}{\partial X_1} \Big|_m &= \left[ \alpha \sin \left( (1 - X_1) \frac{\pi}{2} \right) + \left( 1 - \frac{2\alpha}{\pi} \right) \right] \cos(\alpha + \alpha X_1) \\ &\quad - \alpha \left[ \frac{2\alpha}{\pi} \cos \left( (1 - X_1) \frac{\pi}{2} \right) + \left( 1 - \frac{2\alpha}{\pi} \right) X_1 \right] \sin(\alpha + \alpha X_1) \end{aligned} \quad (\text{A.14a})$$

$$\begin{aligned} \frac{\partial x_2}{\partial X_1} \Big|_m &= \left[ \alpha \sin \left( (1 - X_1) \frac{\pi}{2} \right) + \left( 1 - \frac{2\alpha}{\pi} \right) \right] \sin(\alpha + \alpha X_1) \\ &\quad + \alpha \left[ \frac{2\alpha}{\pi} \cos \left( (1 - X_1) \frac{\pi}{2} \right) + \left( 1 - \frac{2\alpha}{\pi} \right) X_1 \right] \cos(\alpha + \alpha X_1) \end{aligned} \quad (\text{A.14b})$$

The first derivatives of this correlation are

$$\begin{aligned} \frac{\partial}{\partial X_1} \left( \frac{\partial x_1}{\partial X_1} \Big|_m \right) &= -\alpha \frac{\pi}{2} \cos \left( (1 - X_1) \frac{\pi}{2} \right) \cos(\alpha + \alpha X_1) \\ &\quad - 2\alpha \left[ \alpha \sin \left( (1 - X_1) \frac{\pi}{2} \right) + \left( 1 - \frac{2\alpha}{\pi} \right) \right] \sin(\alpha + \alpha X_1) \quad (\text{A.15a}) \\ &\quad - \alpha^2 \left[ \frac{2\alpha}{\pi} \cos \left( (1 - X_1) \frac{\pi}{2} \right) + \left( 1 - \frac{2\alpha}{\pi} \right) X_1 \right] \cos(\alpha + \alpha X_1) \end{aligned}$$

$$\begin{aligned} \frac{\partial}{\partial X_1} \left( \frac{\partial x_2}{\partial X_1} \Big|_m \right) &= -\alpha \frac{\pi}{2} \cos \left( (1 - X_1) \frac{\pi}{2} \right) \sin(\alpha + \alpha X_1) \\ &\quad + 2\alpha \left[ \alpha \sin \left( (1 - X_1) \frac{\pi}{2} \right) + \left( 1 - \frac{2\alpha}{\pi} \right) \right] \cos(\alpha + \alpha X_1) \quad (\text{A.15b}) \\ &\quad - \alpha^2 \left[ \frac{2\alpha}{\pi} \cos \left( (1 - X_1) \frac{\pi}{2} \right) + \left( 1 - \frac{2\alpha}{\pi} \right) X_1 \right] \sin(\alpha + \alpha X_1) \end{aligned}$$

And finally the second derivatives of this expression is,

$$\begin{aligned}
\frac{\partial^2}{(\partial X_1)^2} \left( \frac{\partial x_1}{\partial X_1} \Big|_m \right) &= -\alpha \frac{\pi^2}{4} \sin \left( (1 - X_1) \frac{\pi}{2} \right) \cos(\alpha + \alpha X_1) \\
&+ \alpha^2 \frac{\pi}{2} \cos \left( (1 - X_1) \frac{\pi}{2} \right) \sin(\alpha + \alpha X_1) \\
&+ 2\alpha^2 \frac{\pi}{2} \cos \left( (1 - X_1) \frac{\pi}{2} \right) \sin(\alpha + \alpha X_1) \\
&- 2\alpha^2 \left[ \alpha \sin \left( (1 - X_1) \frac{\pi}{2} \right) + \left( 1 - \frac{2\alpha}{\pi} \right) \right] \cos(\alpha + \alpha X_1) \\
&- \alpha^2 \left[ \alpha \sin \left( (1 - X_1) \frac{\pi}{2} \right) + \left( 1 - \frac{2\alpha}{\pi} \right) \right] \cos(\alpha + \alpha X_1) \\
&+ \alpha^3 \left[ \frac{2\alpha}{\pi} \cos \left( (1 - X_1) \frac{\pi}{2} \right) + \left( 1 - \frac{2\alpha}{\pi} \right) X_1 \right] \sin(\alpha + \alpha X_1)
\end{aligned} \tag{A.16a}$$

$$\begin{aligned}
\frac{\partial^2}{(\partial X_1)^2} \left( \frac{\partial x_2}{\partial X_1} \Big|_m \right) &= -\alpha \frac{\pi^2}{4} \sin \left( (1 - X_1) \frac{\pi}{2} \right) \sin(\alpha + \alpha X_1) \\
&- \alpha^2 \frac{\pi}{2} \cos \left( (1 - X_1) \frac{\pi}{2} \right) \cos(\alpha + \alpha X_1) \\
&- 2\alpha^2 \frac{\pi}{2} \cos \left( (1 - X_1) \frac{\pi}{2} \right) \cos(\alpha + \alpha X_1) \\
&- 2\alpha^2 \left[ \alpha \sin \left( (1 - X_1) \frac{\pi}{2} \right) + \left( 1 - \frac{2\alpha}{\pi} \right) \right] \sin(\alpha + \alpha X_1) \\
&- \alpha^2 \left[ \alpha \sin \left( (1 - X_1) \frac{\pi}{2} \right) + \left( 1 - \frac{2\alpha}{\pi} \right) \right] \sin(\alpha + \alpha X_1) \\
&- \alpha^3 \left[ \frac{2\alpha}{\pi} \cos \left( (1 - X_1) \frac{\pi}{2} \right) + \left( 1 - \frac{2\alpha}{\pi} \right) X_1 \right] \cos(\alpha + \alpha X_1)
\end{aligned} \tag{A.16b}$$

# Appendix B

## Contents

**B.1 Bending Strain and Strain Gradient energy density Function . 163**

**B.2 Stretching Strain and Strain Gradient energy density Function 171**

## B.1 Bending Strain and Strain Gradient energy density Function

The bending energy formulation according to the bernoulli beam beam theory, requires the estimation of the radius of curvature as the other theories, The radius of curvature is taken to be common in sharp and flat length changes,

$$\sin(\alpha^{\sharp}) = \frac{|\mathbf{m}^{\sharp}|}{r} \quad \sin(\alpha^{\flat}) = \frac{|\mathbf{m}^{\flat}|}{r} \quad (\text{B.1})$$

In order to take both effects into account, the following estimation can be done,

$$\begin{aligned} c = r^{-1} &= \frac{\sin(\alpha^{\sharp}) + \sin(\alpha^{\flat})}{|\mathbf{m}^{\sharp}| + |\mathbf{m}^{\flat}|} \\ &= \frac{2\sin((\alpha^{\sharp} + \alpha^{\flat})/2) \cos((\alpha^{\sharp} - \alpha^{\flat})/2)}{|\mathbf{m}^{\sharp}| + |\mathbf{m}^{\flat}|} \\ &\approx \frac{2\sin((\alpha^{\sharp} + \alpha^{\flat})/2)}{|\mathbf{m}^{\sharp}| + |\mathbf{m}^{\flat}|} \end{aligned} \quad (\text{B.2})$$

With the following formulae for the bending energy,

$$\psi^{\kappa} = EIc^2 = EI \frac{4\sin^2((\alpha^{\sharp} + \alpha^{\flat})/2)}{(|\mathbf{m}^{\sharp}| + |\mathbf{m}^{\flat}|)^2} \approx EI \frac{(2 - 2\cos(\alpha^{\sharp} + \alpha^{\flat}))}{(|\mathbf{m}^{\sharp}| + |\mathbf{m}^{\flat}|)^2} \quad (\text{B.3})$$

The cosine of the rotation can be computed by,

$$\cos(\alpha^{\sharp} + \alpha^{\flat}) = \frac{(-\mathbf{m}^{\sharp} \cdot \mathbf{m}^{\flat})}{|\mathbf{m}^{\sharp}| |\mathbf{m}^{\flat}|} \quad (\text{B.4})$$



The minus sign indicates that the sharp tangent to be rotated. The members which are used to compute the invariants then,

$$\begin{aligned} -\mathbf{m}^\sharp &= \mathbf{F} \cdot \mathbf{M} - \frac{1}{2} \mathbf{G} : \mathbf{M}^{\otimes 2} \\ \mathbf{m}^\flat &= \mathbf{F} \cdot \mathbf{M} + \frac{1}{2} \mathbf{G} : \mathbf{M}^{\otimes 2} \end{aligned} \quad (\text{B.5})$$

Together with the definitions above and the introduced invariants, the following invariant formulation can be achieved,

$$\cos(\alpha^\sharp + \alpha^\flat) = \frac{(I_4^\kappa - 0.25I_6^\kappa)}{(I_4^\kappa - I_5^\kappa + 0.25I_6^\kappa)^{1/2} (I_4^\kappa + I_5^\kappa + 0.25I_6^\kappa)^{1/2}} \quad (\text{B.6})$$

For simplicity the following replacements are done,

$$\begin{aligned} \psi^\kappa &= xEI \frac{(2 - 2\cos(\alpha^\sharp + \alpha^\flat))}{(|\mathbf{m}^\sharp| + |\mathbf{m}^\flat|)^2} = EI \frac{2 - 2a}{|\mathbf{m}|^2} \\ a &= \cos(\alpha^\sharp + \alpha^\flat) = \frac{b}{d} \\ b &= (I_4^\kappa - 0.25I_6^\kappa) \\ d &= (I_4^\kappa - I_5^\kappa + 0.25I_6^\kappa)^{1/2} (I_4^\kappa + I_5^\kappa + 0.25I_6^\kappa)^{1/2} \\ |\mathbf{m}| &= (|\mathbf{m}^\sharp| + |\mathbf{m}^\flat|) \end{aligned} \quad (\text{B.7})$$

The first Piola Kirchoff Stress and Hyperstress depends on,

$$\begin{aligned} \mathbf{P}^\kappa &= \frac{\partial \psi^\kappa}{\partial \mathbf{F}} = -2EI \frac{\partial a}{\partial \mathbf{F}} |\mathbf{m}|^{-2} - 2EI |\mathbf{m}|^{-3} \frac{\partial |\mathbf{m}|}{\partial \mathbf{F}} (2 - 2a) \\ \mathbf{Q}^\kappa &= \frac{\partial \psi^\kappa}{\partial \mathbf{G}} = -2EI \frac{\partial a}{\partial \mathbf{G}} |\mathbf{m}|^{-2} - 2EI |\mathbf{m}|^{-3} \frac{\partial |\mathbf{m}|}{\partial \mathbf{G}} (2 - 2a) \end{aligned} \quad (\text{B.8})$$

The necessary three tangent terms are then,

$$\begin{aligned}
 \mathbf{D}_{\mathbf{F}}^{\mathbf{P}^\kappa} &= \frac{\partial \mathbf{P}^\kappa}{\partial \mathbf{F}} = -2EI \frac{\partial^2 a}{\partial \mathbf{F}^2} |\mathbf{m}|^{-2} + 4EI |\mathbf{m}|^{-3} \frac{\partial |\mathbf{m}|}{\partial \mathbf{F}} \otimes \frac{\partial a}{\partial \mathbf{F}} \\
 &+ 6EI |\mathbf{m}|^{-4} \frac{\partial |\mathbf{m}|}{\partial \mathbf{F}} \otimes \frac{\partial |\mathbf{m}|}{\partial \mathbf{F}} (2 - 2a) - 2EI |\mathbf{m}|^{-3} \frac{\partial^2 |\mathbf{m}|}{\partial \mathbf{F}^2} (2 - 2a) \\
 &+ 4EI |\mathbf{m}|^{-3} \frac{\partial a}{\partial \mathbf{F}} \otimes \frac{\partial |\mathbf{m}|}{\partial \mathbf{F}}
 \end{aligned} \tag{B.9a}$$

$$\begin{aligned}
 \mathbf{D}_{\mathbf{G}}^{\mathbf{P}^\kappa} &= \frac{\partial \mathbf{P}^\kappa}{\partial \mathbf{G}} = -2EI \frac{\partial^2 a}{\partial \mathbf{G} \partial \mathbf{F}} |\mathbf{m}|^{-2} + 4EI |\mathbf{m}|^{-3} \frac{\partial |\mathbf{m}|}{\partial \mathbf{G}} \otimes \frac{\partial a}{\partial \mathbf{F}} \\
 &+ 6EI |\mathbf{m}|^{-4} \frac{\partial |\mathbf{m}|}{\partial \mathbf{G}} \otimes \frac{\partial |\mathbf{m}|}{\partial \mathbf{F}} (2 - 2a) - 2EI |\mathbf{m}|^{-3} \frac{\partial^2 |\mathbf{m}|}{\partial \mathbf{G} \partial \mathbf{F}} (2 - 2a) \\
 &+ 4EI |\mathbf{m}|^{-3} \frac{\partial a}{\partial \mathbf{G}} \otimes \frac{\partial |\mathbf{m}|}{\partial \mathbf{F}}
 \end{aligned} \tag{B.9b}$$

$$\begin{aligned}
 \mathbf{D}_{\mathbf{G}}^{\mathbf{Q}^\kappa} &= \frac{\partial \mathbf{Q}^\kappa}{\partial \mathbf{G}} = -2EI \frac{\partial^2 a}{\partial \mathbf{G}^2} |\mathbf{m}|^{-2} + 4EI |\mathbf{m}|^{-3} \frac{\partial |\mathbf{m}|}{\partial \mathbf{G}} \otimes \frac{\partial a}{\partial \mathbf{G}} \\
 &+ 6EI |\mathbf{m}|^{-4} \frac{\partial |\mathbf{m}|}{\partial \mathbf{G}} \otimes \frac{\partial |\mathbf{m}|}{\partial \mathbf{G}} (2 - 2a) - 2EI |\mathbf{m}|^{-3} \frac{\partial^2 |\mathbf{m}|}{\partial \mathbf{G}^2} (2 - 2a) \\
 &+ 4EI |\mathbf{m}|^{-3} \frac{\partial a}{\partial \mathbf{G}} \otimes \frac{\partial |\mathbf{m}|}{\partial \mathbf{G}}
 \end{aligned} \tag{B.9c}$$

The necessary derivations should be introduced one by one,

$$a = \frac{b}{d} \quad \frac{\partial a}{\partial \mathbf{F}} \quad \frac{\partial a}{\partial \mathbf{G}} \quad \frac{\partial^2 a}{\partial \mathbf{F}^2} \quad \frac{\partial^2 a}{\partial \mathbf{G} \partial \mathbf{F}} \quad \frac{\partial^2 a}{\partial \mathbf{G}^2} \tag{B.10}$$

The derivatives in terms of the other values then,

$$\begin{aligned}
\frac{\partial a}{\partial \mathbf{F}} &= \frac{\partial b}{\partial \mathbf{F}} d^{-1} - d^{-2} b \frac{\partial d}{\partial \mathbf{F}} \\
\frac{\partial a}{\partial \mathbf{G}} &= \frac{\partial b}{\partial \mathbf{G}} d^{-1} - d^{-2} b \frac{\partial d}{\partial \mathbf{G}} \\
\frac{\partial^2 a}{\partial \mathbf{F}^2} &= \frac{\partial^2 b}{\partial \mathbf{F}^2} d^{-1} - d^{-2} \frac{\partial d}{\partial \mathbf{F}} \otimes \frac{\partial b}{\partial \mathbf{F}} \\
&\quad + 2d^{-3} b \frac{\partial d}{\partial \mathbf{F}} \otimes \frac{\partial d}{\partial \mathbf{F}} - d^{-2} \frac{\partial b}{\partial \mathbf{F}} \otimes \frac{\partial d}{\partial \mathbf{F}} - d^{-2} b \frac{\partial^2 d}{\partial \mathbf{F}^2} \\
\frac{\partial^2 a}{\partial \mathbf{G} \partial \mathbf{F}} &= \frac{\partial^2 b}{\partial \mathbf{G} \partial \mathbf{F}} d^{-1} - d^{-2} \frac{\partial d}{\partial \mathbf{G}} \otimes \frac{\partial b}{\partial \mathbf{F}} \\
&\quad + 2d^{-3} b \frac{\partial d}{\partial \mathbf{G}} \otimes \frac{\partial d}{\partial \mathbf{F}} - d^{-2} \frac{\partial b}{\partial \mathbf{G}} \otimes \frac{\partial d}{\partial \mathbf{F}} - d^{-2} b \frac{\partial^2 d}{\partial \mathbf{G} \partial \mathbf{F}} \\
\frac{\partial^2 a}{\partial \mathbf{G}^2} &= \frac{\partial^2 b}{\partial \mathbf{G}^2} d^{-1} - d^{-2} \frac{\partial d}{\partial \mathbf{G}} \otimes \frac{\partial b}{\partial \mathbf{G}} \\
&\quad + 2d^{-3} b \frac{\partial d}{\partial \mathbf{G}} \otimes \frac{\partial d}{\partial \mathbf{G}} - d^{-2} \frac{\partial b}{\partial \mathbf{G}} \otimes \frac{\partial d}{\partial \mathbf{G}} - d^{-2} b \frac{\partial^2 d}{\partial \mathbf{G}^2}
\end{aligned} \tag{B.11}$$

Accordingly the derivatives of the directly invariant dependent quantities should be evaluated either

$$b = (I_4^\kappa - 0.25 I_6^\kappa) \quad \frac{\partial b}{\partial \mathbf{F}} \quad \frac{\partial b}{\partial \mathbf{G}} \quad \frac{\partial^2 b}{\partial \mathbf{F}^2} \quad \frac{\partial^2 b}{\partial \mathbf{G} \partial \mathbf{F}} \quad \frac{\partial^2 b}{\partial \mathbf{G}^2} \tag{B.12}$$

The individual derivatives in terms of the invariant derivatives become,

$$\begin{aligned}
\frac{\partial b}{\partial \mathbf{F}} &= \left( \frac{\partial I_4^\kappa}{\partial \mathbf{F}} - 0.25 \frac{\partial I_6^\kappa}{\partial \mathbf{F}} \right) & \frac{\partial b}{\partial \mathbf{G}} &= \left( \frac{\partial I_4^\kappa}{\partial \mathbf{G}} - 0.25 \frac{\partial I_6^\kappa}{\partial \mathbf{G}} \right) \\
\frac{\partial^2 b}{\partial \mathbf{F}^2} &= \left( \frac{\partial^2 I_4^\kappa}{\partial \mathbf{F}^2} - 0.25 \frac{\partial^2 I_6^\kappa}{\partial \mathbf{F}^2} \right) \\
\frac{\partial^2 b}{\partial \mathbf{G} \partial \mathbf{F}} &= \left( \frac{\partial^2 I_4^\kappa}{\partial \mathbf{G} \partial \mathbf{F}} - 0.25 \frac{\partial^2 I_6^\kappa}{\partial \mathbf{G} \partial \mathbf{F}} \right) \\
\frac{\partial^2 b}{\partial \mathbf{G}^2} &= \left( \frac{\partial^2 I_4^\kappa}{\partial \mathbf{G}^2} - 0.25 \frac{\partial^2 I_6^\kappa}{\partial \mathbf{G}^2} \right)
\end{aligned} \tag{B.13}$$

The multiplicative change growth is necessary either

$$d = \left| \mathbf{m}^\# \right| \left| \mathbf{m}^b \right| \quad \frac{\partial d}{\partial \mathbf{F}} \quad \frac{\partial d}{\partial \mathbf{G}} \quad \frac{\partial^2 d}{\partial \mathbf{F}^2} \quad \frac{\partial^2 d}{\partial \mathbf{G} \partial \mathbf{F}} \quad \frac{\partial^2 d}{\partial \mathbf{G}^2} \tag{B.14}$$

The derivatives then,

$$\begin{aligned}
 \frac{\partial d}{\partial \mathbf{F}} &= \frac{\partial |\mathbf{m}^\sharp|}{\partial \mathbf{F}} |\mathbf{m}^\flat| + |\mathbf{m}^\sharp| \frac{\partial |\mathbf{m}^\flat|}{\partial \mathbf{F}} \\
 \frac{\partial d}{\partial \mathbf{G}} &= \frac{\partial |\mathbf{m}^\sharp|}{\partial \mathbf{G}} |\mathbf{m}^\flat| + |\mathbf{m}^\sharp| \frac{\partial |\mathbf{m}^\flat|}{\partial \mathbf{G}} \\
 \frac{\partial^2 d}{\partial \mathbf{F}^2} &= \frac{\partial^2 |\mathbf{m}^\sharp|}{\partial \mathbf{F}^2} |\mathbf{m}^\flat| + \frac{\partial |\mathbf{m}^\flat|}{\partial \mathbf{F}} \otimes \frac{\partial |\mathbf{m}^\sharp|}{\partial \mathbf{F}} + \frac{\partial |\mathbf{m}^\sharp|}{\partial \mathbf{F}} \otimes \frac{\partial |\mathbf{m}^\flat|}{\partial \mathbf{F}} + |\mathbf{m}^\sharp| \frac{\partial^2 |\mathbf{m}^\flat|}{\partial \mathbf{F}^2} \quad (\text{B.15}) \\
 \frac{\partial^2 d}{\partial \mathbf{G} \partial \mathbf{F}} &= \frac{\partial^2 |\mathbf{m}^\sharp|}{\partial \mathbf{G} \partial \mathbf{F}} |\mathbf{m}^\flat| + \frac{\partial |\mathbf{m}^\flat|}{\partial \mathbf{G}} \otimes \frac{\partial |\mathbf{m}^\sharp|}{\partial \mathbf{F}} + \frac{\partial |\mathbf{m}^\sharp|}{\partial \mathbf{G}} \otimes \frac{\partial |\mathbf{m}^\flat|}{\partial \mathbf{F}} + |\mathbf{m}^\sharp| \frac{\partial^2 |\mathbf{m}^\flat|}{\partial \mathbf{G} \partial \mathbf{F}} \\
 \frac{\partial^2 d}{\partial \mathbf{G}^2} &= \frac{\partial^2 |\mathbf{m}^\sharp|}{\partial \mathbf{G}^2} |\mathbf{m}^\flat| + \frac{\partial |\mathbf{m}^\flat|}{\partial \mathbf{G}} \otimes \frac{\partial |\mathbf{m}^\sharp|}{\partial \mathbf{G}} + \frac{\partial |\mathbf{m}^\sharp|}{\partial \mathbf{G}} \otimes \frac{\partial |\mathbf{m}^\flat|}{\partial \mathbf{G}} + |\mathbf{m}^\sharp| \frac{\partial^2 |\mathbf{m}^\flat|}{\partial \mathbf{G}^2}
 \end{aligned}$$

The total length change,

$$|\mathbf{m}| = |\mathbf{m}^\sharp| + |\mathbf{m}^\flat| \quad \frac{\partial |\mathbf{m}|}{\partial \mathbf{F}} \quad \frac{\partial |\mathbf{m}|}{\partial \mathbf{G}} \quad \frac{\partial^2 |\mathbf{m}|}{\partial \mathbf{F}^2} \quad \frac{\partial^2 |\mathbf{m}|}{\partial \mathbf{G} \partial \mathbf{F}} \quad \frac{\partial^2 |\mathbf{m}|}{\partial \mathbf{G}^2} \quad (\text{B.16})$$

The derivatives of the total length change,

$$\begin{aligned}
 \frac{\partial |\mathbf{m}|}{\partial \mathbf{F}} &= \frac{\partial |\mathbf{m}^\sharp|}{\partial \mathbf{F}} + \frac{\partial |\mathbf{m}^\flat|}{\partial \mathbf{F}} \\
 \frac{\partial |\mathbf{m}|}{\partial \mathbf{G}} &= \frac{\partial |\mathbf{m}^\sharp|}{\partial \mathbf{G}} + \frac{\partial |\mathbf{m}^\flat|}{\partial \mathbf{G}} \\
 \frac{\partial^2 |\mathbf{m}|}{\partial \mathbf{F}^2} &= \frac{\partial^2 |\mathbf{m}^\sharp|}{\partial \mathbf{F}^2} + \frac{\partial^2 |\mathbf{m}^\flat|}{\partial \mathbf{F}^2} \quad (\text{B.17}) \\
 \frac{\partial^2 |\mathbf{m}|}{\partial \mathbf{G} \partial \mathbf{F}} &= \frac{\partial^2 |\mathbf{m}^\sharp|}{\partial \mathbf{G} \partial \mathbf{F}} + \frac{\partial^2 |\mathbf{m}^\flat|}{\partial \mathbf{G} \partial \mathbf{F}} \\
 \frac{\partial^2 |\mathbf{m}|}{\partial \mathbf{G}^2} &= \frac{\partial^2 |\mathbf{m}^\sharp|}{\partial \mathbf{G}^2} + \frac{\partial^2 |\mathbf{m}^\flat|}{\partial \mathbf{G}^2}
 \end{aligned}$$

The first derivatives of the sharp fiber length change,

$$\begin{aligned}
 \frac{\partial |\mathbf{m}^\sharp|}{\partial \mathbf{F}} &= \frac{1}{2 [I_4^{EI} - I_5^{EI} + 0.25 I_6^{EI}]^{1/2}} \left( \frac{\partial I_4^{EI}}{\partial \mathbf{F}} - \frac{\partial I_5^{EI}}{\partial \mathbf{F}} + 0.25 \frac{\partial I_6^{EI}}{\partial \mathbf{F}} \right) \quad (\text{B.18a}) \\
 &= \frac{1}{2} |\mathbf{m}^\sharp|^{-1} \left( \frac{\partial I_4^{EI}}{\partial \mathbf{F}} - \frac{\partial I_5^{EI}}{\partial \mathbf{F}} + 0.25 \frac{\partial I_6^{EI}}{\partial \mathbf{F}} \right)
 \end{aligned}$$

$$\frac{\partial |\mathbf{m}^\sharp|}{\partial \mathbf{G}} = \frac{1}{2} |\mathbf{m}^\sharp|^{-1} \left( \frac{\partial I_4^{EI}}{\partial \mathbf{G}} - \frac{\partial I_5^{EI}}{\partial \mathbf{G}} + 0.25 \frac{\partial I_6^{EI}}{\partial \mathbf{G}} \right) \quad (\text{B.18b})$$

The second derivatives of the sharp fiber length change is then,

$$\begin{aligned} \frac{\partial^2 |\mathbf{m}^\sharp|}{\partial \mathbf{F}^2} &= -\frac{1}{2} |\mathbf{m}^\sharp|^{-2} \frac{\partial |\mathbf{m}|}{\mathbf{F}} \otimes \left( \frac{\partial I_4^{EI}}{\partial \mathbf{F}} - \frac{\partial I_5^{EI}}{\partial \mathbf{F}} + 0.25 \frac{\partial I_6^{EI}}{\partial \mathbf{F}} \right) \\ &\quad + \frac{1}{2} |\mathbf{m}^\sharp|^{-1} \left( \frac{\partial^2 I_4^{EI}}{\partial \mathbf{F}^2} - \frac{\partial^2 I_5^{EI}}{\partial \mathbf{F}^2} + 0.25 \frac{\partial^2 I_6^{EI}}{\partial \mathbf{F}^2} \right) \end{aligned} \quad (\text{B.19a})$$

$$\begin{aligned} \frac{\partial^2 |\mathbf{m}^\sharp|}{\partial \mathbf{G}^2} &= -\frac{1}{2} |\mathbf{m}^\sharp|^{-2} \frac{\partial |\mathbf{m}|}{\mathbf{G}} \otimes \left( \frac{\partial I_4^{EI}}{\partial \mathbf{G}} - \frac{\partial I_5^{EI}}{\partial \mathbf{G}} + 0.25 \frac{\partial I_6^{EI}}{\partial \mathbf{G}} \right) \\ &\quad + \frac{1}{2} |\mathbf{m}^\sharp|^{-1} \left( \frac{\partial^2 I_4^{EI}}{\partial \mathbf{G}^2} - \frac{\partial^2 I_5^{EI}}{\partial \mathbf{G}^2} + 0.25 \frac{\partial^2 I_6^{EI}}{\partial \mathbf{G}^2} \right) \end{aligned} \quad (\text{B.19b})$$

$$\begin{aligned} \frac{\partial^2 |\mathbf{m}^\sharp|}{\partial \mathbf{G} \partial \mathbf{F}} &= \frac{\partial^2 |\mathbf{m}^\sharp|}{\partial \mathbf{F} \partial \mathbf{G}} = -\frac{1}{2} |\mathbf{m}^\sharp|^{-2} \frac{\partial |\mathbf{m}|}{\mathbf{G}} \otimes \left( \frac{\partial I_4^{EI}}{\partial \mathbf{F}} - \frac{\partial I_5^{EI}}{\partial \mathbf{F}} + 0.25 \frac{\partial I_6^{EI}}{\partial \mathbf{F}} \right) \\ &\quad + \frac{1}{2} |\mathbf{m}^\sharp|^{-1} \left( \frac{\partial^2 I_4^{EI}}{\partial \mathbf{G} \partial \mathbf{F}} - \frac{\partial^2 I_5^{EI}}{\partial \mathbf{G} \partial \mathbf{F}} + 0.25 \frac{\partial^2 I_6^{EI}}{\partial \mathbf{G} \partial \mathbf{F}} \right) \end{aligned} \quad (\text{B.19c})$$

The first derivatives of the flat fiber length change,

$$\begin{aligned} \frac{\partial |\mathbf{m}^\flat|}{\partial \mathbf{F}} &= \frac{1}{2 [I_4^{EI} - I_5^{EI} + 0.25 I_6^{EI}]^{1/2}} \left( \frac{\partial I_4^{EI}}{\partial \mathbf{F}} + \frac{\partial I_5^{EI}}{\partial \mathbf{F}} + 0.25 \frac{\partial I_6^{EI}}{\partial \mathbf{F}} \right) \\ &= \frac{1}{2} |\mathbf{m}^\flat|^{-1} \left( \frac{\partial I_4^{EI}}{\partial \mathbf{F}} + \frac{\partial I_5^{EI}}{\partial \mathbf{F}} + 0.25 \frac{\partial I_6^{EI}}{\partial \mathbf{F}} \right) \end{aligned} \quad (\text{B.20a})$$

$$\frac{\partial |\mathbf{m}^\flat|}{\partial \mathbf{G}} = \frac{1}{2} |\mathbf{m}^\flat|^{-1} \left( \frac{\partial I_4^{EI}}{\partial \mathbf{G}} + \frac{\partial I_5^{EI}}{\partial \mathbf{G}} + 0.25 \frac{\partial I_6^{EI}}{\partial \mathbf{G}} \right) \quad (\text{B.20b})$$

The second derivatives of the flat fiber length change is then,

$$\begin{aligned} \frac{\partial^2 |\mathbf{m}^\flat|}{\partial \mathbf{F}^2} &= -\frac{1}{2} |\mathbf{m}^\flat|^{-2} \frac{\partial |\mathbf{m}|}{\mathbf{F}} \otimes \left( \frac{\partial I_4^{EI}}{\partial \mathbf{F}} + \frac{\partial I_5^{EI}}{\partial \mathbf{F}} + 0.25 \frac{\partial I_6^{EI}}{\partial \mathbf{F}} \right) \\ &\quad + \frac{1}{2} |\mathbf{m}^\flat|^{-1} \left( \frac{\partial^2 I_4^{EI}}{\partial \mathbf{F}^2} + \frac{\partial^2 I_5^{EI}}{\partial \mathbf{F}^2} + 0.25 \frac{\partial^2 I_6^{EI}}{\partial \mathbf{F}^2} \right) \end{aligned} \quad (\text{B.21a})$$

$$\begin{aligned} \frac{\partial^2 |\mathbf{m}^\flat|}{\partial \mathbf{G}^2} &= -\frac{1}{2} |\mathbf{m}^\flat|^{-2} \frac{\partial |\mathbf{m}|}{\mathbf{G}} \otimes \left( \frac{\partial I_4^{EI}}{\partial \mathbf{G}} + \frac{\partial I_5^{EI}}{\partial \mathbf{G}} + 0.25 \frac{\partial I_6^{EI}}{\partial \mathbf{G}} \right) \\ &\quad + \frac{1}{2} |\mathbf{m}^\flat|^{-1} \left( \frac{\partial^2 I_4^{EI}}{\partial \mathbf{G}^2} + \frac{\partial^2 I_5^{EI}}{\partial \mathbf{G}^2} + 0.25 \frac{\partial^2 I_6^{EI}}{\partial \mathbf{G}^2} \right) \end{aligned} \quad (\text{B.21b})$$

$$\begin{aligned} \frac{\partial^2 |\mathbf{m}^\flat|}{\partial \mathbf{G} \partial \mathbf{F}} &= \frac{\partial^2 |\mathbf{m}^\flat|}{\partial \mathbf{F} \partial \mathbf{G}} = -\frac{1}{2} |\mathbf{m}^\flat|^{-2} \frac{\partial |\mathbf{m}|}{\mathbf{G}} \otimes \left( \frac{\partial I_4^{EI}}{\partial \mathbf{F}} + \frac{\partial I_5^{EI}}{\partial \mathbf{F}} + 0.25 \frac{\partial I_6^{EI}}{\partial \mathbf{F}} \right) \\ &\quad + \frac{1}{2} |\mathbf{m}^\flat|^{-1} \left( \frac{\partial^2 I_4^{EI}}{\partial \mathbf{G} \partial \mathbf{F}} + \frac{\partial^2 I_5^{EI}}{\partial \mathbf{G} \partial \mathbf{F}} + 0.25 \frac{\partial^2 I_6^{EI}}{\partial \mathbf{G} \partial \mathbf{F}} \right) \end{aligned} \quad (\text{B.21c})$$

However, the sharp length change contributes new invariants,

$$\begin{aligned}
 |\mathbf{m}| &= \left[ \left( \mathbf{F} \cdot \mathbf{M} + \frac{1}{2} \mathbf{G} : \mathbf{M}^{\otimes 2} \right) \cdot \left( \mathbf{F} \cdot \mathbf{M} + \frac{1}{2} \mathbf{G} : \mathbf{M}^{\otimes 2} \right) \right]^{1/2} \\
 &+ \left[ \left( -\mathbf{F} \cdot \mathbf{M} + \frac{1}{2} \mathbf{G} : \mathbf{M}^{\otimes 2} \right) \cdot \left( -\mathbf{F} \cdot \mathbf{M} + \frac{1}{2} \mathbf{G} : \mathbf{M}^{\otimes 2} \right) \right]^{1/2} \\
 &= \left[ (\mathbf{F}^T \cdot \mathbf{F}) : \mathbf{M}^{\otimes 2} + \frac{1}{2} (\mathbf{F}^T \cdot (\mathbf{G} \cdot \mathbf{M})) : \mathbf{M}^{\otimes 2} \right. \\
 &\quad \left. + \frac{1}{2} \left( (\mathbf{G} \cdot \mathbf{M})^T \cdot \mathbf{F} \right) : \mathbf{M}^{\otimes 2} + \frac{1}{4} \left( (\mathbf{G} \cdot \mathbf{M})^T \cdot (\mathbf{G} \cdot \mathbf{M}) \right) : \mathbf{M}^{\otimes 2} \right]^{1/2} \\
 &+ \left[ (\mathbf{F}^T \cdot \mathbf{F}) : \mathbf{M}^{\otimes 2} - \frac{1}{2} (\mathbf{F}^T \cdot (\mathbf{G} \cdot \mathbf{M})) : \mathbf{M}^{\otimes 2} \right. \\
 &\quad \left. - \frac{1}{2} \left( (\mathbf{G} \cdot \mathbf{M})^T \cdot \mathbf{F} \right) : \mathbf{M}^{\otimes 2} + \frac{1}{4} \left( (\mathbf{G} \cdot \mathbf{M})^T \cdot (\mathbf{G} \cdot \mathbf{M}) \right) : \mathbf{M}^{\otimes 2} \right]^{1/2}
 \end{aligned} \tag{B.22}$$

Eventough the found invariants are stretch related, and already defined, they are going to be called as bending invariants to preserve consistency,

$$\begin{aligned}
 I_4^\kappa &= (\mathbf{F}^T \cdot \mathbf{F}) : \mathbf{M}^{\otimes 2} = F_{kl} F_{km} M_l M_m \\
 I_5^\kappa &= (\mathbf{F}^T \cdot (\mathbf{G} \cdot \mathbf{M})) : \mathbf{M}^{\otimes 2} = \left( (\mathbf{G} \cdot \mathbf{M})^T \cdot \mathbf{F} \right) : \mathbf{M}^{\otimes 2} = F_{kl} (\mathbf{G} \cdot \mathbf{M})_{km} M_l M_m \\
 I_6^\kappa &= \left( (\mathbf{G} \cdot \mathbf{M})^T \cdot (\mathbf{G} \cdot \mathbf{M}) \right) : \mathbf{M}^{\otimes 2} = (\mathbf{G} \cdot \mathbf{M})_{kl} (\mathbf{G} \cdot \mathbf{M})_{km} M_l M_m
 \end{aligned} \tag{B.23}$$

The second and third contractions are identical since the contracted tensors are transpose of each other,

$$\mathbf{F}^T \cdot (\mathbf{G} \cdot \mathbf{M}) = \left( (\mathbf{G} \cdot \mathbf{M})^T \cdot \mathbf{F} \right)^T \tag{B.24}$$

The full length in the current curved coordinates is the sum of sharp and flat lengths, in terms of the invariants introduced above,

$$|\mathbf{m}| = |\mathbf{m}^\sharp| + |\mathbf{m}^\flat| = \sqrt{(I_4^\kappa + I_5^\kappa + 0.25 I_6^\kappa)} + \sqrt{(I_4^\kappa - I_5^\kappa + 0.25 I_6^\kappa)} \tag{B.25}$$

The derivatives of the last three bending invariants are with respect to the deformation gradient are,

$$\frac{\partial I_4^{EI}}{\partial F_{ij}} = \delta_{ki} \delta_{lj} F_{km} M_l M_m + F_{kl} \delta_{ki} \delta_{mj} M_l M_m = F_{im} M_j M_m + F_{il} M_l M_j \tag{B.26a}$$

$$\frac{\partial I_5^{EI}}{\partial F_{ij}} = \delta_{ki} \delta_{lj} (\mathbf{G} \cdot \mathbf{M})_{km} M_l M_m = (\mathbf{G} \cdot \mathbf{M})_{im} M_j M_m \tag{B.26b}$$

$$\frac{\partial I_6^{EI}}{\partial F_{ij}} = \mathbf{0}_{ij} \tag{B.26c}$$

The derivatives of the last three bending invariants are with respect to the deformation hypergradient are,

$$\frac{\partial I_4^{EI}}{\partial (\mathbf{G} \cdot \mathbf{M})_{ij}} = \mathbf{0}_{ij} \quad (\text{B.27a})$$

$$\frac{\partial I_5^{EI}}{\partial (\mathbf{G} \cdot \mathbf{M})_{ij}} = F_{kl} \delta_{ki} \delta_{mj} M_l M_m = F_{il} M_l M_j \quad (\text{B.27b})$$

$$\begin{aligned} \frac{\partial I_6^{EI}}{\partial (\mathbf{G} \cdot \mathbf{M})_{ij}} &= \delta_{ki} \delta_{lj} (\mathbf{G} \cdot \mathbf{M})_{km} M_l M_m + (\mathbf{G} \cdot \mathbf{M})_{kl} \delta_{ki} \delta_{mj} M_l M_m \\ &= (\mathbf{G} \cdot \mathbf{M})_{im} M_j M_m + (\mathbf{G} \cdot \mathbf{M})_{il} M_l M_j \end{aligned} \quad (\text{B.27c})$$

The second derivatives of the last three bending invariants are with respect to the deformation gradient are,

$$\frac{\partial^2 I_4^\kappa}{\partial F_{kl} \partial F_{ij}} = \frac{1}{\partial F_{kl}} (F_{im} M_j M_m + F_{im} M_m M_j) = 2\delta_{ik} \delta_{ml} M_j M_m = 2\delta_{ik} M_j M_l \quad (\text{B.28a})$$

$$\frac{\partial^2 I_5^\kappa}{\partial F_{kl} \partial F_{ij}} = \mathbf{0}_{ijkl} \quad \frac{\partial^2 I_6^\kappa}{\partial F_{kl} \partial F_{ij}} = \mathbf{0}_{ijkl} \quad (\text{B.28b})$$

The mixed second derivatives of the last three bending invariants with respect to the hypergradients lastly ,

$$\frac{\partial^2 I_4^\kappa}{\partial (\mathbf{G}_M)_{kl} \partial F_{ij}} = \mathbf{0}_{ijkl} \quad (\text{B.29a})$$

$$\frac{\partial^2 I_5^\kappa}{\partial (\mathbf{G}_M)_{kl} \partial F_{ij}} = \frac{\partial (\mathbf{G}_M)_{im} M_j M_m}{\partial (\mathbf{G}_M)_{kl}} = \delta_{ik} M_l M_j \quad (\text{B.29b})$$

$$\frac{\partial^2 I_6^\kappa}{\partial (\mathbf{G}_M)_{kl} \partial F_{ij}} = \mathbf{0}_{ijkl} \quad (\text{B.29c})$$

The second derivatives of the last three bending invariants with respect to the deformation hypergradient are,

$$\frac{\partial^2 I_4^{EI}}{\partial (\mathbf{G}_M)_{kl} \partial (\mathbf{G}_M)_{ij}} = \mathbf{0}_{ijkl} \quad (\text{B.30a})$$

$$\frac{\partial^2 I_5^{EI}}{\partial (\mathbf{G}_M)_{kl} \partial (\mathbf{G}_M)_{ij}} = \mathbf{0}_{ijkl} \quad (\text{B.30b})$$

$$\frac{\partial^2 I_6^{EI}}{\partial (\mathbf{G}_M)_{kl} \partial (\mathbf{G}_M)_{ij}} = 2\delta_{ik} M_j M_l \quad (\text{B.30c})$$

## B.2 Stretching Strain and Strain Gradient energy density Function

The stretching behavior can be represented as, The strain energy density function reads:

$$\psi = \frac{EA}{4} \left( |\mathbf{m}|^2 - 1 \right)^2 \quad (\text{B.31})$$

The first Piola Kirchoff Stress,

$$\mathbf{P} = \frac{\partial \psi}{\partial \mathbf{F}} = \psi = EA \left( |\mathbf{m}|^2 - 1 \right) |\mathbf{m}| \frac{\partial |\mathbf{m}|}{\partial \mathbf{F}} \quad (\text{B.32})$$

The Piola Hyperstress is then,

$$\mathbf{Q} = \frac{\partial \psi}{\partial \mathbf{G}} = \psi = EA \left( |\mathbf{m}|^2 - 1 \right) |\mathbf{m}| \frac{\partial |\mathbf{m}|}{\partial \mathbf{G}} \quad (\text{B.33})$$

The material tangent tensors

$$\begin{aligned} \mathbf{D}_{\mathbf{F}}^{\mathbf{P}} &= \frac{\partial \mathbf{P}}{\partial \mathbf{F}} = 2EA |\mathbf{m}|^2 \frac{\partial |\mathbf{m}|}{\partial \mathbf{F}} \frac{\partial |\mathbf{m}|}{\partial \mathbf{F}} \\ &+ EA \left( |\mathbf{m}|^2 - 1 \right) \frac{\partial |\mathbf{m}|}{\partial \mathbf{F}} \frac{\partial |\mathbf{m}|}{\partial \mathbf{F}} \\ &+ EA \left( |\mathbf{m}|^2 - 1 \right) |\mathbf{m}| \frac{\partial^2 |\mathbf{m}|}{\partial \mathbf{F}^2} \\ \mathbf{D}_{\mathbf{G}}^{\mathbf{P}} &= \frac{\partial \mathbf{P}}{\partial \mathbf{G}} = 2EA |\mathbf{m}|^2 \frac{\partial |\mathbf{m}|}{\partial \mathbf{G}} \frac{\partial |\mathbf{m}|}{\partial \mathbf{F}} \\ &+ EA \left( |\mathbf{m}|^2 - 1 \right) \frac{\partial |\mathbf{m}|}{\partial \mathbf{G}} \frac{\partial |\mathbf{m}|}{\partial \mathbf{F}} \\ &+ EA \left( |\mathbf{m}|^2 - 1 \right) |\mathbf{m}| \frac{\partial |\mathbf{m}|}{\partial \mathbf{G}} \frac{\partial |\mathbf{m}|}{\partial \mathbf{F}} \\ \mathbf{D}_{\mathbf{G}}^{\mathbf{Q}} &= \frac{\partial \mathbf{Q}}{\partial \mathbf{G}} = 2EA |\mathbf{m}|^2 \frac{\partial |\mathbf{m}|}{\partial \mathbf{G}} \frac{\partial |\mathbf{m}|}{\partial \mathbf{G}} \\ &+ EA \left( |\mathbf{m}|^2 - 1 \right) \frac{\partial |\mathbf{m}|}{\partial \mathbf{G}} \frac{\partial |\mathbf{m}|}{\partial \mathbf{G}} \\ &+ EA \left( |\mathbf{m}|^2 - 1 \right) |\mathbf{m}| \frac{\partial^2 |\mathbf{m}|}{\partial \mathbf{G}^2} \end{aligned} \quad (\text{B.34})$$





# Appendix C

## Contents

C.1	Simo-Type geometrically exact anisotropy in hyperelastic form	173
C.2	Tractions and Hypertractions on gradient Cauchy tetrahedra .	176

## C.1 Simo-Type geometrically exact anisotropy in hyperelastic form

Next, we are going to postulate a nonlinear material model consistent with the kinematics given in the first section. The model is motivated principally by the geometrically exact beam formulations covered by the work of Simo, Antman, Reissner and Kirchhoff&Love. We will consider the approach of Simo, and partially adapt the formulation thought to model 3D beams into our material model formulation.

Before starting with the assumptions, we initially define *moving* and *convected* coordinates of a currently curved, and initially straight fiber. The coordinates of the reference moving frame according to the reverse mapping are functions of the current coordinates.

$$\begin{aligned} \mathbf{X}(\mathbf{x}) &= M_1(\mathbf{x}) \hat{\mathbf{M}} + M_2(\mathbf{x}) \hat{\mathbf{M}}_{\perp 1} + M_3(\mathbf{x}) \hat{\mathbf{M}}_{\perp 2} \\ &= (\mathbf{X}^T \cdot \hat{\mathbf{M}}) \hat{\mathbf{M}} + (\mathbf{I} - \hat{\mathbf{M}} \otimes \hat{\mathbf{M}}) \cdot \mathbf{X} \end{aligned} \quad (\text{C.1})$$

The kinematically significant vector component of the moving frame can be defined as a family of level planes. Since inverse mapping is function of current coordinates, the level surface set is in current system and has a cofactor type steepest ascent orthonormal to the level plane, apparent from the gradient of it. Tangent median of the level plane is certainly defined by the deformation gradient along the reference fiber.

$$\begin{aligned} S_{\hat{\mathbf{M}}}^c &= \{ \mathbf{x} \mid \mathbf{X}^T \cdot \hat{\mathbf{M}} = c \} \\ \mathbf{F}^{-T} \cdot \hat{\mathbf{M}} &\perp S_{\hat{\mathbf{M}}}^c \quad \mathbf{F} \cdot \hat{\mathbf{M}} \parallel S_{\hat{\mathbf{M}}}^c \end{aligned} \quad (\text{C.2})$$

The same analogy can be extended to the cofactor of hypergradient as the steepest ascent of level hypersurfaces of deformation gradient. This relevant but contently not necessary

extension is let to be out of the scope. The principle moving and convecting current coordinates around a natural cross section at the flat domain of the fiber,

$$\begin{aligned} S_{\hat{M}^b}^0 \perp (\mathbf{F}^b \cdot \hat{M}^b) &= (\mathbf{F}^b + \mathbf{G} \cdot \hat{M}^b)^{-T} \cdot \hat{M}^b = -(\mathbf{F}^b - \mathbf{G} \cdot \hat{M}^b)^{-T} \cdot \hat{M}^b \\ S_{\hat{M}^b}^0 \parallel (\mathbf{F}^b \cdot \hat{M}^b) &= (\mathbf{F}^b + \mathbf{G} \cdot \hat{M}^b) \cdot \hat{M}^b = (-\mathbf{F}^b + \mathbf{G} \cdot \hat{M}^b) \cdot \hat{M}^b \end{aligned} \quad (\text{C.3})$$

Similarly, the principle moving and convecting current coordinates around a natural cross section at the sharp domain of the fiber,

$$\begin{aligned} S_{\hat{M}^\sharp}^0 \perp (\mathbf{F}^\sharp \cdot \hat{M}^\sharp) &= (\mathbf{F}^\sharp + \mathbf{G} \cdot \hat{M}^\sharp)^{-T} \cdot \hat{M}^\sharp = (\mathbf{F}^\sharp + \mathbf{G} \cdot \hat{M}^\sharp)^{-T} \cdot \hat{M}^\sharp \\ S_{\hat{M}^\sharp}^0 \parallel (\mathbf{F}^\sharp \cdot \hat{M}^\sharp) &= (\mathbf{F}^\sharp + \mathbf{G} \cdot \hat{M}^\sharp) \cdot \hat{M}^\sharp = (\mathbf{F}^\sharp + \mathbf{G} \cdot \hat{M}^\sharp) \cdot \hat{M}^\sharp \end{aligned} \quad (\text{C.4})$$

In this single fiber kinematics, as stated before, we take the natural and sharp directions

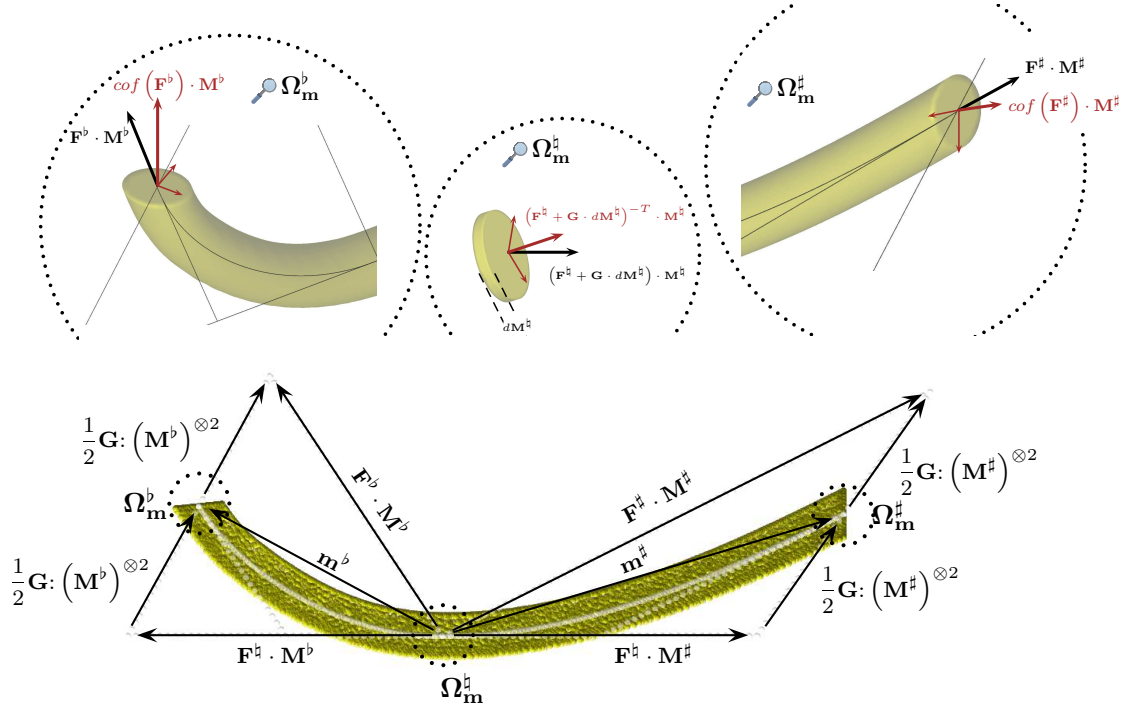


Figure C.1: Kinematics of a single fiber with convecting and moving coordinates at the flat, natural and sharp sections, Change the omega into small one

as identical. We assume an additive orthogonal kinematics for axis apart material points of the fiber exist. The linear momentum material vector field  $\mathbf{\Gamma}$  for the flat and sharp sections

become,

$$\begin{aligned}\Gamma^b &= \Lambda^T \cdot \left( \frac{\left(-\mathbf{F}^\natural + \mathbf{G} \cdot \hat{\mathbf{M}}^\natural\right) \cdot \hat{\mathbf{M}}^\natural}{\left\| \left(-\mathbf{F}^\natural + \mathbf{G} \cdot \hat{\mathbf{M}}^\natural\right) \cdot \hat{\mathbf{M}}^\natural \right\|} - \frac{\left(-\mathbf{F}^\natural + \mathbf{G} \cdot \hat{\mathbf{M}}^\natural\right)^{-T} \cdot \hat{\mathbf{M}}^\natural}{\left\| \left(-\mathbf{F}^\natural + \mathbf{G} \cdot \hat{\mathbf{M}}^\natural\right)^{-T} \cdot \hat{\mathbf{M}}^\natural \right\|} \right) \\ &= \Lambda^T \cdot \frac{\left(-\mathbf{F}^\natural \cdot \hat{\mathbf{M}}^\natural + \mathbf{G} : \hat{\mathbf{M}}^\natural \otimes \hat{\mathbf{M}}^\natural\right)}{\left\| \left(-\mathbf{F}^\natural + \mathbf{G} \cdot \hat{\mathbf{M}}^\natural\right) \cdot \hat{\mathbf{M}}^\natural \right\|} + \hat{\mathbf{M}}^\natural\end{aligned}\quad (\text{C.5})$$

$$\begin{aligned}\Gamma^\natural &= \Lambda^T \cdot \left( \frac{\left(\mathbf{F}^\natural + \mathbf{G} \cdot \hat{\mathbf{M}}^\natural\right) \cdot \hat{\mathbf{M}}^\natural}{\left\| \left(\mathbf{F}^\natural + \mathbf{G} \cdot \hat{\mathbf{M}}^\natural\right) \cdot \hat{\mathbf{M}}^\natural \right\|} - \frac{\left(\mathbf{F}^\natural + \mathbf{G} \cdot \hat{\mathbf{M}}^\natural\right)^{-T} \cdot \hat{\mathbf{M}}^\natural}{\left\| \left(\mathbf{F}^\natural - \mathbf{G} \cdot \hat{\mathbf{M}}^\natural\right)^{-T} \cdot \hat{\mathbf{M}}^\natural \right\|} \right) \\ &= \Lambda^T \cdot \frac{\left(\mathbf{F}^\natural \cdot \hat{\mathbf{M}}^\natural + \mathbf{G} : \hat{\mathbf{M}}^\natural \otimes \hat{\mathbf{M}}^\natural\right)}{\left\| \left(\mathbf{F}^\natural + \mathbf{G} \cdot \hat{\mathbf{M}}^\natural\right) \cdot \hat{\mathbf{M}}^\natural \right\|} - \hat{\mathbf{M}}^\natural\end{aligned}\quad (\text{C.6})$$

The strain energy density function (per unit length) balanced by only linear momentum effects is the parametric integral result in reference volume,

$$\begin{aligned}\psi_{\Gamma^b} &= \mathbf{D}^b : \left(\Gamma^b \otimes \Gamma^b\right) \\ &= E^b A \left(\left(\hat{\mathbf{M}}^\natural \otimes \cdot \hat{\mathbf{M}}^\natural\right) \cdot \Gamma^b \cdot \left(\hat{\mathbf{M}}^\natural \otimes \cdot \hat{\mathbf{M}}^\natural\right) \cdot \Gamma^b\right) \\ &\quad + G^b A \left(\left(\mathbf{I} - \hat{\mathbf{M}}^\natural \otimes \cdot \hat{\mathbf{M}}^\natural\right) \cdot \Gamma^b \cdot \left(\mathbf{I} - \hat{\mathbf{M}}^\natural \otimes \cdot \hat{\mathbf{M}}^\natural\right) \cdot \Gamma^b\right)\end{aligned}\quad (\text{C.7})$$

Linear momentum equation given in this form has the following material tensor,

$$\mathbf{D}^b = E^b A \left(\mathbf{M}^{\otimes 2} \cdot \mathbf{M}^{\otimes 2}\right) + G^b A \left(\mathbf{I} - \mathbf{M}^{\otimes 2}\right) \cdot \left(\mathbf{I} - \mathbf{M}^{\otimes 2}\right) \quad (\text{C.8})$$

By calling the purpose of the additional orthogonal kinematics, the vector of tensile linear momentum part is,

$$\begin{aligned}\left(-\hat{\mathbf{M}}^\natural \otimes -\hat{\mathbf{M}}^\natural\right) \cdot \Gamma^b &= \left(-\hat{\mathbf{M}}^\natural \otimes -\hat{\mathbf{M}}^\natural\right) \cdot \Lambda^T \cdot \frac{\left(-\mathbf{F}^\natural \cdot \hat{\mathbf{M}}^\natural + \mathbf{G} : \hat{\mathbf{M}}^\natural \otimes \cdot \hat{\mathbf{M}}^\natural\right)}{\left\| \left(-\mathbf{F}^\natural + \mathbf{G} \cdot \hat{\mathbf{M}}^\natural\right) \cdot \hat{\mathbf{M}}^\natural \right\|} + \hat{\mathbf{M}}^\natural \\ &= \frac{-\hat{\mathbf{M}}^\natural \otimes \left(-\hat{\mathbf{M}}^\natural \cdot \left(-\mathbf{F}^\natural + \mathbf{G}\right)^{-1} \cdot \left(-\mathbf{F}^\natural + \mathbf{G}\right) \cdot \hat{\mathbf{M}}^\natural\right)}{\left\| \left(-\mathbf{F}^\natural + \mathbf{G} \cdot \hat{\mathbf{M}}^\natural\right)^{-1} \cdot \hat{\mathbf{M}}^\natural \right\| \left\| \left(-\mathbf{F}^\natural + \mathbf{G} \cdot \hat{\mathbf{M}}^\natural\right) \cdot \hat{\mathbf{M}}^\natural \right\|} + \hat{\mathbf{M}}^\natural \\ &= -\left\| -\mathbf{F}^b \cdot \hat{\mathbf{M}}^\natural \right\|^{-1} \left\| -\mathbf{F}^\natural \cdot \hat{\mathbf{M}}^\natural \right\|^{-1} \hat{\mathbf{M}}^\natural + \hat{\mathbf{M}}^\natural \\ \left(\hat{\mathbf{M}}^\natural \otimes \hat{\mathbf{M}}^\natural\right) \cdot \Gamma^\natural &= \left\| \mathbf{F}^\natural \cdot \hat{\mathbf{M}}^\natural \right\|^{-1} \left\| \mathbf{F}^\natural \cdot \hat{\mathbf{M}}^\natural \right\|^{-1} \hat{\mathbf{M}}^\natural - \hat{\mathbf{M}}^\natural\end{aligned}\quad (\text{C.9})$$

Together with the flat contribution, the total tensile momentum free energy becomes,

$$\begin{aligned}
\psi_{\mathbf{F}}^{EA} &= \psi_{\mathbf{F}^b}^{EA} + \psi_{\mathbf{F}^\sharp}^{EA} \\
&= E^b A \left( \|\mathbf{F}^{b^{-1}} \cdot \hat{\mathbf{M}}^\sharp\|^{-2} \|\mathbf{F}^b \cdot \hat{\mathbf{M}}^\sharp\|^{-2} - 2 \|\mathbf{F}^{b^{-1}} \cdot \hat{\mathbf{M}}^\sharp\|^{-1} \|\mathbf{F}^b \cdot \hat{\mathbf{M}}^\sharp\|^{-1} + 1 \right) \\
&\quad + E^\sharp A \left( \|\mathbf{F}^{\sharp^{-1}} \cdot \hat{\mathbf{M}}^\sharp\|^{-2} \|\mathbf{F}^\sharp \cdot \hat{\mathbf{M}}^\sharp\|^{-2} - 2 \|\mathbf{F}^{\sharp^{-1}} \cdot \hat{\mathbf{M}}^\sharp\|^{-1} \|\mathbf{F}^\sharp \cdot \hat{\mathbf{M}}^\sharp\|^{-1} + 1 \right)
\end{aligned} \tag{C.10}$$

Which is clearly zero for absolutely no deformation cases.

## C.2 Traction and Hypertractions on gradient Cauchy tetrahedra

In this section we give an example of fiber anisotropy embedded by a Cauchy tetrahedron. For this purpose we rewrite the strain energy density function in terms of the Cauchy and Finger tensors,

$$\begin{aligned}
\psi_{\mathbf{F}}^{EA} &= E^b A \left[ \left( \mathbf{b}^{b^{-1}} : \hat{\mathbf{M}}^{\sharp\otimes 2} \right)^{-1} \left( \mathbf{C}^b : \hat{\mathbf{M}}^{\sharp\otimes 2} \right)^{-1} - 2 \left( \mathbf{b}^{b^{-1}} : \hat{\mathbf{M}}^{\sharp\otimes 2} \right)^{-1/2} \left( \mathbf{C}^b : \hat{\mathbf{M}}^{\sharp\otimes 2} \right)^{-1/2} + 1 \right] \\
&\quad + E^\sharp A \left[ \left( \mathbf{b}^{\sharp^{-1}} : \hat{\mathbf{M}}^{\sharp\otimes 2} \right)^{-1} \left( \mathbf{C}^\sharp : \hat{\mathbf{M}}^{\sharp\otimes 2} \right)^{-1} - 2 \left( \mathbf{b}^{\sharp^{-1}} : \hat{\mathbf{M}}^{\sharp\otimes 2} \right)^{-1/2} \left( \mathbf{C}^\sharp : \hat{\mathbf{M}}^{\sharp\otimes 2} \right)^{-1/2} + 1 \right]
\end{aligned} \tag{C.11}$$

Where the inverse finger and the Cauchy strains are defined as;

$$\begin{aligned}
\mathbf{b}^{b^{-1}} &= \mathbf{F}^{\sharp^{-T}} \cdot \mathbf{F}^{\sharp^{-1}} & \mathbf{b}^{b^{-1}} &= \mathbf{F}^{b^{-T}} \cdot \mathbf{F}^{b^{-1}} \\
\mathbf{C}^\sharp &= \mathbf{F}^{\sharp T} \cdot \mathbf{F}^\sharp & \mathbf{C}^b &= \mathbf{F}^{b T} \cdot \mathbf{F}^b
\end{aligned} \tag{C.12}$$

Additional material nonlinearity in reference configuration should be defined for more rational approach and for the sake of artificial snap through. Since the modulus is equivalent to slope of incremental load displacement curve, we impose worm-like chain similar exponential type reversible material hardening for the material type nonlinearities.

Quite apparently, the first Piola Kirchhoff stress and hyperstress tensors are,

$$\begin{aligned}
 \mathbf{P}^\sharp &= \frac{\partial \psi_\Gamma^{EA}}{\partial \mathbf{b}^{\flat^{-1}}} : \frac{\partial \mathbf{b}^{\flat^{-1}}}{\partial \mathbf{b}^\flat} : \frac{\partial \mathbf{b}^\flat}{\partial \mathbf{F}^\flat} : \frac{\partial \mathbf{F}^\flat}{\partial \mathbf{F}^\sharp} + \frac{\partial \psi_\Gamma^{EA}}{\partial \mathbf{b}^{\sharp^{-1}}} : \frac{\partial \mathbf{b}^{\sharp^{-1}}}{\partial \mathbf{b}^\sharp} : \frac{\partial \mathbf{b}^\sharp}{\partial \mathbf{F}^\sharp} : \frac{\partial \mathbf{F}^\sharp}{\partial \mathbf{F}^\sharp} \\
 &+ \frac{\partial \psi_\Gamma^{EA}}{\partial \mathbf{C}^\flat} : \frac{\partial \mathbf{C}^\flat}{\partial \mathbf{F}^\flat} : \frac{\partial \mathbf{F}^\flat}{\partial \mathbf{F}^\sharp} + \frac{\partial \psi_\Gamma^{EA}}{\partial \mathbf{C}^\sharp} : \frac{\partial \mathbf{C}^\sharp}{\partial \mathbf{F}^\sharp} : \frac{\partial \mathbf{F}^\sharp}{\partial \mathbf{F}^\sharp} \\
 \mathbf{Q}^\sharp &= \frac{\partial \psi_\Gamma^{EA}}{\partial \mathbf{b}^{\flat^{-1}}} : \frac{\partial \mathbf{b}^{\flat^{-1}}}{\partial \mathbf{b}^\flat} : \frac{\partial \mathbf{b}^\flat}{\partial \mathbf{F}^\flat} : \frac{\partial \mathbf{F}^\flat}{\partial \mathbf{G}^\sharp} + \frac{\partial \psi_\Gamma^{EA}}{\partial \mathbf{b}^{\sharp^{-1}}} : \frac{\partial \mathbf{b}^{\sharp^{-1}}}{\partial \mathbf{b}^\sharp} : \frac{\partial \mathbf{b}^\sharp}{\partial \mathbf{F}^\sharp} : \frac{\partial \mathbf{F}^\sharp}{\partial \mathbf{G}^\sharp} \\
 &+ \frac{\partial \psi_\Gamma^{EA}}{\partial \mathbf{C}^\flat} : \frac{\partial \mathbf{C}^\flat}{\partial \mathbf{F}^\flat} : \frac{\partial \mathbf{F}^\flat}{\partial \mathbf{G}^\sharp} + \frac{\partial \psi_\Gamma^{EA}}{\partial \mathbf{C}^\sharp} : \frac{\partial \mathbf{C}^\sharp}{\partial \mathbf{F}^\sharp} : \frac{\partial \mathbf{F}^\sharp}{\partial \mathbf{G}^\sharp}
 \end{aligned} \tag{C.13}$$

Where, the intrinsic dependence of the incremental modulus to the Cauchy deformation measures are taken to be,

$$E^\sharp A = E_0 A_0 \exp\left(\mathbf{C}^\sharp : \hat{\mathbf{M}}^{\sharp \otimes 2}\right) \quad E^\flat A = E_0 A_0 \exp\left(\mathbf{C}^\flat : \hat{\mathbf{M}}^{\flat \otimes 2}\right) \tag{C.14}$$

As above, among the derivations, no pull back transformation is applied on the area elements, towards which we implicitly imply that the balance of angular momentum is quantitatively negligible besides of the linear momentum effects as a consequence of small enough area assumption. The following parts are to be put into the appendix, but I'll write down for programming purposes,

$$\begin{aligned}
 \frac{\partial \psi_\Gamma^{EA}}{\partial \mathbf{b}^{\flat^{-1}}} &= -EA \left(\mathbf{b}^{\flat^{-1}} : \hat{\mathbf{M}}^{\flat \otimes 2}\right)^{-2} \left(\mathbf{C}^\flat : \hat{\mathbf{M}}^{\flat \otimes 2}\right)^{-1} \hat{\mathbf{M}}^{\flat \otimes 2} \\
 &\quad - EA \left(\mathbf{b}^{\flat^{-1}} : \hat{\mathbf{M}}^{\flat \otimes 2}\right)^{-3/2} \left(\mathbf{C}^\flat : \hat{\mathbf{M}}^{\flat \otimes 2}\right)^{-1/2} \hat{\mathbf{M}}^{\flat \otimes 2} \\
 \frac{\partial \psi_\Gamma^{EA}}{\partial \mathbf{b}^{\sharp^{-1}}} &= -EA \left(\mathbf{b}^{\sharp^{-1}} : \hat{\mathbf{M}}^{\sharp \otimes 2}\right)^{-2} \left(\mathbf{C}^\sharp : \hat{\mathbf{M}}^{\sharp \otimes 2}\right)^{-1} \hat{\mathbf{M}}^{\sharp \otimes 2} \\
 &\quad - EA \left(\mathbf{b}^{\sharp^{-1}} : \hat{\mathbf{M}}^{\sharp \otimes 2}\right)^{-3/2} \left(\mathbf{C}^\sharp : \hat{\mathbf{M}}^{\sharp \otimes 2}\right)^{-1/2} \hat{\mathbf{M}}^{\sharp \otimes 2}
 \end{aligned} \tag{C.15}$$

Again for programming purposes, the derivatives of the strain energy density density function with respect to the sharp and flat Cauchy strain measure,

$$\begin{aligned}
 \frac{\partial \psi_\Gamma^{EA}}{\partial \mathbf{C}^\flat} &= -EA \left(\mathbf{C}^\flat : \hat{\mathbf{M}}^{\flat \otimes 2}\right)^{-2} \left(\mathbf{b}^{\flat^{-1}} : \hat{\mathbf{M}}^{\flat \otimes 2}\right)^{-1} \hat{\mathbf{M}}^{\flat \otimes 2} \\
 &\quad - EA \left(\mathbf{C}^\flat : \hat{\mathbf{M}}^{\flat \otimes 2}\right)^{-3/2} \left(\mathbf{b}^{\flat^{-1}} : \hat{\mathbf{M}}^{\flat \otimes 2}\right)^{-1/2} \hat{\mathbf{M}}^{\flat \otimes 2} \\
 \frac{\partial \psi_\Gamma^{EA}}{\partial \mathbf{C}^\sharp} &= -EA \left(\mathbf{C}^\sharp : \hat{\mathbf{M}}^{\sharp \otimes 2}\right)^{-2} \left(\mathbf{b}^{\sharp^{-1}} : \hat{\mathbf{M}}^{\sharp \otimes 2}\right)^{-1} \hat{\mathbf{M}}^{\sharp \otimes 2} \\
 &\quad - EA \left(\mathbf{C}^\sharp : \hat{\mathbf{M}}^{\sharp \otimes 2}\right)^{-3/2} \left(\mathbf{b}^{\sharp^{-1}} : \hat{\mathbf{M}}^{\sharp \otimes 2}\right)^{-1/2} \hat{\mathbf{M}}^{\sharp \otimes 2}
 \end{aligned} \tag{C.16}$$

Additionally, the inverse derivatives of the finger tensor and the derivatives of the Cauchy and Finger tensors are given,

$$\begin{aligned} \left(\frac{\partial \mathbf{b}^{-1}}{\partial \mathbf{b}}\right)_{ijkl} &= \frac{1}{2} \left(b_{ik}^{-1} b_{lj}^{-1} + b_{il}^{-1} b_{kj}^{-1}\right) \\ \left(\frac{\partial \mathbf{C}}{\partial \mathbf{F}}\right)_{ijkl} &= \delta_{il} F_{kj} + \delta_{ki} F_{jl} & \left(\frac{\partial \mathbf{b}}{\partial \mathbf{F}}\right)_{ijkl} &= \delta_{ik} F_{jl} + \delta_{jk} F_{il} \\ \left(\frac{\partial \mathbf{F}^b}{\partial \mathbf{F}^a}\right)_{ijkl} &= \frac{\partial (-\mathbf{F}^a + \mathbf{G}^a \cdot \mathbf{M}^a)_{ij}}{\partial (\mathbf{F}^a)_{kl}} = -\delta_{ik} \delta_{jl} & \left(\frac{\partial \mathbf{F}^b}{\partial \mathbf{G}^a}\right)_{ijkln} &= \delta_{ik} \delta_{jl} M_n \end{aligned} \quad (\text{C.17})$$

The last two equations is due to the fact that the reference coordinates are fixed and divergence-free near to the material point.

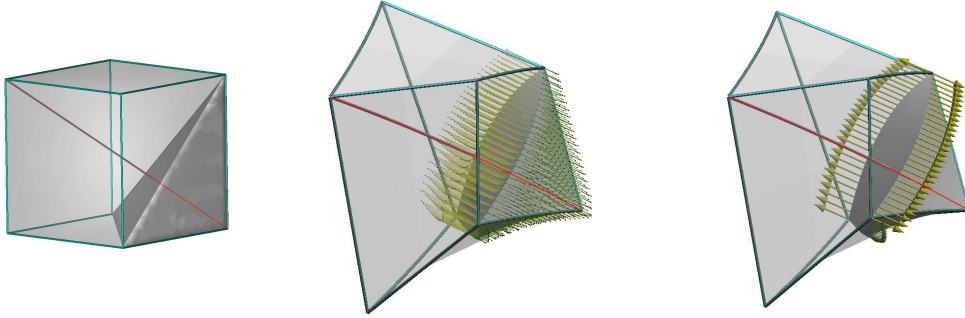


Figure C.2: From left to right, undeformed straight Cauchy tetrahedron, traction forces on deformed body hypertraction forces on deformed body.

It does worth to comment further on the quantitative proportion of traction forces, hypertraction forces as well as traction stresses with each other. For this purpose we use the extended Cauchy Tetrahedron which we call as *Hyper-Cauchy tetrahedron*. The Hyper-Cauchy tetrahedron (for this case) represents a volume division of a fiber reinforced unit cell. Like in Cauchy-tetrahedron, it is assumed that the cell is balanced by volumetrically divergence-free stress and volumetrically double divergence-free hyperstress, indicating the absence of body forces. Analogously, the hyperstress is facially divergence-free and do act on interfaces of the further divisions of surface patches and balance those surface patches.

Figure 9 on the left shows the traction and hypertraction forces developing with the deformation factor of an example case. As can be seen the exponential hardening does not undergo any artificial snap-through or artificial softening which may be caused if only the geometrical nonlinearities were considered in the material. At this stage, we state that the exponential hardening of the elastic modulus of simo-type geometrically exact anisotropy can be replaced by any type of material model. In case, St. Venant-Kirchhoff material is used, some softening, even snap through in exceeding deformations can be observable, because the stress functions of this model linear in isotropic material parameter couples.

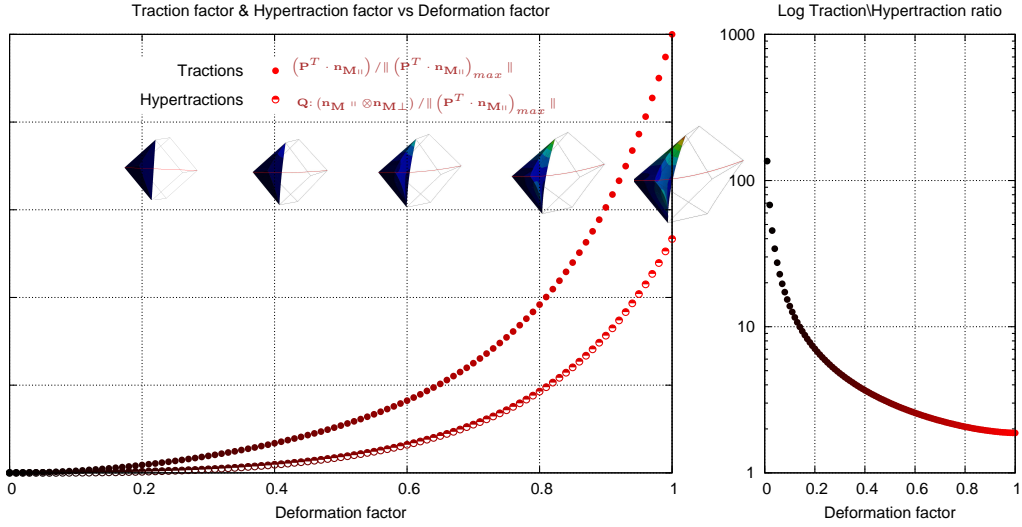


Figure C.3: Left, traction and hypertraction force factors depending on the deformation factors. Right The logarithmic ratio of traction to hypertraction forces.

Instead, a Neo-Hookean material update can be used, however it would be quite difficult to argue on phenomenological reasoning of dependence of incremental material properties of fibers on the cofactor update. In fact, the increase of incremental effective values depending on the tangential stretch of radially packed fibers is stated many times in the literature. Therefore, we took exponential incremental update driven by the deformation gradient and deformation hypergradient.

Figure 9 on the right shows the proportional development of traction forces with respect to hypertractions forces with increasing displacement factor. In spite, this behavior can not be taken as general, it is still evidential that the hypertractive effects may be quantitatively equivalent to tractive effects. Additionally, it is again evidential that this proportion may ascent with deformation.

For weighting those two effects, instead of an energy based comparison approach, we compared the tractions and hypertractions. Because the L:SA:V ratios of Hyper-Cauchy geometries (in general geometries) are size dependent, the energy tracked by the surface forces of different sized surfaces does not allow an objective comparison. Besides, the energy function is not straightforwardly additively splittable into those pieces. However tractions and surface tractions do allow an objective comparison, due to the fact that L:SA of surfaces is proportional with L, and L is proportional with  $\|\mathbf{M}\|$  and  $\|\mathbf{M}\|$  is proportional with  $\|\mathbf{Q} : \mathbf{n}_{\parallel} \otimes \mathbf{n}_{\perp}\| / \|\mathbf{P}^T \cdot \mathbf{n}_{\parallel}\|$ .





# Appendix D

## Contents

<b>D.1 Stationary configurational energy and kinematics</b> . . . . .	181
<b>D.2 Maximization of Configurational Energy</b> . . . . .	185

## D.1 Stationary configurational energy and kinematics

The strain energy of energetically equal configurations of gradient-only systems can be represented by the following composite function.

$$\psi^c = \psi \circ \mathbf{E}^* \circ \mathbf{Q}^* \quad (\text{D.1})$$

Where the finite rotation tensor  $\mathbf{Q}$  and the rotation angle scaled skew rotation axis tensor  $\alpha\mathbf{A}$  are mapped onto each other by means of matrix exponential and matrix natural logarithm functions. Even though the matrix logarithm function has a radius of convergence, we write down to show the invertibility of the skew symmetric and orthogonal matrix functions.

$$\mathbf{Q} = \exp(\alpha\mathbf{A}) \quad \alpha\mathbf{A} = \log_e(\mathbf{Q}) \quad (\text{D.2})$$

According to this, we can express the composite function as,

$$\psi^c = \psi \circ \mathbf{E}^* \circ (\alpha\mathbf{A})^* \circ \mathbf{Q}^* \quad (\text{D.3})$$

$\mathbf{E}^*$  being the configurational Green-Lagrange strain tensor where the configuration is driven by the  $\mathbf{Q}^*$  orthonormal tensor rotating the material frame. The coefficient matrices of configurational Green-Lagrange strain tensor, the rotation axis  $\mathbf{a}$  and the skew rotation axis tensor  $\mathbf{A}^*$  are represented in the eigenvector space of Green lagrange strain.

$$\begin{aligned} \mathbf{E}^* &= \frac{1}{2} (\lambda_i^{*2} - 1) \mathbf{N}_i^* \otimes \mathbf{N}_i^* \\ \hat{\mathbf{a}}^* &= \hat{a}_i^* \mathbf{N}_i^* \\ \mathbf{A}^* &= A_{ij}^* (\mathbf{N}_i^* \otimes \mathbf{N}_j^*) = -\varepsilon_{ijk} a_k^* (\mathbf{N}_i^* \otimes \mathbf{N}_j^*) \end{aligned} \quad (\text{D.4})$$

Where, the axis is perpendicular to the plane of *two different configurational fiber directions*. This means, one of the configurational fiber direction given as unremodeled, the axis  $\mathbf{a}^*$  represents

one of infinitely many axis of remodeling rotations. As stated before, since we consider energetically equal configurations, in this stage the remodeling assumes to change the kinematics. Thus, kinematics  $\mathbf{E}^*$  is configural either. The variation of the strain energy function in the direction of the rotations,

$$\frac{\partial \psi^c}{\partial \mathbf{Q}^*} : \delta \mathbf{Q}^* = \frac{\partial \psi}{\partial \mathbf{E}^*} : \frac{\partial \mathbf{E}^*}{\partial \hat{\mathbf{a}}^*} \cdot \frac{\partial \hat{\mathbf{a}}^*}{\partial (\alpha^* \mathbf{A}^*)} : \frac{\partial (\alpha^* \mathbf{A}^*)}{\partial \mathbf{Q}^*} : \delta \mathbf{Q}^* \quad (\text{D.5})$$

In the indicial notation we have,

$$\frac{\partial \psi^c}{Q_{ij}^*} \delta Q_{ij}^* = \frac{\partial \psi}{\partial E_{ij}^*} \frac{\partial E_{ij}^*}{\partial \hat{a}_k^*} \frac{\partial \hat{a}_k^*}{\partial (\alpha^* A_{lm}^*)} \frac{\partial (\alpha^* A_{lm}^*)}{Q_{no}^*} \delta Q_{no}^* \quad (\text{D.6})$$

Defining the non-remodeled configuration vector by  $\mathbf{m}$  and new configuration vector by  $\mathbf{q}^*$  in Green Lagrange eigenvector bases,

$$\mathbf{m} = m_i \mathbf{N}_i^* \quad \mathbf{q}^* = q_i^* \mathbf{N}_i^* \quad (\text{D.7})$$

The new configuration is obtained by a  $k$ 'th contravariant unit base vector as the axis  $\hat{\mathbf{a}}^*$  of the  $j$ 'th and  $i$ 'th unit covariant base vectors as non-remodeled configuration vector and new configuration vector.

$$\mathbf{m} = \mathbf{G}_i \|\mathbf{G}_j\|_2 \|\mathbf{G}_i\|_2^{-1} \quad \mathbf{q}^* = \mathbf{G}_j \quad \hat{\mathbf{a}}^* = \mathbf{G}^k \|\mathbf{G}^k\|_2^{-1} \quad (\text{D.8})$$

Following this, there is a unit contravariant axis  $\hat{\mathbf{a}}^*$  which rotates  $i$ 'th covariant unit base into  $j$ 'th covariant and similarly the axis  $-\hat{\mathbf{a}}^*$  rotates  $j$ 'th base into  $i$ 'th base with the same angle of rotation  $\alpha^*$  with positive sinus. According to this idea we can write down the forward and backward Euler-Rodrigues rotation formula,

$$\mathbf{Q}^* = \hat{\mathbf{a}}^* \otimes \hat{\mathbf{a}}^* + \cos(\alpha^*) (\mathbf{I}_N - \hat{\mathbf{a}}^* \otimes \hat{\mathbf{a}}^*) + \sin(\alpha^*) \mathbf{A} \quad (\text{D.9})$$

$$\mathbf{Q}^{*T} = \hat{\mathbf{a}}^* \otimes \hat{\mathbf{a}}^* + \cos(\alpha^*) (\mathbf{I}_N - \hat{\mathbf{a}}^* \otimes \hat{\mathbf{a}}^*) - \sin(\alpha^*) \mathbf{A}$$

The elements of the Rodrigues formulation are,

$$\mathbf{I}_N = \mathbf{N}_i^* \otimes \mathbf{N}_i^*$$

$$\hat{\mathbf{a}} \otimes \hat{\mathbf{a}} = \hat{a}_i \hat{a}_j \mathbf{N}_i^* \otimes \mathbf{N}_j^* = \varepsilon_{ikl} \varepsilon_{jmn} q_l q_n m_k m_m \|\mathbf{a}\|^{-2} \mathbf{N}_i^* \otimes \mathbf{N}_j^*$$

$$\mathbf{A} = A_{ij} \mathbf{N}_i^* \otimes \mathbf{N}_j^* = -\varepsilon_{ijk} \hat{a}_k \mathbf{N}_i^* \otimes \mathbf{N}_j^* = -\varepsilon_{ijk} \varepsilon_{klm} q_m m_l \|\mathbf{a}\|^{-1} \mathbf{N}_i^* \otimes \mathbf{N}_j^*$$

$$\cos(\alpha^*) = q_i m_i (\|\mathbf{q}\| \|\mathbf{m}\|)^{-1}$$

$$\sin(\alpha^*) = \|\mathbf{a}\| (\|\mathbf{q}\| \|\mathbf{m}\|)^{-1} = (\varepsilon_{ikl} \varepsilon_{imn} q_l q_n m_k m_m)^{1/2} (\|\mathbf{q}\| \|\mathbf{m}\|)^{-1} \quad (\text{D.10})$$

It should be stated here that among the infinitely many orthonormal tensors, the spin-free one is presented here. According to the equation (D.9), the logarithm of the angle-scaled skew matrix and the derivative appearing in the equation (D.5) is given as,

$$\log_e(\mathbf{Q}^*) = \alpha^* \mathbf{A}^* = \frac{\alpha^*}{\sin(\alpha^*)} (\mathbf{Q}^* - \mathbf{Q}^{*T}) \quad \frac{\partial (\alpha^* \mathbf{A}^*)}{\partial \mathbf{Q}^*} = \frac{\alpha^*}{\sin(\alpha^*)} (\hat{\mathbb{I}} - \hat{\mathbb{I}}) \quad (\text{D.11})$$

Now we chose the new configuration coaxial with the eigenvalue scaled eigenvector. With this post statement, we will be looking for the variational stability of the energetically equal configurations for the rotations steered by the axis of one eigenvector direction. Say,

$$\mathbf{q}^* = \lambda_1^* \mathbf{N}_1 \quad (\text{D.12})$$

If we reduce the target into one eigenvector the Rodrigues formula compatible to equation (D.10) is,

$$\begin{aligned} \mathbf{Q}^* = & \left( \varepsilon_{ik1} \varepsilon_{jm1} \lambda_1^* \lambda_1^* m_k m_m \|\mathbf{a}\|^{-2} + m_1 \lambda_1^{*-1} (\delta_{ij} + \varepsilon_{ik1} \varepsilon_{jm1} \lambda_1^* \lambda_1^* m_k m_m \|\mathbf{a}\|^{-1}) \right) \mathbf{N}_i^* \otimes \mathbf{N}_j^* \\ & - \left( \varepsilon_{ijk} \varepsilon_{klm} q_m m_l \|\mathbf{a}\|^{-1} (\varepsilon_{np1} \varepsilon_{nr1} \lambda_1^* \lambda_1^* m_p m_r)^{1/2} \lambda_1^{*2} \right) \mathbf{N}_i^* \otimes \mathbf{N}_j^* \end{aligned} \quad (\text{D.13})$$

The coefficient matrix of the rotation tensor becomes,

$$[\mathbf{Q}^*] = \begin{bmatrix} (m_1 \lambda_1^{*-1}) & (m_2 \lambda_1^{*-1}) & (m_3 \lambda_1^{*-1}) \\ - (m_2 \lambda_1^{*-1}) & \begin{pmatrix} m_1 \lambda_1^{*-1} + m_3^2 (m_2^2 + m_3^2)^{-1} \\ -m_1 m_3^2 \lambda_1^{*-1} (m_3^2 + m_2^2)^{-1} \end{pmatrix} & \begin{pmatrix} -m_3 m_2 (m_3^2 + m_2^2)^{-1} \\ +m_1 m_3 m_2 \lambda_1^{*-1} (m_3^2 + m_2^2)^{-1} \end{pmatrix} \\ - (m_3 \lambda_1^{*-1}) & \begin{pmatrix} -m_2 m_3 (m_3^2 + m_2^2)^{-1} \\ +m_1 m_2 m_3 \lambda_1^{*-1} (m_3^2 + m_2^2)^{-1} \end{pmatrix} & \begin{pmatrix} m_1 \lambda_1^{*-1} + m_2^2 (m_3^2 + m_2^2)^{-1} \\ -m_1 m_2^2 \lambda_1^{*-1} (m_3^2 + m_2^2)^{-1} \end{pmatrix} \end{bmatrix} \quad (\text{D.14})$$

Equation (D.5) becomes,

$$\frac{\partial \psi^c}{\partial \mathbf{Q}^*} : \delta \mathbf{Q}^* = \mathbf{S}^* : \frac{\partial \mathbf{E}^*}{\partial \hat{\mathbf{a}}^*} \cdot \frac{-\mathcal{E}}{\alpha^*} : \frac{\alpha^*}{\sin(\alpha^*)} (\hat{\mathbb{I}} - \hat{\mathbb{I}}) : \delta \mathbf{Q}^* = \mathbf{S}^* : \left( \frac{-2}{\sin \alpha^*} \frac{\partial \mathbf{E}^*}{\partial \hat{\mathbf{a}}^*} \cdot \mathcal{E} : \delta \mathbf{Q}^* \right) \quad (\text{D.15})$$

Where, the symbol  $\mathcal{E}$  stands for the isotropic permutation pseudotensor. Since, the second Piola Kirchhoff stress tensor is nondecreasing for nondecreasing Green-Lagrange Strain tensor, we are going to expand the remaining product. The variation of the Green-Lagrange tensor in formula above in indicial notation,

$$\frac{\partial E_{ij}^* (-\varepsilon_{lnk})}{\partial \hat{a}_k^* \sin(\alpha^*)} \left( \frac{\partial Q_{lm}^*}{\partial Q_{no}^*} - \frac{\partial Q_{ml}^*}{\partial Q_{no}^*} \right) \delta Q_{no} = \frac{-2}{\sin \alpha^*} \left( \frac{\partial E_{ij}^*}{\partial \hat{a}_k^*} \varepsilon_{nok} \right) \delta Q_{no} = \frac{-2}{\sin \alpha^*} \left( \frac{\partial E_{ii}^*}{\partial \hat{a}_k^*} \varepsilon_{nok} \right) \delta Q_{no} \quad (\text{D.16})$$

The last kronecker insertion is due to the nonexistence of the non-diagonal terms of the Green-Lagrange strain tensor coefficients in the eigenvector base system. *Unfolding* the permutation pseudotensor and multiplying it with the directional derivative of the Green-Lagrange strain tensor in the direction of the rotation axis, one would get the the *unfolded* form of the third order result of the round brackets of last part of equation (D.16). The permutation pseudotensor is independent of any coordinate system and can be represented in terms of the foldings of eigenbases as,

$$\begin{aligned} \mathcal{E} = & (\mathbf{N}_2^* \otimes \mathbf{N}_3^* - \mathbf{N}_3^* \otimes \mathbf{N}_2^*) \otimes \mathbf{N}_1^* \\ & + (\mathbf{N}_3^* \otimes \mathbf{N}_1^* - \mathbf{N}_1^* \otimes \mathbf{N}_3^*) \otimes \mathbf{N}_2^* \\ & + (\mathbf{N}_1^* \otimes \mathbf{N}_2^* - \mathbf{N}_2^* \otimes \mathbf{N}_1^*) \otimes \mathbf{N}_3^* \end{aligned} \quad \text{unfold}_i(\mathcal{E}) = \mathcal{E} \cdot \mathbf{N}_i^* \quad (\text{D.17})$$

The tensor order of the Green Lagrange strain tensor is reduced for practical reasons. Even though the tensor itself can not be extracted from the reduced representation for arbitrary coordinate system (from 3 parameter space into 6 parameter space), it is still valid to vectorize the Green-Lagrange strain tensor. Since we define the coefficients in eigenspace, the conversion in this space is self-verified (from 3 parameter space into 3 parameter space). The length of the vector form is equal to the second invariant of the second order form. Thus, this vector form has an invariant and is a tensor.

$$\hat{\mathbf{E}}^* = \frac{1}{2} (\lambda_i^{*2} - 1) \mathbf{N}_i^* \quad \|\hat{\mathbf{E}}^*\|_2^2 = I_2^{\mathbf{E}^*} \quad (\text{D.18})$$

So, the derivative in the round brackets of equation (D.16) and the unfolded second order tensorial components of it are given below,

$$\frac{\partial \hat{\mathbf{E}}^*}{\partial \hat{\mathbf{a}}^*} \cdot \mathcal{E} = \frac{\partial \hat{\mathbf{E}}^*}{\partial (\hat{\mathbf{a}}^* \cdot \mathbf{N}_j^*)} \otimes \text{unfold}_j(\mathcal{E}) \quad (\text{D.19})$$

The matrix coefficients of the unfolding of equation (D.19) with the combination of equation (D.17) is given below,

$$\text{unfold}_i \left( \frac{\partial \hat{\mathbf{E}}^*}{\partial \hat{\mathbf{a}}^*} \cdot \mathcal{E} \right) = \frac{\partial \hat{E}_i^*}{\partial \hat{a}_j^*} \varepsilon_{jkl} (\mathbf{N}_k^* \otimes \mathbf{N}_l^*) \quad (\text{D.20})$$

Enforcing the anisotropy in the direction of the target configuration,

$$\begin{aligned} \frac{\partial \hat{\mathbf{E}}^*}{\partial \hat{\mathbf{a}}^*} &= \frac{\partial \hat{\mathbf{E}}^*}{\partial (\mathbf{E}^* : \mathbf{q}^* \otimes \mathbf{q}^*)} \otimes \frac{\partial (\mathbf{E}^* : \mathbf{q}^* \otimes \mathbf{q}^*)}{\partial \mathbf{q}^*} \cdot \frac{\partial \mathbf{q}^*}{\partial \hat{\mathbf{a}}^*} \\ &= \lambda_1^* (\mathbf{N}_1^* \otimes \mathbf{N}_1^*) \cdot (m_3^{-1} (\mathbf{N}_1^* \otimes \mathbf{N}_2^*) - m_2^{-1} (\mathbf{N}_1^* \otimes \mathbf{N}_3^*)) \end{aligned} \quad (\text{D.21})$$

Inserting back into equation (D.20) gives us the only nonzero component in matrix form,

$$\left[ \text{unfold}_1 \left( \frac{\partial \hat{\mathbf{E}}^*}{\partial \hat{\mathbf{a}}^*} \cdot \mathcal{E} \right) \right] = \begin{bmatrix} 0 & -\lambda_1^* m_2^{-1} & -\lambda_1^* m_3^{-1} \\ \lambda_1^* m_2^{-1} & 0 & 0 \\ \lambda_1^* m_3^{-1} & 0 & 0 \end{bmatrix} \quad (\text{D.22})$$

The total derivative in the direction of the orthonormal tensor variation vanishes as shown below.

$$\begin{aligned} \frac{\partial \hat{\mathbf{E}}^*}{\partial \hat{\mathbf{a}}^*} \cdot \mathcal{E} : \delta \mathbf{Q}^* &= \left( -\lambda_1^* m_3^{-1} \frac{\partial Q_{13}^*}{\partial \lambda_1^*} + \lambda_1^* m_3^{-1} \frac{\partial Q_{31}^*}{\partial \lambda_1^*} \right) \delta \lambda_1^* \mathbf{N}_1^* \\ &\quad + \left( -\lambda_1^* m_2^{-1} \frac{\partial Q_{12}^*}{\partial \lambda_1^*} + \lambda_1^* m_2^{-1} \frac{\partial Q_{21}^*}{\partial \lambda_1^*} \right) \delta \lambda_1^* \mathbf{N}_1^* \\ &= 2\lambda_1^* m_3^{-1} \frac{m_3}{\lambda_1^{*2}} \delta \lambda_1^* \mathbf{N}_1^* - 2\lambda_1^* m_2^{-1} \frac{m_2}{\lambda_1^{*2}} \delta \lambda_1^* \mathbf{N}_1^* \\ &= 2\lambda_1^{*-1} \delta \lambda_1^* \mathbf{N}_1^* - 2\lambda_1^{*-1} \delta \lambda_1^* \mathbf{N}_1^* = \mathbf{0} \end{aligned} \quad (\text{D.23})$$

This indicates that the configurational kinematics as well as configurational energy is stationary for the given type of rotations. Next, we will discuss about the convexity of this type of rotations.

## D.2 Maximization of Configurational Energy

In this section the duality of the optimization manifolds will be shown and proven to be holding at the location of stationary point shown in the previous section. The only nonzero part of the coefficient of the variation of Green Lagrange strain tensor in the direction of virtual rotation is,

$$\begin{aligned} \mathit{unfold}_1 \left( \frac{\partial \hat{\mathbf{E}}^*}{\partial \hat{\mathbf{a}}^*} \cdot \boldsymbol{\varepsilon} \right) &= -\lambda_1^* m_2^{-1} (\mathbf{N}_1^* \otimes \mathbf{N}_2^*) - \lambda_1^* m_3^{-1} (\mathbf{N}_1^* \otimes \mathbf{N}_3^*) \\ &+ \lambda_1^* m_2^{-1} (\mathbf{N}_2^* \otimes \mathbf{N}_1^*) + \lambda_1^* m_3^{-1} (\mathbf{N}_3^* \otimes \mathbf{N}_1^*) \end{aligned} \quad (\text{D.24})$$

The second variation of the Green Lagrange Strain tensor with respect to the rotation tensor gives us information about the convexity of the Green Lagrange Strain tensor in terms of the rotations.

$$\frac{-2}{\sin \alpha^*} \left[ \frac{\partial}{\partial \mathbf{Q}^*} \left( \mathit{unfold}_1 \left( \frac{\partial \hat{\mathbf{E}}^*}{\partial \hat{\mathbf{a}}^*} \cdot \boldsymbol{\varepsilon} \right) \right) : \delta \mathbf{Q}^* \right] : \delta \mathbf{Q}^* \quad (\text{D.25})$$

The derivative with respect to the rotation tensor in the brackets right before the second variational double contraction is,

$$\frac{\partial}{\partial \mathbf{Q}^*} \left( \mathit{unfold}_1 \left( \frac{\partial \hat{\mathbf{E}}^*}{\partial \hat{\mathbf{a}}^*} \cdot \boldsymbol{\varepsilon} \right) \right) = \frac{-2}{\sin \alpha^*} \frac{\partial}{\partial \mathbf{a}^*} \left( \mathit{unfold}_1 \left( \frac{\partial \hat{\mathbf{E}}^*}{\partial \hat{\mathbf{a}}^*} \cdot \boldsymbol{\varepsilon} \right) \right) \cdot \boldsymbol{\varepsilon} \quad (\text{D.26})$$

The derivative with respect to the rotation axis is,

$$\begin{aligned} \frac{\partial}{\partial \mathbf{a}^*} \left( \mathit{unfold}_1 \left( \frac{\partial \hat{\mathbf{E}}^*}{\partial \hat{\mathbf{a}}^*} \cdot \boldsymbol{\varepsilon} \right) \right) &= \\ &-m_2^{-1} m_3^{-1} (\mathbf{N}_1^* \otimes \mathbf{N}_2^* \otimes \mathbf{N}_2^*) - m_3^{-2} (\mathbf{N}_1^* \otimes \mathbf{N}_3^* \otimes \mathbf{N}_2^*) \\ &+ m_2^{-1} m_3^{-1} (\mathbf{N}_2^* \otimes \mathbf{N}_1^* \otimes \mathbf{N}_2^*) + m_3^{-2} (\mathbf{N}_3^* \otimes \mathbf{N}_1^* \otimes \mathbf{N}_2^*) \\ &+ m_2^{-2} (\mathbf{N}_1^* \otimes \mathbf{N}_2^* \otimes \mathbf{N}_3^*) + m_2^{-1} m_3^{-1} (\mathbf{N}_1^* \otimes \mathbf{N}_3^* \otimes \mathbf{N}_3^*) \\ &- m_2^{-2} (\mathbf{N}_2^* \otimes \mathbf{N}_1^* \otimes \mathbf{N}_3^*) - m_2^{-1} m_3^{-1} (\mathbf{N}_3^* \otimes \mathbf{N}_1^* \otimes \mathbf{N}_3^*) \end{aligned} \quad (\text{D.27})$$

Dot product with the permutation pseudotensor,

$$\begin{aligned}
\frac{\partial}{\partial \mathbf{a}^*} \left( \text{unfold}_1 \left( \frac{\partial \hat{\mathbf{E}}^*}{\partial \hat{\mathbf{a}}^*} \cdot \boldsymbol{\varepsilon} \right) \right) \cdot \boldsymbol{\varepsilon} = & \\
& -m_2^{-1} m_3^{-1} (\mathbf{N}_1^* \otimes \mathbf{N}_2^* \otimes (\mathbf{N}_3^* \otimes \mathbf{N}_1^* - \mathbf{N}_1^* \otimes \mathbf{N}_3^*)) \\
& -m_3^{-2} (\mathbf{N}_1^* \otimes \mathbf{N}_3^* \otimes (\mathbf{N}_3^* \otimes \mathbf{N}_1^* - \mathbf{N}_1^* \otimes \mathbf{N}_3^*)) \\
& +m_2^{-1} m_3^{-1} (\mathbf{N}_2^* \otimes \mathbf{N}_1^* \otimes (\mathbf{N}_3^* \otimes \mathbf{N}_1^* - \mathbf{N}_1^* \otimes \mathbf{N}_3^*)) \\
& +m_3^{-2} (\mathbf{N}_3^* \otimes \mathbf{N}_1^* \otimes (\mathbf{N}_3^* \otimes \mathbf{N}_1^* - \mathbf{N}_1^* \otimes \mathbf{N}_3^*)) \\
& +m_2^{-2} (\mathbf{N}_1^* \otimes \mathbf{N}_2^* \otimes (\mathbf{N}_1^* \otimes \mathbf{N}_2^* - \mathbf{N}_2^* \otimes \mathbf{N}_1^*)) \\
& +m_2^{-1} m_3^{-1} (\mathbf{N}_1^* \otimes \mathbf{N}_3^* \otimes (\mathbf{N}_1^* \otimes \mathbf{N}_2^* - \mathbf{N}_2^* \otimes \mathbf{N}_1^*)) \\
& -m_2^{-2} (\mathbf{N}_2^* \otimes \mathbf{N}_1^* \otimes (\mathbf{N}_1^* \otimes \mathbf{N}_2^* - \mathbf{N}_2^* \otimes \mathbf{N}_1^*)) \\
& -m_2^{-1} m_3^{-1} (\mathbf{N}_3^* \otimes \mathbf{N}_1^* \otimes (\mathbf{N}_1^* \otimes \mathbf{N}_2^* - \mathbf{N}_2^* \otimes \mathbf{N}_1^*))
\end{aligned} \tag{D.28}$$

The variation in the direction of the secondary virtual rotations,

$$\begin{aligned}
\left[ \frac{\partial}{\partial \mathbf{Q}^*} \left( \text{unfold}_1 \left( \frac{\partial \hat{\mathbf{E}}^*}{\partial \hat{\mathbf{a}}^*} \cdot \boldsymbol{\varepsilon} \right) \right) : \delta \mathbf{Q}^* \right] = & \\
& -2m_2^{-1} \lambda_1^{*-2} \delta \lambda_1^* (\mathbf{N}_1^* \otimes \mathbf{N}_2^*) - 2m_3^{-1} \lambda_1^{*-2} \delta \lambda_1^* (\mathbf{N}_1^* \otimes \mathbf{N}_3^*) \\
& +2m_2^{-1} \lambda_1^{*-2} \delta \lambda_1^* (\mathbf{N}_2^* \otimes \mathbf{N}_1^*) + 2m_3^{-1} \lambda_1^{*-2} \delta \lambda_1^* (\mathbf{N}_3^* \otimes \mathbf{N}_1^*) \\
& -2m_2^{-1} \lambda_1^{*-2} \delta \lambda_1^* (\mathbf{N}_1^* \otimes \mathbf{N}_2^*) - 2m_3^{-1} \lambda_1^{*-2} \delta \lambda_1^* (\mathbf{N}_1^* \otimes \mathbf{N}_3^*) \\
& +2m_2^{-1} \lambda_1^{*-2} \delta \lambda_1^* (\mathbf{N}_2^* \otimes \mathbf{N}_1^*) + 2m_3^{-1} \lambda_1^{*-2} \delta \lambda_1^* (\mathbf{N}_3^* \otimes \mathbf{N}_1^*)
\end{aligned} \tag{D.29}$$

The total variation is then,

$$\frac{-2}{\sin \alpha^*} \left[ \frac{\partial}{\partial \mathbf{Q}^*} \left( \text{unfold}_1 \left( \frac{\partial \hat{\mathbf{E}}^*}{\partial \hat{\mathbf{a}}^*} \cdot \boldsymbol{\varepsilon} \right) \right) : \delta \mathbf{Q}^* \right] : \delta \mathbf{Q}^* = 64 \sin^{-2}(\alpha^*) \delta \lambda_1^* \delta \lambda_1^* \tag{D.30}$$

Which shows that the eigenvalue based rotation can be represented as a convex optimization problem. Stretch and thus strain have their minimum value independent of the energy constraint and the initial position. Since we have a stationary point at the locus of interest, we can not comment (not straightforwardly) further on the convexity of the strain energy density function about the orthonormal tensor, using the tensor composition higher order derivatives. To show that there is the maximization perspective of the same objective and subjective we will use next the Lagrange duality. The problem above without the inclusion of the composition and energetically equal restriction, can be interpreted as the minimization of the anisotropic ingredient of the Green-Lagrange Strain measure. As shown

in the previous section, the stated stationary point is minimum kinematic configuration and is the solution of the following primal objective and subjective set,

$$\begin{aligned}
\text{minimize} \quad & I_4 = \mathbf{m}^T \cdot (\mathbf{Q}^T \cdot \mathbf{E} \cdot \mathbf{Q}) \cdot \mathbf{m} = \mathbf{E} : ((\mathbf{Q} \cdot \mathbf{m}) \otimes (\mathbf{Q} \cdot \mathbf{m})) \\
\text{subject to} \quad & (\mathbf{Q} \cdot \mathbf{m}) \cdot (\mathbf{Q} \cdot \mathbf{m}) = 1 \\
& \mathbf{Q}^T \cdot \mathbf{Q} = \mathbf{I}
\end{aligned} \tag{D.31}$$

Since  $\mathbf{m}$  is arbitrary, thus nor configurational, neither a parameter of the optimization. Hence, is not listed explicitly in the constraints. Reformulating the problem,

$$\begin{aligned}
\text{minimize} \quad & \mathbf{E} : (\mathbf{q} \otimes \mathbf{q}) \\
\text{subject to} \quad & \mathbf{q} \cdot \mathbf{q} = 1
\end{aligned} \tag{D.32}$$

The Lagrangian of the minimization of the convex quadratic function on the unit ball constraint is,

$$\begin{aligned}
L(\mathbf{q}, \mu) &= \mathbf{E} : (\mathbf{q} \otimes \mathbf{q}) + \mu (\mathbf{q} \cdot \mathbf{q} - 1) \\
&= \mathbf{q}^T \cdot (\mathbf{E} - \mu \mathbf{I}) \cdot \mathbf{q} + \mathbf{q}^T \cdot \mu \mathbf{I} \cdot \mathbf{q} + \mu (\mathbf{q} \cdot \mathbf{q} - 1) \\
&= \mathbf{q}^T \cdot (\mathbf{E} - \mu \mathbf{I}) \cdot \mathbf{q} - \mu
\end{aligned} \tag{D.33}$$

The cost  $\mu$  is set to be the Lagrange multiplier of the single equality constraint. The dual form is then,

$$g(\mu) = \inf_{\mathbf{q}} (L(\mathbf{q}, \mu)) = \inf_{\mathbf{q}} (\mathbf{q}^T \cdot (\mathbf{E} - \mu \mathbf{I}) \cdot \mathbf{q}) - \mu \tag{D.34}$$

Since the infimum of the quadratic form is zero if the form is positive definite, else negatively unbounded,

$$g(\mu) = \begin{cases} -\mu & (\mathbf{E} - \mu \mathbf{I}) \cdot \mathbf{q} \succeq \mathbf{0} \\ -\infty & \text{otherwise} \end{cases} \tag{D.35}$$

Moving on with the assumption of strong duality (zero duality gap), the Lagrange multiplier component of the Karush-Kuhn-Tucker point of the quadratic problem with quadratic equality constraint can be found. For zero duality gap, the gradient of the Lagrangian (Lagrangian with the optimal dual parameter) evaluated at the optimal primary variable should vanish.

$$\nabla_{\mathbf{q}} L(\mathbf{q}, \mu^*)|_{\mathbf{q}^*} = \nabla_{\mathbf{q}} \mathbf{E} : (\mathbf{q} \otimes \mathbf{q})|_{\mathbf{q}^*} + \nabla_{\mathbf{q}} \mu^* (\mathbf{q} \cdot \mathbf{q} - 1)|_{\mathbf{q}^*} = 2(\mathbf{E} + \mu^* \mathbf{I}) \cdot \mathbf{q}^* = \mathbf{0} \tag{D.36}$$

Quite clearly the solutions which imposes redundancy to the term in brackets and satisfies the KKT condition above is,

$$\mu^* = \{-\lambda^{*2} + 1 \mid \lambda^{*2} \geq 1\} \tag{D.37}$$



Which is feasible according to the dual constraint. The additional constraint in equation (72) is a reinterpretation of the dual constraint of (70). In matrix vector form the constraint of (70) for a stationary point,

$$\lambda_1^{*2} \geq 1 \implies \begin{bmatrix} 2\lambda_1^{*2} - 2 & 0 & 0 \\ 0 & \lambda_1^{*2} + \lambda_2^{*2} - 2 & 0 \\ 0 & 0 & \lambda_1^{*2} + \lambda_3^{*2} - 2 \end{bmatrix} \cdot \begin{bmatrix} 1 \\ 0 \\ 0 \end{bmatrix} \succeq \begin{bmatrix} 0 \\ 0 \\ 0 \end{bmatrix} \quad (\text{D.38})$$

The strain energy density function of the remodeled configuration is a nondecreasing function of the given eigenvalues of the Green-Lagrange strain tensor. According to the dual form, the remodeling search can be interpreted as the maximization of the energy subjected to a kinematic inequality constraint.

# Bibliography

- [A.Laub 2008] UCLA Department of Mathematics A.Laub. *Notes on Moore-Penrose pseudoinverse*. url:  
<http://www.math.ucla.edu/laub/33a.2.12s/mpseudoinverse.pdf>, 2008. (Cited on page 143.)
- [A.Menzel 2004] A.Menzel. *Modelling of anisotropic growth in fibrous tissue*. (3(3): 147 – 171). Biomechan. Model. Mechanobiol., pages –, 2004. (Cited on pages 49, 100, 108 and 113.)
- [A.Menzel 2006] A.Menzel. *A fibre reorientation model for orthotropic multiplicative growth*. (DOI : 10.1007/s10237 – 006 – 0061 – y). Biomechan Model Mechanobiol., pages –, 2006. (Cited on page 113.)
- [B.Barber 1996] H.Huhdanpaa B.Barber D.P. Dobkin. *The Quickhull algorithm for convex hulls*. (22(4): 469 – 483). ACM TRANSACTIONS ON MATHEMATICAL SOFTWARE, url:<http://www.qhull.org/>, 1996. (Cited on page 132.)
- [Beta 2009] Cae Systems SA Beta. *Metapost postprocessor*. 2009. (Cited on page 47.)
- [Bischoff 2004] W.A.Wall Bischoff Bletzinger and E.Ramm. *Models and Finite Elements for Thin-Walled Structures* (DOI : 10.1002/0470091355.ecm026). Encyclopedia of Computational Mechanics, 2004. (Cited on page 154.)
- [Bletzinger 2009] K.U. Bletzinger. *Ergaenzungskurs Statik* (url : <https://campus.tum.de/>; Modul – Kennung : 240079716). TUM-online, 2009. (Cited on page 2.)
- [Boehler 1979] Jean-Paul Boehler. *A simple derivation of representations for non-polynomial constitutive equations in some cases of anisotropy*. (DOI : 10.1002/zamm.19790590403). Zeitschrift fuer Angewandte Mathematik und Mechanik, V59, I4, pages 157–167, 1979. (Cited on pages 102, 103 and 104.)
- [Buckley 2008] Buckley. *Mapping the depth dependence of shear properties in articular cartilage*. (DOI : 10.1016/j.jbiomech.2008.05.021). Orthopedic research society, 2008. (Cited on pages 99 and 100.)
- [C.J. Chuong 1986] Y.C. Fung C.J. Chuong. *On Residual Stress in Arteries*. (DOI : 10.1007/978 – 1 – 4612 – 4866 – 8<sub>9</sub>). Journal of Biomechanics, no. 108(2), pages 189–192, 1986. (Cited on page iv.)
- [C.L.Stanfield 2012] W.J.Germann C.L.Stanfield. *Principles of Human Physiology*. (ISBN – 10 : 0321819349). Pearson, 2012. (Cited on page 78.)

- [C.Miehe 1996] C.Miehe. *Numerical computation of algorithmic consistent tangent moduli in large-strain computational inelasticity.* (DOI : [doi.org/10.1016/0045-7825\(96\)01019-5](https://doi.org/10.1016/0045-7825(96)01019-5)). Computer Methods in Applied Mechanics and Engineering 134(3-4), pages 223-240, 1996. (Cited on page 108.)
- [C.Sansour 2007] C.Sansour. *On the physical assumptions underlying the volumetric-isochoric split and the case of anisotropy.* (DOI : [doi.org/10.1016/j.euromechsol.2007.04.001](https://doi.org/10.1016/j.euromechsol.2007.04.001)). European Journal of Mechanics and Solids, V27, I1, pages 28-39, 2007. (Cited on page 103.)
- [C.Truesdell 1960] R.A.Toupin C.Truesdell. *The classical field theories.* (DOI : [10.1007/978-3-642-45943-6\\_2](https://doi.org/10.1007/978-3-642-45943-6_2)). Handbuch der Physik, Springer Verlag, pages -, 1960. (Cited on pages 2 and 10.)
- [David Boal 2010] Simon Fraser University David Boal. *Lecture notes on statistical physics and biophysics, Simon Fraser University.* url: <http://www.sfu.ca/boal/teaching.html>, pages -, 2010. (Cited on page 101.)
- [de Boer 1996] R. de Boer. *Highlights in the historical development of the porous media theor: Toward a consistent macroscopic theory* (DOI : [10.1115/1.3101926](https://doi.org/10.1115/1.3101926)). Appl.Mech.Rev., no. 49, pages 201-262, 1996. (Cited on page 3.)
- [deHoff 2006] R. deHoff. *Thermodynamics in Material Science* (ISBN9780849340659 - CAT4065). Taylor and Francis, 2006. (Cited on pages 11 and 16.)
- [D.F.Styer 2007] D.F.Styer. *Statistical Mechanics,* (<http://www.oberlin.edu/physics/dstyer/StatMech/book.pdf>). Oberlin Collage, Department of Physics and Astronomy, Class Matter, 2007. (Cited on page 15.)
- [Dolbow 1998] John Dolbow and Ted Belytschko. *Numerical Integration of the Galerkin Weak Form in Meshfree Methods.* (DOI : [10.1007/s004660050403](https://doi.org/10.1007/s004660050403)). Departments of Civil and Mechanical Engineering, Northwestern University, 1998. (Cited on page 136.)
- [Edelsbrunner 1983] Seidel Edelsbrunner Kirkpatrick. *On the shape of a set of points in the plane.* (DOI : [10.1109/TIT.1983.1056714](https://doi.org/10.1109/TIT.1983.1056714)). IEEE Transactions on Information Theory 29 (4), pages 551-559, 1983. (Cited on pages 124 and 125.)
- [E.Kuhl 2008] E.Kuhl. *Remodeling of biological Tissue: Mechanically induced reorientation of a transversely isotropic chain network.* (DOI : [doi.org/10.1016/j.jmps.2005.03.002](https://doi.org/10.1016/j.jmps.2005.03.002)). Biomechan. Model. Mechanobiol., pages -, 2008. (Cited on pages 49, 100, 104, 108 and 113.)
- [E.Onate 2004] F. D.Pin E.Onate S.R.Idelshon and R.Aubry. *The particle finite element method - An Overview.* DOI: (<http://dx.doi.org/10.1142/S0219876204000204>).

- International Journal of Computational Methods Vol1 No2, pages 167–307, 2004. (Cited on page 123.)
- [Erdemir 2014] Ahmet Erdemir. *Open Knee(s): Virtual Biomechanical Representations of the Knee Joint*. url: <https://simtk.org/projects/openknee>, 2014. (Cited on page 57.)
- [F.C.MacKintosh 2009] F.C.MacKintosh. *Polymer-based models of cytoskeletal networks*. (url : <http://www.nat.vu.nl/fcm/Papers/CytoMechChapter.pdf>). Cambridge University Press, pages 152–169, 2009. (Cited on page 101.)
- [Federico 2008] Federico. *Towards an analytical model of soft biological tissues*. (DOI : 10.1016/j.jbiomech.2008.05.039). Journal of Biomechanics, 2008. (Cited on pages 99 and 100.)
- [Fung 1993] Y.-C. Fung. *Biomechanics: Mechanical Properties of Living Tissues*. (DOI : 10.1007/978-1-4757-2257-4). New York: Springer-Verlag, page 568, 1993. (Cited on pages iii, iv and 2.)
- [G.A.Ateshian 2008] G.A.Ateshian. *Mixture Theory for Biological Tissues*. Notes of Summer School on "Modeling and Computation in Biomechanics" in Graz, 2008. (Cited on page 4.)
- [G.Bradoski 2008] A.Kaehler G.Bradoski. *Learning OpenCV Computer Vision with the OpenCV Library*. (ISBN – 10 : 0596516134). O'Reilly, pages 479–480, 2008. (Cited on page 127.)
- [G.Holzzapfel 2006] E. Kuhl G.Holzzapfel. *A continuum model for remodeling in living structures*. (DOI : 10.1007/s10853-007-1917-y). Nano- and micromechanical properties of Hierarchical biological materials, pages –, 2006. (Cited on pages 49, 100 and 108.)
- [GNU 2009] The Project GNU. <http://gcc.gnu.org/>. 2009. (Cited on page 46.)
- [Green 1970] A.E. Green. *Large Elastic Deformations*. (ISBN – 13 : 978-0198533344). Oxford University Press; 2nd Revised edition edition (Dec1970), 1970. (Cited on page iv.)
- [Hariton 2007] Holzzapfel Hariton. *Stress modulated collagen fibre remodeling in a human carotid bifurcation*. (DOI : [doi.org/10.1016/j.jtbi.2007.05.037](https://doi.org/10.1016/j.jtbi.2007.05.037)). Journal of theoretical biology, pages –, 2007. (Cited on page 113.)
- [Hatze 1974] Herbert Hatze. *The meaning of the term biomechanics*. (DOI : [http://dx.doi.org/10.1016/0021-9290\(74\)90060-8](http://dx.doi.org/10.1016/0021-9290(74)90060-8)). Journal of Biomechanics, no. 7, pages 189–190, 1974. (Cited on page iii.)
- [H.C.Prk 1997] S.K.Youn H.C.Prk. *Finite element analysis and constitutive modelling of anisotropic nonlinear hyperelastic bodies with convected frames*.

- (DOI : 10.1016/S0045 – 7825(97)00172 – 2). Computer methods in applied mechanics and engineering. V151, 13-4, pages 605–618, 1997. (Cited on page 103.)
- [H.Darcy 1856] H.Darcy. *Les Fontaines Publiques de la Ville de Dijon*. Dalmont, Paris, 1856. (Cited on page 24.)
- [Hic.et.nunc 2012] Hic.et.nunc. *Uterine fibroids url:*  
([https://commons.wikimedia.org/wiki/File:Uterine\\_fibroids.png](https://commons.wikimedia.org/wiki/File:Uterine_fibroids.png)).  
Wikipedia Commons -  
(<https://creativecommons.org/licenses/by-sa/3.0/legalcode>), 2012. (Cited on page 49.)
- [Himpel 2007] Kuhl Himpel Menzel and Steinmann. *Time dependent fibre reorientation of transversely isotropic continua- Finite element formulation and consistent linearization*. (DOI : 10.1002/nme.2124). International journal for numerical methods in engineering, pages –, 2007. (Cited on page 113.)
- [Holzapfel 2006] G.A. Holzapfel. *Nonlinear Solid Mechanics, A continuum Approach for Engineering*. (ISBN : 978 – 0 – 471 – 82319 – 3). John Wiley and Sons Ltd., 2006. (Cited on page 7.)
- [Holzapfel 2008] G.A. Holzapfel. *Collagen in Arterial Walls: Biomechanical Aspects*. (DOI : 10.1007/978 – 0 – 387 – 73906 – 9<sub>1</sub>1). Collagen:Structure and Mechanics, Springer Science+Business Media, pages 285–324, 2008. (Cited on page iv.)
- [Humphrey 2003] D. Jay Humphrey. *Continuum biomechanics of soft biological tissues*. (DOI : 10.1098/rspa.2002.1060). In The Royal Society. Proceedings of the Royal Society of London A 459 (2029), pages 3–46, 2003. (Cited on page iii.)
- [I.Hariton 2007] G.Holzapfel I.Hariton. *Stress-driven collagen fiber remodeling in arterial walls*. (DOI : 10.1007/s10237 – 006 – 0049 – 7). Biomechan. Model. Mechanobiol., pages –, 2007. (Cited on pages 49, 100 and 113.)
- [J.Bonet 2008] R.D.Wood J.Bonet. *Nonlinear Continuum Mechanics for Finite Element Analysis* (ISBN – 13 : 978 – 0521838702). Cambridge University Press, 2008. (Cited on pages 7, 8, 26 and 38.)
- [J.Braun 2006] M.Sambridge J.Braun. *A numerical method for solving partial differential equations on highly irregular evolving grids*. (DOI : 10.1038/376655a0). Nature Vol 376, pages 655–660, 2006. (Cited on page 124.)
- [J.E.Bischoff 2002] K.Grosh J.E.Bischoff E.Arruda. *Finite element simulations of orthotropic hyperelasticity*. (DOI : doi.org/10.1016/S0168 – 874X(02)00089 – 6). Finite Elements in Analysis and Design, V38, 110, pages 983–998, 2002. (Cited on pages 108 and 110.)

- [J.M. Guccione 1991] L.K. Waldman J.M. Guccione A.D. McCulloch. *Passive material properties of intact ventricular myocardium determined from a cylindrical model.* (*PubMedID* : 2020175). *J. Biomech Eng.*, no. 113(1), pages 42–55, 1991. (Cited on page iv.)
- [J.M.Clark 1990] J.M.Clark. *The organisation of collagen fibrils in the superficial zones of articular cartilage.* (*PMCID* : PMC1257132). *J.Anat.*, pages 117–130, 1990. (Cited on pages 61 and 62.)
- [J.M.Clark 1991] J.M.Clark. *Variation of Collagen Fiber Alignment in a Joint Surface: Scanning Electron Microscope Study of the Tibia Plateau in Dog, Rabbit, and Man.* (*DOI* : 10.1002/jor.1100090213). *Journal of Orthopaedic Research*, pages 246–257, 1991. (Cited on pages xvii and 62.)
- [J.S.Chen 2001] S.Yoon J.S.Chen C.T.Wux and Y.You. *A stabilized conforming nodal integration for Galerkin mesh-free methods.* (*DOI* : 10.1002/1097 – 0207(20010120)50 : 2 < 435 :: AID – NME32 > 3.0.CO;2 – A). *International Journal for numerical methods in engineering* 50, pages 435–456, 2001. (Cited on page 135.)
- [J.W.Delleur 2007] J.W.Delleur. *The handbook of groundwater engineering.* (*ISBN* : 978 – 3 – 540 – 64745 – 4). Taylor and Francis, 2007. (Cited on page 24.)
- [J.W.Yoo 2004] J.S.Chen J.W.Yoo B.Moran. *Stabilized conforming nodal integration in the natural-element method.* (*DOI* : 10.1002/nme.972). *International Journal for numerical methods in engineering* 60, pages 861–890, 2004. (Cited on page 136.)
- [K.Garikipati 2005] K.Garikipati. *Biological remodelling: Stationary energy, Configurational change, internal variables and dissipation.* (*DOI* : //doi.org/10.1016/j.jmps.2005.11.011). *Journal of the Mechanics and Physics of Solids*, pages –, 2005. (Cited on pages 49, 100 and 113.)
- [K.U.Bletzinger 2011] Lehrstuhl fuer Statik TUMuenchen K.U.Bletzinger. *Lehrveranstaltung - Structural Optimization 1.* url: <https://campus.tum.de/tumonline/LV.detail?clvnr=950033069f>, 2011. (Cited on page 143.)
- [L.C.Hughes 2005] I.Gwynn L.C.Hughes C.W.Archer. *The Ultrastructure of Mouse Articular Cartilage: Collagen Orientation and Implications for Tissue Functionality. A Polarized Light and Scanning Electron Microscope Study and Review.* (*PMID* : 15968593). *European Cells and Materials*, pages 68–84, 2005. (Cited on page 62.)
- [Library-MKL 2008] Intel Math Kernel Library-MKL. <http://software.intel.com/en-us/intel-mkl>. 2008. (Cited on page 46.)

- [M.Duflot 2002] H. N.Dang M.Duflot. *A truly meshless Galerkin method based on a moving least squares quadrature.* (DOI : 10.1002/cnm.503). Marc Duflot, Fracture mechanics department, University of Liege, 2002. (Cited on page 123.)
- [M.J.Buehler 2006] M.J.Buehler. *Atomistic and continuum modeling of mechanical properties of collagen: Elasticity, fracture and self-assembly.* (DOI : <https://doi.org/10.1557/jmr.2006.0236>). J. Mater. Res., 2006. (Cited on pages 78 and 124.)
- [Monaghan 1992] J.J. Monaghan. *Smoothed Particle Hydrodynamics.* (DOI : 10.1146/annurev.aa.30.090192.002551). Annu. Rev. Astrophys., 1992. (Cited on page 123.)
- [M.Serrano 2005] I.Zuniga M.Serrano P.Espanol. *Voronoi Fluid Particle Model for Euler Equations.* (DOI : 10.1007/s10955 – 005 – 8414 – y). Journal of Statistical Physics, Vol. 121, 2005. (Cited on page 124.)
- [Mueller 2009] G. Mueller. *Kontinuumsmechanik* ([url : https://campus.tum.de/](https://campus.tum.de/); Modul – Kennung : BV020001). TUM-online, 2009. (Cited on page 10.)
- [N.Bicanic 2004] N.Bicanic. *Discrete Element Methods.* (DOI : 10.1002/0470091355.ecm006). Stein, de Borst, Hughes Encyclopedia of Computational Mechanics, Vol. 1. Wiley, 2004. (Cited on page 123.)
- [Newmark 1959] N. M. Newmark. *A method of computation for structural dynamics.* Journal of Engineering Mechanics ASCE, pages 85 (EM3) 67–94, 1959. (Cited on page 33.)
- [N.J.Driessen 2003] N.J.Driessen. *Remodeling of continuously distributed collagen fibres in soft connective tissue.* (PMID : 12831741). Journal of Biomechanics, pages –, 2003. (Cited on pages 49, 100 and 113.)
- [Norris 2005] Norris. *Optimal orientation of anisotropic solids.* (DOI : 10.1093/qjmam/hbi030). Mech. Appl. Math., pages –, 2005. (Cited on page 113.)
- [N.Sasaki 1996] S.Odajimat N.Sasaki. *Stress strain curve and youngs modulus of a collagen molecule as determined by the xray diffraction technique.* (PMID : 8707794). Journal of Biomechanics, pages 655–658, 1996. (Cited on page 78.)
- [N.Sukumar 1998] T.Belytschko N.Sukumar B.Moran. *The Natural Element Method in Solid Mechanics.* (DOI : 10.1002/(SICI)1097 – 0207(19981115)43 : 5 < 839 :: AID – NME423 > 3.0.CO;2 – R). International Journal for Numerical Methods in Engineering, 43, pages 839–887, 1998. (Cited on page 123.)

- [O.C.Zienkiewicz 2000a] J.Z.Zhu O.C.Zienkiewicz R.L.Taylor. *The Finite Element Method, Volume 1: The Finite Element Method Its Basis and Fundamentals*. (ISBN – 13 : 978 – 0750663212). Elsevier, Butterworth and Heinemann, pages –, 2000. (Cited on pages 62, 92 and 135.)
- [O.C.Zienkiewicz 2000b] R.L.Taylor O.C.Zienkiewicz. *The Finite Element Method, Volume 2: For Solid and Structural Mechanics*. (ISBN – 13 : 978 – 0750663212). Butterworth and Heinemann, pages –, 2000. (Cited on pages 34, 108 and 109.)
- [O.C.Zienkiewicz 2000c] R.L.Taylor O.C.Zienkiewicz. *The Finite Element Method, Volume 3: Fluid Dynamics*. (ISBN – 13 : 978 – 0750663229). Butterworth and Heinemann, pages –, 2000. (Cited on page 9.)
- [Ogden 2003] R.W. Ogden. *Nonlinear Elasticity, Anisotropy, Material Stability and Residual stresses in Soft Tissue* (DOI : 10.1007/978 – 3 – 7091 – 2736 – 0<sub>3</sub>). Biomechanics of Soft Tissue in Cardiovascular Systems CISM Courses and Lectures Series, Springer, Wien, no. 441, pages 65–108, 2003. (Cited on page iv.)
- [OpenStax 2016] OpenStax. *Muscle Fibers*, url: ([https://commons.wikimedia.org/wiki/File:1007\\_Muscle\\_Fibres\\_large.jpg](https://commons.wikimedia.org/wiki/File:1007_Muscle_Fibres_large.jpg)). Wikipedia Commons - (<https://creativecommons.org/licenses/by/4.0/legalcode>), 2016. (Cited on pages xviii and 78.)
- [P.Alliez 2006] P.Alliez. <http://visionair.ge.imati.cnr.it/ontologies/shapes/view.jsp?id=422-Skull>. Visionair - A world class Infrastructure for Advanced 3D Visualization-based Research. Visualization Virtual Services, AIM@SHAPE Digital Shape Workbench v5.0, 2006. (Cited on pages xix, 129, 130 and 133.)
- [Pardiso 2009] Software Pardiso. <http://www.pardiso-project.org/>. 2009. (Cited on page 46.)
- [personal post processor GiD 2009] The personal post processor GiD. <http://gid.cimne.upc.es/>. 2009. (Cited on page 47.)
- [P.Fischer 2010] P.Steinmann P.Fischer J.Mergheim. *On the C1 continuous discretization of non-linear gradient elasticity: A comparison of NEM and FEM based on Bernstein-Bezier patches*. (DOI : 10.1002/nme.2802). International Journal for Numerical Methods in Engineering, 2010. (Cited on pages 80 and 81.)
- [R.A.Bank 2000] J.M.TeKoppele R.A.Bank. *The increased swelling and instantaneous deformation of osteoarthritic cartilage is highly correlated with collagen degradation* (DOI : 10.1002/1529 – 0131(200010)43 : 10 < 2202 :: AID – ANR7 > 3.0.CO; 2 – E). Arthritis and Rheumatism, pages 2202–2210, 2000. (Cited on page 78.)



- [R.Baierlein 2010] R.Baierlein. *Thermal physics*. (ISBN – 10 : 0521658381). Cambridge University Press, pages –, 2010. (Cited on page 101.)
- [R.E.Sonntag 1998] G.J.Wylen R.E.Sonntag C.Borgnakke. *Fundamentals of Thermodynamics*. (ISBN : 978 – 1 – 119 – 32145 – 3). John Wiley and Sons Inc., 1998. (Cited on pages 11 and 15.)
- [R.J.Atkin 1976] R.E.Crain R.J.Atkin. *Continuum theories of mixtures: Basic theory and hixtorical development* (DOI : <https://doi.org/10.1093/qjmam/29.2.209>). J. Mech. and Appl. Math., no. 29, pages 209–244, 1976. (Cited on page 2.)
- [R.Shirazi 2008] M.Hurtig R.Shirazi A.S.Adl. *Role of cartilage collagen fibrils networks in knee joint biomechanics under compression*. (DOI : 10.1016/j.jbiomech.2008.09.033). Journal of Biomechanics, 2008. (Cited on page 78.)
- [R.W.Ogden 2008] R.W.Ogden. *Nonlinear elasticity and fibrous structure in arterial wall mechanics*. Lecture notes for summer school on Modeling and Computation in Biomechanics, Graz 2008, pages 152–169, 2008. (Cited on pages 101 and 108.)
- [Schinagl 1997] Schinagl. *Depth dependent confined compression modulus of full thickness bovine articular cartilage*. (DOI : 10.1002/jor.1100150404). Orthopedic research society, 1997. (Cited on pages 99 and 100.)
- [Simulia 2011] Dassault Systems Simulia. *Abaqus Scripting Reference Manual*. 2011. (Cited on page 46.)
- [S.Kobayashiv 1995] Y.Kurogouchi S.Kobayashiv S.Yonekubo. *Cryoscanning electron microscopic study of the surface amorphous layer of articular cartilage*. (PMCID : PMC1167438). J.Anat., pages 117–130, 1995. (Cited on page 62.)
- [Smith 2013] I. Smith. *Smith's elements of solid mechanics*. (ISBN : 978 – 0 – 470 – 67339 – 3). John Wiley and Sons Inc., 2013. (Cited on page 24.)
- [S.R.Idelshon 2006] E.Onate S.R.Idelshon. *To mesh or not to mesh. That is the question. . .* (DOI : <https://doi.org/10.1016/j.cma.2005.11.006>). Comput. Methods Appl. Mech. Engrg. 195, pages 4681–4696, 2006. (Cited on page 124.)
- [S.R.Idelsohn 2002] N.Calvo S.R.Idelsohn E.Onate and F.D.Pin. *The meshless finite element method*. (DOI : 10.1002/nme.798). International Center for Computational Mechanics in Engineering (CIMEC) ,International Center for Numerical Methods in Engineering (CIMNE), 2002. (Cited on page 123.)
- [S.Timoshenko 1951] J.N.Goodier S.Timoshenko. *Theory of Elasticity*. (ISBN – 13 : 978 – 0070647206). Engineering Societies Monographs, McGraw-Hill Book Company,Inc, page 1, 1951. (Cited on page iv.)

- [Thewlis 1973] J. Thewlis. *Concise dictionary of physics and related subjects*. (ISBN : 0080169007). Oxford: Pergamon Press., page 248, 1973. (Cited on page 154.)
- [T.M.Quinn 2005] T.M.Quinn. *Microstructural modelling of collagen network mechanics and interactions with the proteoglycan gel in articular cartilage*. (DOI : 10.1007/s10237 – 006 – 0036 – z). Biomechan Model Mechanobiol, 2005. (Cited on page 99.)
- [V.C.Mow 1980] W.M.Lai V.C.Mow S.C.Kuei and C.G.Armstrong. *Biphasic creep and stress relaxation of articular cartilage in compression: theory and experiments*. (PMID : 7382457). J.Biomech.Engng., no. 102, pages 73–84, 1980. (Cited on page 3.)
- [Vianello 1995] Vianello. *Optimization of the stored energy and coaxiality of strain and stress in finite elasticity*. (DOI : 10.1007/BF00042131). Journal of Elasticity, pages –, 1995. (Cited on page 113.)
- [Vianello 1996a] Vianello. *Coaxiality of strain and stress for anisotropic linear elasticity*. (DOI : 10.1007/BF00041794). Journal of Elasticity, pages –, 1996. (Cited on page 113.)
- [Vianello 1996b] Vianello. *Rotations which make strain and stress coaxial*. (DOI : 10.1023/A : 1007492301537). Journal of Elasticity, pages –, 1996. (Cited on page 114.)
- [W.Ehlers 2002] J.Bluhm W.Ehlers. *Porous Media. Theory, Experiments and Numerical Applications*. (DOI : 10.1007/978 – 3 – 662 – 04999 – 0). Springer Verlag, 2002. (Cited on pages 3 and 5.)
- [W.Wilson 2003] W.Wilson. *Stresses in the local collagen network of articular cartilage: A poroviscoelastic fibril-reinforced finite element study*. (PMID : 14757455). Journal of Biomechanics, 2003. (Cited on page 99.)
- [W.Wilson 2005] W.Wilson. *Depth-dependent Compressive equilibrium properties of articular cartilage explained by its composition*. (DOI : 10.1007/s10237 – 006 – 0044 – z). Biomechan Model Mechanobiol, 2005. (Cited on page 99.)
- [W.Wilson 2006] W.Wilson. *Prediction of collagen orientation in articular cartilage by a collagen remodeling algorithm*. (DOI : <http://dx.doi.org/10.1016/j.joca.2006.05.006>). Osteoarthritis and Cartilage, pages –, 2006. (Cited on pages 49, 100 and 113.)
- [Yang 1996] Daoqi Yang. *C++ and Object-Oriented Numeric Computing for Scientists and Engineers*. Springer Science+Business Media New York, no. ISBN: 978-1-4612-6566-5, pages 1–440, 1996. (Cited on page 46.)

- [Y.Chen 2006] A.Eskandarian Y.Chen J.D.Lee. *Meshless Methods in Solid Mechanics*. (DOI : 10.1007/0 – 387 – 33368 – 1). Springer Science Business Media Inc., 2006. (Cited on pages [124](#) and [136](#).)

## Present Publication Series



**Band Titel**

- 1 Frank Koschnick, *Geometrische Lockingeffekte bei Finiten Elementen und ein allgemeines Konzept zu ihrer Vermeidung*, 2004.
- 2 Natalia Camprubi, *Design and Analysis in Shape Optimization of Shells*, 2004.
- 3 Bernhard Thomee, *Physikalisch nichtlineare Berechnung von Stahlfaserbetonkonstruktionen*, 2005.
- 4 FernaßDaoud, *Formoptimierung von Freiformschalen - Mathematische Algorithmen und Filtertechniken*, 2005.
- 5 Manfred Bischoff, *Models and Finite Elements for Thin-walled Structures*, 2005.
- 6 Alexander Hörmann, *Ermittlung optimierter Stabwerkmodelle auf Basis des Kraftflusses als Anwendung plattformunabhängiger Prozeßkopplung*, 2006.
- 7 Roland Wüchner, *Mechanik und Numerik der Formfindung und Fluid-Struktur-Interaktion von Membrantragwerken*, 2006.
- 8 Florian Jurecka, *Robust Design Optimization Based on Metamodeling Techniques*, 2007.
- 9 Johannes Linhard, *Numerisch-mechanische Betrachtung des Entwurfsprozesses von Membrantragwerken*, 2009.
- 10 Alexander Kupzok, *Modeling the Interaction of Wind and Membrane Structures by Numerical Simulation*, 2009.
- 11 Bin Yang, *Modified Particle Swarm Optimizers and their Application to Robust Design and Structural Optimization*, 2009.
- 12 Michael Fleischer, *Absicherung der virtuellen Prozeßkette für Folgeoperationen in der Umformtechnik*, 2009.
- 13 Amphon Jrusjrungkiat, *Nonlinear Analysis of Pneumatic Membranes - From Subgrid to Interface*, 2009.
- 14 Alexander Michalski, *Simulation leichter Flächentragwerke in einer numerisch generierten atmosphärischen Grenzschicht*, 2010.
- 15 Matthias Firl, *Optimal Shape Design of Shell Structures*, 2010.
- 16 Thomas Gallinger, *Effiziente Algorithmen zur partitionierten Lösung stark gekoppelter Probleme der Fluid-Struktur-Wechselwirkung*, 2011.
- 17 Josef Kiendl, *Isogeometric Analysis and Shape Optimal Design of Shell Structures*, 2011.
- 18 Joseph Jordan, *Effiziente Simulation großer Mauerwerkßstrukturen mit diskreten Reißmodellen*, 2011.
- 19 Albrecht von Boetticher, *Flexible Hangmurenbarrieren: Eine numerische Modellierung des Tragwerks, der Hangmure und der Fluid-Struktur-Interaktion*, 2012.
- 20 Robert Schmidt, *Trimming, Mapping, and Optimization in Isogeometric Analysis of Shell Structures*, 2013.

---

**Band Titel**

- 21 Michael Fischer, *Finite Element Based Simulation, Design and Control of Piezoelectric and Lightweight Smart Structures*, 2013.
- 22 Falko Hartmut Dieringer, *Numerical Methods for the Design and Analysis for Tensile Structures*, 2014.
- 23 Rupert Fisch, *Code Verification of Partitioned FSI Environments for Lightweight Structures*, 2014.
- 24 Stefan Sicklinger, *Stabilized Co-Simulation of Coupled Problems Including Fields and Signals*, 2014.
- 25 Madjid Hojjat, *Node-based parametrization for shape optimal design*, 2015.
- 26 Ute Israel, *Optimierung in der Fluid-Struktur-Interaktion - Sensitivitätsanalyse für die Formoptimierung auf Grundlage des partitionierten Verfahrens*, 2015.
- 27 Electra Stavropoulou, *Sensitivity analysis and regularization for shape optimization of coupled problems*, 2015.
- 28 Daniel Markus, *Numerical and Experimental Modeling for Shape Optimization of Offshore Structures*, 2015.
- 29 Pablo Suárez, *Design Process for the Shape Optimization of Pressurized Bulkheads as Components of Aircraft Structures*, 2015.
- 30 Armin Widhammer, *Variation of Reference Strategy - Generation of Optimized Cutting Patterns for Textile Fabrics*, 2015.
- 31 Helmut Masching, *Parameter Free Optimization of Shape Adaptive Shell Structures*, 2016.
- 32 Hao Zhang, *A General Approach for Solving Inverse Problems in Geophysical Systems by Applying Finite Element Method and Metamodel Techniques*, 2016.
- 33 Tianyang Wang, *Development of Co-Simulation Environment and Mapping Algorithms*, 2016.
- 34 Michael Breitenberger, *CAD-integrated Design and Analysis of Shell Structures*, 2016.
- 35 Önay Can, *Functional Adaptation with Hyperkinematics using Natural Element Method: Application for Articular Cartilage*, 2016.

